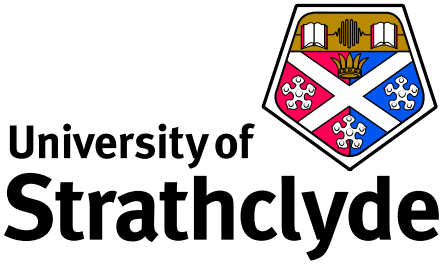

Stents and Arterial Flows

Sean McGinty

Department of Mathematics and Statistics

University of Strathclyde

Glasgow, UK

March 2010

A thesis submitted to the University of Strathclyde for the degree of Doctor of Philosophy in the Faculty of Science.

Acknowledgements

Whilst I will ultimately take the credit for the writing of this thesis, it would not have been possible without the crucial input of several people. I thank my supervisor, Prof. Sean McKee, for providing me with the opportunity to undertake this research. For his guidance and encouragement alone over the past three years, he deserves immense credit. There were, inevitably, times when the research became incredibly frustrating, when codes weren't working or when contour integration appeared, but this is just the nature of research, and the sense of achievement when the problem is overcome far outweighs the frustration. Carefully timed research trips to such places as Brazil have helped make it all bearable. I do regret not having the same love for golf as Sean; had I the same enthusiasm for the sport my PhD would no doubt have been finished much sooner!

Due to the nature of this interdisciplinary research, several meetings have been necessary with colleagues from the Strathclyde Institute of Pharmacology and Biomedical Sciences. In particular, I would like to thank Prof. Roger Wadsworth and Dr. Christopher McCormick, for their unending patience and invaluable input. At various points I have also consulted colleagues from the Department of Mathematics. In particular, I would like to thank Prof. Adam McBride, Dr. Brian Duffy, Dr. Wilson Lamb and Dr. Chris Coles for their advice.

My thanks does not extend only to academics. The Department's administrative staff, Mary McAuley, Irene Spencer and Sandra Miller have been employed by me extensively, and their assistance has been extremely useful. I have made many good friends in the Department and I thank them for their support, good humour, and for letting me kick them at Friday football when I'm frustrated by my research.

I also wish to express my gratitude to The Carnegie Trust for the Universities of Scotland for providing a generous amount of funding over the past three years.

Finally, I wish to express my unending thanks to my fiancee, Michelle, for putting up with my research related mood swings: she may now have her fiance back. I would also like to thank my parents for providing me with the platform to excel and who may now, at last, have their son back.

"Everything is simpler than you think and at the same time more complex than you imagine"

Johann Wolfgang von Goethe

Contents

Chapter 1

General Introduction & Outline of Thesis

Mathematics is not (as is the common perception) a subject restricted to classroom teachings of topics that have no use in the real World. In fact, mathematics is at the heart of everything; a living subject which underpins the modern world of science, technology and business. Mathematical models are increasingly being developed to solve real problems across all disciplines and this is what makes the subject so useful and exciting.

In particular, mathematical biology is a booming area and its applications in the life sciences are helping us understand phenomena which could previously only be explained by experimentation. Every experiment has an associated cost, and verifying the results via further experiments can increase costs significantly. Furthermore, experiments are often carried out for one particular set of physical parameters when perhaps a whole range of physical parameters may need to be tested. Hence, mathematical models can often prove to be a useful generic tool.

The two main topics considered in this thesis, the reaction-advection-diffusion

equation and pipe flow, are quite different and yet connected in their application to the life sciences. The motivation for studying these topics is clear; cardiovascular disease, being the disease that involves the heart or blood vessels, is the most common cause of death and disability in the Western World. Thus any understanding that can be gained from mathematical modelling is welcome.

This thesis has two parts. In the first part, mathematical models are proposed and developed for the transport of a drug from a medical device known as a drug eluting stent into the arterial wall. In the second part, models of Newtonian and non-Newtonian pipe flow are developed and solved analytically for the fluid velocity, allowing simulations of blood flow in a dog's femoral artery to be produced, direct from the analytic solution.

In Chapter 2, the topic of drug eluting stents is introduced through a thorough description of the medical condition that the stent has been designed to relieve. A brief background of the history of treatment strategies is discussed before describing the stent itself. The chapter concludes with a description of some of the types of drugs and polymers used in drug eluting stents. Chapter 3 details previous work that has been done in this field and describes existing models in the literature. Starting from a description of the basic mechanisms of transport, four models are then proposed for the elution of a drug from polymer coated stents and the subsequent uptake into the arterial wall. These models are non-dimensionalized. Chapter 4 deals with analytic methods of solution and these solutions are derived for a number of simpler cases. The full solution, in Laplace transform space, is provided for model I. In Chapter 5, a numerical scheme is devised to compute the solution to the models described in Chapter 3. A thorough sensitivity analysis is carried out to determine the relative importance of transmural convection, diffusion and drug-dependent parameters in drug delivery and deposition, and drug

release from the stent is displayed graphically. Finally, some concentration profiles are displayed. A common theme in mathematical biology is the difficulty in obtaining required parameter values. Chapter 6 explores an inverse problem which allows some of these difficult-to-determine parameters to be obtained by comparing experimental data to a derived analytic solution. Interestingly, there are three characterizations of this solution, which are shown to be equivalent. In Chapter 7, a model is proposed for drug release from a polymer-free micro-porous stent, and the consequent uptake into arterial tissue. Analytic solutions are derived for both extracellular and cellular drug concentration and mass. The results are compared with novel experimental data.

In the penultimate chapter, the second main research topic is described. A brief history of the literature on pipe flow is provided, before a new solution of Newtonian pipe flow is derived for an arbitrary initial condition. Models of cylindrical and annular pulsatile pipe flow subject to an arbitrary time-dependent pressure gradient and arbitrary initial flow are then proposed for an Oldroyd B fluid and solved analytically. Maxwellian flow, Newtonian flow and Poiseuille flow are readily shown to be special cases of the Oldroyd B solutions. Finally, graphical results for blood flow in a dog's femoral artery are presented and discussed. In chapter 9, the main conclusions from this work are presented and some future research directions are suggested.

Chapter 2

Drug Eluting Stents: Introduction and Background

2.1 Introduction

Coronary heart disease is the biggest killer in the UK. Such is the extent of the condition, one in every four male deaths and one in every six female deaths are attributed to the disease in the UK each year. In simple terms, the condition is caused by a blockage or interruption to blood flow and often results in heart attacks and strokes (NHS 2009). It is reasonable to ask what causes the blockage in the first place. The general consensus (e.g. NHS 2009, Beers 2004) is that this problem is the result of fatty deposits accumulating and lining the arterial walls over a period of many years. This, in part, may explain why people who suffer from coronary heart disease tend to do so later in life. The fatty deposits are called atheroma and the process during which the atheroma accumulates is termed atherosclerosis. Indeed the word atherosclerosis itself comes from the Greek words *atheroma* and *sklerosis*, meaning 'tumour full of grainy matter' and 'hardening'.

On average, men develop coronary heart disease around ten years earlier than women. The reason for this is that women are protected by high levels of estrogen until the menopause (after which the disease becomes more common in women) (Beers 2004). It may come as no surprise then that among people aged over seventy five, the disease is more common in women, since women on average live longer than men. An important risk factor, other than age or sex is a family history of early coronary heart disease. In this context, 'early' refers to a father or brother being diagnosed with heart disease before the age of fifty five, or a mother or sister being diagnosed with the condition before the age of sixty five. Other factors include diet and exercise and the related problems of high cholesterol, high blood pressure, diabetes and obesity (Beers 2004). We often hear of "Britain's expanding waistline" and this, it is felt, is only making the problem worse.

2.2 The structure of the arterial wall

An understanding of the arterial wall is essential and is provided at the outset. The arterial wall has three distinct layers: the intima, the media and the adventitia (Yang & Burt 2006) (Figure 2.1). The intima is the innermost region, closest to the lumen. The main constituent of the intima is the endothelial layer of cells. These cells provide a barrier between the flowing blood in the lumen and the rest of the arterial wall and regulate uptake of molecules into the wall. They are also involved in vasoconstriction and vasodilation, and hence the control of blood pressure. Endothelial dysfunction is the starting point of atherosclerosis. The internal elastic lamina (a fenestrated layer of elastic tissue) forms the outermost part of the intima. Moving outwards, we next meet the media (middle) region containing smooth muscle cells, collagen and elastin. Migration and proliferation

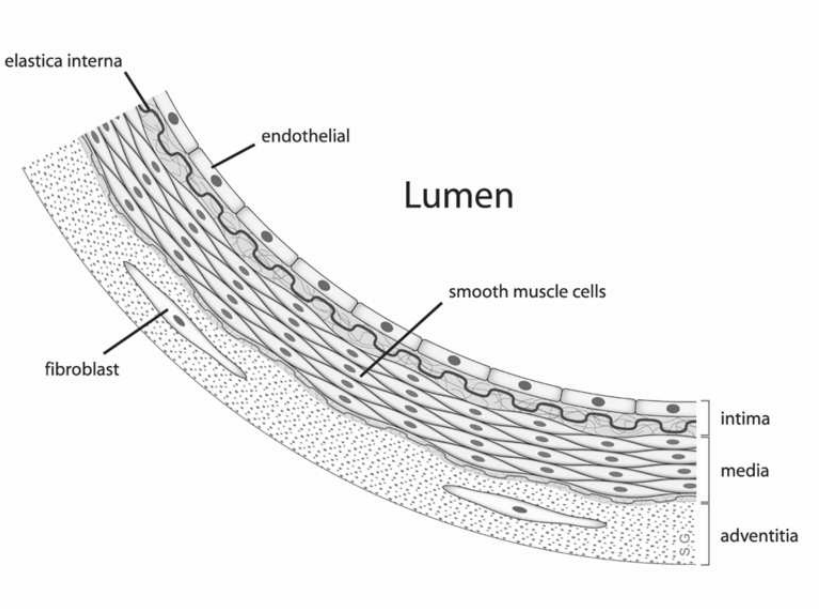

Figure 2.1: The structure of the arterial wall

of smooth muscle cells are important in the development of atherosclerotic plaques. Finally, the outermost layer of the arterial wall is the adventitia. The adventitia essentially tethers the artery to perivascular tissue, and contains cells known as fibroblast. There is also the presence of a network of small blood vessels, termed *vasa vasorum*, which act as a blood (and therefore oxygen) supply to the adventitia and provide nutrients as well as removing waste products.

2.3 Atherosclerosis - a progressive disease

Having provided a very simple description of this condition, one must emphasize that atherosclerosis is in fact a complex progressive disease that is not entirely understood. It is, however, reasonably well established (e.g. Beers 2004, Ai & Vafai 2006) that the initial stages of the disease are characterized by abnormal accumulation of white blood cells in the arterial wall, especially macrophages that

have taken up oxidized low-density lipoprotein (LDL). These molecules enter the arterial wall via the endothelium, the layer of cells which act as a barrier between the wall and the lumen. It is believed that conditions such as high blood pressure and high cholesterol can result in endothelial dysfunction, thus allowing these molecules to enter the wall more readily. As this process continues, and the disease progresses, these macrophages become foam cells. The death of the foam cell releases debris which attracts more macrophages and so the process continues. This is the basis of the formation of atherosclerotic plaque. The plaque is known to contain a fibrous cap of variable thickness as well as a necrotic core made up of cellular debris, cholesterol cleft and cell membranes. Furthermore the plaque also contains macrophages and smooth muscle cells as well as a lipid pool containing lipid dispersed in a collagen matrix (Waksman & Serruys 2004). As the disease progresses, the ever growing plaque bulges into the artery, resulting in stenosis (the narrowing of the lumen), and thus acts as a restriction to blood flow. Perhaps it should be stressed that it is essential that blood flow is maintained since blood, by virtue of its very purpose, serves to distribute oxygen to the various muscles and tissues throughout the body. When the supply of oxygen to the heart muscle (myocardium) falls below the necessary level, the heart can no longer function properly and this may result in myocardial infarction (heart attack, the death of an area of heart muscle) or stroke (a sudden loss of consciousness resulting when the rupture or occlusion of a blood vessel leads to lack of oxygen in the brain) (e.g. NHS 2009, Beers 2004). Clearly, the larger the atheroma (the narrower the artery), the greater the chance of this type of incident. However, there is always the possibility that an atheroma may rupture suddenly, even in relatively wide arteries, causing the onset of thrombus (blood clot) which results in further narrowing or blockage which again can lead to heart attack or stroke. Sudden ruptures are

common in one particular class of plaque called vulnerable plaque. This type of plaque is identifiable by its very thin fibrous cap and large and soft lipid pool underneath (Waksman & Serruys 2004).

2.4 A brief history of treatment strategies

Traditional treatment strategies for coronary heart disease were limited to coronary bypass surgery, known widely as 'open heart surgery'. This type of surgery involves diverting blood around blocked arteries in the heart using a healthy blood vessel taken from elsewhere in the body. However, this was, and to some extent still is, a notoriously dangerous procedure with many associated risks. Some of the possible complications include transient ischemic attacks, internal bleeding and infection as well as neurological damage and stroke (Buzzle 2009). Despite the fact that the surgery has improved through the years, with an increased survival rate, the risk factor is definitely higher in the case of older people and those with related medical conditions of a serious nature.

In the late 1960's, the vascular radiologist Charles Dotter first described the minimally invasive treatment known as angioplasty, from the Greek for 'vessel moulding', as an alternative to open surgery (Duraiswamy *et al.* 2007). This procedure involved using catheters, of various sizes, to try to widen blocked arteries and increase blood flow. However, it was not until the late 1980's/early 1990's that Julio Palmaz developed the stent as a form of angioplasty. Over the past twenty years, stents have become commonplace, with various different designs and levels of complexity added. Being a minimally invasive procedure, the use of a stent to unblock an artery holds many advantages for the patient. The procedure can be performed under local anaesthetic and recovery times can be greatly reduced. In

fact, it is not uncommon for a patient to be admitted in the morning, undergo the procedure, and be discharged the following morning. With the first stent being approved for use in humans as recently as 1994 (drug eluting stents were first approved more recently, in 2002) (Cordis 2009), limited data is available on the long term safety and effectiveness of stenting. Because of the complexity of the problem, mathematical modelling is helpful in characterizing stent release kinetics and arterial drug deposition and thus in improving upon the current 'trial and error' philosophy.

2.5 The stent

The stent itself is essentially a small metal mesh tube which can be inserted into an artery to increase the lumen and act as a scaffold to hold the arterial walls apart. The stent, in collapsed form, is mounted on the back of a balloon catheter and is fed into the body, usually via the groin. The surgeon then guides the stent to the site of stenosis, at which point the balloon is inflated, causing the stent to expand and push the artery walls apart. Next, the balloon is deflated and the catheter removed, leaving the stent *in situ*. Figure 2.2 displays a schematic of the stenting procedure. On the face of it, this procedure may seem too good to be true, in comparison with open heart surgery. Naturally, complications can arise. However, the main risks associated with open heart surgery are either erradicated or greatly reduced. As one may expect, the insertion of a stent can cause injury to the vessel, and in particular the endothelium layer of cells. Until the endothelium is restored (a period of around four weeks, personal communication, Roger Wadsworth), the ability to inhibit smooth muscle cell proliferation is lost and the vessel wall may thicken over, a process known as restenosis, the re-narrowing

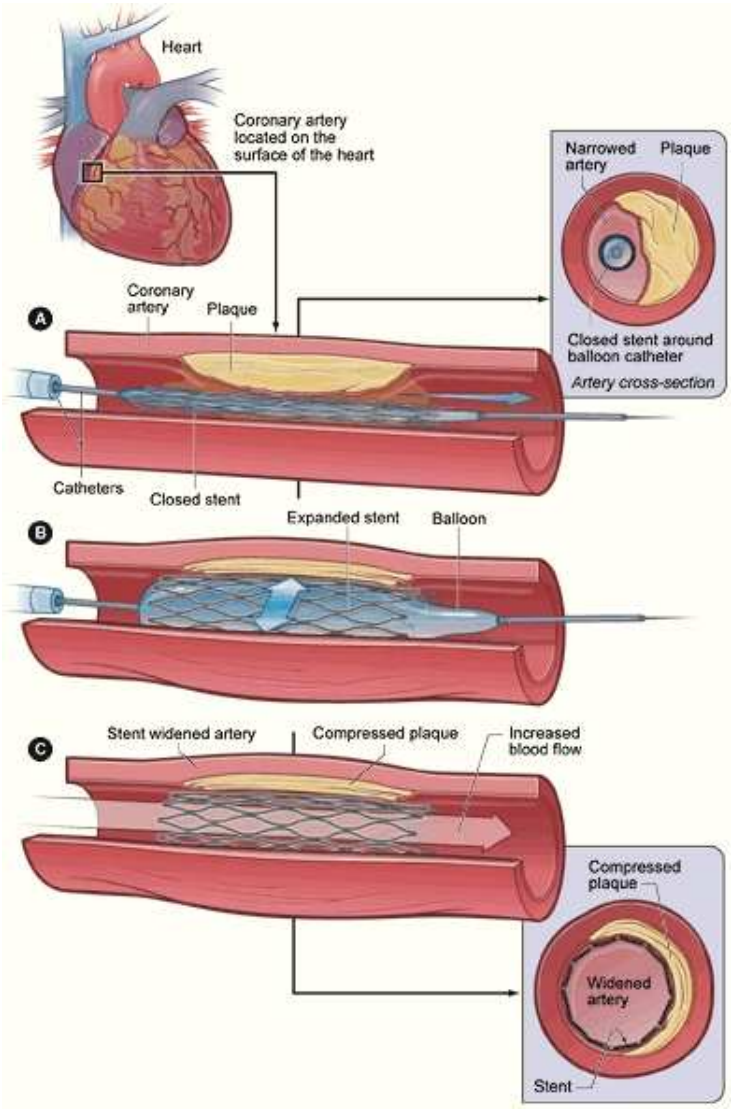

Figure 2.2: The illustration shows a cross-section of a coronary artery with plaque buildup. The coronary artery is located on the surface of the heart. In A we see the deflated balloon catheter inserted into the narrowed coronary artery. In B, the balloon is inflated, compressing the plaque and restoring the size of the artery. Finally, C shows the widened artery. (Credit: US National Heart Lung and Blood institute)

of the vessel. Restenosis occurs in $15 - 20\%$ of patients with bare metal stents (Angioplasty.org 2009). (In those patients a second angioplasty is needed to re-open an artery that closed). This is the major problem with deploying stents as a treatment for stenosis and has led to the development of drug eluting stents. The idea is a simple one; the stent is coated with a drug designed to combat smooth muscle cell proliferation and thus reduce the onset of restenosis. Drug eluting-stents, however, are not without complications of their own. Some studies have indicated that there is a higher incidence of thrombosis when drug coated stents are used, in comparison with bare metal stents. However, most researchers believe that the chance of late stent thrombosis is less than 0.6 % (Angioplasty.org 2009).

2.6 The current 'trial and error' philosophy

Although the deployment of stents as a means of treating coronary heart disease is now well established, it may come as a surprise to learn that the procedure is far from an exact science and relies on a certain degree of trial and error. Although there are a number of stents commercially available, of varying sizes, shapes and materials, and loaded with different types of drugs, no-one really knows what form the ideal stent should take. Clearly, the size of atherosclerotic lesion varies from vessel to vessel and from patient to patient and this explains why stents of different sizes are necessary. The clinician is able to use instrumentation to make a reasonable guess as to the correct size of stent to use. This guess, of course, will depend much on the experience of the clinician. But there are many questions which remain unanswered. Figure 2.3 shows several different stent designs, each with an elaborate mesh-like design. The design must be such that the stent can be collapsed and then expanded inside the artery, but other than this pre-requisite,

it is by no means clear why these complex designs have been chosen. Generally speaking, the struts of the stent are metal or metal alloy with a polymer coating containing the drug. Naively, one might initially think that the ideal stent should have as many struts as possible to deliver the maximum amount of drug to the wall. Then one might think that perhaps a hollow cylinder is the best design so that there is a uniform drug delivery from the stent. Of course, this would not be practical since blood interaction with the wall is essential. Also, there is the possibility that the more struts that are forced against the wall, the more damage to the arterial wall. Research has shown (Pache *et al.* 2003) that thinner struts can reduce the degree of restenosis, but the stability of the stent must also be kept in mind; if the stent were to collapse under the strain of the artery, the procedure would be a disaster. The only way that insight has been gained into the problem of stent design is by trial and error. The more procedures performed using different stents, the more the clinician gets a feel for the best stent for the circumstances. An interesting problem would be to consider the optimal design of a stent, but due to the differences in vessels between patients, and due to differences in the extent of the disease, this problem is far from trivial.

2.7 Drugs and polymers

A number of different drugs and polymers have been used in the design of drug eluting stents. The first clinically approved stent in Europe, the sirolimus eluting CYPHER stent system, arrived in 2002. The stent consists of a stainless steel repeat-pattern design and is coated with a controlled-release, nonresorbable, elastomeric polymer coating containing the drug sirolimus. Sirolimus, also known as rapamycin, is an anti-rejection drug, whose anti-proliferative properties are ideal

Figure 2.3: A selection of stent designs.

for reducing smooth muscle cell proliferation after the implantation of the stent, and thus reducing the on-set of restenosis. The drug is hydrophobic ('water fearing') and thus partitions highly into arterial tissue. To date, the Cypher stent has been used to unblock the arteries of over three million patients (Cordis 2009). A trial showing the efficacy of the CYPHER Stent found that up to 5 years after receiving a CYPHER Stent, the risk of re-blockage in the treated part of the artery is about 10%, compared to about 26% for an uncoated stent. Eighty percent (80%) of the sirolimus is released during the first 30 days. The rest is released by the end of 90 days. A series of trials involving a different drug, paclitaxel, led to the FDA approval of the Taxus paclitaxel eluting stent in the USA in 2004. The stent consists of a stainless steel design which mimics the natural contours of the arterial wall and is coated with Translute Polymer, a proprietary polymer carrier technology, containing the drug paclitaxel. The manufacturer claims that the polymer "controls the release of paclitaxel, which may allow for consistent drug release and more uniform drug distribution" (Rogers *et al.* 2000). Paclitaxel binds specifically to intracellular proteins (Levin *et al.* 2004), and like sirolimus has anti-proliferative properties making it ideal for the prevention of restenosis. Paclitaxel is highly lipophilic, a property that may contribute to a more uniform drug distribution (Creel *et al.* 2000). Several other drugs have been considered for use in drug eluting stents. For example, everolimus (similar in nature to sirolimus) and heparin (a hydrophilic drug). The hydrophilicity and hydrophobicity of a drug can have an enormous effect on arterial drug concentrations delivered from drug eluting stents. Generally speaking, hydrophobic drugs such as paclitaxel lead to higher arterial wall deposition than hydrophilic drugs such as heparin (e.g. Hwang *et al.* 2001, Creel *et al.* 2000). The reason for this is that heparin, by its hydrophilic nature, binds easily to water and is washed through the system more readily than

paclitaxel, which binds tenaciously to tissue. The effect of varying lipophilicity is considered in Table 5.6. Several different polymer platforms have been considered for use with drug eluting stents. These include PLGA poly(lactic-co-glycolic acid) (personal communication, Christopher McCormick), PDLLA poly(D,L-lactide) and PDLLGA poly(D,L-lactide-co-glycolide) biodegradable helical stent systems (Alexis *et al.* 2004). It is suggested in the literature (Labinaz *et al.* 2007) that the way forward is biodegradable stents which control the inflammation effects of restenosis and then completely degrade, leaving no trace in the artery.

Chapter 3

Mathematical Models of Drug Eluting Stents

3.1 Existing Models

There have been a number of studies investigating various different problems relating to arterial stents. Garasic *et al.* (2000) experimentally investigated whether design-dependent post-depolyment luminal geometry affects late restenosis independently of strut induced injury. Their results show that stents designed with twelve struts per cross section had two-fold less neointimal thickening than identical stents with only eight struts per cross section. Using straightforward mathematics, they sought to determine if eventual lumen shape is a function of the shape of the polygon that can be formed between struts and the largest circular lumen that can be inscribed within it. They calculated the predicted area of neointimal hyperplasia (polyglon) minus eventual lumen area (circle) and found that increasing the number of struts led to an advantageous circular post deployment shape. In trials, as stent struts became more numerous and evenly distributed, neointi-

mal area fell and lumen size rose in a predictable manner. Hwang *et al.* (2001) experimentally found that stent based delivery leads to large tissue concentration gradients. The mere proximity of delivery device to tissue does not ensure adequate drug targeting, because physiological transport forces cause local concentrations to deviate significantly from mean concentrations. The authors commented that the partition coefficients for hydrophilic drugs differ dramatically from those of hydrophobic drugs. It is suggested that, given their lower concentration variability, the hydrophilic nature of a drug may be advantageous when that drug possesses a small therapeutic window, whereas the hydrophobic nature of a drug may be advantageous to maintain high therapeutic doses closer to the intima. The flow instabilities induced by coronary artery stents were examined by Peacock *et al.* (1995). The results show that under resting conditions, all coronary waveforms remained laminar, even after stent deployment. However, disturbances were found downstream from a stent placed in the proximal left anterior descending coronary artery under mild exercise conditions. The shear stress from these disturbances is sufficient to delay re-endothelialisation and promote restenosis.

The first full mathematical treatment of drug eluting stents appears to have been by Zunino (2004). Zunino neglects the endothelium layer of cells, the intima tissue and internal elastic lamina and considers only the stent coating and the media. The coating and arterial wall are taken to be porous. There is a leakage of plasma from the lumen into the arterial wall resulting in a fluid flow in the porous media, driven by the pressure gradient across the wall. Darcy's Law is used to estimate the magnitude of this filtration velocity and it is found to be of the order of 10^{-8} ms^{-1}. Zunino couples Darcy's law with the advection-diffusion equation in two dimensions to study the release of the drug from the stent over the first six hours and also

the drug lost to the lumen. The procedure employed is numerical and uses finite elements. Two different drugs are considered, allowing for a variation in some parameters. Zunino concludes that most of the drug is lost from the stent to the wall within the first hour of implantation, and that a significant fraction of the drug is lost to the lumen after six hours, more so with one of the drugs (heparin) than the other (taxus). Zunino argues that the difference in drug loss strictly depends on the properties of the drug inside the wall and is not influenced by the characteristics of the carrier. It is suggested that a slower release rate may reduce the amount of drug lost to the blood. Pontrelli & de Monte (2007) use the corresponding one dimensional equations to solve the problem analytically using the separation of variables technique and then proceed to perform a sensitivity analysis on some of the non-dimensional parameters characterizing the system. Similarly to Zunino, Pontrelli & de Monte use Darcy's law to estimate the magnitude of the filtration velocity to be of the order of 10^{-8} ms^{-1}, although they conclude that convection is negligible in comparison with diffusion. The authors then proceed to neglect the effect of convection, which leads to a significantly simplified model. Uptake into cells is not considered, but a concentration jump at the interfaces is accounted for. Some very recent work by Zunino *et al.* (2009) investigates models which couple the stent dynamics, blood flow and drug transport into the tissue. A mechanical analysis of stent expansion into a coronary artery is carried out and simulated numerically. Numerical methods are also employed to simulate the fluid dynamics and drug release, and the authors find that there is evidence that the interaction between the stent and the blood stream generates complex flow patterns, where recirculation zones interact with the main flow. Another recent paper by Pontrelli & de Monte (2009) builds upon their aforementioned earlier work by adding a reaction term to their one-dimensional model, and this time including the effect

of convection in their numerical computations, finding that even a relatively small advection lowers the concentration curves at all times. Davia *et al.* (2009) present numerical results in two dimensions for release of nucleic acid based drugs from a gel paved stent. Their models include advection as well as diffusion and reaction. Their simulations, which are computed using control volume methods, reveal that drug spreading strongly depends on reaction rate and on the ratio between the diffusion coefficient of the drug in the gel and the wall. They find that by adjusting the drug diffusion coefficent accordingly, an almost constant mean drug concentration can be obtained over a period of several months.

3.2 Mechanisms of transport

The main mechanisms of drug transport in the arterial wall are molecular diffusion and convection. Molecular diffusion involves the net transport of molecules from an area of higher concentration to one of lower concentration by random molecular motions. In the absence of convection or other external forces, the diffusion process will eventually result in complete mixing or a state of equilibrium. Convection, on the other hand, is the transfer of molecules within fluid, caused by relative molecular motion. One can think of the subsequent spreading from dropping a blob of ink into a pond as an example of diffusion. If instead we drop the blob of ink into a river, the ink not only diffuses into the surrounding water, but is also carried downstream by the river (convection).

3.2.1 Fick's laws of diffusion

In the mid Nineteenth Century, Adolf Fick developed the theory of diffusion, realising that in an isotropic substance, the rate of transfer of diffusing substance

through unit area of a section is proportional to the concentration gradient measured normal to the section. This statement, Fick's first law of diffusion, is expressed mathematically as

$$F = -D\frac{\partial C}{\partial x}, \tag{3.2.1}$$

where F is the rate of transfer per unit area, C is the concentration of diffusing substance, and x is the usual space co-ordinate measured normal to the section. The parameter D is the so-called diffusion coefficient with dimensions $[L]^2/[T]$. The presence of the negative sign indicates that the direction of diffusion is opposite to that of increasing concentration.

By considering the rate at which a diffusing substance is transferred through an element of volume of a rectangular parallelpiped (Crank 1956), one can derive the differential equation of diffusion in an isotropic medium, known as Fick's second Law:

$$\frac{\partial C}{\partial t} = D\frac{\partial^2 C}{\partial x^2}, \tag{3.2.2}$$

where, clearly, one-dimensional diffusion only has been considered. Equation (3.2.2) can easily be generalised to two or more space dimensions by use of the Gradient operator. Equation (3.2.2) will be the foundation of the preceding models of arterial drug transport from a drug eluting stent.

3.3 New Models

In the remainder of the chapter, a hierarchical family of one-dimensional models for the elution of a drug from a polymer coated stent into the arterial wall is developed. Adopting a different approach from the works of Zunino (2004) and Pontrelli & de Monte (2007, 2009), the following models are not only concerned with investigating the release of drug from the stent, but also in the uptake into cells within the

arterial wall. The action of the drug is to inhibit smooth muscle cell proliferation and thus it is the cells within the tissue that are targeted. Indeed, Pontrelli (2007) comments that to have a desired effect, drug concentration should lie withing some given range, below which the drug is ineffective, and above which toxicity is reached. Thus models have been developed which discriminate between the drug concentration in the cellular and extracellular regions, to allow one to ascertain the levels of drug that can be maintained in the cells. The starting point is a model composed of only the polymer and media layers. More sophisticated models, with the addition of the adventitia, a polymer topcoat layer and atherosclerotic plaque are then developed.

3.3.1 Assumptions

In all of the models it has been necessary to make some simplifying assumptions which will be stated at the outset. All of the preceding models have a fundamental assumption: the transport of drug may be represented by a one-space dimensional Cartesian model with the single space dimension in the direction normal to the artery. This assumption is justified, since experimental data suggests (at least for the calf carotid artery) an arterial radius of 6mm and a wall thickness of 0.7mm (Levin *et al.* 2004), and so the radius of the artery is considerably greater than the distance the drug penetrates into the arterial wall. It is assumed that the insertion of a stent removes or damages the endothelium to such an extent that it can be neglected. Furthermore, the intima layer including the internal elastic lamina is not considered. Thus, all the models consider the polymer (covering a stent strut) to be the region closest to the lumen, followed by the media region. The diffusion of drug in tissue is known to be anisotropic (Levin *et al.* 2004), but since our attention is restricted to one-dimension, it is not possible to account for

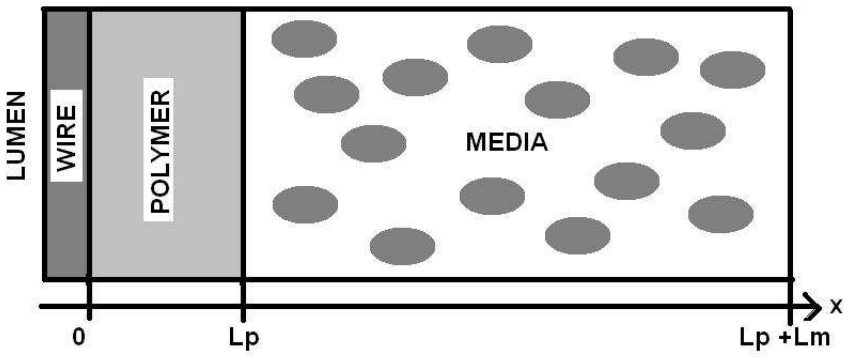

Figure 3.1: Model I: Consists of a drug-filled polymer region and media region containing smooth muscle cells and extracellular space.

the anisotropic nature of diffusion within the tissue. The strut is considered to be in contact with the arterial wall; in reality, the struts are likely to be embedded in the artery. Finally, the flow interaction problem between the blood and the struts is not investigated, and drug loss to the lumen is only considered when investigating release from the stent.

3.3.2 Model I: polymer and media

Consider initially a polymer region of thickness l_p and a media region of thickness l_m, as shown in Figure 3.1. The media region is considered to be a porous medium, of porosity ϕ_m, with two distinct phases: C_e will denote the extracellular fluid drug concentration, and C_i will denote the internal cellular drug concentration. The model then consists of three coupled differential equations: one diffusion equation for the drug concentration in the polymer, C_p; one advection-diffusion equation for the drug concentration in the extracellular region of the media; and an equation for the drug concentration in the cells. Associated with the first two equations are their respective diffusion coefficients, D_p and D_m. The parameter D_m is interpreted

as $\phi_m \bar{D_m}$ where $\bar{D_m}$ is the interstitial diffusion coefficient.

$$\frac{\partial C_p}{\partial t} = D_p \frac{\partial^2 C_p}{\partial x^2}, \qquad x \in (0, l_p)\,, \tag{3.3.3}$$

$$\phi_m \frac{\partial C_e}{\partial t} + v\frac{\partial C_e}{\partial x} = D_m \frac{\partial^2 C_e}{\partial x^2} - \alpha_i \left(C_e - \frac{C_i}{K_i} \right), \quad x \in (l_p, l_p + l_m)\,, \tag{3.3.4}$$

$$(1 - \phi_m)\frac{\partial C_i}{\partial t} = \alpha_i \left(C_e - \frac{C_i}{K_i} \right), \qquad x \in (l_p, l_p + l_m)\,. \tag{3.3.5}$$

There is a leakage of plasma from the lumen into the arterial wall resulting in a fluid flow of magnitude v in the extracellular phase, driven by the pressure gradient across the wall. The parameter v, which is taken to be constant, will be referred to as the transmural velocity. The second equation contains a convective term to account for this. Again, v must be interpreted as $\phi_m \bar{v}$, where $\bar{v}$ is the interstitial fluid velocity. In addition, there is a sink term which describes how the drug is lost from the extracellular fluid into the cells. The parameter α_i is a drug uptake rate constant (units s^{-1}) and K_i is the dimensionless partition coefficient. The partition coefficient is the equilibrium ratio of concentrations of a compound in two different phases, here the extracellular fluid and the cells (Sangster 1997). Thus the partition coefficient is a measure of how hydrophilic ("water loving") or hydrophobic ("water fearing") the substance is. Both α_i and K_i are drug-dependent, but are assumed to be spatially independent. The third equation expresses the rate of uptake of the drug by the cells: it is initially proportional to C_e but that proportionality diminishes with increasing C_i until the carrying capacity (or partition coefficient) of the cells is reached, at which point the uptake rate becomes zero. Subsequently, drug begins to be transferred from the cells back into the extracellular space. The factor $(1 - \phi_m)$ represents the cellular fraction. It should be stressed that diffusion within cells is not considered in this analysis.

Furthermore, it is believed that the drug is not used up during the interaction with smooth muscle cells (personal communication, Roger Wadsworth), and that it is released back into the system in proportion to α_i. After a cell has uptaken and released drug, it is assumed to have the same ability to uptake/release drug, i.e. its properties do not change.

The boundary conditions are as follows:

$$-D_p \frac{\partial C_p}{\partial x} = 0, \qquad x = 0, \tag{3.3.6}$$

$$C_p = C_e, \qquad x = l_p, \tag{3.3.7}$$

$$-D_p \frac{\partial C_p}{\partial x} = -D_m \frac{\partial C_e}{\partial x} + vC_e, \qquad x = l_p, \tag{3.3.8}$$

$$-D_m \frac{\partial C_e}{\partial x} + vC_e = \beta C_e, \qquad x = l_p + l_m. \tag{3.3.9}$$

The initial conditions are given by

$$C_p(x,0) = C_0, \tag{3.3.10}$$

$$C_e(x,0) = C_i(x,0) = 0. \tag{3.3.11}$$

The first boundary condition stipulates no flux of the drug into the "wire". This is probably unrealistic as there is likely to be drug washed away by the blood flow at this boundary, and an argument could be made for choosing the boundary condition to be $C_p = 0$. However, for the purposes of the one-dimensional model, the no-flux condition is a reasonable choice, given that there is likely to be regrowth of endothelial cells and tissue around any one strut on the stent. However, the condition $C_p = 0$ as well as the more general boundary condition $-D_p\ \partial C_p/\partial x = \gamma C_p$ (γ constant) are considered in Chapter 5. The second and third conditions stipulate continuity of both the drug concentration and advective

and diffusive fluxes across the polymer/media interface. This is different from the work of Zunino (2004, 2009) and Pontrelli & de Monte (2007, 2009) (who consider a thin film coating the polymer, and a permeable membrane at the interface, respectively) in that a concentration jump across the interface is not considered here, in the interest of avoiding unnecessary complication. Since the stent only covers a fraction of the surface of the arterial wall, an argument could be made for the inclusion of an area coverage factor. In the one-dimensional averaging, this has been implicitly added to the boundary condition across the interface. The final condition states that the flux of the drug out of the media is proportional to C_e at the interface between the media and the adventitia; β is a constant of proportionality. There is no immediately obvious boundary condition to employ at the far media boundary. It was felt the conditions $C_e = 0$ and $\partial C_e/\partial x = 0$ were inappropriate since the drug is known to be transported into the adventitia region of the arterial wall. The chosen boundary condition (3.3.9) has been discussed in Beavers & Joseph (1967) (albeit in the context of fluid velocity rather than drug transport) where it is recognized that the parameter β must be determined experimentally. Furthermore, Davia *et al.* (2009) employ this type of condition.

3.3.3 Model II: polymer, media and adventitia

There are several ways in which one can attempt to improve on Model I. One such way is by including the adventitia, the outermost layer of the arterial wall, as in Figure 3.2. The advantage of this model is that the difficult-to-determine constant of proportionality, β, in the media/adventitia boundary condition can be replaced with the more natural continuity of flux condition. At the far adventitia boundary, the concentration of extracellular drug is assumed to be zero. The structure of the adventitia is similar to the media. There exists cells (fibroblast) which, although

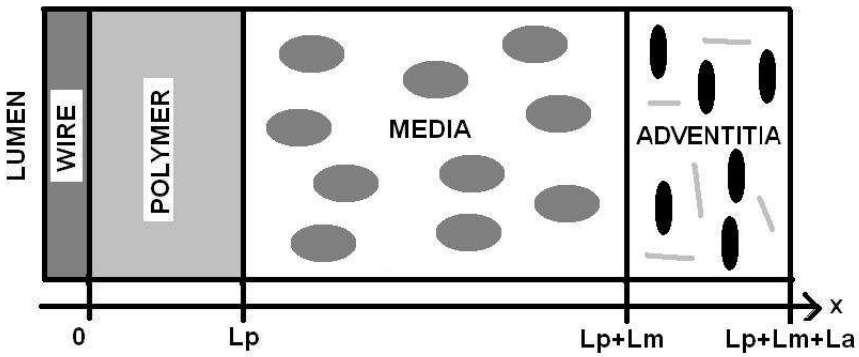

Figure 3.2: Model II: Builds upon Model I by including the adventitia region containing fibroblast cells and *vasa vasorum*, as well as a drug-filled polymer region and media region containing smooth muscle cells and extracellular space.

different in nature to the media's smooth muscle cells, can be modelled in a similar way. There may be fewer cells in the adventitia and thus the porosity may be greater than in the media. The adventitia does, however, contain *vasa vasorum* which are essentially small veins that can act as a sink and carry drug away in the bloodstream. The additional equations are essentially the same as (3.3.4) and (3.3.5) except that here, differences in adventitial porosity, diffusion coefficient, drug uptake and partition coefficient are allowed for by assigning the subscript a to these parameters. Furthermore, a sink term is included to account for the extraction (in proportion to some rate constant, α_v) of drug by the vasa vasorum, and the drug is expected to decay rapidly with distance into the adventitia as a result of this. Thus the additional equations, boundary conditions and initial

conditions are

$$\phi_a \frac{\partial C_a}{\partial t} + v\frac{\partial C_a}{\partial x} = D_a \frac{\partial^2 C_a}{\partial x^2} - \alpha_a \left(C_a - \frac{C_f}{K_a} \right) - \alpha_v C_a, \tag{3.3.12}$$

$$(1-\phi_a)\frac{\partial C_f}{\partial t} = \alpha_a \left(C_a - \frac{C_f}{K_a} \right), \quad x \in (l_p + l_m, l_p + l_m + l_a), \tag{3.3.13}$$

$$-D_m \frac{\partial C_e}{\partial x} = -D_a \frac{\partial C_a}{\partial x}, \qquad x = l_p + l_m, \tag{3.3.14}$$

$$C_e = C_a, \qquad x = l_p + l_m, \tag{3.3.15}$$

$$C_a = 0, \qquad x = l_p + l_m + l_a, \tag{3.3.16}$$

$$C_a = C_f = 0, \qquad t = 0, \tag{3.3.17}$$

where C_a and C_f denote the adventitial extracellular drug concentration and the concentration of drug in fibroblast cells, respectively. It should be stressed that equation (3.3.14) assumes that the velocity, v, is the same in the media and the adventitia, which in turn implies that porosities in each layer should be the same. Certainly, for comparable porosities, this will be a good approximation.

3.3.4 Model III: polymer, topcoat, media and adventitia

Whilst models I and II above are a reasonable first attempt at modelling the problem, there are ways in which these models can be easily adapted to account for some of the extra features seen in stents. Authors such as Venkatraman and Boey (2007) indicate that release rates can be controlled by merely coating a drug-free top layer onto the drug reservoir polymer layer. The properties of the topcoat layer can, in principle, be adjusted to alter the release characteristics. In fact, the Cypher sirolimus-eluting Coronary Stent system (Venkatraman & Boey 2007) uses this principle: a combination of polymers mixed with sirolimus makes up the base coat while a drug-free polymer is applied to the stent surface to control the

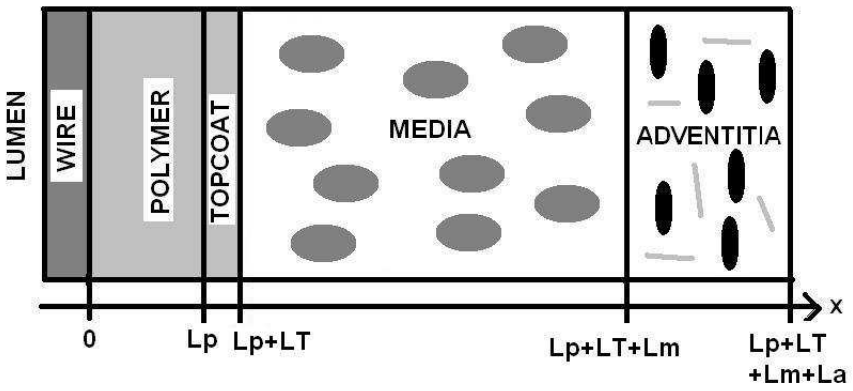

Figure 3.3: Model III: Builds upon Model II by including a drug-free topcoat polymer layer on top of the drug-filled polymer layer, as well as the media region containing smooth muscle cells and extracellular space and the adventitia region containing fibroblast cells and *vasa vasorum*.

release kinetics of the drug. It appears that for both sirolimus and paclitaxel, a slow-releasing drug-eluting stent leads to slightly more favourable angiographic outcomes than one with a more rapid release (Venkatraman & Boey 2007), and so it is interesting to examine the model to see under what circumstances the release of the drug may be increased or reduced.

Mathematically, the addition of the topcoat layer, as shown in Figure 3.3, simply requires an extra layer between the polymer and the media with the drug transport described by the diffusion equation:

$$\frac{\partial C_T}{\partial t} = D_T \frac{\partial^2 C_T}{\partial x^2}, \tag{3.3.18}$$

where the subscript T denotes topcoat. The boundary conditions at the polymer/topcoat and the topcoat/media interfaces are continuity of drug concentration and continuity of the relative fluxes of the drug. Consequently, the boundary

conditions at the polymer/topcoat interface are

$$C_p = C_T, \tag{3.3.19}$$

$$-D_p \frac{\partial C_p}{\partial x} = -D_T \frac{\partial C_T}{\partial x}, \tag{3.3.20}$$

and the boundary conditions at the topcoat/media interface are

$$C_T = C_e, \tag{3.3.21}$$

$$-D_T \frac{\partial C_T}{\partial x} = -D_m \frac{\partial C_e}{\partial x} + vC_e. \tag{3.3.22}$$

Since the topcoat is a drug-free polymer layer, the initial condition in the topcoat layer is simply

$$C_T(x, 0) = 0. \tag{3.3.23}$$

The boundary conditions at the media/adventitia interface, and the equations in the adventitia region are the same as in Model II.

3.3.5 Model IV: polymer, media, plaque and adventitia

In reality, when a stent is inserted into a diseased artery, the atherosclerotic plaque will not be removed and is likely to be smeared into the tissue. The plaque may thus play an important role in the transport of the drug across the wall, and yet does not appear to have been previously modelled. Baldwin *et al.* (1997) have indicated that the presence of plaque may increase transmural velocity by a factor of ten. This may be because patients with atherosclerosis are likely to have high blood pressure, or it could be that the addition of the stent has caused initial damage to the endothelial cells. Pulsatility may also have an effect. The effect of increasing transmural velocity with proportion of plaque will be explicitly consid-

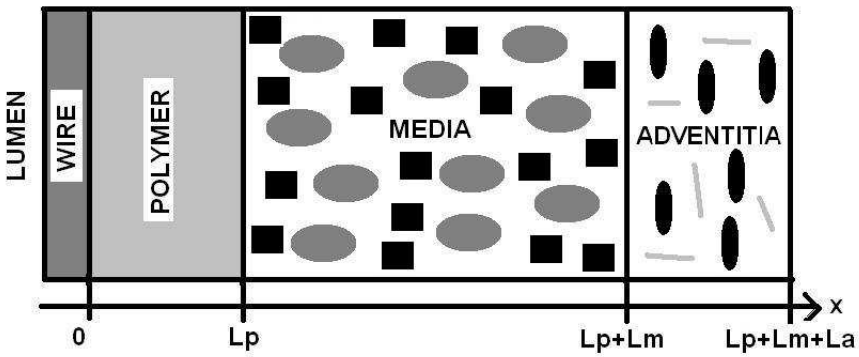

Figure 3.4: Model IV: Builds upon Model II by including a modified media region, containing plaque and smooth muscle cells as well as a drug filled polymer region and the adventitia region containing fibroblast cells and *vasa vasorum* .

ered in the sensitivity analysis, Table 5.13.

The plaque is modelled as a modified media region (see Figure 3.4) with the subscript pl indicating the quantities relating to the plaque. By varying the values of ϕ_m and ϕ_{pl}, the relative proportion of space and the relative amount of cells and plaque may be altered. Furthermore, a partition coefficient and drug uptake rate into plaque are suggested, although at the time of writing there would appear to be little data available on such quantities. The following equations are valid for $x \in (l_p, l_p + l_m)$:

$$\phi_m \frac{\partial C_e}{\partial t} + v\frac{\partial C_e}{\partial x} = D_m \frac{\partial^2 C_e}{\partial x^2} - \alpha_{pl}\left(C_e - \frac{C_{pl}}{K_{pl}}\right) - \alpha_i\left(C_e - \frac{C_i}{K_i}\right), \quad (3.3.24)$$

$$\phi_{pl}\frac{\partial C_{pl}}{\partial t} = \alpha_{pl}\left(C_e - \frac{C_{pl}}{K_{pl}}\right), \quad (3.3.25)$$

$$\phi_i \frac{\partial C_i}{\partial t} = \alpha_i\left(C_e - \frac{C_i}{K_i}\right). \quad (3.3.26)$$

$$C_{pl}(x, 0) = 0. \quad (3.3.27)$$

Note that in this case $\phi_m + \phi_i + \phi_{pl} = 1$. The polymer and adventitia equations,

as well as the boundary and initial conditions, are the same as in Model II.

3.3.6 Non-dimensionalization

The process of non-dimensionalization involves the removal of units from a system of equations by a change of variables. Non-dimensionalization is useful since it often simplifies the problem, and replaces a set of dimensional parameters with a new (usually smaller) set of parameters which are characteristic of the system. This is valuable for it allows one to ascertain which terms are significant and which may be possibly neglected. Non-dimensionalization is especially useful when numerical techniques are to be used to obtain a solution. The reason for this is that the new scaled parameters are closer to each other in size, and do not differ by many orders of magnitude, thus reducing the chance of ill-conditioning. The following non-dimensional variables are employed:

$$t^N = \frac{D_m t}{(l_p + l_m)^2}, \quad x^N = \frac{x}{l_p + l_m}, \quad C_p^N = \frac{C_p}{C_0}, \quad C_e^N = \frac{C_e}{C_0}, \quad C_i^N = \frac{C_i}{C_0},$$

where C_0 is the initial concentration in the polymer. Thus the equations in model I reduce to

$$\frac{\partial C_p}{\partial t} = D\frac{\partial^2 C_p}{\partial x^2}, \qquad x \in (0, L), \tag{3.3.28}$$

$$\phi_m \frac{\partial C_e}{\partial t} + v^\star \frac{\partial C_e}{\partial x} = \frac{\partial^2 C_e}{\partial x^2} - \alpha_i^\star \left(C_e - \frac{C_i}{K_i} \right), \quad x \in (L, 1), \tag{3.3.29}$$

$$(1 - \phi_m)\frac{\partial C_i}{\partial t} = \alpha_i^\star \left(C_e - \frac{C_i}{K_i} \right), \qquad x \in (L, 1), \tag{3.3.30}$$

subject to

$$
\begin{aligned}
-\frac{\partial C_p}{\partial x} &= 0, & x = 0, \quad & (3.3.31)\\
C_p &= C_e, & x = L, \quad & (3.3.32)\\
D\frac{\partial C_p}{\partial x} &= \frac{\partial C_e}{\partial x} - v^\star C_e, & x = L, \quad & (3.3.33)\\
\frac{\partial C_e}{\partial x} &= \lambda C_e, & x = 1, \quad & (3.3.34)\\
C_p &= 1, & t = 0, \quad & (3.3.35)\\
C_e = C_i &= 0, & t = 0, \quad & (3.3.36)
\end{aligned}
$$

where

$$D = \frac{D_p}{D_m}, \quad v^\star = \frac{v\,(l_p + l_m)}{D_m}, \quad \alpha_i^\star = \frac{\alpha_i\,(l_p + l_m)^2}{D_m}, \quad \lambda = \frac{(v - \beta)\,(l_p + l_m)}{D_m},$$

with

$$L = \frac{l_p}{l_p + l_m},$$

and the superscript N has been omitted for convenience. Note also that the non-dimensional parameter $v^\star$ is the Peclet number of the system. The same non-dimensionalization is applied to models II-IV, giving rise to the following additional non-dimensional parameters:

$$D_{am} = \frac{D_a}{D_m}, \quad D_{pT} = \frac{D_p}{D_T}, \quad D_{Tm} = \frac{D_T}{D_m}, \quad \alpha_a^\star = \frac{\alpha_a\,(l_p + l_m)^2}{D_m},$$

$$\alpha_v^\star = \frac{\alpha_v\,(l_p + l_m)^2}{D_m}, \quad \alpha_{pl}^\star = \frac{\alpha_{pl}\,(l_p + l_m)^2}{D_m}.$$

Chapter 4

Analytic Methods

There is both beauty and elegance in analytic solutions. Whilst they are not always achievable, analytic solutions are usually the aim at the outset. The attraction of these solutions lies not only in their very existence, but also in the fact that they can provide a 'full picture' of how the dependent variables depend upon the independent variables and any parameters. Thus one can readily see how the solution behaves in small and large limits. Numerical solutions, on the other hand, need to be computed for each new set of parameters. In general, the more complicated the problem is, the less chance there is of obtaining an analytic solution.

4.1 Method of solution: The Laplace transformation

The method of solution chosen to solve the resulting partial differential equations that arise in these diffusion-based problems is the application of Laplace transforms. The Laplace transform of a function $f(t)$, defined for all positive values of

t, is given by

$$L[f(t)] = \bar{f}(s) = \int_0^\infty \exp\{-st\}\ f(t)\ dt. \tag{4.1.1}$$

The models described in the previous chapter are all linear and so, in principle at least, it should be possible to solve them using Laplace transforms. However, as will become evident, for even the simplest model, model I, this is far from trivial. The difficulty lies not in obtaining the solution in Laplace transform space, but in inverting the solution to return to functions of space and time. For simple functions, Laplace transforms and their corresponding inverses appear in tables in the literature (e.g. Carslaw & Jaeger 1986, Gradshteyn & Ryzhik 2007). Formally, the inverse Laplace transform can be found using the complex inversion formula contained in the following theorem.

Theorem 1 *The Complex Inversion Formula. If* $\bar{f}(s) = L[f(t)]$, *then* $L^{-1}\left[\bar{f}(s)\right]$ *is given by*

$$f(t) = \frac{1}{2\pi \mathrm{i}} \int_{\beta-\mathrm{i}\infty}^{\beta+\mathrm{i}\infty} \exp\{st\}\ \bar{f}(s)\ ds, \quad t > 0 \tag{4.1.2}$$

and $f(t) = 0$ *for* $t < 0$.

The real number β *is to be chosen such that* $s = \beta$ *lies to the right of all the singularities of the integrand, but is otherwise arbitrary.*

In practice, the integral (4.1.2) is evaluated using contour integration, and in particular the Bromwich contour, C, displayed in Figure 4.1. The integral (4.1.2) is evaluated by considering the integral around the closed contour C and subtracting the integral around the curved part of the contour ($BJKLA$), namely Ω:

$$\begin{aligned} f(t) &= \lim_{R\to\infty} \frac{1}{2\pi \mathrm{i}} \int_{\beta-\mathrm{iT}}^{\beta+\mathrm{iT}} \exp\{st\}\ \bar{f}(s)\ ds \\ &= \left\{ \frac{1}{2\pi \mathrm{i}} \oint_C \exp\{st\}\ \bar{f}(s)\ ds - \frac{1}{2\pi \mathrm{i}} \int_\Omega \exp\{st\}\ \bar{f}(s)\ ds \right\}, \end{aligned} \tag{4.1.3}$$

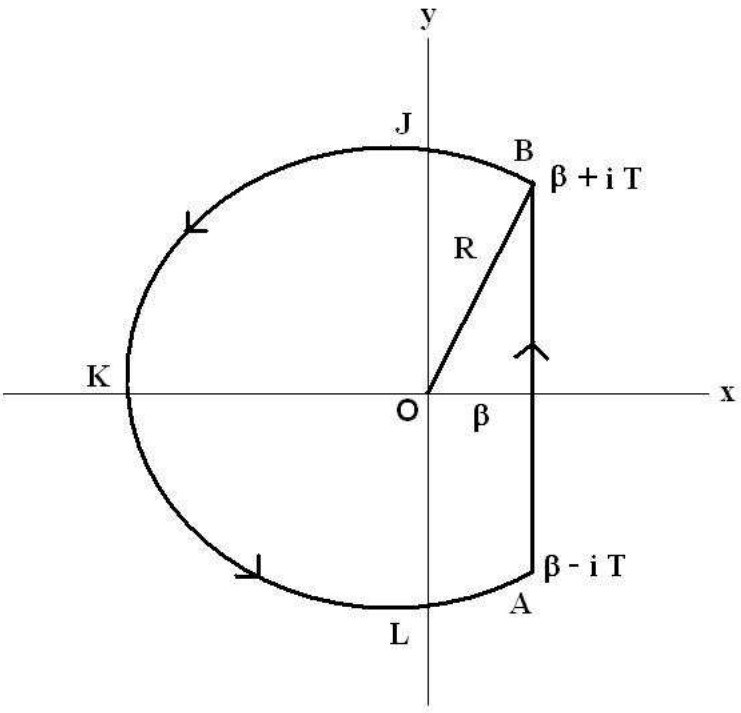

Figure 4.1: The Bromwich Contour, C

since as $R \to \infty$, $T \to \infty$. Use can then be made of Cauchy's Theorem, as outlined in the following theorem.

Theorem 2 *Cauchy's Theorem. If $g(s)$ is analytic in some region bounded by the closed curve C then*

$$\oint_C g(s)\, ds = 0$$

for $s \, \varepsilon \, C$.

A sufficient condition for the integral around Ω to approach zero as $R \to \infty$ is contained in the following Theorem.

Theorem 3 *If there exists constants, $M > 0$, $k > 0$ such that on Ω (where $s = Re^{i\theta}$),*

$$|\bar{f}(s)| < \frac{M}{R^k}, \tag{4.1.4}$$

then the integral around Ω *of* $\exp\{st\}\ \bar{f}(s)$ *approaches zero as* $R \to \infty$*, i.e.*

$$\lim_{R\to\infty} \int_{\Omega} \exp\{st\}\ \bar{f}(s)\ ds = 0. \tag{4.1.5}$$

When the only singularities of $\bar{f}(s)$ are poles, the inversion process can be significantly simplified by using the Residue Theorem:

Theorem 4 *The Residue Theorem. Suppose that the only singularities of* $\bar{f}(s)$ *are poles, all of which lie to the left of the line* $s = \beta$*. Suppose further that the integral around* Ω *approaches zero as* $R \to \infty$*. Then, by the Residue Theorem,*

$$f(t) = 2\pi\mathrm{i} \sum \text{residues of } \big(\exp\{st\}\ \bar{f}(s)\big) \text{ at the poles of } \bar{f}(s). \tag{4.1.6}$$

Extensive use will be made of these theorems in the remainder of the chapter, as well as throughout this thesis.

4.2 Diffusion in composite media

The models described in the previous chapter involve a level of complexity which suggests that analytic solutions will not easily be obtainable. In this case, it is usual to consider a series of simpler problems, adding an extra level of complexity from one to the other. Here, purely diffusion in composite regions of infinite and finite length, with differing boundary conditions is considered.

4.2.1 Diffusion in infinite composite media

Consider firstly the diffusion of a drug between infinite composite media having diffusion coefficients D_p and D_m, respectively. The drug concentration in the first region, occupying the whole of the negative axis, is denoted by C_p. It should be

stressed that the second region, occupying the whole of the positive axis, is not treated as a porous medium here: there is only one concentration phase, denoted by C_e. The equations describing the diffusion of a drug between the two media are the following:

$$\frac{\partial C_p}{\partial t} = D_p \frac{\partial^2 C_p}{\partial x^2}, \quad x \in (-\infty, 0), \tag{4.2.7}$$

$$\frac{\partial C_e}{\partial t} = D_m \frac{\partial^2 C_e}{\partial x^2}, \quad x \in (0, \infty), \tag{4.2.8}$$

subject to

$$C_p = C_e, \quad x = 0, \tag{4.2.9}$$

$$-D_p \frac{\partial C_p}{\partial x} = -D_m \frac{\partial C_e}{\partial x}, \quad x = 0, \tag{4.2.10}$$

$$C_p(x, 0) = C_0, \tag{4.2.11}$$

$$C_e(x, 0) = 0. \tag{4.2.12}$$

Furthermore, it is assumed that both $C_p(x, t)$ and $C_e(x, t)$ remain bounded $\forall\, x, t$. Taking Laplace transforms of (4.2.7) provides

$$s\bar{C}_p(x, s) - C_p(x, 0) = D_p \frac{d^2 \bar{C}_p}{dx^2}(x, s). \tag{4.2.13}$$

Rearranging (4.2.13) and making use of the initial condition in the polymer region (4.2.11) gives rise to

$$\frac{d^2 \bar{C}_p}{dx^2}(x, s) - \frac{s}{D_p}\bar{C}_p(x, s) = -\frac{C_0}{D_p}. \tag{4.2.14}$$

Solving (4.2.14) results in

$$\bar{C_p}(x,s) = A(s)\exp\left\{-\sqrt{\frac{s}{D_p}}x\right\} + B(s)\exp\left\{\sqrt{\frac{s}{D_p}}x\right\} + \frac{C_0}{s}, \quad x < 0, \quad (4.2.15)$$

where C_0/s is the particular integral.

Since the solution satisfies the boundedness condition, it is necessary to set $A(s) = 0$, so that (4.2.15) reduces to

$$\bar{C_p}(x,s) = B(s)\exp\left\{\sqrt{\frac{s}{D_p}}x\right\} + \frac{C_0}{s}, \quad x < 0. \quad (4.2.16)$$

It is then straightforward to write down the Laplace transform of the media diffusion equation (4.2.8), subject to the initial (4.2.12) and boundedness conditions:

$$\bar{C_e}(x,s) = C(s)\exp\left\{-\sqrt{\frac{s}{D_m}}x\right\}, \quad x > 0. \quad (4.2.17)$$

Taking the Laplace transform of boundary conditions (4.2.9-4.2.10), and applying to expressions (4.2.16-4.2.17), implies, respectively,

$$B(s) = C(s) - \frac{C_0}{s}, \quad (4.2.18)$$

$$B(s) = -\sqrt{\frac{D_m}{D_p}}C(s). \quad (4.2.19)$$

Equating (4.2.18) with (4.2.19) and rearranging gives

$$C(s) = \frac{C_0\sqrt{D_p}}{s\left(\sqrt{D_p} + \sqrt{D_m}\right)}. \quad (4.2.20)$$

Returning to (4.2.18), and making use of (4.2.20), $B(s)$ is then given as

$$B(s) = -\frac{C_0\sqrt{D_m}}{s\left(\sqrt{D_p}+\sqrt{D_m}\right)}. \tag{4.2.21}$$

Thus, substituting (4.2.21) into (4.2.16) and (4.2.20) into (4.2.17) provides the solution, in Laplace transform space, for the drug concentration in the polymer and media regions:

$$\bar{C}_p(x,s) = \frac{C_0}{s}\left(1-\frac{\sqrt{D_m}\exp\left\{\sqrt{\frac{s}{D_p}}x\right\}}{\sqrt{D_p}+\sqrt{D_m}}\right), \quad x<0, \tag{4.2.22}$$

$$\bar{C}_e(x,s) = \frac{C_0\sqrt{D_p}\exp\left\{-\sqrt{\frac{s}{D_m}}x\right\}}{s\left(\sqrt{D_p}+\sqrt{D_m}\right)}, \quad x>0. \tag{4.2.23}$$

It is straightforward to invert (4.2.23) since it is well established (e.g. Carslaw & Jaeger 1986, Crank 1956) that

$$L^{-1}\left[\frac{\exp\left\{-\sqrt{\frac{s}{k}}x\right\}}{s}\right] = \operatorname{erfc}\left(\frac{x}{2\sqrt{kt}}\right),$$

where the complementary error function is defined in terms of the error function as

$$\begin{aligned}\operatorname{erfc}(x) &= 1-\operatorname{erf}(x)\\ &= 1-\frac{2}{\sqrt{\pi}}\int_0^x \exp\left\{-\xi^2\right\}d\xi\\ &= \frac{2}{\sqrt{\pi}}\int_x^\infty \exp\left\{-\xi^2\right\}d\xi.\end{aligned} \tag{4.2.24}$$

The solution for $C_e(x,t)$ is thus

$$C_e(x,t) = \frac{C_0\sqrt{D_p}}{\sqrt{D_p}+\sqrt{D_m}}\,\mathrm{erfc}\left(\frac{x}{2\sqrt{D_m t}}\right). \tag{4.2.25}$$

Now, the inverse Laplace transform of (4.2.22) is given by

$$\begin{aligned} C_p(x,t) &= L^{-1}\left[\frac{C_0}{s}\left(1-\frac{\sqrt{D_m}\exp\left\{\sqrt{\frac{s}{D_p}}x\right\}}{\sqrt{D_p}+\sqrt{D_m}}\right)\right] \\ &= C_0 - \frac{C_0\sqrt{D_m}}{\sqrt{D_p}+\sqrt{D_m}}L^{-1}\left[\frac{\exp\left\{\sqrt{\frac{s}{D_p}}x\right\}}{s}\right] \end{aligned} \tag{4.2.26}$$

Making the change of variable, $x=-x'$,

$$\begin{aligned} L^{-1}\left[\frac{\exp\left\{\sqrt{\frac{s}{D_p}}x\right\}}{s}\right] &= L^{-1}\left[\frac{\exp\left\{-\sqrt{\frac{s}{D_p}}x'\right\}}{s}\right] \\ &= \mathrm{erfc}\left(\frac{x'}{2\sqrt{D_p t}}\right) \\ &= 1-\frac{2}{\sqrt{\pi}}\int_0^{\frac{x'}{2\sqrt{D_p t}}}\exp\left\{-\xi^2\right\}d\xi \\ &= 1-\frac{2}{\sqrt{\pi}}\int_0^{\frac{-x}{2\sqrt{D_p t}}}\exp\left\{-\xi^2\right\}d\xi, \quad x<0. \end{aligned} \tag{4.2.27}$$

Making a further change of variable, $\xi' = -\xi$, it is evident that

$$\begin{aligned} 1 - \frac{2}{\sqrt{\pi}} \int_0^{\frac{-x}{2\sqrt{D_p t}}} \exp\left\{-\xi^2\right\} d\xi &= 1 - \frac{2}{\sqrt{\pi}} \int_0^{\frac{x}{2\sqrt{D_p t}}} \exp\left\{-\xi'^2\right\} (-d\xi') \\ &= 1 + \frac{2}{\sqrt{\pi}} \int_0^{\frac{x}{2\sqrt{D_p t}}} \exp\left\{-\xi'^2\right\} d\xi' \\ &= 1 + \operatorname{erf}\left(\frac{x}{2\sqrt{D_p t}}\right). \end{aligned} \tag{4.2.28}$$

Thus, making use of (4.2.26 -4.2.28), the solution for $C_p(x,t)$ is

$$C_p(x,t) = C_0 - \frac{C_0\sqrt{D_m}}{\sqrt{D_p} + \sqrt{D_m}} \left[1 + \operatorname{erf}\left(\frac{x}{2\sqrt{D_p t}}\right)\right]. \tag{4.2.29}$$

4.2.2 Diffusion in semi-infinite regions

Clearly, the polymer and media are not of infinite thickness. In reality, $l_m >> l_p$, and so the case of a polymer of finite thickness and media of infinite thickness is an appropriate case to consider. Equations (4.2.8-4.2.12) are still valid; however, equation (4.2.7) now becomes

$$\frac{\partial C_p}{\partial t} = D_p \frac{\partial^2 C_p}{\partial x^2}, \quad x \in (-l_p, 0) \tag{4.2.30}$$

and the more realistic zero-flux boundary condition is supposed at $x = -l_p$:

$$-D_p \frac{\partial C_p}{\partial x} = 0, \quad x = -l_p. \tag{4.2.31}$$

In this case, the hyperbolic form of the solution for $\bar{C_p}$ is chosen when solving the resulting second order ordinary differential equation in Laplace transform space:

$$\bar{C_p}(x,s) = A(s)\cosh\left(\sqrt{\frac{s}{D_p}}x\right) + B(s)\sinh\left(\sqrt{\frac{s}{D_p}}x\right) + \frac{C_0}{s}. \tag{4.2.32}$$

Application of the boundary condition at $x = -l_p$, (4.2.31), gives rise to

$$B(s) = \frac{A(s)\sinh\left(\sqrt{\frac{s}{D_p}}l_p\right)}{\cosh\left(\sqrt{\frac{s}{D_p}}l_p\right)}. \tag{4.2.33}$$

With no changes to the media equations, $\bar{C}_e$ is still given by (4.2.17), and the continuity of concentration condition across the interface results in

$$A(s) = C(s) - \frac{C_0}{s}. \tag{4.2.34}$$

Now, the continuity of flux condition (4.2.10) implies

$$B(s) = -\sqrt{\frac{D_m}{D_p}}C(s), \tag{4.2.35}$$

or, after substituting the expression for $B(s)$ from (4.2.33) into (4.2.35), and rearranging, supplies an expression for $A(s)$ in terms of $C(s)$

$$A(s) = -\sqrt{\frac{D_m}{D_p}}C(s)\frac{\cosh\left(\sqrt{\frac{s}{D_p}}l_p\right)}{\sinh\left(\sqrt{\frac{s}{D_p}}l_p\right)}. \tag{4.2.36}$$

An expression for $C(s)$ can be obtained by equating (4.2.34) with (4.2.36) and rearranging:

$$C(s) = \frac{C_0\sqrt{D_p}\sinh\left(\sqrt{\frac{s}{D_p}}l_p\right)}{s\left(\sqrt{D_p}\sinh\left(\sqrt{\frac{s}{D_p}}l_p\right) + \sqrt{D_m}\cosh\left(\sqrt{\frac{s}{D_p}}l_p\right)\right)}. \tag{4.2.37}$$

Substitution of (4.2.37) into (4.2.36) and (4.2.35) gives expressions for $A(s)$ and $B(s)$ immediately

$$A(s) = -\frac{C_0\sqrt{D_m}\cosh\left(\sqrt{\frac{s}{D_p}}l_p\right)}{s\left(\sqrt{D_p}\sinh\left(\sqrt{\frac{s}{D_p}}l_p\right)+\sqrt{D_m}\cosh\left(\sqrt{\frac{s}{D_p}}l_p\right)\right)}, \quad (4.2.38)$$

$$B(s) = -\frac{C_0\sqrt{D_m}\sinh\left(\sqrt{\frac{s}{D_p}}l_p\right)}{s\left(\sqrt{D_p}\sinh\left(\sqrt{\frac{s}{D_p}}l_p\right)+\sqrt{D_m}\cosh\left(\sqrt{\frac{s}{D_p}}l_p\right)\right)}. \quad (4.2.39)$$

Finally, the substitution of equations (4.2.37-4.2.39) into (4.2.17) and (4.2.32) provides the solution in Laplace transform space:

$$\bar{C}_p(x,s) = \frac{C_0}{s}\left[1-\frac{\sqrt{D_m}\cosh\left(\sqrt{\frac{s}{D_p}}(x-l_p)\right)}{\sqrt{D_p}\sinh\left(\sqrt{\frac{s}{D_p}}l_p\right)+\sqrt{D_m}\cosh\left(\sqrt{\frac{s}{D_p}}l_p\right)}\right], \quad (4.2.40)$$

$$\bar{C}_e(x,s) = \frac{C_0\sqrt{D_p}\sinh\left(\sqrt{\frac{s}{D_p}}l_p\right)\exp\left\{-\sqrt{\frac{s}{D_m}}x\right\}}{s\left(\sqrt{D_p}\sinh\left(\sqrt{\frac{s}{D_p}}l_p\right)+\sqrt{D_m}\cosh\left(\sqrt{\frac{s}{D_p}}l_p\right)\right)}. \quad (4.2.41)$$

To invert (4.2.40-4.2.41), the Residue Theorem (Theorem 4) is employed. The application of the Residue Theorem is demonstrated in detail in the following section.

4.2.3 Diffusion in composite finite regions

The next level of sophistication is to consider the media region also to be of finite thickness, say l_m. In this case a change is made to the geometry for simplicity; the composite media are now both along the positive x axis. Again, the polymer

region, of thickness l_p, is initially filled with drug of concentration C_0. Zero-flux conditions are now imposed at both ends, and continuity of drug concentration as well as continuity of the relative fluxes are imposed across the boundary between the polymer and the media. The equations are then:

$$\frac{\partial C_p}{\partial t} = D_p \frac{\partial^2 C_p}{\partial x^2}, \quad x \in (0, l_p), \tag{4.2.42}$$

$$\frac{\partial C_e}{\partial t} = D_m \frac{\partial^2 C_e}{\partial x^2}, \quad x \in (l_p, l_p + l_m), \tag{4.2.43}$$

subject to

$$-D_p \frac{\partial C_p}{\partial x} = 0, \quad x = 0, \tag{4.2.44}$$

$$C_p = C_e, \quad x = l_p, \tag{4.2.45}$$

$$-D_p \frac{\partial C_p}{\partial x} = -D_m \frac{\partial C_e}{\partial x}, \quad x = l_p, \tag{4.2.46}$$

$$-D_m \frac{\partial C_e}{\partial x} = 0, \quad x = l_p + l_m, \tag{4.2.47}$$

$$C_p(x, 0) = C_0, \tag{4.2.48}$$

$$C_e(x, 0) = 0. \tag{4.2.49}$$

It should be stressed that these equations are exactly the equations of Model I, in the limit $v, \alpha, \beta \to 0$, $\phi \to 1$. So that the solution to both problems can be compared, equations (4.2.42-4.2.49) are non-dimensionalized as before using the same non-dimensionalization as in §3.36. Equations (4.2.42-4.2.49) then become, after dropping the superscript N for convenience,

$$\frac{\partial C_p}{\partial t} = D \frac{\partial^2 C_p}{\partial x^2}, \quad x \in (0, L), \tag{4.2.50}$$

$$\frac{\partial C_e}{\partial t} = \frac{\partial^2 C_e}{\partial x^2}, \quad x \in (L, 1), \tag{4.2.51}$$

subject to

$$-\frac{\partial C_p}{\partial x} = 0, \quad x = 0, \tag{4.2.52}$$

$$C_p = C_e, \quad x = L, \tag{4.2.53}$$

$$D\frac{\partial C_p}{\partial x} = \frac{\partial C_e}{\partial x}, \quad x = L, \tag{4.2.54}$$

$$-\frac{\partial C_e}{\partial x} = 0, \quad x = 1, \tag{4.2.55}$$

$$C_p(x,0) = 1, \tag{4.2.56}$$

$$C_e(x,0) = 0, \tag{4.2.57}$$

where D and L are the same non-dimensional parameters given in §3.36. In line with the case of semi-infinite composite regions the hyperbolic form is chosen for C_p, but also now for C_e:

$$\bar{C_p}(x,s) = A(s)\cosh\left(\sqrt{\frac{s}{D}}x\right) + B(s)\sinh\left(\sqrt{\frac{s}{D}}x\right) + \frac{1}{s}, \tag{4.2.58}$$

$$\bar{C_e}(x,s) = C(s)\cosh\left(\sqrt{s}x\right) + D(s)\sinh\left(\sqrt{s}x\right). \tag{4.2.59}$$

Application of the boundary condition at $x = 0$ gives rise to

$$B(s) = 0, \tag{4.2.60}$$

so that (4.2.58) reduces to

$$\bar{C_p}(x,s) = A(s)\cosh\left(\sqrt{\frac{s}{D}}x\right) + \frac{1}{s}. \tag{4.2.61}$$

The interface conditions (4.2.53-4.2.54) then imply

$$A(s) = \frac{C(s)\cosh\left(\sqrt{s}L\right) + D(s)\sinh\left(\sqrt{s}L\right) - 1/s}{\cosh\left(\sqrt{\frac{s}{D}}L\right)}, \tag{4.2.62}$$

$$A(s) = \frac{C(s)\sinh\left(\sqrt{s}L\right) + D(s)\cosh\left(\sqrt{s}L\right)}{\sqrt{D}\sinh\left(\sqrt{\frac{s}{D}}L\right)}. \tag{4.2.63}$$

Finally, employing condition (4.2.55) gives an expression for $C(s)$ in terms of $D(s)$:

$$C(s) = -\frac{D(s)\cosh\left(\sqrt{s}\right)}{\sinh\left(\sqrt{s}\right)}. \tag{4.2.64}$$

Eliminating $C(s)$ between equations (4.2.63-4.2.64) results in the following expression for $A(s)$ in terms of $D(s)$:

$$\begin{aligned} A(s) &= \frac{D(s)\left[\cosh\left(\sqrt{s}L\right)\sinh\left(\sqrt{s}\right) - \cosh\left(\sqrt{s}\right)\sinh\left(\sqrt{s}L\right)\right]}{\sqrt{D}\sinh\left(\sqrt{\frac{s}{D}}L\right)\sinh\left(\sqrt{s}\right)} \\ &= \frac{D(s)\sinh\left(\sqrt{s}\left(1-L\right)\right)}{\sqrt{D}\sinh\left(\sqrt{\frac{s}{D}}L\right)\sinh\left(\sqrt{s}\right)}. \end{aligned} \tag{4.2.65}$$

Similarly, eliminating $C(s)$ between equations (4.2.62) and (4.2.64) results in the following expression for $A(s)$ in terms of $D(s)$:

$$A(s) = -\frac{sD(s)\cosh\left(\sqrt{s}\left(1-L\right)\right) + \sinh\left(\sqrt{s}\right)}{s\cosh\left(\sqrt{\frac{s}{D}}L\right)\sinh\left(\sqrt{s}\right)}. \tag{4.2.66}$$

Now, equating (4.2.65) with (4.2.66) provides $D(s)$:

$$D(s) = -\frac{\sqrt{D}\sinh\left(\sqrt{s}\right)\sinh\left(\sqrt{\frac{s}{D}}L\right)}{s\left[\sinh\left(\sqrt{s}\left(1-L\right)\right)\cosh\left(\sqrt{\frac{s}{D}}L\right) + \sqrt{D}\cosh\left(\sqrt{s}\left(1-L\right)\right)\sinh\left(\sqrt{\frac{s}{D}}L\right)\right]}. \tag{4.2.67}$$

Returning to (4.2.64), it is clear that the substitution of $D(s)$ from (4.2.67) immediately provides an expression for $C(s)$:

$$C(s) = \frac{\sqrt{D}\sinh\left(\sqrt{\frac{s}{D}}L\right)\cosh\left(\sqrt{s}\right)}{s\left[\sinh\left(\sqrt{s}\left(1-L\right)\right)\cosh\left(\sqrt{\frac{s}{D}}L\right)+\sqrt{D}\cosh\left(\sqrt{s}\left(1-L\right)\right)\sinh\left(\sqrt{\frac{s}{D}}L\right)\right]}. \tag{4.2.68}$$

Finally, $A(s)$ is determined by substituting (4.2.67) into (4.2.65) to obtain

$$A(s) = -\frac{\sinh\left(\sqrt{s}\left(1-L\right)\right)}{s\left[\sinh\left(\sqrt{s}\left(1-L\right)\right)\cosh\left(\sqrt{\frac{s}{D}}L\right)+\sqrt{D}\cosh\left(\sqrt{s}\left(1-L\right)\right)\sinh\left(\sqrt{\frac{s}{D}}L\right)\right]}. \tag{4.2.69}$$

Now that the 'constants' $A(s)$, $C(s)$ and $D(s)$ have been determined, expressions, in Laplace transform space, for the concentration of the drug in the polymer and the media regions are easily obtained by substitution of (4.2.69) into (4.2.61), and (4.2.67-4.2.68) into (4.2.59):

$$\bar{C}_p(x,s) = \frac{\left[\begin{array}{c}\sqrt{D}\sinh\left(\sqrt{\frac{s}{D}}L\right)\cosh\left(\sqrt{s}\left(1-L\right)\right)\\ +\sinh\left(\sqrt{s}\left(1-L\right)\right)\left\{\cosh\left(\sqrt{\frac{s}{D}}L\right)-\cosh\left(\sqrt{\frac{s}{D}}x\right)\right\}\end{array}\right]}{s\left[\begin{array}{c}\sinh\left(\sqrt{s}\left(1-L\right)\right)\cosh\left(\sqrt{\frac{s}{D}}L\right)\\ +\sqrt{D}\sinh\left(\sqrt{\frac{s}{D}}L\right)\cosh\left(\sqrt{s}\left(1-L\right)\right)\end{array}\right]}, \tag{4.2.70}$$

$$\bar{C}_e(x,s) = \frac{\sqrt{D}\sinh\left(\sqrt{\frac{s}{D}}L\right)\cosh\left(\sqrt{s}\left(1-x\right)\right)}{s\left[\begin{array}{c}\sinh\left(\sqrt{s}\left(1-L\right)\right)\cosh\left(\sqrt{\frac{s}{D}}L\right)\\ +\sqrt{D}\sinh\left(\sqrt{\frac{s}{D}}L\right)\cosh\left(\sqrt{s}\left(1-L\right)\right)\end{array}\right]}. \tag{4.2.71}$$

The expressions (4.2.70-4.2.71) may be inverted using the Complex Inversion Theorem (Theorem 1). Consider firstly $\left(\bar{C}_e(x,s)\ \exp\{st\}\right)$ (see equation 4.2.71):

$$\bar{C}_e(x,s)\ \exp\{st\} = \frac{\sqrt{D}\sinh\left(\sqrt{\frac{s}{D}}L\right)\cosh\left(\sqrt{s}\,(1-x)\right)\exp\{st\}}{s\left[\begin{array}{c}\sinh\left(\sqrt{s}\,(1-L)\right)\cosh\left(\sqrt{\frac{s}{D}}L\right)\\ +\sqrt{D}\sinh\left(\sqrt{\frac{s}{D}}L\right)\cosh\left(\sqrt{s}\,(1-L)\right)\end{array}\right]}. \tag{4.2.72}$$

Clearly there is a simple pole at $s=0$. The other poles are found by solving:

$$\sinh\left(\sqrt{s}\,(1-L)\right)\cosh\left(\sqrt{\frac{s}{D}}L\right)+\sqrt{D}\sinh\left(\sqrt{\frac{s}{D}}L\right)\cosh\left(\sqrt{s}\,(1-L)\right)=0. \tag{4.2.73}$$

Letting $s=-D\eta^2$, these poles are located at $s_n=-D\eta_n^2$, $n=1,2,3...$, where η_n are the roots of the following transcendental equation:

$$\sqrt{D}\cos\left(\sqrt{D}\eta(1-L)\right)\sin(\eta L)+\sin\left(\sqrt{D}\eta(1-L)\right)\cos(\eta L)=0. \tag{4.2.74}$$

The roots of equations of the form (4.2.74) are real and simple (see, for example, Carslaw & Jaeger 1986, page 324). A method for solving equations such as (4.2.74) is provided in the following section.

Now, the residue at the simple pole $s = 0$ is

$$
\begin{aligned}
&\operatorname{Res}(s=0)\left\{C_e(x,s)e^{st}\right\} \\
&= \lim_{s\to 0}\left\{\frac{\sqrt{D}\sinh\left(\sqrt{\frac{s}{D}}L\right)\cosh\left(\sqrt{s}\,(1-x)\right)e^{st}}{\left(\begin{array}{c}\sinh\left(\sqrt{s}\,(1-L)\right)\cosh\left(\sqrt{\frac{s}{D}}L\right)\\ +\sqrt{D}\sinh\left(\sqrt{\frac{s}{D}}L\right)\cosh\left(\sqrt{s}\,(1-L)\right)\end{array}\right)}\right\} \\
&= \lim_{s\to 0}\left\{\sqrt{D}e^{st}\right\} \\
&\times \lim_{s\to 0}\left\{\frac{\left(\begin{array}{c}\frac{L}{\sqrt{D}}\cosh\left(\sqrt{s}(1-x)\right)\cosh\left(\sqrt{\frac{s}{D}}L\right)\\ +(1-x)\sinh\left(\sqrt{s}(1-x)\right)\sinh\left(\sqrt{\frac{s}{D}}L\right)\end{array}\right)}{\left(\begin{array}{c}\cosh\left(\sqrt{s}(1-L)\right)\cosh\left(\sqrt{\frac{s}{D}}L\right)\\ +\left(\sqrt{D}\,(1-L)+\frac{L}{\sqrt{D}}\right)\sinh\left(\sqrt{s}(1-L)\right)\sinh\left(\sqrt{\frac{s}{D}}L\right)\end{array}\right)}\right\} \\
&= L,
\end{aligned}
\tag{4.2.75}
$$

making use of L'Hôpital's rule. The residue at s_n is given by the following:

$$
\begin{aligned}
&\mathrm{Res}(s = s_n)\left\{C_e(x,s)e^{st}\right\} \\
&= \lim_{s\to s_n}\left\{\frac{(s-s_n)\sqrt{D}\sinh\left(\sqrt{\frac{s}{D}}L\right)\cosh\left(\sqrt{s}\,(1-x)\right)e^{st}}{s\begin{pmatrix}\sinh\left(\sqrt{s}\,(1-L)\right)\cosh\left(\sqrt{\frac{s}{D}}L\right)\\ +\sqrt{D}\sinh\left(\sqrt{\frac{s}{D}}L\right)\cosh\left(\sqrt{s}\,(1-L)\right)\end{pmatrix}}\right\} \\
&= \lim_{s\to s_n}\left\{\frac{\sqrt{D}\sinh\left(\sqrt{\frac{s}{D}}L\right)\cosh\left(\sqrt{s}\,(1-x)\right)e^{st}}{s}\right\} \\
&\times \lim_{s\to s_n}\left\{\frac{s-s_n}{\begin{pmatrix}\sinh\left(\sqrt{s}\,(1-L)\right)\cosh\left(\sqrt{\frac{s}{D}}L\right)\\ +\sqrt{D}\sinh\left(\sqrt{\frac{s}{D}}L\right)\cosh\left(\sqrt{s}\,(1-L)\right)\end{pmatrix}}\right\} \\
&= \frac{2\cos\left(\sqrt{D}\eta_n(1-x)\right)\sin\left(\eta_n L\right)e^{-D\eta_n^2 t}}{\eta_n\begin{bmatrix}\cos\left(\sqrt{D}\eta_n(1-L)\right)\cos\left(\eta_n L\right)\\ -\left(\sqrt{D}\,(1-L)+\frac{L}{\sqrt{D}}\right)\sin\left(\sqrt{D}\eta_n(1-L)\right)\sin\left(\eta_n L\right)\end{bmatrix}},
\end{aligned}
\tag{4.2.76}
$$

again using L'Hôpital's rule. In a similar manner, the residues at the poles of $\bar{C}_p(x,s)\ \exp\{st\}$ are found to be

$$\mathrm{Res}(s=0)\left\{C_p(x,s)e^{st}\right\} = L, \tag{4.2.77}$$

$$\begin{aligned}&\mathrm{Res}(s=s_n)\left\{C_p(x,s)e^{st}\right\}\\ &= \frac{2}{\sqrt{D}}\frac{\begin{bmatrix}\sqrt{D}\sin(\eta_n L)\cos\left(\sqrt{D}\eta_n(1-L)\right)\\ +\sin\left(\sqrt{D}\eta_n(1-L)\right)\{\cos(\eta_n L)-\cos(\eta_n x)\}\end{bmatrix}e^{-D\eta_n^2 t}}{\eta_n\begin{bmatrix}\cos\left(\sqrt{D}\eta_n(1-L)\right)\cos(\eta_n L)\\ -\left(\sqrt{D}(1-L)+\frac{L}{\sqrt{D}}\right)\sin\left(\sqrt{D}\eta_n(1-L)\right)\sin(\eta_n L)\end{bmatrix}}.\end{aligned} \tag{4.2.78}$$

Finally, the solutions $C_p(x,t)$ and $C_e(x,t)$ are obtained using the Residue Theorem (Theorem 4) and are provided in (4.2.79) and (4.2.80).

$$\begin{aligned}&C_p(x,t) = L\\ &+\frac{2}{\sqrt{D}}\sum_{n=1}^{\infty}\left\{\frac{\begin{pmatrix}\sqrt{D}\sin(\eta_n L)\cos\left(\sqrt{D}\eta_n(1-L)\right)\\ +\sin\left(\sqrt{D}\eta_n(1-L)\right)\{\cos(\eta_n L)-\cos(\eta_n x)\}\end{pmatrix}e^{-D\eta_n^2 t}}{\eta_n\begin{pmatrix}\cos\left(\sqrt{D}\eta_n(1-L)\right)\cos(\eta_n L)\\ -\left(\sqrt{D}(1-L)+\frac{L}{\sqrt{D}}\right)\sin\left(\sqrt{D}\eta_n(1-L)\right)\sin(\eta_n L)\end{pmatrix}}\right\},\end{aligned} \tag{4.2.79}$$

$$\begin{aligned}&C_e(x,t) = L\\ &+2\sum_{n=1}^{\infty}\left\{\frac{\sin(\eta_n L)\cos\left(\sqrt{D}\eta_n(1-x)\right)e^{-D\eta_n^2 t}}{\eta_n\begin{pmatrix}\cos\left(\sqrt{D}\eta_n(1-L)\right)\cos(\eta_n L)\\ -\left(\sqrt{D}(1-L)+\frac{L}{\sqrt{D}}\right)\sin\left(\sqrt{D}\eta_n(1-L)\right)\sin(\eta_n L)\end{pmatrix}}\right\}.\end{aligned} \tag{4.2.80}$$

4.3 Solving transcendental equations

A transcendental equation is an equation containing transcendental functions. Such functions do not satisfy a polynomial equation whose coefficients are themselves polynomials, in contrast to algebraic functions, which do satisfy such an equation. Equation (4.2.74) is such an equation. A simple root finding method such as the bisection method can be used to find the roots of (4.2.74). A plot of the function allows one to get an indication of the interval between roots, thus allowing the bisection method to be easily implemented.

4.3.1 The bisection method

To solve

$$f(x) = 0,$$

where f is a continuous function, two initial points, say a and b, are required such that $f(a)$ and $f(b)$ have different signs. This indicates that at least one root must lie in the interval (a, b). The method computes the midpoint $c = (a + b)/2$ which divides the interval in two. The method is then repeated on either the interval (a, c) or the interval (c, b), depending on whether $f(a)f(c) < 0$ or $f(c)f(b) < 0$. The process is repeated until a root is found to within some specified tolerance. This method was implemented in Matlab to solve equation (4.2.74). It should be noted that because there are infinitely many roots of (4.2.74), only the first hundred were computed since it was found that additional roots did not significantly alter the solutions (4.2.79-4.2.80).

4.4 Model I: Solution in Laplace transform space

Having examined a number of simpler cases, involving only diffusion, an attempt is now made to derive an analytic solution for the equations proposed in model I. Equation (3.3.30) can be rearranged to give

$$\begin{aligned}\frac{\partial C_i}{\partial t}(x,t) &= -\frac{\alpha_i^\star}{K_i\,(1-\phi_m)}C_i(x,t) + \frac{\alpha_i^\star}{1-\phi_m}C_e(x,t) \\ &= -\frac{\gamma}{K_i}C_i(x,t) + \gamma C_e(x,t), \end{aligned} \tag{4.4.81}$$

where $\gamma = \alpha_i^\star/(1-\phi_m)$. Equation (4.4.81) can be re-expressed (using the initial condition $C_i(x,0) = 0$) to obtain an integral relationship between $C_i(x,t)$ and $C_e(x,t)$:

$$C_i(x,t) = \gamma \int_0^t e^{-\gamma(t-t')/K_i}\; C_e(x,t')\; dt'. \tag{4.4.82}$$

Now, taking Laplace transforms of (3.3.28) with respect to time and rearranging provides

$$\frac{d^2\bar{C}_p}{dx^2}(x,s) - \frac{s}{D}\bar{C}_p(x,s) = -\left(\frac{1}{D}\right) C_p(x,0). \tag{4.4.83}$$

Equation (4.4.83) has a general solution given by

$$\bar{C}_p(x,s) = A(s)\cosh\left(\sqrt{\frac{s}{D}}x\right) + B(s)\sinh\left(\sqrt{\frac{s}{D}}x\right) + \frac{1}{s}, \tag{4.4.84}$$

where $1/s$ is the particular integral. Now, substituting (4.4.82) into (3.3.29) gives rise to

$$\phi_m\frac{\partial C_e}{\partial t} + v^\star\frac{\partial C_e}{\partial x} = \frac{\partial^2 C_e}{\partial x^2} - \alpha_i^\star\left(C_e - \frac{\gamma}{K_i}\int_0^t e^{-\gamma(t-t')/K_i}\; C_e(x,t')\; dt'\right). \tag{4.4.85}$$

Taking the Laplace transform of (4.4.85), making use of the initial condition $C_e(x,0) = 0$, and rearranging provides

$$\frac{d^2\bar{C}_e}{dx^2}(x,s) - v^\star \frac{d\bar{C}_e}{dx}(x,s) + \Gamma(s)\bar{C}_e(x,s) = 0, \tag{4.4.86}$$

with

$$\Gamma(s) = \frac{\alpha_i^\star \gamma}{K_i s + \gamma} - \alpha_i^\star - \phi_m s.$$

It is straightforward to solve (4.4.86) to obtain

$$\bar{C}_e(x,s) = e^{v^\star x/2}\left[C(s)\cosh\left(m(s)x\right) + D(s)\sinh\left(m(s)x\right)\right], \tag{4.4.87}$$

where

$$2m(s) = \sqrt{v^{\star 2} - 4\Gamma(s)}. \tag{4.4.88}$$

Taking Laplace transforms of (4.4.82) then yields

$$\begin{aligned} \bar{C}_i(x,s) &= \frac{K_i\gamma}{K_i s + \gamma}\bar{C}_e(x,s) \\ &= \frac{K_i\gamma e^{v^\star x/2}}{K_i s + \gamma}\left[C(s)\cosh\left(mx\right) + D(s)\sinh\left(mx\right)\right]. \end{aligned} \tag{4.4.89}$$

Note that the dependence of m on s has been suppressed here and hereafter for convenience. Now the (transformed) boundary conditions can be used to determine $A(s), B(s), C(s)$ and $D(s)$. The Laplace transform of condition (3.3.31) implies that

$$B(s) = 0. \tag{4.4.90}$$

Thus, (4.4.84) simplifies to

$$\bar{C}_p(x,s) = A(s)\cosh\left(\sqrt{\frac{s}{D}}x\right) + \frac{1}{s}. \tag{4.4.91}$$

Next considered is the Laplace transform of condition (3.3.34):

$$\frac{d\bar{C}_e}{dx} = \lambda \bar{C}_e, \qquad\qquad x = 1. \tag{4.4.92}$$

Differentiating (4.4.87) with respect to x provides

$$\frac{d\bar{C}_e}{dx} = e^{v^\star x/2}\left\{\begin{array}{c} C(s)\left(m\sinh(mx) + \frac{v^\star}{2}\cosh(mx)\right) \\ +D(s)\left(m\cosh(mx) + \frac{v^\star}{2}\sinh(mx)\right) \end{array}\right\}. \tag{4.4.93}$$

Substituting (4.4.93) and (4.4.87) at $x = 1$ into (4.4.92) leads to

$$C(s) = -\frac{D(s)\left[m\cosh(m) + \left(\frac{v^\star}{2} - \lambda\right)\sinh(m)\right]}{m\sinh(m) + \left(\frac{v^\star}{2} - \lambda\right)\cosh(m)}. \tag{4.4.94}$$

Making use of (4.4.87), (4.4.91) and(4.4.94), the Laplace transform of condition (3.3.32) then implies that

$$A(s) = -\frac{\left[\begin{array}{c} sD(s)e^{v^\star L/2}\left(m\cosh(m(1-L)) + \left(\frac{v^\star}{2} - \lambda\right)\sinh(m(1-L))\right) \\ +m\sinh(m) + \left(\frac{v^\star}{2} - \lambda\right)\cosh(m) \end{array}\right]}{s\cosh\left(\sqrt{\frac{s}{D}}L\right)\left(m\sinh(m) + \left(\frac{v^\star}{2} - \lambda\right)\cosh(m)\right)}. \tag{4.4.95}$$

Differentiating (4.4.91) provides

$$\frac{d\bar{C}_p}{dx} = \sqrt{\frac{s}{D}}A(s)\sinh\left(\sqrt{\frac{s}{D}}x\right). \tag{4.4.96}$$

Making use of (4.4.96), (4.4.87) and (4.4.93), the Laplace transform of condition (3.3.33) then implies that

$$A(s) = \frac{e^{v^\star L/2} D(s) \left[\begin{array}{c} \left(m^2 + \frac{v^\star}{2}\left(\frac{v^\star}{2} - \lambda\right)\right) \sinh\left(m(1-L)\right) \\ +m\left(v^\star - \lambda\right) \cosh\left(m(1-L)\right) \end{array} \right]}{\sqrt{sD} \sinh\left(\sqrt{\frac{s}{D}} L\right) \left(m \sinh\left(m\right) + \left(\frac{v^\star}{2} - \lambda\right) \cosh\left(m\right)\right)}. \tag{4.4.97}$$

Eliminating $A(s)$ in (4.4.95) and (4.4.97), the following expression for $D(s)$ is obtained:

$$D(s) = \frac{-\sqrt{sD} \sinh\left(\sqrt{\frac{s}{D}} L\right) \left(m \sinh\left(m\right) + \left(\frac{v^\star}{2} - \lambda\right) \cosh\left(m\right)\right)}{s e^{v^\star L/2} \left[\begin{array}{l} \cosh\left(\sqrt{\frac{s}{D}} L\right) \left\{ \begin{array}{c} \left(m^2 + \frac{v^\star}{2}\left(\frac{v^\star}{2} - \lambda\right)\right) \sinh\left(m(1-L)\right) \\ +m\left(v^\star - \lambda\right) \cosh\left(m(1-L)\right) \end{array} \right\} \\ +\sqrt{sD} \sinh\left(\sqrt{\frac{s}{D}} L\right) \left\{ \begin{array}{c} m \cosh\left(m(1-L)\right) \\ +\left(\frac{v^\star}{2} - \lambda\right) \sinh\left(m(1-L)\right) \end{array} \right\} \end{array} \right]}. \tag{4.4.98}$$

It is now possible to employ (4.4.98) in (4.4.97) to solve for $A(s)$:

$$A(s) = \frac{- \left[\begin{array}{c} \left(m^2 + \frac{v^\star}{2}\left(\frac{v^\star}{2} - \lambda\right)\right) \sinh\left(m(1-L)\right) \\ +m\left(v^\star - \lambda\right) \cosh\left(m(1-L)\right) \end{array} \right]}{s \left[\begin{array}{l} \cosh\left(\sqrt{\frac{s}{D}} L\right) \left\{ \begin{array}{c} \left(m^2 + \frac{v^\star}{2}\left(\frac{v^\star}{2} - \lambda\right)\right) \sinh\left(m(1-L)\right) \\ +m\left(v^\star - \lambda\right) \cosh\left(m(1-L)\right) \end{array} \right\} \\ +\sqrt{sD} \sinh\left(\sqrt{\frac{s}{D}} L\right) \left\{ \begin{array}{c} m \cosh\left(m(1-L)\right) \\ +\left(\frac{v^\star}{2} - \lambda\right) \sinh\left(m(1-L)\right) \end{array} \right\} \end{array} \right]}. \tag{4.4.99}$$

Substituting the expression for $D(s)$ (4.4.98) into (4.4.94) delivers

$$C(s) = \frac{\sqrt{sD}\sinh\left(\sqrt{\frac{s}{D}}L\right)\left(m\cosh\left(m\right) + \left(\frac{v^\star}{2} - \lambda\right)\sinh\left(m\right)\right)}{se^{v^\star L/2}\left[\begin{array}{l} \cosh\left(\sqrt{\frac{s}{D}}L\right)\left\{\begin{array}{c}\left(m^2 + \frac{v^\star}{2}\left(\frac{v^\star}{2} - \lambda\right)\right)\sinh\left(m(1-L)\right) \\ +m\left(v^\star - \lambda\right)\cosh\left(m(1-L)\right)\end{array}\right\} \\ +\sqrt{sD}\sinh\left(\sqrt{\frac{s}{D}}L\right)\left\{\begin{array}{c} m\cosh\left(m(1-L)\right) \\ +\left(\frac{v^\star}{2} - \lambda\right)\sinh\left(m(1-L)\right)\end{array}\right\}\end{array}\right]}. \tag{4.4.100}$$

Now that expressions for $A(s), B(s), C(s)$ and $D(s)$ have been obtained, substitution of (4.4.98), (4.4.99) and (4.4.100) into (4.4.91), (4.4.87) and (4.4.89) delivers the solution in Laplace transform space:

$$\bar{C_p}(x,s) = \frac{\left[\begin{array}{l}\sqrt{sD}\sinh\left(\sqrt{\frac{s}{D}}L\right)\left\{\begin{array}{c} m\cosh\left(m(1-L)\right) \\ +\left(\frac{v^\star}{2} - \lambda\right)\sinh\left(m(1-L)\right)\end{array}\right\} \\ -\left\{\begin{array}{c}\left[\begin{array}{c}\left(m^2 + \frac{v^\star}{2}\left(\frac{v^\star}{2} - \lambda\right)\right)\sinh\left(m(1-L)\right) \\ +m\left(v^\star - \lambda\right)\cosh\left(m(1-L)\right)\end{array}\right] \\ \times\left[\cosh\left(\sqrt{\frac{s}{D}}L\right) - \cosh\left(\sqrt{\frac{s}{D}}x\right)\right]\end{array}\right\}\end{array}\right]}{s\left[\begin{array}{l} \cosh\left(\sqrt{\frac{s}{D}}L\right)\left\{\begin{array}{c}\left(m^2 + \frac{v^\star}{2}\left(\frac{v^\star}{2} - \lambda\right)\right)\sinh\left(m(1-L)\right) \\ +m\left(v^\star - \lambda\right)\cosh\left(m(1-L)\right)\end{array}\right\} \\ +\sqrt{sD}\sinh\left(\sqrt{\frac{s}{D}}L\right)\left\{\begin{array}{c} m\cosh\left(m(1-L)\right) \\ +\left(\frac{v^\star}{2} - \lambda\right)\sinh\left(m(1-L)\right)\end{array}\right\}\end{array}\right]}, \tag{4.4.101}$$

$$\bar{C}_e(x,s) = \frac{\sqrt{sD}\sinh\left(\sqrt{\frac{s}{D}}L\right)\left\{\begin{array}{c} m\cosh\left(m(1-x)\right) \\ +\left(\frac{v^\star}{2}-\lambda\right)\sinh\left(m(1-x)\right)\end{array}\right\}e^{v^\star(x-L)/2}}{s\left[\begin{array}{l}\cosh\left(\sqrt{\frac{s}{D}}L\right)\left\{\begin{array}{c}\left(m^2+\frac{v^\star}{2}\left(\frac{v^\star}{2}-\lambda\right)\right)\sinh\left(m(1-L)\right) \\ +m\left(v^\star-\lambda\right)\cosh\left(m(1-L)\right)\end{array}\right\} \\ +\sqrt{sD}\sinh\left(\sqrt{\frac{s}{D}}L\right)\left\{\begin{array}{c} m\cosh\left(m(1-L)\right) \\ +\left(\frac{v^\star}{2}-\lambda\right)\sinh\left(m(1-L)\right)\end{array}\right\}\end{array}\right]}. \tag{4.4.102}$$

Finally, $\bar{C}_i(x,s)$ is given by

$$\begin{aligned}&\bar{C}_i(x,s) \\ &= \frac{\sqrt{sD}\left(K_i\gamma\right)\sinh\left(\sqrt{\frac{s}{D}}L\right)\left\{\begin{array}{c} m\cosh\left(m(1-x)\right) \\ +\left(\frac{v^\star}{2}-\lambda\right)\sinh\left(m(1-x)\right)\end{array}\right\}e^{v^\star(x-L)/2}}{s\left(K_is+\gamma\right)\left[\begin{array}{l}\cosh\left(\sqrt{\frac{s}{D}}L\right)\left\{\begin{array}{c}\left(m^2+\frac{v^\star}{2}\left(\frac{v^\star}{2}-\lambda\right)\right)\sinh\left(m(1-L)\right) \\ +m\left(v^\star-\lambda\right)\cosh\left(m(1-L)\right)\end{array}\right\} \\ +\sqrt{sD}\sinh\left(\sqrt{\frac{s}{D}}L\right)\left\{\begin{array}{c} m\cosh\left(m(1-L)\right) \\ +\left(\frac{v^\star}{2}-\lambda\right)\sinh\left(m(1-L)\right)\end{array}\right\}\end{array}\right]}.\end{aligned} \tag{4.4.103}$$

Inversion of (4.4.101-4.4.103) provides the solution to the system of partial differential equations (3.3.28-3.3.30) subject to (3.3.31-3.3.36). Because of the complexity of the problem it is impractical to invert (4.4.101-4.4.103). As well as the transformed variable, s, appearing explicitly, expressions (4.4.101-4.4.103) also contain the more complicated $m(s)$, as given by equation (4.4.88). It is not clear at all how one would determine the location of all the branch points, nor how one would proceed to draw and implement a suitable contour to invert the expressions.

Chapter 5

Numerical and Experimental Work

Often, when it is not possible nor practical to obtain an analytic solution, numerical methods are adopted to compute a numerical solution. This type of solution is an approximation, but depending on the method used, accurate solutions can be obtained. When dealing with partial differential equations, both finite element and finite difference approximations are often used. In this thesis, the latter will be employed, and in particular, a variation of the Crank-Nicolson scheme. The Crank-Nicolson scheme is known to be unconditionally stable, at least for the diffusion equation, and whilst an adaption of this method is implemented here, it was felt that it would nevertheless possess favourable stability properties. Developing this scheme was preferred to utilizing commercial software, such as COMSOL, since it allows one to easily keep track of exactly how the problem is being solved as well as providing the user with greater control over accuracy. In the absence of data on the somewhat vexatious constant of proportionality β, the main focus of attention will be the non-dimensional version of models $II - IV$.

5.1 Numerical scheme

In this section the numerical scheme is described. The scheme is based on the well known implicit Crank-Nicolson method (Crank 1956) and makes use of central differences in space and the average of forward Euler and backward Euler in time.

5.1.1 Polymer region

Let the polymer region P be such that $x \in P := [0, L]$. Let the points x_j belong to a uniform mesh $P_j = \{x_j = (j-1)\Delta x_p : j = 1, 2, ..., N_p + 1\}$, where $\Delta x_p = L/N_p$. Furthermore, let Δt be the non-dimensional time spacing. Then the Crank-Nicolson scheme for the concentration diffusion equation (3.3.28) in the polymer region is given by

$$\left(1 - \frac{r_p}{2}\,\delta_x^2\right) C_{p_j}^{n+1} = \left(1 + \frac{r_p}{2}\,\delta_x^2\right) C_{p_j}^{n} \quad , \qquad r_p = D\frac{\Delta t}{\Delta x_p^2}, \tag{5.1.1}$$

where the grid function $C_{p_j}^n$ denotes an approximation to the polymer drug concentration at (x_j, t_n) and the second order central difference operator is defined as $\delta_x^2 C_j^n = C_{j-1}^n - 2C_j^n + C_{j+1}^n$. Equation (5.1.1) is employed on the internal points, x_j, $j = 2, 3, ..., N_p$.

5.1.2 Wire/polymer boundary

The derivative boundary condition (3.3.31) is approximated as follows

$$\frac{C_{p_2}^n - C_{p_0}^n}{2\Delta x_p} = 0,$$

or, equivalently,

$$C_{p_2}^n = C_{p_0}^n, \tag{5.1.2}$$

where C_{p_0} denotes the concentration of drug at a fictitious point. Applying (5.1.2) to the polymer scheme (5.1.1) at the wire/polymer boundary point gives rise to

$$(1+r_p)\,C_{p_1}^{n+1} - r_p C_{p_2}^{n+1} = (1-r_p)\,C_{p_1}^{n} + r_p C_{p_2}^{n}, \tag{5.1.3}$$

where C_{p_1} denotes the concentration of drug at the wire/polymer boundary.

5.1.3 Media region

Let the media region M be such that $x \in M := [L, 1]$. Let the points x_j belong to a uniform mesh $M_j = \{x_j = L+(j-N_p-1)\Delta x_m : j = N_p+1, N_p+2, ..., N_p+N_m+1\}$, where $\Delta x_m = (1-L)/N_m$. Equation (3.3.29) is approximated in a similar way to the polymer diffusion equation. Here, $C_{e_j}^n$ and $C_{i_j}^n$ denote an approximation to the media extracellular concentration and smooth muscle cell concentration, respectively, at (x_j, t_n). A central difference approximation for the convective term is employed, again taking the average of forward and backward Euler in line with the Crank-Nicolson method. Arguably a one-sided (i.e. upwinding) finite difference approximation of the convective term might have been more stable; however, excessive computation was not incurred by using a small time step which precluded any 'wiggles'. The cellular concentration, C_i, appearing in the loss term, is approximated at the back level:

$$\begin{aligned}
\phi_m \frac{\left(C_{e_j}^{n+1} - C_{e_j}^{n}\right)}{\Delta t} &= -\frac{v^\star}{2}\frac{\left(C_{e_{j+1}}^{n+1} - C_{e_{j-1}}^{n+1}\right)}{2\Delta x_m} - \frac{v^\star}{2}\frac{\left(C_{e_{j+1}}^{n} - C_{e_{j-1}}^{n}\right)}{2\Delta x_m} \\
&+ \frac{\left(C_{e_{j-1}}^{n+1} - 2C_{e_j}^{n+1} + C_{e_{j+1}}^{n+1}\right)}{2\Delta x_m^2} + \frac{\left(C_{e_{j-1}}^{n} - 2C_{e_j}^{n} + C_{e_{j+1}}^{n}\right)}{2\Delta x_m^2} \\
&- \alpha_i \star \left(C_{e_j}^{n+1} - \frac{C_{i_j}^{n}}{K_i}\right),
\end{aligned} \tag{5.1.4}$$

or, after letting $r_{m_1} = v^\star \Delta t/2\phi_m \Delta x_m, \quad r_{m_2} = \Delta t/\phi_m \Delta x_m^2, \quad r_{m_3} = \alpha_i^\star \Delta t/\phi_m$, the scheme can be written as

$$\begin{aligned} - & \frac{1}{2}\left(r_{m_1} + r_{m_2}\right)\, C_{e_{j-1}}^{n+1} + \left(1 + r_{m_2} + r_{m_3}\right)\, C_{e_j}^{n+1} - \frac{1}{2}\left(r_{m_2} - r_{m_1}\right)\, C_{e_{j+1}}^{n+1} \\ = & \frac{1}{2}\left(r_{m_1} + r_{m_2}\right)\, C_{e_{j-1}}^{n} + \left(1 - r_{m_2}\right)\, C_{e_j}^{n} + \frac{1}{2}\left(r_{m_2} - r_{m_1}\right)\, C_{e_{j+1}}^{n} + \frac{r_{m_3}}{K_i} C_{i_j}^{n}. \end{aligned} \tag{5.1.5}$$

The cellular uptake equation is handled as follows,

$$\frac{C_{i_j}^{n+1} - C_{i_j}^{n}}{\Delta t} = \frac{\alpha_i^\star}{1 - \phi_m}\left(C_{e_j}^{n+1} - \frac{C_{i_j}^{n}}{K_i}\right),$$

which can be rearranged to give

$$C_{i_j}^{n+1} = \left(1 - r_i/K_i\right)\, C_{i_j}^{n} + r_i\, C_{e_j}^{n+1}, \tag{5.1.6}$$

where $r_i = \alpha_i^\star \Delta t/(1 - \phi)$. Both schemes (5.1.5) and (5.1.6) should be applied to the internal media points, x_j, $j = N_p + 2, ..., N_p + N_m$.

5.1.4 Polymer/media boundary

Here, conditions (3.3.32) and (3.3.33), applied at the point x_j, $j = N_p + 1$, are considered. The latter is approximated in the following way:

$$D\left[\frac{C_{p_{N_p+2}}^{n} - C_{p_{N_p}}^{n}}{\Delta x_p + \Delta x_m}\right] = \frac{C_{e_{N_p+2}}^{n} - C_{e_{N_p}}^{n}}{\Delta x_p + \Delta x_m} - v^\star C_{e_{N_p+1}}^{n} \tag{5.1.7}$$

where $C_{p_{N_p+2}}^{n}$ and $C_{e_{N_p}}^{n}$ both denote the concentration of drug at fictitious points and $C_{e_{N_p+1}}$ denotes the drug concentration at the polymer/media boundary point. Rearranging gives an expression for the concentration at the polymer fictitious

points in terms of the concentration at the media fictitious points

$$C^n_{p_{N_p+2}} = C^n_{p_{N_p}} + \frac{C^n_{e_{N_p+2}} - C^n_{e_{N_p}}}{D} - \frac{v^\star \left(\Delta x_p + \Delta x_m\right) C^n_{e_{N_p+1}}}{D} \tag{5.1.8}$$

To eliminate the fictitious terms, both the polymer and media schemes are evaluated at this boundary point. If $\Delta x_p = \Delta x_m$ then this is trivial and the schemes are simply given by (5.1.1) and (5.1.5) respectively. For the general case, $\Delta x_p \neq \Delta x_m$, central differences should be defined. The first consideration is the general problem of two regions, 1 and 2, each of uniform spacing Δx_1 and Δx_2, respectively. The boundary point is the Nth point.

$$\delta_x C^n_N = \frac{C^n_{N+1/2} - C^n_{N-1/2}}{\left(\Delta x_1 + \Delta x_2\right)/2} \tag{5.1.9}$$

$$\begin{aligned}
\delta_x^2 C^n_N &= \frac{\delta_x C^n_{N+1/2} - \delta_x C^n_{N-1/2}}{\left(\Delta x_1 + \Delta x_2\right)/2} \\
&= \frac{\left(C^n_{N+1} - C^n_N\right)/\Delta x_2 - \left(C^n_N - C^n_{N-1}\right)/\Delta x_1}{\left(\Delta x_1 + \Delta x_2\right)/2} \\
&= 2\left(\frac{1}{\Delta x_1\left(\Delta x_1 + \Delta x_2\right)} C^n_{N-1} - \frac{1}{\Delta x_1 \Delta x_2} C^n_N + \frac{1}{\Delta x_2\left(\Delta x_1 + \Delta x_2\right)} C^n_{N+1}\right).
\end{aligned} \tag{5.1.10}$$

Equation (5.1.10) is now applied to (3.3.28). In the polymer region, this gives

$$\frac{\left(C^{n+1}_{p_{N_p+1}} - C^n_{p_{N_p+1}}\right)}{\Delta t} = D\left[\begin{array}{c} \frac{C^{n+1}_{p_{N_p}}}{\Delta x_p(\Delta x_p+\Delta x_m)} - \frac{C^{n+1}_{p_{N_p+1}}}{\Delta x_p \Delta x_m} + \frac{C^{n+1}_{p_{N_p+2}}}{\Delta x_m(\Delta x_p+\Delta x_m)} \\ + \frac{C^n_{p_{N_p}}}{\Delta x_p(\Delta x_p+\Delta x_m)} - \frac{C^n_{p_{N_p+1}}}{\Delta x_p \Delta x_m} + \frac{C^n_{p_{N_p+2}}}{\Delta x_m(\Delta x_p+\Delta x_m)} \end{array}\right]. \tag{5.1.11}$$

Rearranging, the polymer scheme at the boundary point can be written as

$$\begin{aligned} - & \frac{\Delta x_p}{\Delta x_p + \Delta x_m} r_p \, C^{n+1}_{p_{N_p}} + \left(1 + \frac{\Delta x_p}{\Delta x_m} r_p\right) \, C^{n+1}_{p_{N_p+1}} - \frac{\Delta x_p^2}{\Delta x_m \left(\Delta x_p + \Delta x_m\right)} r_p \, C^{n+1}_{p_{N_p+2}} \\ = & \frac{\Delta x_p}{\Delta x_p + \Delta x_m} r_p \, C^{n}_{p_{N_p}} + \left(1 - \frac{\Delta x_p}{\Delta x_m} r_p\right) \, C^{n}_{p_{N_p+1}} + \frac{\Delta x_p^2}{\Delta x_m \left(\Delta x_p + \Delta x_m\right)} r_p \, C^{n}_{p_{N_p+2}}. \end{aligned} \tag{5.1.12}$$

In a similar manner, the expressions for δ_x and δ_x^2 can be applied to the media region, equation (3.3.29), and rearranged to give

$$\begin{aligned} - & \frac{\Delta x_m}{\Delta x_p + \Delta x_m} \left(r_{m_1} + \frac{\Delta x_m}{\Delta x_p} r_{m_2}\right) \, C^{n+1}_{e_{N_p}} + \left(1 + \frac{\Delta x_m}{\Delta x_p} r_{m_2} + r_{m_3}\right) \, C^{n+1}_{e_{N_p+1}} \\ + & \frac{\Delta x_m}{\Delta x_p + \Delta x_m} \left(r_{m_1} - r_{m_2}\right) \, C^{n+1}_{e_{N_p+2}} \\ = & \frac{\Delta x_m}{\Delta x_p + \Delta x_m} \left(r_{m_1} + \frac{\Delta x_m}{\Delta x_p} r_{m_2}\right) \, C^{n}_{e_{N_p}} + \left(1 - \frac{\Delta x_m}{\Delta x_p} r_{m_2}\right) \, C^{n}_{e_{N_p+1}} \\ + & \frac{\Delta x_m}{\Delta x_p + \Delta x_m} \left(r_{m_2} - r_{m_1}\right) \, C^{n}_{e_{N_p+2}} + \frac{r_{m_3}}{K_i} \, C^{n}_{i_{N_p+1}}. \end{aligned} \tag{5.1.13}$$

Substituting (5.1.8) into (5.1.12) and simplifying gives

$$\begin{aligned} C^{n+1}_{e_{N_p}} + C^{n}_{e_{N_p}} = & \frac{D \Delta x_m \left(\Delta x_p + \Delta x_m\right)}{\Delta x_p^2 r_p} \\ & \times \begin{bmatrix} \frac{\Delta x_p r_p}{\Delta x_p + \Delta x_m} \left(1 + \frac{\Delta x_p}{\Delta x_m}\right) \, C^{n}_{p_{N_p}} \\ + \left(1 - \frac{\Delta x_p}{\Delta x_m} r_p - \frac{v^\star \Delta x_p^2 r_p}{D \Delta x_m}\right) \, C^{n}_{p_{N_p+1}} \\ + \frac{\Delta x_p^2 r_p}{D \Delta x_m (\Delta x_p + \Delta x_m)} \left(C^{n+1}_{e_{N_p+2}} + C^{n}_{e_{N_p+2}}\right) \\ + \frac{\Delta x_p r_p}{\Delta x_p + \Delta x_m} \left(1 + \frac{\Delta x_p}{\Delta x_m}\right) \, C^{n+1}_{p_{N_p}} \\ - \left(1 + \frac{\Delta x_p}{\Delta x_m} r_p + \frac{v^\star \Delta x_p^2 r_p}{D \Delta x_m}\right) \, C^{n+1}_{p_{N_p+1}} \end{bmatrix}. \end{aligned} \tag{5.1.14}$$

At this point, use is made of the condition (3.3.32), so that $C^n_{p_{N_p+1}} = C^n_{e_{N_p+1}}$. Rearranging (5.1.13) provides

$$\begin{aligned} C^{n+1}_{e_{N_p}} + C^n_{e_{N_p}} &= \frac{\Delta x_p + \Delta x_m}{\Delta x_m \left(r_{m_1} + \Delta x_m r_{m_2}/\Delta x_p\right)} \\ &\times \left[\begin{array}{c} \left(1 + \frac{\Delta x_m}{\Delta x_p} r_{m_2} + r_{m_3}\right) C^{n+1}_{e_{N_p+1}} + \frac{\Delta x_m \left(r_{m_1} - r_{m_2}\right)}{\Delta x_p + \Delta x_m} C^{n+1}_{e_{N_p+2}} \\ -\left(1 - \frac{\Delta x_m}{\Delta x_p} r_{m_2}\right) C^n_{e_{N_p+1}} - \frac{\Delta x_m \left(r_{m_2} - r_{m_1}\right)}{\Delta x_p + \Delta x_m} C^n_{e_{N_p+2}} \\ -\frac{r_{m_3}}{K_i} C^n_{i_{N_p+1}} \end{array}\right]. \end{aligned} \tag{5.1.15}$$

Hence by equating (5.1.14) with (5.1.15), one can eliminate the remaining fictitious points. The result, after simplification is the following condition for the polymer/media boundary

$$\begin{aligned} &- \frac{\Delta x_p}{\Delta x_m} r_p \, C^{n+1}_{p_{N_p}} \\ &+ \left(1 + \frac{\Delta x_p}{\Delta x_m} r_p \left(1 + \frac{v^\star \Delta x_p}{D} + \frac{r_{m_2} + \left(1 + r_{m_3}\right) \Delta x_p/\Delta x_m}{D\left(r_{m_1} + r_{m_2} \Delta x_m/\Delta x_p\right)}\right)\right) C^{n+1}_{p_{N_p+1}} \\ &+ \frac{\Delta x_p^2 r_p}{D \Delta x_m \left(\Delta x_p + \Delta x_m\right)} \left(\frac{r_{m_1} - r_{m_2}}{r_{m_1} + r_{m_2} \Delta x_m/\Delta x_p} - 1\right) C^{n+1}_{e_{N_p+2}} \\ &= \frac{\Delta x_p}{\Delta x_m} r_p \, C^n_{p_{N_p}} \\ &+ \left(1 - \frac{\Delta x_p}{\Delta x_m} r_p \left(1 + \frac{v^\star \Delta x_p}{D} - \frac{\Delta x_p/\Delta x_m - r_{m_2}}{D\left(r_{m_1} + r_{m_2} \Delta x_m/\Delta x_p\right)}\right)\right) C^n_{p_{N_p+1}} \\ &+ \frac{\Delta x_p^2 r_p}{D \Delta x_m \left(\Delta x_p + \Delta x_m\right)} \left(\frac{r_{m_2} - r_{m_1}}{r_{m_1} + r_{m_2} \Delta x_m/\Delta x_p} + 1\right) C^n_{e_{N_p+2}} \\ &+ \frac{\Delta x_p^2 r_p r_{m_3}}{\Delta x_m^2 K_i D \left(r_{m_1} + r_{m_2} \Delta x_m/\Delta x_p\right)} C^n_{i_{N_p+1}}. \end{aligned} \tag{5.1.16}$$

5.1.5 Media/adventitia boundary

Condition (3.3.34) is approximated at the point x_j, $j = N_p + N_m + 1$ as follows:

$$\frac{C^n_{e_{N_p+N_m+2}} - C^n_{e_{N_p+N_m}}}{2\Delta x_m} - \lambda C^n_{e_{N_p+N_m+1}} = 0, \tag{5.1.17}$$

where $C^n_{e_{N_p+N_m+2}}$ denotes the drug concentration at a fictitious point. Rearranging equation (5.1.17), one can obtain the following expression for the fictitious term

$$C^n_{e_{N_p+N_m+2}} = C^n_{e_{N_p+N_m}} + 2\Delta x_m \lambda C^n_{e_{N_p+N_m+1}}. \tag{5.1.18}$$

Applying the media scheme (5.1.5) to the point x_j, $j = N_p + N_m + 1$ gives

$$\begin{aligned}
- \quad & \frac{1}{2}\left(r_{m_1} + r_{m_2}\right)\, C^{n+1}_{e_{N_p+N_m}} + \left(1 + r_{m_2} + r_{m_3}\right)\, C^{n+1}_{e_{N_p+N_m+1}} \\
- \quad & \frac{1}{2}\left(r_{m_2} - r_{m_1}\right)\, C^{n+1}_{e_{N_p+N_m+2}} \\
= \quad & \frac{1}{2}\left(r_{m_1} + r_{m_2}\right)\, C^{n}_{e_{N_p+N_m}} + \left(1 - r_{m_2}\right)\, C^{n}_{e_{N_p+N_m+1}} \\
+ \quad & \frac{1}{2}\left(r_{m_2} - r_{m_1}\right)\, C^{n}_{e_{N_p+N_m+2}} \\
+ \quad & \frac{r_{m_3}}{K_i} C^n_{i_{N_p+N_m+1}}.
\end{aligned} \tag{5.1.19}$$

Substituting (5.1.18) into (5.1.19) and rearranging gives

$$\begin{aligned}
- \quad & r_{m_2}\, C^{n+1}_{e_{N_p+N_m}} + \left(1 + r_{m_2} + r_{m_3} + \left(r_{m_1} - r_{m_2}\right)\lambda\Delta x_m\right)\, C^{n+1}_{e_{N_p+N_m+1}} \\
= \quad & +r_{m_2}\, C^{n}_{e_{N_p+N_m}} + \left(1 - r_{m_2} + \left(r_{m_2} - r_{m_1}\right)\lambda\Delta x_m\right)\, C^{n}_{e_{N_p+N_m+1}} \\
+ \quad & \frac{r_{m_3}}{K_i}\, C^n_{i_{N_p+N_m+1}}.
\end{aligned} \tag{5.1.20}$$

5.1.6 The inclusion of the adventitia, topcoat and plaque

The adventitia and plaque equations are approximated in the same way as the media equations; thus the detail is omitted. The topcoat diffusion equation is approximated in the same way as the polymer diffusion equation, and the interface boundary conditions are approximated in the same way as the polymer/media boundary conditions. The far adventitia boundary condition, $C_a = 0$, is handled in the usual way.

5.1.7 Implementation of numerical scheme in Matlab

The scheme is implemented in Matlab by considering the matrix equation

$$\boldsymbol{A_1 C^{n+1} = A_2 C^n + A_3 C_i^n + A_4 C_f^n,} \tag{5.1.21}$$

where C^{n+1} and C^n denote the vectors containing polymer, media and adventita (extracellular) concentration values at time levels $n+1$ and n, respectively. The vectors C_i^n and C_f^n represent the drug concentration in smooth muscle cells and fibroblast cells, respectively, at the back time level n. The matrices $A_1 - A_4$ (all of the same order) are derived by consideration of equations (5.1.1-5.1.20). By firstly computing the vector b,

$$\boldsymbol{b = A_2 C^n + A_3 C_i^n + A_4 C_f^n,} \tag{5.1.22}$$

the solution is obtained using the Matlab built-in backslash operator:

$$\boldsymbol{C^{n+1} = A_1 \backslash b.} \tag{5.1.23}$$

The smooth muscle cell concentration is then obtained from (5.1.6), since the $C_{e_j}^{n+1}$ values can be extracted from (5.1.23), and the $C_{i_j}^{n}$ values will be known. The fibroblast cellular values are computed in a similar way. This process is repeated, increasing the time level by the timestep Δt each time, until the solution for the desired time is achieved. The Matlab built-in backslash operator employs matrix factorization (LU, Cholesky, QR, or other methods) and is commonly used to solve matrix equations. The disadvantage of using such a solver, of course, is that the user has no control over which particular factorization is employed. Clearly, the obvious alternative would be to directly use one of the aforementioned factorizations best suited to the problem being solved.

5.2 Validation

In the absence of an analytic solution to the full model, the code is verified by setting $v = \alpha_i = \beta = 0$ and $\phi_m = 1$ and comparing it to the analytic solution (computed in Matlab using the first 100 terms) for the case of diffusion in composite finite regions (§4.2.3). Table 5.1 shows that as the mesh spacing is decreased in the polymer and media regions, the numerical solution converges to the analytic solution. While maintaining a mesh ratio of less than 1 for reasons of stability, a dimensional time of 4000 s was used for comparison. This time choice for comparison is reasonable since, with the parameter values selected, the system adjusts over a shorter period of time than the full problem and reaches a steady state within the first day. Whilst this method only validates the diffusive part of the problem, the other aspects of the problem (advection and reaction) may be tested in a more thorough validation by making use of a suitable analytic solution (for example, the analytic solutions derived in Chapters 6 and 7).

'Strips' ratio $N_p : N_m$	Polymer mid-point concentration	polymer/media boundary concentration	Media mid-point concentration
10:20	0.4825	0.1695	0.0090
100:200	0.4039	0.0950	0.0030
200:400	0.3995	0.0908	0.0026
1000:2000	0.3960	0.0875	0.0024
5000:10000	0.3953	0.0869	0.0023
Analytic	0.3951	0.0867	0.0023

Table 5.1: Comparison of analytic and numerical results at $t = 4000$s. Note that all concentrations are non-dimensional

5.3 Source of parameter data

An extensive literature search has been performed to obtain estimates of the various parameters in the aforementioned models. This has posed many difficulties. Ideally all the parameters should be measured experimentally using the same type of stent and the same type of artery in the same species. However, the experimental data used has been drawn from a variety of studies, using differing stents, arteries and species. Furthermore, many experiments have been carried out *in vitro* when the transmural velocity, v, has necessarily been neglected.

For polymer coated stents which do not contain an additional polymer topcoat layer, the polymer thickness, l_p, appears to be reasonably well established. A polymer thickness of $l_p = 5 - 10$ μm is quoted by McLean and Litvack (2005) for some commercially available stents and a similar thickness of $l_p = 1.57 \times 10^{-5}$ m has been measured experimentally for an Iloprost in PLGA poly(lactic-co-glycolic acid) coated stent (Christopher McCormick, personal communication). Sternberg *et al.* (2007) use the absorbable polymer PLLA poly(L-lactide) with a coating of thickness $l_p = 5 - 10$ μm, whilst in a study by Alexis *et al.* (2004) a polymer film thickness of $l_p = 120 \pm 20$ μm was employed for PDLLA poly(D,L-lactide) and PDLLGA poly(D,L-lactide-co-glycolide) biodegradable helical stent systems.

Clearly, the media thickness, l_m, and adventitia thickness, l_a, vary from artery to artery and species to species. Levin *et al.* (2004) segregated tissue segments of calf internal carotid arteries of thickness 7×10^{-4} m into two parts, defining the media region to have a thickness 4×10^{-4} m and the adventitia region to have a thickness 3×10^{-4} m. The media thickness in a rabbit's iliac artery has been measured to be 2×10^{-4} m (Roger Wadsworth, personal communication). Karner and Perktold (2000) in their mathematical study of albumin accumulation in the arterial wall considered a media thickness of 300 μm.

Data for the polymer diffusion coefficient, D_p, is believed to lie in the range $10^{-13} - 10^{-16}$ m^2 s^{-1} (Green *et al.* 2005, Zunino 2004, Alexis *et al.* 2004) depending on the type of polymer used. The diffusion coefficients in the media, D_m, and adventitia, D_a, are drug-dependent. Lovich and Edelman (1995) measured the media and adventitia diffusion coefficients for heparin to be $D_m = 7.7 \times 10^{-12}$ m^2 s^{-1} and $D_a = 12 \times 10^{-12}$ m^2 s^{-1} respectively, whereas the corresponding media figure for paclitaxel is quoted by Zunino (2004) as $D_m = 2.6 \times 10^{-12}$ m^2 s^{-1} . Creel *et al.* (2000) measure a lumped effective diffusivity for paclitaxel which includes effects such as convection and binding. Their values are of the same order of magnitude, $D_m = 1.26 - 4.87 \times 10^{-12}$ m^2 s^{-1}. Levin *et al.* (2004) also measured effective diffusivities: their values were calculated from the early time solution of a diffusion equation. They do report different transmural diffusivities for dextran, paclitaxel and rapamycin, with the paclitaxel value given as $D_m = 5 \times 10^{-13}$ m^2 s^{-1}. Interestingly, the corresponding value for dextran ($D_m = 5 \times 10^{-11}$ m^2 s^{-1}) is considerably higher whereas the value for rapamycin ($D_m = 1 \times 10^{-13}$ m^2 s^{-1}) is comparable with the paclitaxel value.

Data on the drug uptake parameter is limited. One can fit a first order reaction kinetics model to data from Levin *et al.* (2004) to obtain a drug uptake rate con-

stant for paclitaxel of $\alpha_i = 2 \times 10^{-5}$ s^{-1}. No other measurements of this parameter appear to have been made for paclitaxel. Zhu *et al.* (2006) use a similar method to Green *et al.* (2005) to obtain the drug uptake rate for the drug dipyridamole of 3×10^{-6} s^{-1}. The porosity in the media is quoted as $\phi_m = 0.61$ (Lovich and Edelman 1999, Zunino 2004), whereas the value in the adventitia, where there are fewer cells, is stated as $\phi_a = 0.85$ (Lovich & Edelman 1999). The paclitaxel partition coefficient in the media, found by calculating the tissue drug concentration normalized by bulk fluid drug concentration was found in separate studies to lie in the range $13 - 25$ (Levin *et al.* 2004) and $10 - 20$ (Creel *et al.* 2000). The corresponding value for heparin is 1 (Zunino 2004). The partition coefficient for paclitaxel in the adventitia was found to be more variable, in the range $15 - 45$ (Levin *et al.* 2004). The representative values, $K_i = 15$ and $K_a = 20$ are taken here.

Although there is a plethora of data available for the transmural velocity, the measurements do vary considerably. Zunino (2004) uses Darcy's law to estimate a transmural velocity of $v = 10^{-8}$ ms^{-1} for a pressure difference across the artery wall of 100 mmHg. This estimate is comparable with data from Lever *et al.* (1992) where the transmural velocity at 110.5 mmHg is found to be $v = 1.85 \pm 0.33 \times 10^{-8}$ ms^{-1}. In another study by Alberding *et al.* (1992) the velocity varied from $v = 2.1 - 15.7 \times 10^{-8}$ ms^{-1} for the case of intact arteries to $v = 1.29 - 5.94 \times 10^{-7}$ ms^{-1} for arteries where the endothelium had been removed (assuming a standard physiological pressure of 60 mmHg). They concluded that both the removal of the endothelium and pulsatility resulted in increased transmural velocity. An interesting study by Baldwin *et al.* (1997) measured transmural velocities at different physiological pressures and found that the value of the transmural velocity increased with pressure. In a control artery, the measurements were

$v = 2 - 4.5 \times 10^{-8}$ ms^{-1} at 30 mmHg, but rose to $v = 7.4 - 12.4 \times 10^{-8}$ ms^{-1} at a pressure of 90 mmHg. This group also measured v in arteries which had been subject to a fatty diet (but no lesion) as well as a fatty diet resulting in a lesion. For the case of no lesion, the measurements ranged from $v = 5.1 - 7.5 \times 10^{-8}$ ms^{-1} at 30 mmHg to $v = 7.3 - 16.4 \times 10^{-8}$ ms^{-1} at a pressure of 90 mmHg. The corresponding values for the arteries with a lesion ranged from $v = 3.6 - 9.7 \times 10^{-8}$ ms^{-1} at 30 mmHg to $v = 10 - 18 \times 10^{-8}$ ms^{-1} at a pressure of 90 mmHg. These results seems to indicate that not only does transmural velocity increase with pressure, but also that transmural velocity may increase with disease. This increase could be an order of magnitude resulting in a transmural velocity of order 10^{-7} ms^{-1}.

5.3.1 Timescales

This section provides some estimates of the timescales for diffusion, convection and reaction in the system, based on parameter values for the drug paclitaxel. The timescale associated with diffusion is given by L^2/D, where L and D are the typical length scale and diffusion coefficient respectively. The timescales for diffusion in the polymer, T_{D_p}, range from $10^4 - 10^6$ s for diffusion coefficients in the range $10^{-14} - 10^{-16}$m^{2}s^{-1}. In the media, the timescale for diffusion, T_{D_m}, ranges from $1.6 \times (10^5 - 10^6)$ s for diffusion coefficients in the range $10^{-12} - 10^{-13}$m^{2}s^{-1}. The timescale associated with convection, T_v, is given by L/v, where L is a typical length scale and v is the velocity. The timescales for convection in the media range from $4 \times (10^3 - 10^4)$s for transmural velocities $10^{-7} - 10^{-8}$ms^{-1}. Finally, the timescale associated with reaction, T_{α_i}, is given by $1/\alpha_i$, where α_i is the reaction rate. For an uptake rates of 2×10^{-5}s^{-1}, the corresponding timescale for reaction is 5×10^4s.

The Peclet number $Pe = L\ v/D$ compares the relative diffusive and convective

fluxes. Using the range of values for v and D_m (for paclitaxel), the Peclet number ranges from 4 (convection and diffusion more or less of equal importance) to 400 (convection dominated). Thus the system appears not to be a diffusion dominated system, contrary to what had been reported in the literature (e.g. Pontrelli & de Monte 2007) and so convective terms cannot be neglected. Indeed, it has been shown experimentally (Lovich and Edelman 1995, 1999) that the addition of a transmural hydrostatic pressure gradient, where both diffusive and convective transport existed, can lead to significantly increased drug deposition compared to diffusive transport alone. The Damköhler number, defined as the ratio of the timescale for convection to the timescale for reaction, ranges from around 0.1 to unity, depending on the value of the transmural velocity.

5.4 Sensitivity analysis

Now that the numerical scheme has been devised, and a range of parameter values to consider have been established, some results may be obtained from the code. The following markers are introduced:

- $C_i(max)$: The non-dimensional maximum cellular concentration across the media
- $maxgrad$: The maximum gradient $((C_i(1,t) - C_i(L,t))/(1-L))$ of the line which joins the cellular concentration value at the polymer/media boundary and the media/adventitia boundary. This provides some measure of the uniformity of the drug within the media.
- $T_{>min}$: The time (in hours) taken for every cellular point in the media to exceed the minimum therapeutic value (defined to be $C_i(max)/1000$, see §5.4.1)

- $T_{therapeutic}$: The time (in hours) during which all the cells in the media are exposed to levels of drug greater than the minimum therapeutic level, but lower than the toxic level

- T_{empty}: The time (in hours) taken for 99 % of the drug to be released from the polymer. This is calculated by integrating the concentration of drug over the polymer region numerically using the trapezoidal rule (see §5.5)

- C^0_{equiv}: The equivalent dimensional initial stent coating concentration required such that the toxic level of drug is never reached. This is useful since the models are non-dimensionalized so that the initial concentration is 1. The parameter C^0_{equiv} then tells us what the initial stent coating should be such that the results can be compared (i.e., so that the maximum cellular concentration reached is always the maximum therapeutic concentration, 0.15 mol m^{-3})

The control values for the parameters (see §5.3) are:

- transmural velocity, $v = 10^{-8}\mathrm{ms}^{-1}$

- polymer diffusion coefficient, $D_p = 10^{-14}\mathrm{m}^2\mathrm{s}^{-1}$

- media diffusion coefficient, $D_m = D_a = 10^{-12}\mathrm{m}^2\mathrm{s}^{-1}$

- drug uptake rate, $\alpha_i = \alpha_a = 2 \times 10^{-5}\mathrm{s}^{-1}$

- partition coefficient, $K_i = 15$, $K_a = 20$, $K_{pl} = 20$

- polymer thickness, $l_p = 10^{-5}\mathrm{m}$

- media thickness, $l_m = 4 \times 10^{-4}\mathrm{m}$

- adventitia thickness, $l_a = 3 \times 10^{-4}\mathrm{m}$

- $\phi_m = 0.6$, $\phi_a = 0.8$
- *vasa vasorum* drug uptake rate, $\alpha_v = 2 \times 10^{-5}\text{s}^{-1}$

Note that these values are for the drug Paclitaxel.

5.4.1 Therapeutic ratios

Experimental data (Toiyama *et al.* 2007) suggests that the minimum therapeutic and toxic tissue concentrations for Paclitaxel are 10 μ mol m^{-3} and 10 m mol m^{-3} respectively. To find the corresponding lower and upper bounds on the C_i concentrations, consider the equilibrium ratio C_i/C_e.
Recall that the cellular uptake equation is

$$(1-\phi_m)\frac{\partial C_i}{\partial t} = \alpha_i \left(C_e - \frac{C_i}{K_i} \right). \tag{5.4.24}$$

In equilibrium, $\partial C_i/\partial t = 0$. Thus

$$C_i = K_i C_e. \tag{5.4.25}$$

So with $K_i = 15$ for Paclitaxel, it is expected that the C_i concentrations will be 15 times greater than the corresponding extracellular concentrations. This would suggest a therapeutic cellular concentration lower and upper bound of 150 μ mol m^{-3} and 150 m mol m^{-3}. This gives a therapeutic ratio C_i(toxic)/C_i(min therapeutic) of 1000. In the chosen non-dimensionalisation, all concentrations are scaled with the initial concentration coated on the stent, so that the initial concentration in the non-dimensional model is $C_0^N = C_0/C_0 = 1$, where N stands for normalized. Because all concentrations are normalized in the same way, the therapeutic ratio

in both the dimensional and the non-dimensional model is 1000.

5.4.2 Estimating initial drug concentration on the stent

In the non-dimensional model,

$$C_i^N(max) = \frac{C_i(max)}{C_0}. \tag{5.4.26}$$

Here $C_i^N(max)$ denotes the normalized maximum cellular concentration obtained by the model, and $C_i(max)$ denotes the actual experimental toxic cellular concentration. C_0 is the initial stent coating concentration. Hence, using (5.4.26) the drug concentration required to be coated on the stent initially, such that the toxic concentration level is never surpassed, can be computed. Rearranging (5.4.26) gives

$$C_0 = \frac{C_i(max)}{C_i^N(max)} = \frac{0.15 \text{ mol m}^{-3}}{C_i^N(max)}. \tag{5.4.27}$$

It must be stressed that C^0_{equiv} (see §5.4) assumes a therapeutic ratio of 1000 and that other drugs with different properties may have different therapeutic ratios.

5.4.3 Results

In the sensitivity analysis that follows, ξ represents the control value of the parameter considered: $\xi^{(-)}$ an order of magnitude lower; $\xi^{(+)}$ and order of magnitude higher; $\xi^{(--)}$ two orders of magnitude lower, and so on. By varying the model parameters in this way, one can ascertain their relative importance. Firstly, the parameters in the model II are varied before considering the effect of the topcoat and plaque. The results are presented in Tables $5.2 - 5.13$.

It should be emphasized that the results are based on the assumption that the toxic

	$v^{(+)}$	v	$v^{(-)}$
$C_i(max)$ @ time (h)	0.0058 @4.6	0.0472 @8.4	0.1030 @17.4
$maxgrad$ @ time (h)	0.0030 @0.5	0.0389 @ 4	0.0903 @ 12.5
$T_{>min}$ (h)	0.4	1.4	2
$T_{therapeutic}$	564 h (24d)	715 h (30d)	1795 h (62d)
T_{empty} (h)	5	7	15
C^0_{equiv}	25.9	3.2	1.5

Table 5.2: Varying transmural velocity, v

level should never be reached. In practice it is, of course, possible for toxic levels of the drug to be achieved due to the enormous variation in the various properties of diseased arteries between patients. In most cases, the numerical results indicated that when some physiological initial polymer paclitaxel concentrations (such as 20 mol m^{-3} and 100 mol m^{-3}) were used, toxicity was reached very quickly, usually within the first hour of implantation and frequently within the first fifteen minutes. For this reason, and also since polymer coating drug concentrations vary, the sensitivity analysis was conducted on the assumption that the maximum possible cellular concentration is the toxic one; the C^0_{equiv} value then gives the maximum C_0 such that toxicity is never reached. In some cases, such as $\alpha_i^{(-)}$ coupled with $v^{(+)}$, it was observed that large C_0 values of up to 247 mol m^{-3} were possible without toxicity ever being reached. In the tables which follow, 'h' represents hours and 'd' represents days.

5.4.4 Model II

Table 5.2 clearly shows that model II is very sensitive to the parameter v. Increasing v by a factor of ten reduces the maximum cellular concentration by a factor of eight. This implies that the polymer would need to be coated with eight

	$D_p^{(+)}$	D_p	$D_p^{(-)}$	$D_p^{(--)}$
$C_i(max)$ @ time (h)	0.0476 @7	0.0472 @8.4	0.0396 @24.4	0.0197 @ 50.1
$maxgrad$ @ time (h)	0.0418 @2.9	0.0389 @ 4	0.0222 @10.6	0.0109 @4.2
$T_{>min}$ (h)	1.3	1.4	1.4	1.3
$T_{therapeutic}$	710 h (29.6d)	715 h (30d)	744 h (31d)	1044 h (44d)
T_{empty}	4 h	7 h	51 h	497 h (21d)
C^0_{equiv}	3.2	3.2	3.8	7.6

Table 5.3: Varying polymer diffusion coefficient, D_p

	$D_m^{(+)}, D_a^{(+)}$	D_m, D_a	$D_m^{(-)}, D_a^{(-)}$	$D_m^{(-)}, D_a$	$D_m, D_a^{(+)}$
$C_i(max)$ @ time (h)	0.0229 @8.7	0.0472 @8.4	0.0557 @5.7	0.0557 @5.7	0.0472 @8.3
$maxgrad$ @ time (h)	0.0132 @ 6.4	0.0389 @ 4	0.0542 @ 4.5	0.0544 @ 4.6	0.0428 @ 5.7
$T_{>min}$ (h)	0.3	1.4	3.9	4	1.5
$T_{therapeutic}$	673 h (28d)	715 h (30d)	574 h (24d)	577 h (24d)	693 h (29d)
T_{empty} (h)	6	7	6	6	7
C^0_{equiv}	6.6	3.2	2.7	2.7	3.2

Table 5.4: Varying media and adventitia diffusion coefficients, D_m, D_a

	$\alpha_i^{(+)}$	α_i	$\alpha_i^{(-)}$
$C_i(max)$ @ time (h)	0.2289 @3.2	0.0472 @8.4	0.0059 @18
$maxgrad$ @ time (h)	0.2316 @3	0.0389 @ 4	0.0042 @4
$T_{>min}$ (h)	1.5	1.4	1.4
$T_{therapeutic}$	290 h (12d)	715 h (30d)	5737 h (239d)
T_{empty} (h)	7	7	8
C^0_{equiv}	0.7	3.2	25.4

Table 5.5: Varying drug uptake rate, α_i

	$K_i^{(+)}, K_a^{(+)}$	K_i, K_a	$K_i^{(-)}, K_a^{(-)}$
$C_i(max)$ @ time (h)	0.0513 @14.2	0.0472 @8.4	0.0326 @3.9
$maxgrad$ @ time (h)	0.0401 @4.1	0.0389 @ 4	0.0306 @3
$T_{>min}$ (h)	1.4	1.4	1.3
$T_{therapeutic}$	7810 h (325d)	715 h (30d)	83 h (3.5d)
T_{empty} (h)	7	7	7
C^0_{equiv}	2.9	3.2	4.6

Table 5.6: Varying partition coefficient, K_i

	$\alpha_v = 0$	α_v	$\alpha_v^{(++)}$	$\alpha_v^{(++++)}$
$C_i(max)$ @ time (h)	0.0472 @ 8.4	0.0472 @8.4	0.0472 @8.3	0.0471 @ 8.2
$maxgrad$ @ time (h)	0.0388 @ 4	0.0389 @ 4	0.0429 @6.1	0.0478 @8.1
$T_{>min}$ (h)	1.4	1.4	1.4	2.2
$T_{therapeutic}$	712 h (30d)	715 h (30d)	663 h (28d)	360 h (15d)
T_{empty} (h)	7	7	7	7
C^0_{equiv}	3.2	3.2	3.2	3.2

Table 5.7: Varying drug loss to *vasa vasorum*, α_v

times the initial concentration to reach the same $C_i(max)$ as the $v = 10^{-8}\text{ms}^{-1}$ case. The media profile is significantly more uniform, as can be seen by comparing the $maxgrad$ values. With a larger v, the drug takes less time to have an effect, but the effect does not last as long ($T_{therapeutic}$ reduced by six days in this case). The effect of reducing v by a factor of ten is to more than double $C_i(max)$, give a less uniform profile, and to significantly increase $T_{therapeutic}$ by 32 days (more than double). As has already been discussed, there is the implication in the literature (for example in Pontrelli and de Monte 2007 and Zunino 2004) that the magnitude of the transmural velocity should be of order 10^{-8}ms^{-1} and negligible in comparison with diffusion. However, there is some clinical evidence (Baldwin, Wilson, Gradus-Pizlo, Wilensky & March 1997) from experiments on diseased arteries that suggests that the value may be an order of magnitude larger. This difference is quite significant since it results in an order of magnitude increase in the Peclet number. Clearly, because of the significant effect it has on the markers, it is important that the parameter v is measured accurately.

Varying the polymer diffusivity in Table 5.3, it is found that this has little effect on most of the markers. However, the value of D_p has a substantial influence on T_{empty}. By reducing D_p by one or two orders of magnitude, the polymer empty time can be increased by factors of seven (44 hours) and 71 (20 days), respectively. The lowest of these values, $D_p^{(--)}$, reduces $C_i(max)$ by a factor of two which implies that one would be required to double C_0 (the initial drug concentration in the polymer) to reach the same maximum concentration as obtained by the standard D_p value. However, this may be beneficial since the therapeutic time is increased by two weeks.

Turning to Table 5.4 and the effect of the media diffusion coefficient, it is found that $D_m^{(+)}$ would require C_0 to be twice as large to reach the same $C_i(max)$

as the control D_m value, with the result that $T_{therapeutic}$ is reduced by two days. The diffusion coefficient $D_m^{(-)}$ has a limited effect on the markers, with the only significant result being that $T_{therapeutic}$ is reduced by six days. This appears to be counter-intuitive, since one would not expect both a higher and a lower D_m to give rise to a reduction in $T_{therapeutic}$. One might expect a faster diffusion to result in a quicker clearance of drug and thus a lower $T_{therapeutic}$. It seems the interplay between diffusion and binding in the media is non-trivial, and may lead to trade-offs. Varying D_m has little effect on polymer empty time and changing D_a relative to D_m does not significantly affect the results.

The markers appear to be extremely sensitive to the value chosen for the smooth muscle cell drug uptake rate, α_i, as can be seen in Table 5.5. It is observed that $\alpha_i^{(+)}$ increases $C_i(max)$ by a factor of five, whilst $\alpha_i^{(-)}$ can reduce $C_i(max)$ by a factor of eight. Changes to α_i have a large effect on the therapeutic time. The larger value, $\alpha_i^{(+)}$, reduces $T_{therapeutic}$ by a factor of 2.5 (i.e. 18 days) whereas $\alpha_i^{(-)}$ increases $T_{therapeutic}$ significantly to 209 days, a factor of eight.

In Table 5.6, changes in smooth muscle cell partition coefficient are considered. Noticeably, $K_i^{(+)}$ can greatly increase $T_{therapeutic}$ by a factor of eleven (an increase of almost ten months) without significantly changing $C_i(max)$. Decreasing K_i by a factor of ten has the opposite effect, reducing $T_{therapeutic}$ by a factor of nine to 3.5 days. The value of K_i appears to have little effect on T_{empty}. It is interesting to compare the results from Table 5.6 with two experimental observations in the literature. Creel *et al.* (2000) concluded that drugs which have a higher degree of liphophilia (higher K_i) may result in a more uniform drug distribution in the arterial wall. The results from Table 5.6 show that increasing K_i actually increases $maxgrad$, suggesting a less uniform profile. This apparent discrepancy may be due to the rather simplistic measure of uniformity used, that being the gradient

of the line joining the cellular concentration points at the polymer/media and media/adventitia interfaces. Clearly, this method is unable to account for the possible significant variation between the two endpoints. The results do, however, agree with experimental results in the literature (Hwang *et al.* 2001, Creel *et al.* 2000) which suggest that lipophilic (hydrophobic) drugs lead to higher arterial wall deposition than lipophobic (hydrophilic) drugs. This is demonstrated through the increase in $C_i(max)$ with increasing K_i.

The only markers that vary with the parameter α_v are $maxgrad$ and $T_{therapeutic}$. In Table 5.7 it is clear that increasing α_v (uptake rate into *vasa vasorum*) results in a less uniform distribution and also a reduction in the therapeutic time. However, increasing α_v by two orders of magnitude results in only two less therapeutic days. The parameter α_v must be increased by a factor of 10^4 for the therapeutic time to be reduced by a half. If it is reasonable to assume that the rate at which drug is lost to the vasa vasorum is approximately of the order of α_i, or even negligible, then the control value is acceptable, and indicates that the adventitia does not have a large effect on the results in the media region.

5.4.5 Model III: The effect of adding a topcoat

In this section an examination is carried out into how the presence of a drug-free polymer topcoat layer can affect the results. The thickness of the topcoat as well as the topcoat diffusion coefficient are varied. Table 5.8 compares the topcoat code with $l_T^{(1)} = 0$m (no topcoat), $l_T^{(2)} = 10^{-6}$m, $l_T^{(3)} = 2 \times 10^{-6}$m, $l_T^{(4)} = 5 \times 10^{-6}m$. The effect of adding a topcoat with the same diffusion coefficient as the drug-filled polymer is to reduce $C_i(max)$. The presence of the topcoat has little effect on $T_{therapeutic}$, even if the total polymer length (polymer + topcoat) is increased by 50%. There is also no significant effect on T_{empty}. For $l_T^{(4)}$, $C_i(max)$ is five times

	$l_T^{(1)}$	$l_T^{(2)}$	$l_T^{(3)}$	$l_T^{(4)}$
$C_i(max)$	0.0472	0.0399	0.0206	0.0099
@ time (h)	@8.4	@ 9.2	@ 8.9	@ 9.0
$maxgrad$	0.0389	0.0322	0.0168	0.0081
@ time (h)	@ 4	@ 4.6	@ 4.5	@ 4.7
$T_{>min}$ (h)	1.4	1.5	1.5	1.7
$T_{therapeutic}$	715 h (30d)	713 h (30d)	712 h (30d)	753 h (31d)
T_{empty} (h)	7	8	7	7
C^0_{equiv}	3.2	3.8	7.3	15.2

Table 5.8: Varying topcoat thickness, l_T

	$D_T^{(+)}$	D_T	$D_T^{(-)}$	$D_T^{(--)}$
$C_i(max)$	0.0400	0.0399	0.0378	0.0258
@ time (h)	@ 8.6	@ 9.2	@ 15.1	@ 51.9
$maxgrad$	0.0329	0.0322	0.0259	0.0129
@ time (h)	@ 4.2	@ 4.6	@ 7.8	@ 3.6
$T_{>min}$ (h)	1.4	1.5	1.9	2.9
$T_{therapeutic}$	710 h (30d)	713 h (30d)	722 h (30d)	793 h (33d)
T_{empty} (h)	5	8	19	138
C^0_{equiv}	3.8	3.8	4.0	5.8

Table 5.9: Varying topcoat diffusion coefficient, D_T

lower, so C_0 is five times that of the case when there is no topcoat present. From Table 5.9 it is clear that the effect of decreasing the topcoat diffusion coefficient by a factor of ten is essentially the same as the effect of decreasing D_p. Decreasing D_T results in a reduction in $C_i(max)$. However, the most significant effect is on T_{empty}, which increases by eleven hours (over twice as long) for a tenfold reduction in D_T. Decreasing D_T further by another factor of ten has a similar effect, further increasing T_{empty} to 138 days, a factor of seventeen greater than that of the control case. Hence it is clear that by adding a topcoat and reducing D_T, T_{empty} can be significantly increased.

5.4.6 Model IV: The effect of the plaque

It would be useful to gain an understanding of how the relative proportion of plaque affects the results. Furthermore, as there is no data available for drug uptake to the plaque or its corresponding partition coefficient, it would be interesting to vary ϕ_{pl} and K_{pl} and observe the effect on the various markers. It is assumed (unless otherwise stated) that there is a standard cellular ratio of $\phi_i = 0.4$, a plaque uptake rate of $\alpha_{pl} = 2 \times 10^{-5}\text{s}^{-1}$, partition coefficient of $K_{pl} = 20$ and any additional plaque fills the extracellular space (thus decreasing ϕ_m). In Table 5.10, the plaque results are compared with $\phi_{pl}^{(1)} = 0$ (no plaque), $\phi_{pl}^{(2)} = 0.1$, $\phi_{pl}^{(3)} = 0.2$, $\phi_{pl}^{(4)} = 0.5$. Increasing the proportion of plaque has little effect on $C_i(max)$, $maxgrad$, and T_{empty}. However, there is a notable increase in $T_{therapeutic}$ with increasing plaque proportion. This seems to suggest that a patient with a higher degree of atherosclerosis may receive therapeutic levels of drug for a longer period of time than those with a lower degree of disease, reinforcing the idea that the plaque may act as a reservoir for drug. For a very high proportion of plaque, $\phi_{pl}^{(4)}$, $T_{therapeutic}$ is increased by over two weeks (50% greater than the no plaque case).

Table 5.11 displays the results of varying the plaque uptake parameter, α_{pl}, with $\phi_{pl} = 0.2$. The value of α_{pl} has little effect on most of the markers. However, the effect of $\alpha_{pl}^{(+)}$ is to slightly reduce $C_i(max)$ as well as reducing $T_{therapeutic}$ by one day. It does, however, take almost three times as long to reach this maximum concentration. For $\alpha_{pl}^{(-)}$ there is a slight increase in $C_i(max)$, whilst $T_{therapeutic}$ is increased by five days.

The only result of real interest, due to varying K_{pl}, is $T_{therapeutic}$ which reduces by two days for $K_{pl}^{(1)}$ and increases by three days for $K_{pl}^{(3)}$. This can be seen in Table 5.12.

	$\phi_{pl}^{(1)} = 0$	$\phi_{pl}^{(2)} = 0.1$	$\phi_{pl}^{(3)} = 0.2$	$\phi_{pl}^{(4)} = 0.5$
$C_i(max)$	0.0472	0.0427	0.0426	0.0430
@ time (h)	@8.4	@7.5	@6.8	@5.6
$maxgrad$	0.0389	0.0360	0.0354	0.0322
@ time (h)	@ 4	@ 3.8	@ 3.6	@ 3.6
$T_{>min}$ (h)	1.4	1.1	0.9	0.3
$T_{therapeutic}$	715 h (30d)	758 h (32d)	805 h (34d)	1071 h (45d)
T_{empty} (h)	7	7	6	6
C_{equiv}^0	3.2	3.5	3.5	3.5

Table 5.10: Varying the proportion of plaque, ϕ_{pl}

	$\alpha_{pl}^{(+)}$	α_{pl}	$\alpha_{pl}^{(-)}$
$C_i(max)$	0.0364	0.0426	0.0464
@ time (h)	@ 19.6	@6.8	@ 7.2
$maxgrad$	0.0331	0.0360	0.0363
@ time (h)	@10.7	@ 3.6	@ 3.3
$T_{>min}$ (h)	1.2	0.9	0.9
$T_{therapeutic}$	797 h (33d)	805 h (34d)	943 h (39d)
T_{empty} (h)	7	6	7
C_{equiv}^0	4.1	3.5	3.2

Table 5.11: Varying plaque uptake rate, α_{pl}

Finally, in Table 5.13 the effect of varying the transmural velocity with plaque is considered. Four cases are examined (i) $\phi_{pl}^{(3)}$, $v = 10^{-8}\text{ms}^{-1}$, (ii) $\phi_{pl}^{(3)}$, $v = 10^{-7}\text{ms}^{-1}$, (iii) $\phi_{pl}^{(4)}$, $v = 10^{-8}\text{ms}^{-1}$, (iv) $\phi_{pl}^{(4)}$, $v = 10^{-7}\text{ms}^{-1}$. If the presence of plaque resulted in a greater transmural velocity of $10^{-7}ms^{-1}$, then the effect would be to significantly reduce $C_i(max)$, whilst at the same time reducing $T_{therapeutic}$.

	$K_{pl}^{(1)} = 10$	$K_{pl}^{(2)} = 20$	$K_{pl}^{(3)} = 30$
$C_i(max)$ @ time (h)	0.0429 @ 7	0.0426 @ 6.8	0.0426 @ 6.7
$maxgrad$ @ time (h)	0.0354 @3.6	0.0354 @ 3.6	0.0354 @ 3.6
$T_{>min}$ (h)	0.9	0.9	0.9
$T_{therapeutic}$	756 h (32d)	805 h (34d)	880 h (37d)
T_{empty} (h)	7	6	6
C_{equiv}^{0}	3.5	3.5	3.5

Table 5.12: Varying plaque partition coefficient, K_{pl}

	(i)	(ii)	(iii)	(iv)
$C_i(max)$ @ time (h)	0.0426 @6.8	0.0056 @ 4.6	0.0430 @ 5.6	0.0056 @4.6
$maxgrad$ @ time (h)	0.0354 @ 3.6	0.0026 @ 0.3	0.0322 @ 3.6	0.0018 @ 0.1
$T_{>min}$ (h)	0.9	0.3	0.3	0.1
$T_{therapeutic}$	805 h (34d)	580 h (24 d)	1071 h (45d)	586 h (24d)
T_{empty} (h)	6	5	6	5
C_{equiv}^{0}	3.5	27	3.5	27

Table 5.13: Varying transmural velocity with plaque: (i) $\phi_{pl}^{(3)}$, $v = 10^{-8}\text{ms}^{-1}$, (ii) $\phi_{pl}^{(3)}$, $v = 10^{-7}\text{ms}^{-1}$, (iii) $\phi_{pl}^{(4)}$, $v = 10^{-8}\text{ms}^{-1}$, (iv) $\phi_{pl}^{(4)}$, $v = 10^{-7}\text{ms}^{-1}$

	(1) v, α_i, K_i	(2) v^+	(3) α_i^+	(4) K_i^+	(5) v^-	(6) α_i^-
$C_i(max)$	0.0472 @8.4 h	0.0058 @4.6 h	0.2289 @3.2h	0.0513 @14.2 h	0.1030 @17.4 h	0.0059 @18 h
Change		↓	↑	↑	↑	↓

Table 5.14: varying v, α_i and K_i

	(7) K_i^-	(8) v^+, α_i^+	(9) v^+, α_i^-	(10) v^+, α_i^+, K_i^+
$C_i(max)$	0.0326 @3.9 h	0.0439 @2.2 h	6.0758×10^{-4} @7.1 h	0.0563 @4.6h
Change	↓	↓	↓	↑

Table 5.15: varying v, α_i and K_i

5.4.7 Closer analysis of the most sensitive parameters

The sensitivity analysis revealed that the most sensitive parameters to change were the drug uptake rate, α_i, the transmural velocity, v, and the partition coefficient, K_i. Here the effect of varying combinations of these parameters on the maximum cellular concentration obtained is investigated. The values considered are:

- $v^{(-)} = 10^{-9} ms^{-1}$, $v^{(+)} = 10^{-7} ms^{-1}$,
- $\alpha_i^{(-)} = 2 \times 10^{-6} s^{-1}$, $\alpha_i^{(+)} = 2 \times 10^{-4} s^{-1}$,
- $K_i^{(-)} = 1.5$, $K_i^{(+)} = 150$.

The following conclusions are drawn from Tables $5.14 - 5.17$:

- The effect of increasing v is greater than the effect of increasing α_i [(2), (3) and (8)]

	(11) v^-, α_i^-	(12) v^-, α^+	(13) v^-, α_i^-, K_i^-	(14) v^+, α_i^+, K_i^-
$C_i(max)$	0.3194 @3.8 h	0.0230 @75.1 h	0.0163 @33.2 h	0.0214 @0.5 h
Change	↑	↓	↓	↓

Table 5.16: varying v, α_i and K_i

	(15) v^+, α_i^-, K_i^-	(16) v^-, α_i^+, K_i^+	(17) v^-, α_i^+, K_i^-	(18) v^-, α_i^-, K_i^+
$C_i(max)$	5.7745×10^{-4} @4.6h	0.4059 @6.7 h	0.1286 @1.4 h	0.0248 @123 h
Change	$\downarrow$	$\uparrow$	$\uparrow$	$\downarrow$

Table 5.17: varying v, α_i and K_i

- The effects of increasing v whilst decreasing α_i are additive as are the effects of decreasing v while increasing α_i [(2-3), (5-6), (9) and (11)]
- The effect of increasing α_i with K_i is greater than the effect of increasing v [(2) and (10)]
- The effect of reducing α_i is greater than the effect of reducing v [(5), (6) and (11)]. Also, the effect of reducing α_i with K_i is greater than the effect of reducing v [(5) and (13)]
- The effect of increasing v whilst decreasing K_i is greater than the effect of increasing α_i [(3) and (14)]
- The effects of increasing v whilst reducing α_i with K_i are additive [(2) and (15)] as are the effects of decreasing v whilst increasing α_i with K_i [(5) and (16)]
- The effect of reducing v whilst increasing α_i is greater that the effect of reducing K [(5) and (17)]
- The effect of decreasing α_i is greater than the effect of decreasing v whilst increasing K_i [(6) and (18)]

5.5 Release profiles

Experimentalists are principally interested in release rates from different types of stents. Here it is indicated how release profiles can be computed, while, at the same time, establishing drug empty times from the polymer. The mass (in *mol*) of drug on the polymer coated stent at time t is given by

$$M(t) = \int_0^{l_p} C_p(x,t)dx. \tag{5.5.28}$$

Clearly, for a constant initial stent concentration, C_0, then

$$M(0) = M_0 = l_p C_0. \tag{5.5.29}$$

The mass is non-dimensionalized with respect to the initial mass coating on the stent, M_0

$$M^N = M/M_0 = M/(l_p C_0)$$

Applying this non-dimensionalization to (5.5.28) gives rise to

$$M^N(t^N) = \frac{1}{L}\int_0^L C_p^N(x^N,t^N)dx^N. \tag{5.5.30}$$

Using the extended trapezoidal rule, the integral (5.5.30) can be approximated for each time t as follows

$$M(t) = \frac{1}{2n}\left[C_p(x_1,t) + 2\left(C_p(x_2,t) + C_p(x_3,t) + ... + C_p(x_n,t)\right) + C_p(x_{n+1},t)\right], \tag{5.5.31}$$

where

$$x_i = (i-1)\Delta x, \quad i = 1,2,...,n+1, \quad \Delta x = L/n.$$

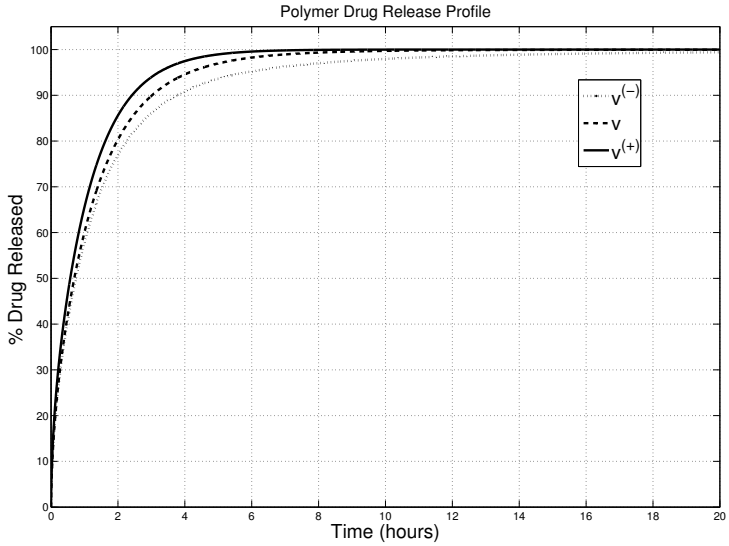

Figure 5.1: The effect of transmural velocity on release

Note that the superscript N has been omitted for convenience. Figures $5.1 - 5.7$ display the release profiles for variations in the parameters.

Figure 5.1 clearly shows that, as expected, the greater the value of the transmural velocity, the greater the release. With the control value, v, it takes approximately seven hours for the stent to empty, compared with five hours and fifteen hours for $v^{(+)}$ and $v^{(-)}$, respectively. One parameter that does have a large effect on the release characteristics is the polymer diffusion coefficient, D_p, as can be seen in Figure 5.2. By reducing the control value by two orders of magnitude, one can extend the residence time of the drug in the polymer by three weeks. It is noticeable, however, that over 30% of the drug is released within the first day, and 65% within the first four days. The effect of varying the media diffusion coefficient, D_m, on release is not significant (Figure 5.3). However, it is not found that greater values of D_m result in a significantly more rapid empty time, as one might expect. Similarly the drug uptake rate has virtually no effect on release from the stent as

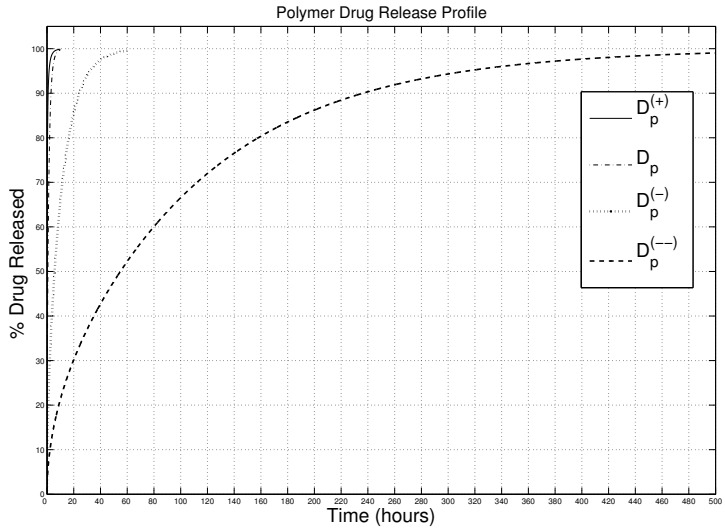

Figure 5.2: The effect of polymer diffusion coefficient on release. Note that the profiles for $D_p^{(+)}$, D_p and $D_p^{(-)}$ are only shown until the time when the polymer has emptied.

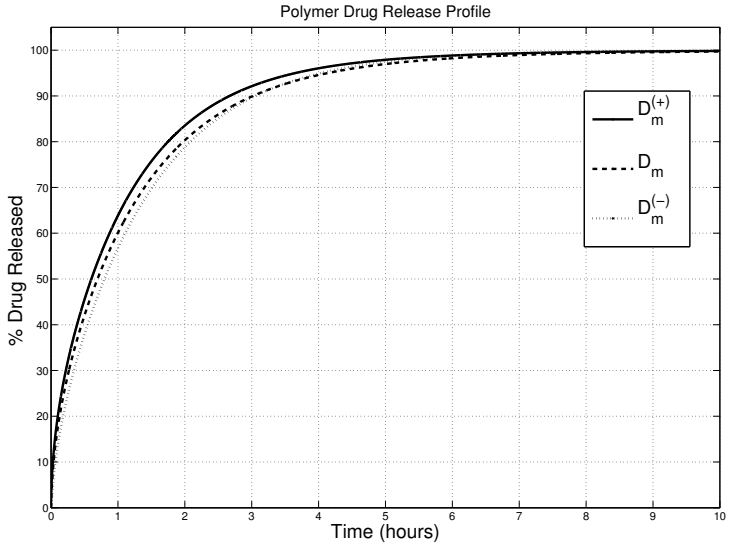

Figure 5.3: The effect of media diffusion coefficient on release

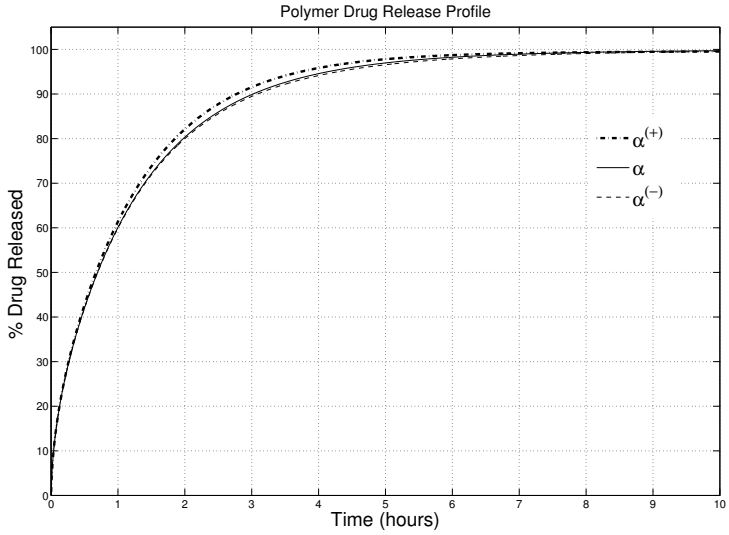

Figure 5.4: The effect of smooth muscle cell drug uptake rate on release

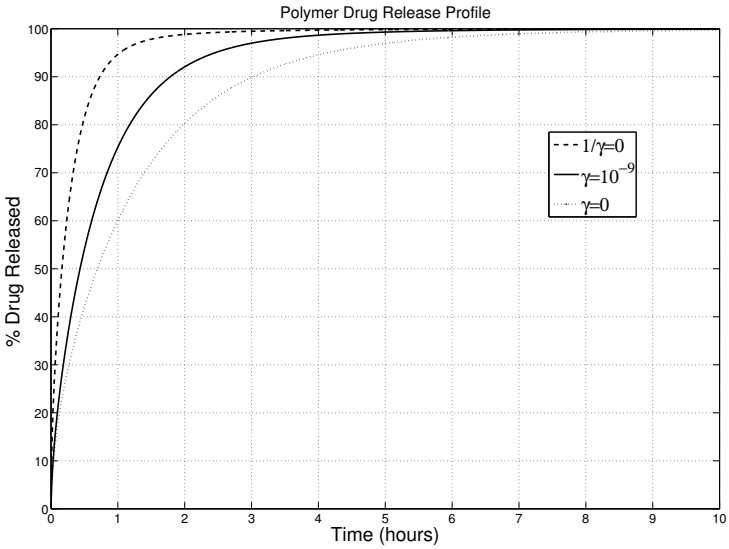

Figure 5.5: The effect of wire/polymer boundary condition on release

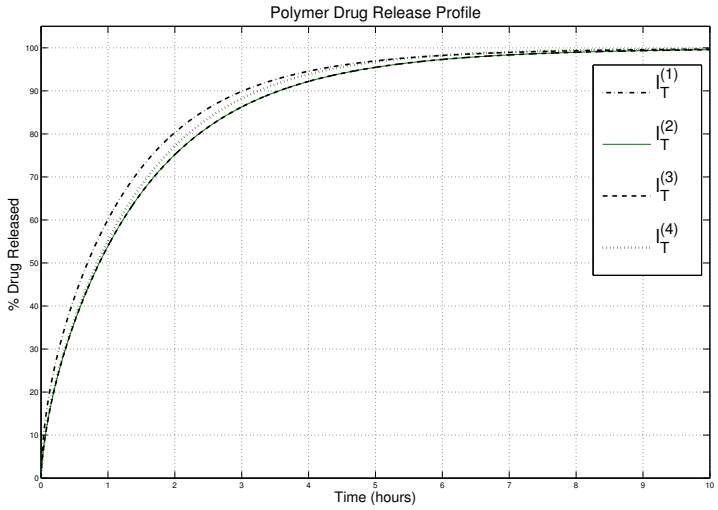

Figure 5.6: The effect of topcoat thickness on release

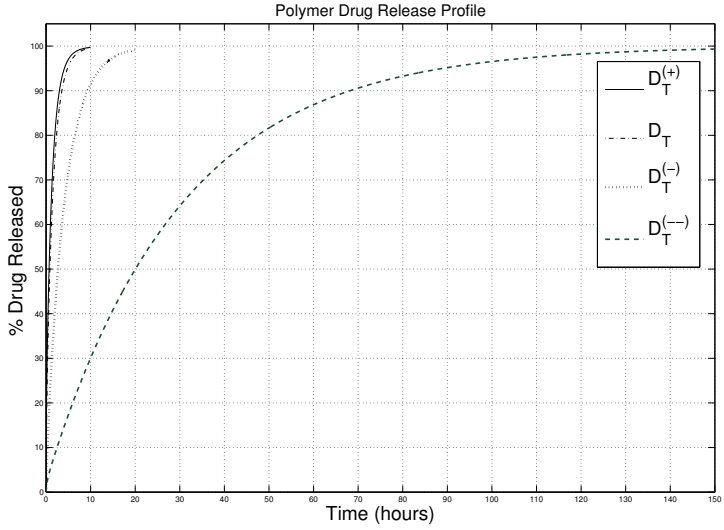

Figure 5.7: The effect of topcoat diffusion coefficient on release. Note that the profiles for $D_T^{(+)}$, D_T and $D_T^{(-)}$ are only shown until the time when the polymer has emptied.

can be seen in Figure 5.4. The same was true for changes in K_i and α_v. In Figure 5.5 the effect of the wire/polymer boundary condition on release is considered. The following general boundary condition is also employed:

$$-D_p \, \partial C_p / \partial x = \gamma C_p, \quad x = 0,$$

with γ constant. The control no-flux condition corresponds to $\gamma = 0$; the case $1/\gamma = 0$ is equivalent to the condition $C_p = 0$; that is, all the drug is washed away at the lumen. Also considered is an intermediate value, $\gamma = 10^{-9}\text{ms}^{-1}$. As one would expect, the $C_p = 0$ condition results in a considerably faster release from the stent. Decreasing the value of γ (which corresponds to a smaller flux out of the 'wire' end) results in a slower release from the polymer again as one would expect. Figure 5.6 confirms that increasing the thickness of a topcoat would slow down release and Figure 5.7, similar in nature to Figure 5.2, confirms that slower release can be obtained by choosing a smaller topcoat diffusion coefficient. Varying the properties of the plaque had virtually no effect on release from the stent and thus these profiles are not illustrated here.

5.6 Concentration Profiles

Whilst the sensitivity analysis has provided several interesting numerical results, it is often useful to represent results pictorially. In this section, normalized cellular concentration profiles are provided. In the first part, graphs of normalized cellular concentration versus time (over a three day period) at the polymer/media boundary, the media midpoint and the media/adventitia boundary are provided for the standard parameters (see §5.4), as well as variations of these. In the second part, normalized cellular concentration versus media thickness is plotted at five different

times over the first three days (1 hour, 4 hours, 1 day, 2 days, 3 days), again for the standard parameters as well as variations of these.

5.6.1 Normalized cellular concentration versus time

In Figure 5.8, it is observed that at each considered point, the cellular concentration rapidly builds up to some maximum value before slowly decreasing with time. As one might expect, the greatest concentrations are observed closest to the drug source, and the lowest concentrations are observed closed to the adventitia. The remaining figures will be compared to Figure 5.8. For the case of a faster transmural velocity (Figure 5.9), the three curves are much closer together, indicating a much more uniform drug concentration profile. In this case the maximum cellular concentration, which is significantly lower than the previous case, does not occur at the polymer/media boundary as one might expect; the maximum concentration at the media midpoint appears to be higher. In line with the sensitivity analysis, the maximum cellular concentration clearly occurs sooner when a faster transmural velocity is driving the drug through the system. In Figure 5.10, it is evident that the reduced polymer diffusion coefficient results in a slower transport of drug through the system. The maximum cellular concentration at each of the three considered points is not acheived as rapidly as with the faster polymer diffusion case. In Figure 5.11 the time taken to reach a maximum cellular concentration at each point is prolonged. The profiles in Figure 5.12 are similar to those in Figure 5.8. However, the faster media diffusion coefficient results in an increased maximum cellular concentration at each of the three considered points and less drug is uptaken into the media midpoint and media/adventita boundary cells in the first few hours. Perhaps this is due to the faster diffusion resulting in less drug being available for uptake into the cells in early stages. Decreasing the

drug uptake rate, as in Figure 5.13, results in the drug concentration at each of the considered points being maintained at high levels for a longer period of time. Thus despite the actual cellular concentrations being significantly lower than the case of a higher uptake rate constant, the drug is retained in the cells for longer. Figure 5.14 is similar to Figure 5.9 and shows that a s transmural velocity coupled with a slower media diffusion coefficient results in slower clearance of drug from the system, as one might expect. Finally, it is interesting to compare Figures 5.8, 5.13 and 5.15. These results clearly demonstrate that, decreasing the drug uptake rate at the same time as increasing the transmural velocity results in significanltly reduced maximum cellular concentrations; these concentrations are reached more rapidly and are maintained for significantly longer.

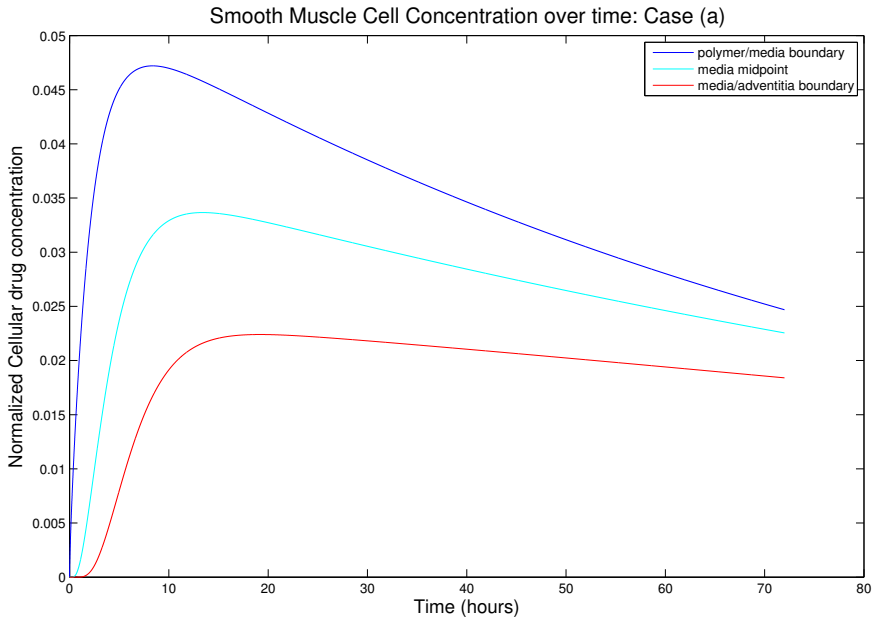

Figure 5.8: Standard parameters. Upper curve: polymer/media boundary. Middle curve: media midpoint. Lower curve: media/adventitia boundary

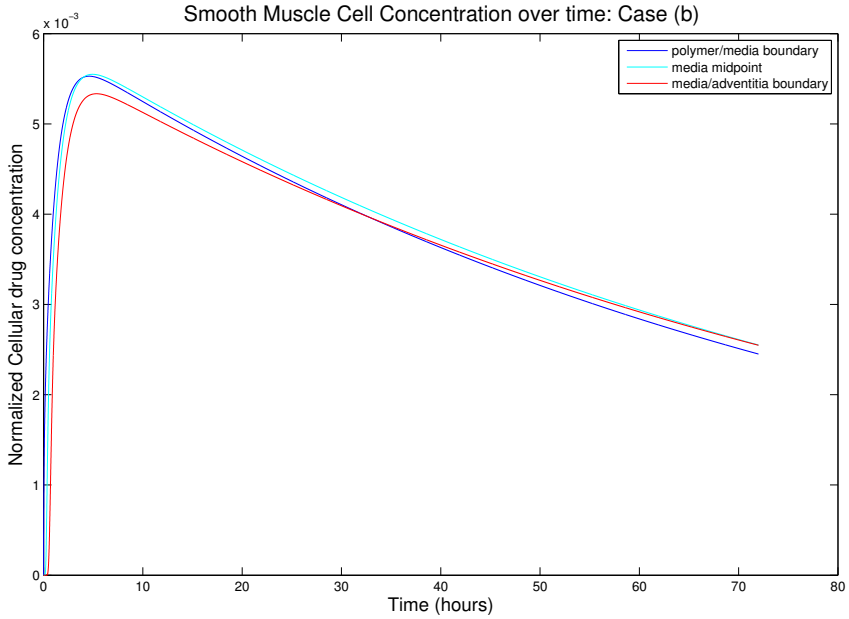

Figure 5.9: $v = 10^{-7}$ m s^{-1}. At early times: Upper curve: polymer/media boundary. Middle curve: media midpoint. Lower curve: media/adventitia boundary. At late times: Upper curve: media/midpoint. Middle curve: media/adventitia boundary. Lower curve: polymer/media boundary.

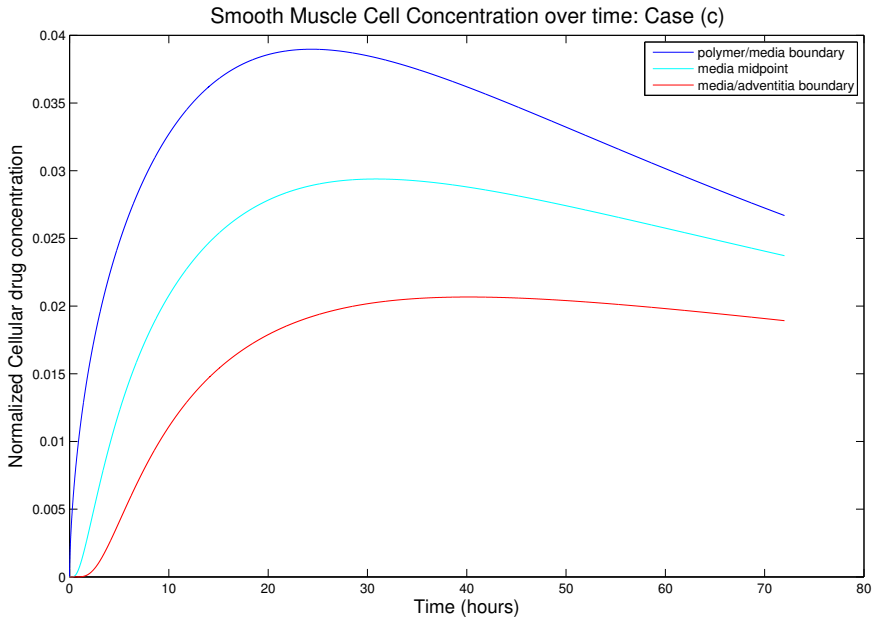

Figure 5.10: $D_p = 10^{-15}$ m^2 s^{-1}. Upper curve: polymer/media boundary. Middle curve: media midpoint. Lower curve: media/adventitia boundary

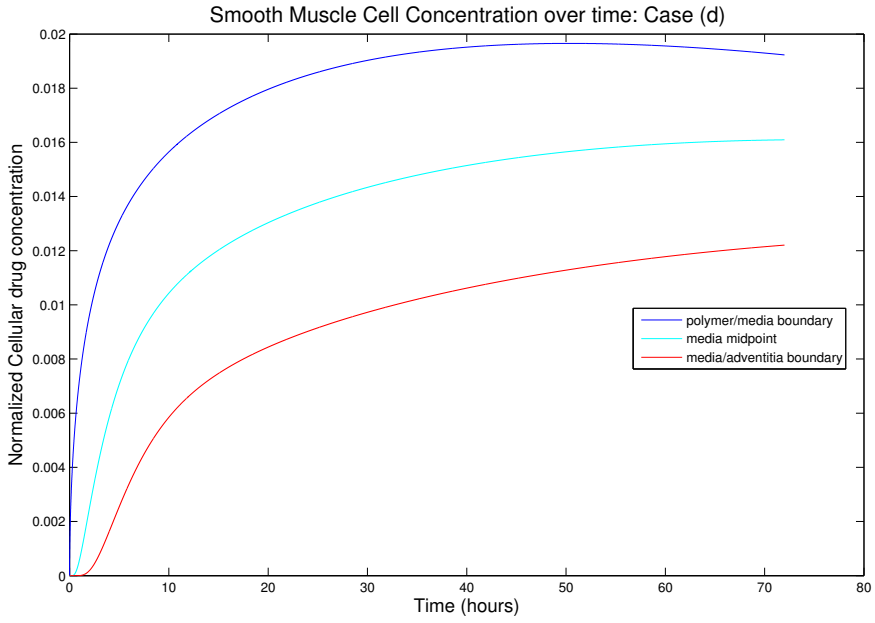

Figure 5.11: $D_p = 10^{-16}$ m^2 s^{-1}. Upper curve: polymer/media boundary. Middle curve: media midpoint. Lower curve: media/adventitia boundary

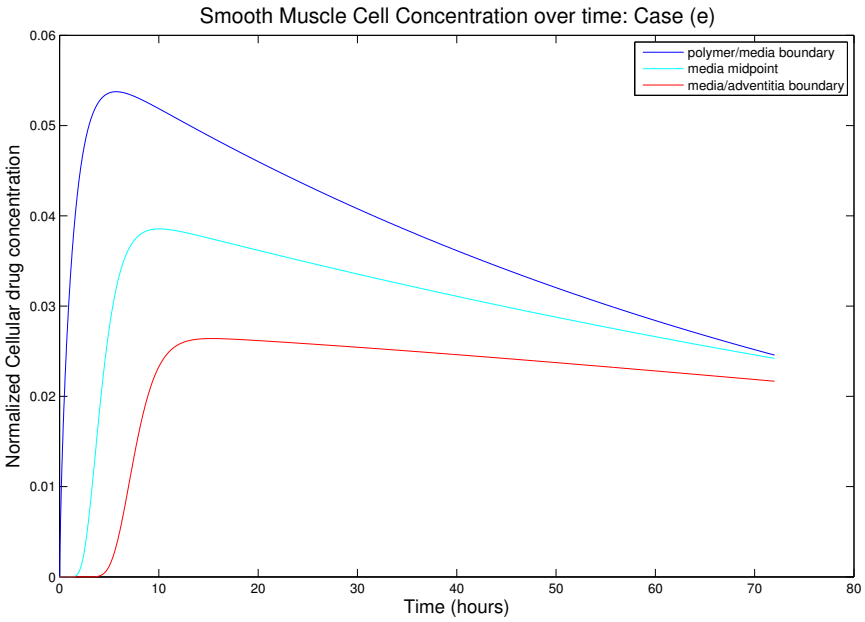

Figure 5.12: $D_m = 10^{-13}$ m^2 s^{-1}. Upper curve: polymer/media boundary. Middle curve: media midpoint. Lower curve: media/adventitia boundary

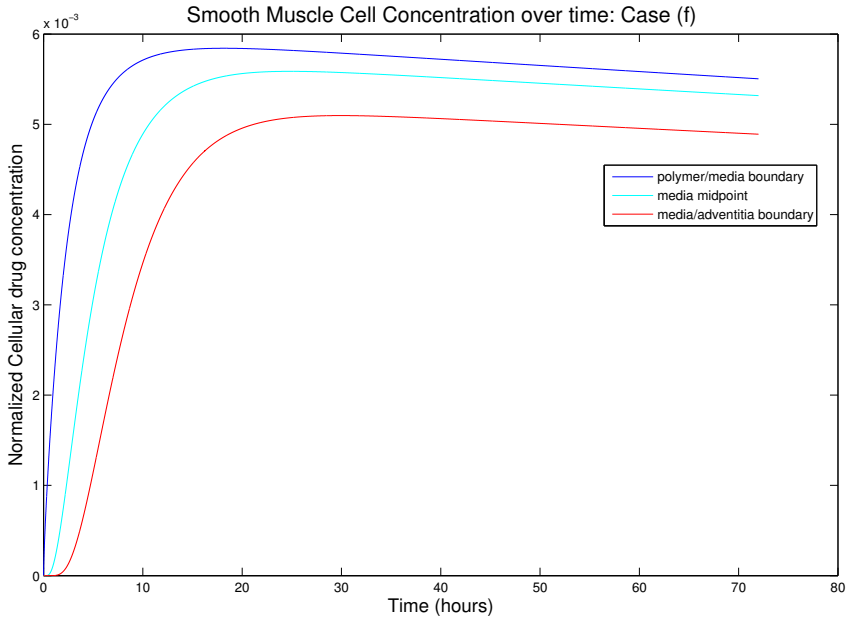

Figure 5.13: $\alpha_i = 2{\times}10^{-6}$ m^2 s^{-1}. Upper curve: polymer/media boundary. Middle curve: media midpoint. Lower curve: media/adventitia boundary

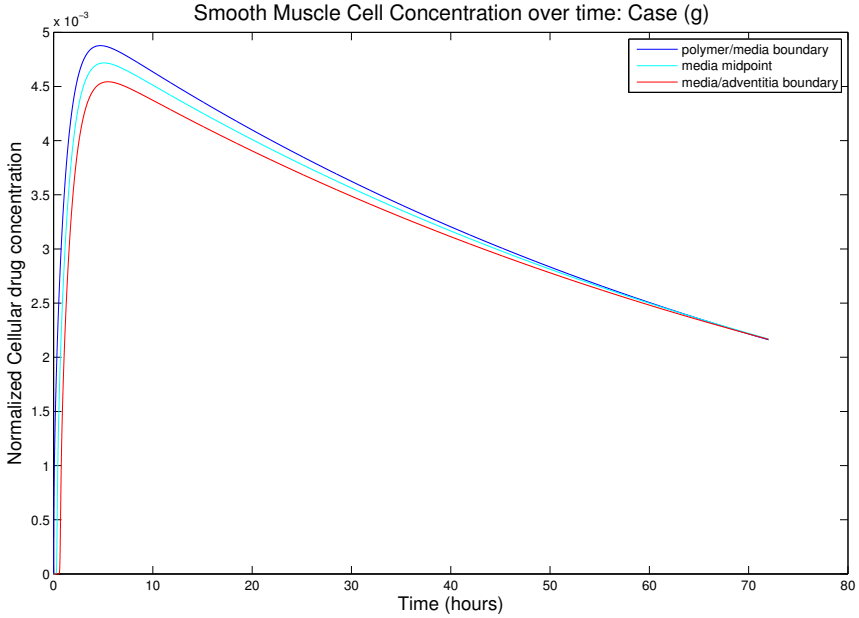

Figure 5.14: $v = 10^{-7}$ m s^{-1} and $D_m = 10^{-13}$ m^2 s^{-1}. Upper curve: polymer/media boundary. Middle curve: media midpoint. Lower curve: media/adventitia boundary

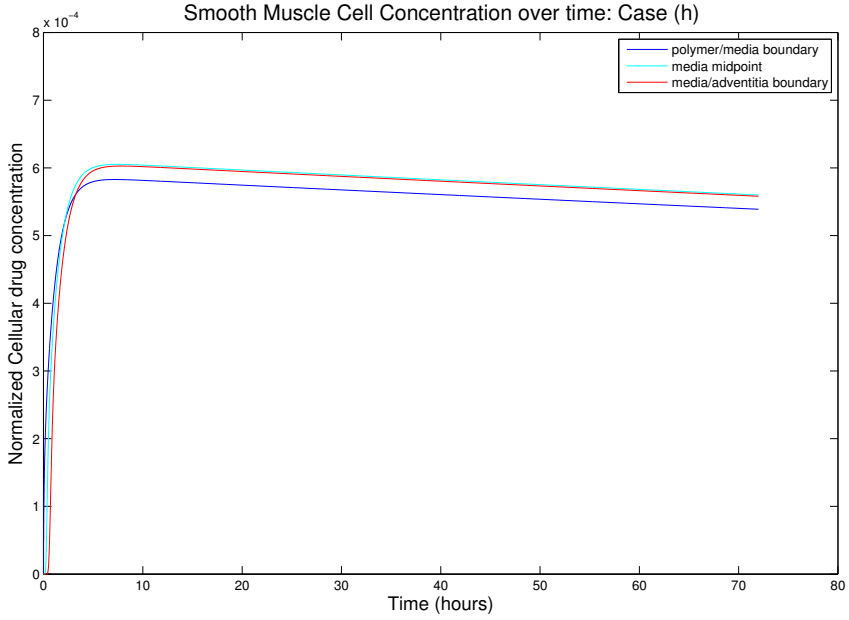

Figure 5.15: $v = 10^{-7}$ m s^{-1} and $\alpha_i = 2 \times 10^{-6}$ m^2 s^{-1}. At early times: Upper curve: polymer/media boundary. Middle curve: media midpoint. Lower curve: media/adventitia boundary. At late times: Upper curve: media/midpoint. Middle curve: media/adventitia boundary. Lower curve: polymer/media boundary.

5.6.2 Normalized cellular concentration versus media thickness

In Figure 5.16 it is observed that after one hour, the drug has begun to be uptake into cells closest to the drug source, but that the cellular concentrations nearest the adventitia are still zero. As time progresses, and the drug diffuses through the media, the concentration in cells nearest the source begins to decrease whilst the concentrations nearest the adventitia begin to increase. In Figure 5.17, the most noticeable feature is undoubtedly the significantly more uniform profiles due to the significantly increased Peclet number. The decreased transport resulting from a decreased polymer diffusion coefficient is displyed in Figures $5.18 - 5.19$. Figures 5.16 and 5.20 are comparable, indicating that a decreased media diffusion coefficient does not have a large effect on cellular concentration profiles. In Figure 5.22, similar profiles to 5.17 are observed, although a faster transmural velocity coupled with a slower media diffusion coefficient does result in faster clearance of drug from the system. The increased retention of drug by cells due to a lower drug uptake rate is displayed clearly in Figure 5.21. The retention of drug by cells is more striking when a faster transmural velocity is coupled with a slower drug uptake rate, as in Figure 5.23. It should be noted that in Figures 5.17, 5.19, 5.20 and 5.23 the 'kinks' at early times have been attributed to under-resolution and are remedied by choosing a finer mesh.

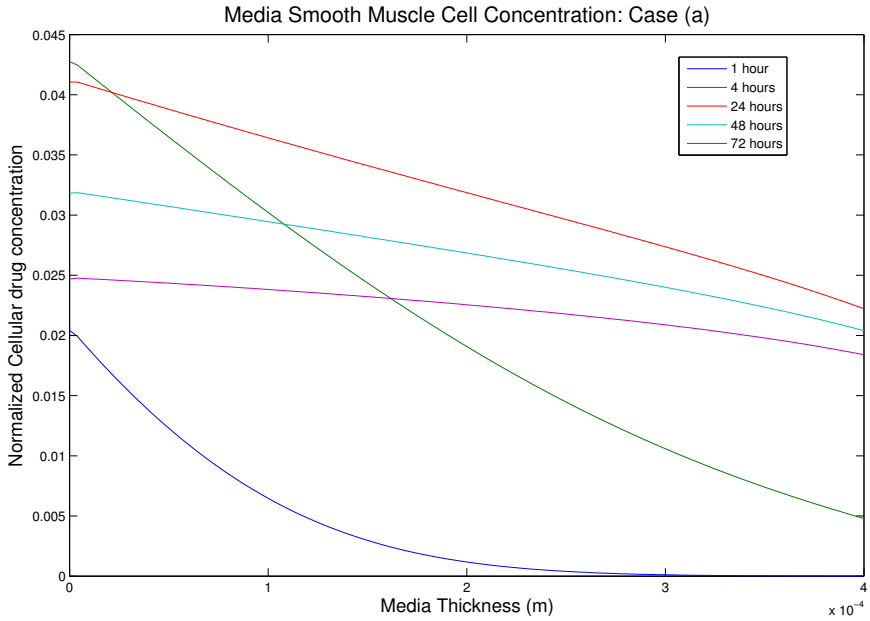

Figure 5.16: standard parameters. At $x = 0$, the lower and upper curves represent 1 hour and 4 hours respectively. Between 4 hours and 72 hours the drug concentration decreases in a monotonic fashion.

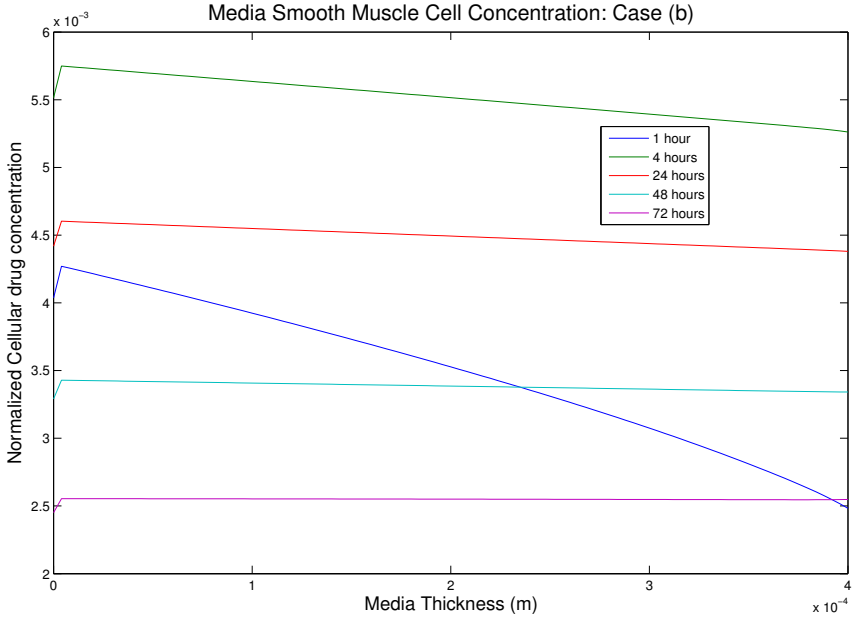

Figure 5.17: $v = 10^{-7}$ m s^{-1}. The middle and upper curves represent 1 hour and 4 hours respectively. Between 4 hours and 72 hours the drug concentration decreases in a monotonic fashion.

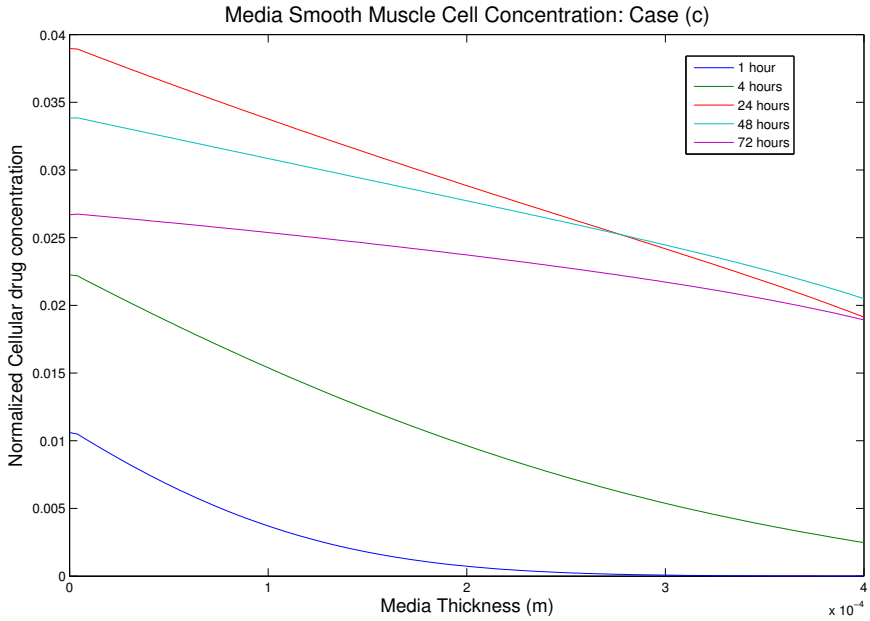

Figure 5.18: $D_p = 10^{-15}$ m^2 s^{-1}. At $x = 0$, the lowest curve represents 1 hour. Moving upwards, next is the 4 hour curve, followed by 72 hours, 48 hours and 24 hours.

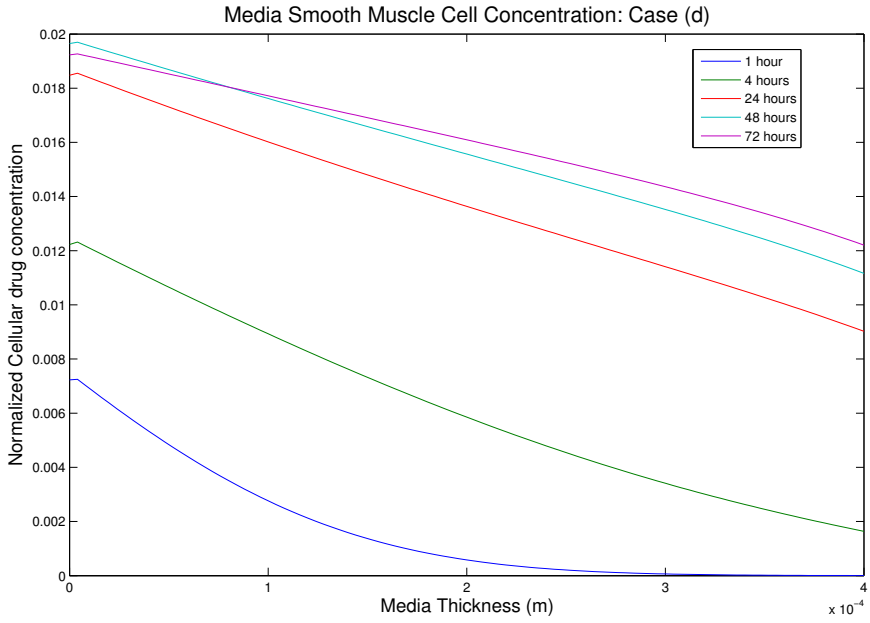

Figure 5.19: $D_p = 10^{-16}$ m^2 s^{-1}. At $x = 0$, the lowest curve represents 1 hour. Moving upwards, next is the 4 hour curve, followed by 24 hours, 72 hours and 48 hours.

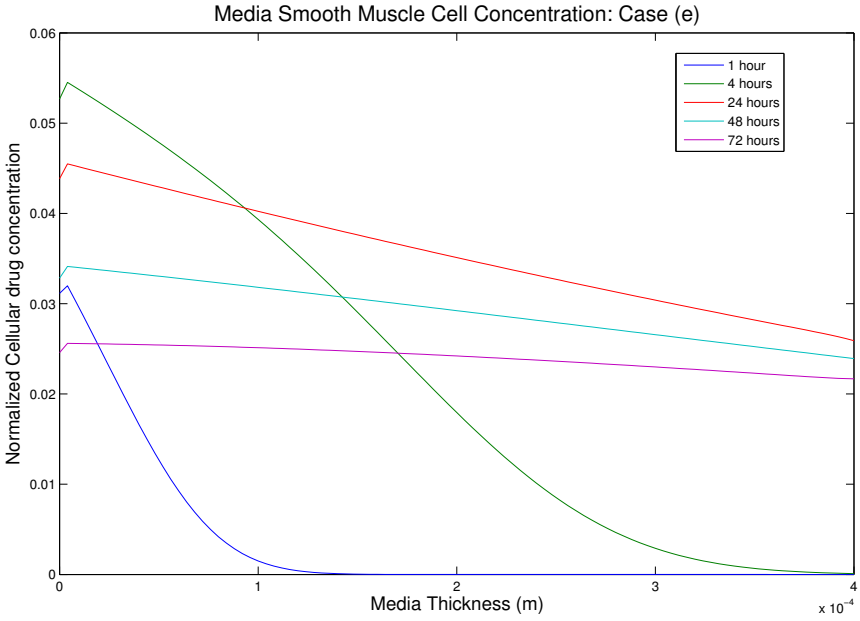

Figure 5.20: $D_m = 10^{-13}$ m^2 s^{-1}. At $x = 0$, the lower and upper curves represent 1 hour and 4 hours respectively. Between 4 hours and 72 hours the drug concentration decreases in a monotonic fashion.

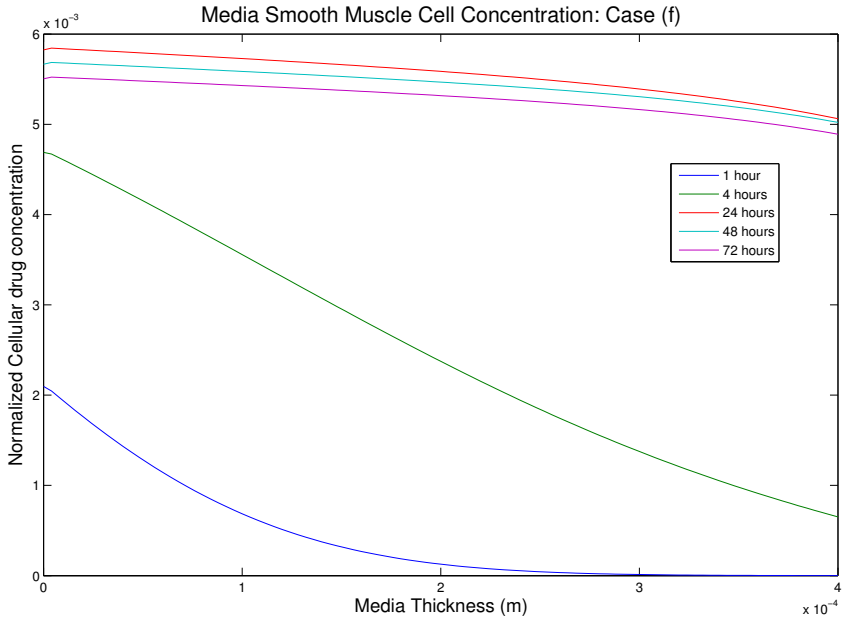

Figure 5.21: $\alpha_i = 2 \times 10^{-6}$ m^2 s^{-1}. The lowest curve represents 1 hour. Moving upwards, next is the 4 hour curve, followed by 72 hours, 48 hours and 24 hours.

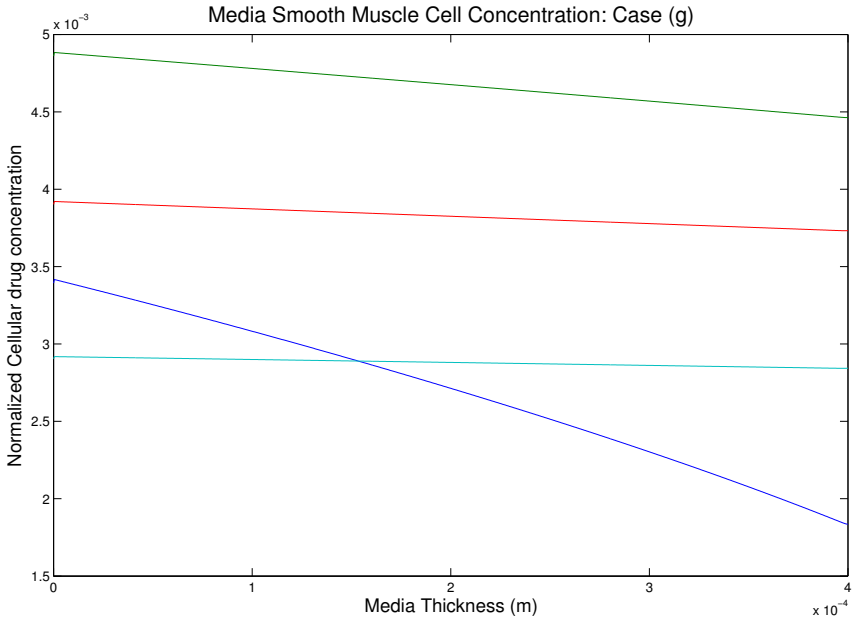

Figure 5.22: $v = 10^{-7}$ m s^{-1} and $D_m = 10^{-13}$ m^2 s^{-1}. At $x = 4 \times 10^{-4}$m, The lowest curve represents 1 hour. Moving upwards, next is the 48 hour curve, followed by 24 hours and 4 hours.

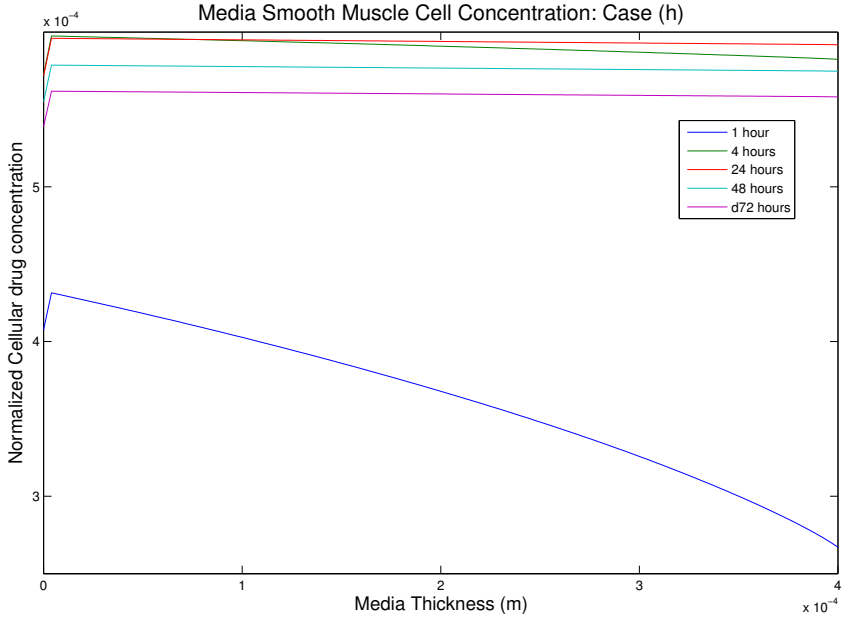

Figure 5.23: $v = 10^{-7}$ m s^{-1} and $\alpha_i = 2 \times 10^{-6}$ m^2 s^{-1}. At $x = 4 \times 10^{-4}$m, The lowest curve represents 1 hour. Moving upwards, next is the 72 hour curve, followed by 48 hours, 4 hours and 24 hours.

Chapter 6

Determining Physiological Parameters from Experimental Data

In many physiological processes, it is extremely difficult in practice to measure diffusion coefficients, particularly in interstitial regions between cells. This is in part, at least, because there is often a small but significant convection flow; this is particularly true near to arterial walls where there is a transmural pressure gradient and a consequent transmural flow. In addition, the species diffusing may interact with proteins or other lipids masking the true diffusion rate. In this chapter, it is indicated how a simple mathematical approach may allow the diffusion coefficient to be uncoupled from these other effects.

6.1 Inverse Problem

Consider the initial value problem

$$\frac{\partial C}{\partial t}(x,t) + v\frac{\partial C}{\partial x}(x,t) = D\frac{\partial^2 C}{\partial x^2}(x,t) - \alpha C(x,t) \tag{6.1.1}$$

subject to

$C(x,0) = 0$, $C(0,t) = C^0$, $t \geq 0$, $C(x,t)$ bounded for all x, t,

where C^0 is some given (constant) concentration, v is the magnitude of the transmural velocity, D is the diffusion coefficient and drug is removed from the system in proportion to α. For the case of the drug eluting stent, the media is considered to be the region $(0 < x < \infty)$ and while a constant applied concentration of drug at the polymer/media interface is somewhat unrealistic, it may, nonetheless provide a good approximation for early times.
The following lemmas will be used in solving equation (6.1.1) and are stated at the outset.

Lemma 1 *Let $f(t)$ be any continuous function and let $\bar{f}(s) = L[f(t)]$ be its corresponding Laplace transform. Then if*

$$\bar{f}(s) = \frac{1}{s}\ \exp\left\{-\sqrt{a(s+b)}\right\},$$

then

$$f(t) = \frac{1}{2}\left[\exp\{-\sqrt{ab}\}\ \text{erfc}\left(-\sqrt{bt} + \frac{1}{2}\sqrt{\frac{a}{t}}\right) + \exp\{\sqrt{ab}\}\ \text{erfc}\left(\sqrt{bt} + \frac{1}{2}\sqrt{\frac{a}{t}}\right)\right].$$

Proof Note that one can write

$$\frac{1}{s}\ \exp\left\{-\sqrt{a(s+b)}\right\} = \left[\frac{-1}{\sqrt{s+b}+\sqrt{b}} + \frac{1}{\sqrt{s+b}-\sqrt{b}}\right] \frac{\exp\left\{-\sqrt{a(s+b)}\right\}}{2\sqrt{b}}. \tag{6.1.2}$$

Employing the Shifting Theorem,

$L^{-1}[\bar{f}(s+b)] = \exp\{-bt\}L^{-1}[\bar{f}(s)] = \exp\{-bt\}f(t)$,

results in

$$\begin{aligned}
& L^{-1}\left[\frac{1}{s}\ \exp\left\{-\sqrt{a(s+b)}\right\}\right] \\
= & \frac{\exp\{-bt\}}{2\sqrt{b}}\ L^{-1}\left[\left\{\frac{1}{\sqrt{s}-\sqrt{b}} - \frac{1}{\sqrt{s}+\sqrt{b}}\right\}\exp\left\{-\sqrt{as}\right\}\right] \\
= & \frac{\exp\{-bt\}}{2\sqrt{b}} \\
\times & \left[\begin{array}{l} \frac{1}{\sqrt{\pi t}}\ \exp\left\{-\frac{a}{4t}\right\} + \sqrt{b}\ \exp\left\{-\sqrt{ab}\right\}\ \exp\{bt\}\ \operatorname{erfc}\left(-\sqrt{bt}+\frac{1}{2}\sqrt{\frac{a}{t}}\right) \\ -\left(\frac{1}{\sqrt{\pi t}}\ \exp\left\{-\frac{a}{4t}\right\} - \sqrt{b}\ \exp\left\{\sqrt{ab}\right\}\ \exp\{bt\}\ \operatorname{erfc}\left(\sqrt{bt}+\frac{1}{2}\sqrt{\frac{a}{t}}\right)\right) \end{array}\right] \\
= & \frac{1}{2}\left[\exp\left\{-\sqrt{ab}\right\}\ \operatorname{erfc}\left(-\sqrt{bt}+\frac{1}{2}\sqrt{\frac{a}{t}}\right) + \exp\left\{\sqrt{ab}\right\}\ \operatorname{erfc}\left(\sqrt{bt}+\frac{1}{2}\sqrt{\frac{a}{t}}\right)\right].
\end{aligned} \tag{6.1.3}$$

Lemma 2 *Let $f(t)$ be any continuous function and let $\bar{f}(s) = L[f(t)]$ be its corresponding Laplace transform. Then if*

$$\bar{f}(s) = \frac{1}{s}\ \exp\left\{-\sqrt{a(s+b)}\right\},$$

then

$$f(t) = \exp\{-bt\}\ \operatorname{erfc}\left(\frac{1}{2}\sqrt{\frac{a}{t}}\right) + b\int_0^t \exp\{-b\tau\}\ \operatorname{erfc}\left(\frac{1}{2}\sqrt{\frac{a}{\tau}}\right)\ d\tau.$$

Proof It is well established that $L^{-1}[\exp\{-\sqrt{as}\}/s)] = \text{erfc}(\sqrt{(a/t)}/2)$. Also, from the first Shifting Theorem:

$$L^{-1}\left[\frac{1}{s+b}\ \exp\left\{-\sqrt{a(s+b)}\right\}\right] = \exp\{-bt\}\ L^{-1}\left[\frac{1}{s}\ \exp\left\{-\sqrt{as}\right\}\right]. \quad (6.1.4)$$

Now

$$\frac{1}{s} = \left(1+\frac{b}{s}\right)\frac{1}{s+b} \quad (6.1.5)$$

so that

$$\begin{aligned} & L^{-1}\left[\frac{1}{s}\ \exp\left\{-\sqrt{a(s+b)}\right\}\right] \\ = & L^{-1}\left[\left(1+\frac{b}{s}\right)\frac{1}{s+b}\ \exp\left\{-\sqrt{a(s+b)}\right\}\right] \\ = & \int_0^t [\delta(t-\tau)+b]\exp\{-b\tau\}\ \text{erfc}\left(\frac{1}{2}\sqrt{\frac{a}{\tau}}\right)\ d\tau \\ = & \exp\{-bt\}\ \text{erfc}\left(\frac{1}{2}\sqrt{\frac{a}{t}}\right) + b\int_0^t \exp\{-b\tau\}\ \text{erfc}\left(\frac{1}{2}\sqrt{\frac{a}{\tau}}\right)\ d\tau. \end{aligned} \quad (6.1.6)$$

Taking Laplace transforms of (6.1.1) leads to

$$s\bar{C}(x,s) - C(x,0) + v\frac{d\bar{C}}{dx}(x,s) = D\frac{d^2\bar{C}}{dx^2}(x,s) - \alpha\bar{C}(x,s). \quad (6.1.7)$$

Rearranging (6.1.7) and making use of the initial condition provides

$$\frac{d^2\bar{C}}{dx^2}(x,s) - \frac{v}{D}\frac{d\bar{C}}{dx}(x,s) - \frac{(s+\alpha)}{D}\bar{C}(x,s) = 0, \quad (6.1.8)$$

which along with the boundary conditions admits the solution

$$\bar{C}(x,s) = \frac{C^0}{s}\exp\left\{\left(\frac{v-\sqrt{v^2+4D(\alpha+s)}}{2D}\right)x\right\}. \quad (6.1.9)$$

It is convenient to re-write (6.1.9) in the form

$$\bar{C}(x,s) = C^0 \exp\left\{\frac{v}{2D}x\right\} \cdot \frac{1}{s} \exp\left\{-\frac{x}{\sqrt{D}}\sqrt{s + \frac{v^2}{4D} + \alpha}\right\}. \tag{6.1.10}$$

Now let $x/\sqrt{D} = \sqrt{a}$ and $(v^2/4D) + \alpha = b$, so that (6.1.10) can be written in the more concise form

$$\bar{C}(x,s) = C^0 \exp\left\{\frac{v}{2D}x\right\} \cdot \frac{1}{s} \exp\left\{-\sqrt{a(s+b)}\right\}. \tag{6.1.11}$$

Applying Lemma 1 and Lemma 2 directly provides two forms of the solution:

$$\begin{aligned} C(x,t) &= \frac{C^0}{2} \exp\left\{\frac{v}{2D}x\right\} \\ &\times \left[\begin{array}{c} \exp\left\{-x\sqrt{\frac{v^2}{4D^2} + \frac{\alpha}{D}}\right\} \operatorname{erfc}\left(-\sqrt{\left(\frac{v^2}{4D} + \alpha\right)t} + \frac{x}{2\sqrt{Dt}}\right) \\ + \exp\left\{x\sqrt{\frac{v^2}{4D^2} + \frac{\alpha}{D}}\right\} \operatorname{erfc}\left(\sqrt{\left(\frac{v^2}{4D} + \alpha\right)t} + \frac{x}{2\sqrt{Dt}}\right) \end{array}\right] \end{aligned} \tag{6.1.12}$$

$$\begin{aligned} C(x,t) &= C^0 \exp\left\{\frac{v}{2D}x\right\} \\ &\times \left[\begin{array}{c} \exp\left\{-\left(\frac{v^2}{4D} + \alpha\right)t\right\} \operatorname{erfc}\left(\frac{1}{2}\frac{x}{\sqrt{Dt}}\right) \\ + \left(\frac{v^2}{4D} + \alpha\right)\int_0^t \exp\left\{-\left(\frac{v^2}{4D} + \alpha\right)\tau\right\} \operatorname{erfc}\left(\frac{1}{2}\frac{x}{\sqrt{D\tau}}\right) d\tau \end{array}\right], \end{aligned} \tag{6.1.13}$$

where the complementary error function is defined by (4.2.24) (Chapter 4). Clearly, letting $v, \alpha \to 0$ in (6.1.12) and (6.1.13), returns the well known solution for the diffusion equation, that is (eg. Carslaw & Jaeger 1986, Crank 1956)

$$C(x,t) = C^0 \operatorname{erfc}\left(\frac{x}{2\sqrt{Dt}}\right). \tag{6.1.14}$$

6.2 Equivalence of the two solutions

The two forms of solution, (6.1.12) and (6.1.13), can be shown to be equivalent. Consider firstly the results from Lemma 1 and Lemma 2:

$$\begin{aligned} & L^{-1}\left[\frac{1}{s}\exp\left\{\sqrt{a(s+b)}\right\}\right] \\ = \; & \frac{1}{2}\left[\exp\left\{-\sqrt{ab}\right\}\operatorname{erfc}\left(-\sqrt{bt}+\frac{1}{2}\sqrt{\frac{a}{t}}\right)+\exp\left\{\sqrt{ab}\right\}\operatorname{erfc}\left(\sqrt{bt}+\frac{1}{2}\sqrt{\frac{a}{t}}\right)\right]. \end{aligned} \tag{6.2.15}$$

$$\begin{aligned} & L^{-1}\left[\frac{1}{s}\exp\left\{\sqrt{a(s+b)}\right\}\right] \\ = \; & \exp\{-bt\}\operatorname{erfc}\left(\frac{1}{2}\sqrt{\frac{a}{t}}\right)+b\int_0^t \exp\{-b\tau\}\operatorname{erfc}\left(\frac{1}{2}\sqrt{\frac{a}{\tau}}\right)d\tau. \end{aligned} \tag{6.2.16}$$

Recall the definition of erfc(z)

$$\operatorname{erfc(z)} = \frac{2}{\sqrt{\pi}}\int_z^\infty \exp\left\{-u^2\right\}du. \tag{6.2.17}$$

Consider

$$\operatorname{erfc}\left(\frac{A}{k}+Bk\right) = \frac{2}{\sqrt{\pi}}\int_{\frac{A}{k}+Bk}^\infty \exp\left\{-u^2\right\}du. \tag{6.2.18}$$

Now, differentiating (6.2.18) with respect to k provides (making use of Leibnitz rule)

$$\begin{aligned} & \frac{d}{dk}\left[\operatorname{erfc}\left(\frac{A}{k}+Bk\right)\right] \\ = \; & -\frac{2}{\sqrt{\pi}}\exp\left\{-\left(\frac{A}{k}+Bk\right)^2\right\}\left(B-\frac{A}{k^2}\right) \\ = \; & -\frac{2}{\sqrt{\pi}}\left(B-\frac{A}{k^2}\right)\exp\{-2AB\}\exp\left\{-\left(\frac{A}{k}\right)^2-(Bk)^2\right\}. \end{aligned} \tag{6.2.19}$$

Similarly,

$$\frac{d}{dk}\left[\text{erfc}\left(\frac{A}{k}-Bk\right)\right]=-\frac{2}{\sqrt{\pi}}\left(-B-\frac{A}{k^2}\right)\ \exp\left\{2AB\right\}\ \exp\left\{-\left(\frac{A}{k}\right)^2-(Bk)^2\right\}. \tag{6.2.20}$$

Thus one may write

$$\begin{aligned}&\exp\left\{2AB\right\}\frac{d}{dk}\left[\text{erfc}\left(\frac{A}{k}+Bk\right)\right]-\exp\left\{-2AB\right\}\frac{d}{dk}\left[\text{erfc}\left(\frac{A}{k}-Bk\right)\right]\\ =\ &-\frac{4B}{\sqrt{\pi}}\ \exp\left\{-\left(\frac{A}{k}\right)^2-(Bk)^2\right\}.\end{aligned} \tag{6.2.21}$$

Noting that $-\text{erfc}(z)=\text{erfc}(-z)$, it then follows that

$$\begin{aligned}&\int_{\frac{1}{2}\sqrt{\frac{a}{t}}}^{\infty}\exp\left\{2AB\right\}\frac{d}{dk}\text{erfc}\left(\frac{A}{k}+Bk\right)dk\\ +\ &\int_{\frac{1}{2}\sqrt{\frac{a}{t}}}^{\infty}\exp\left\{-2AB\right\}\frac{d}{dk}\text{erfc}\left(-\frac{A}{k}+Bk\right)dk\\ =\ &-\frac{4B}{\sqrt{\pi}}\int_{\frac{1}{2}\sqrt{\frac{a}{t}}}^{\infty}\exp\left\{-\left(\frac{A}{k}\right)^2-(Bk)^2\right\}dk.\end{aligned} \tag{6.2.22}$$

Simplifying (6.2.22) provides

$$\begin{aligned}&\exp\left\{2AB\right\}\left[\text{erfc}\left(\infty\right)-\text{erfc}\left(\frac{2A\sqrt{t}}{\sqrt{a}}+\frac{B\sqrt{a}}{2\sqrt{t}}\right)\right]\\ +\ &\exp\left\{-2AB\right\}\left[\text{erfc}\left(\infty\right)-\text{erfc}\left(-\frac{2A\sqrt{t}}{\sqrt{a}}+\frac{B\sqrt{a}}{2\sqrt{t}}\right)\right]\\ =\ &-\frac{4B}{\sqrt{\pi}}\int_{\frac{1}{2}\sqrt{\frac{a}{t}}}^{\infty}\exp\left\{-\left(\frac{A}{k}\right)^2-(Bk)^2\right\}dk.\end{aligned} \tag{6.2.23}$$

Noting that $\operatorname{erfc}(\infty) = 0$, equation (6.2.23) can be simplified further to give

$$\begin{aligned} & \frac{1}{2}\left[\exp\{2AB\}\operatorname{erfc}\left(\frac{2A\sqrt{t}}{\sqrt{a}}+\frac{B\sqrt{a}}{2\sqrt{t}}\right)+\exp\{-2AB\}\operatorname{erfc}\left(-\frac{2A\sqrt{t}}{\sqrt{a}}+\frac{B\sqrt{a}}{2\sqrt{t}}\right)\right] \\ = \; & \frac{2B}{\sqrt{\pi}}\int_{\frac{1}{2}\sqrt{\frac{a}{t}}}^{\infty}\exp\left\{-\left(\frac{A}{k}\right)^2-(Bk)^2\right\}dk. \end{aligned} \tag{6.2.24}$$

Making the substitution $B = 1$, $A = \sqrt{ab}/2$ in (6.2.24) results in the following expression

$$\begin{aligned} & \frac{1}{2}\left[\exp\left\{-\sqrt{ab}\right\}\operatorname{erfc}\left(-\sqrt{bt}+\frac{1}{2}\sqrt{\frac{a}{t}}\right)+\exp\left\{\sqrt{ab}\right\}\operatorname{erfc}\left(\sqrt{bt}+\frac{1}{2}\sqrt{\frac{a}{t}}\right)\right] \\ = \; & \frac{2}{\sqrt{\pi}}\int_{\frac{1}{2}\sqrt{\frac{a}{t}}}^{\infty}\exp\left\{-\frac{ab}{4k^2}-k^2\right\}dk, \end{aligned} \tag{6.2.25}$$

whose right hand side is a further characterization of the inverse Laplace transform:

$$L^{-1}\left[\frac{1}{s}\;\exp\left\{\sqrt{a(s+b)}\right\}\right] = \frac{2}{\sqrt{\pi}}\int_{\frac{1}{2}\sqrt{\frac{a}{t}}}^{\infty}\exp\left\{-\frac{ab}{4k^2}-k^2\right\}dk. \tag{6.2.26}$$

Using (6.2.17), equation (6.2.16) can be manipulated as follows:

$$\begin{aligned}
& \exp\{-bt\}\,\mathrm{erfc}\left(\frac{1}{2}\sqrt{\frac{a}{t}}\right) + b\int_0^t \exp\{-b\tau\}\,\mathrm{erfc}\left(\frac{1}{2}\sqrt{\frac{a}{\tau}}\right)d\tau \\
= \;& \exp\{-bt\}\,\mathrm{erfc}\left(\frac{1}{2}\sqrt{\frac{a}{t}}\right) + \frac{2b}{\sqrt{\pi}}\int_0^t\int_{\frac{1}{2}\sqrt{\frac{a}{\tau}}}^{\infty} \exp\left\{-b\tau - u^2\right\}du\,d\tau \\
= \;& \exp\{-bt\}\;\mathrm{erfc}\left(\frac{1}{2}\sqrt{\frac{a}{t}}\right) + \frac{2b}{\sqrt{\pi}}\int_{\frac{1}{2}\sqrt{\frac{a}{t}}}^{\infty}\int_{\frac{a}{4u^2}}^{t} \exp\left\{-b\tau - u^2\right\}d\tau du \\
= \;& \exp\{-bt\}\;\mathrm{erfc}\left(\frac{1}{2}\sqrt{\frac{a}{t}}\right) \\
& -\frac{2}{\sqrt{\pi}}\int_{\frac{1}{2}\sqrt{\frac{a}{t}}}^{\infty} \exp\left\{-u^2\right\}\left(\exp\{-bt\} - \exp\left\{-\frac{ab}{4u^2}\right\}\right)du \\
= \;& \exp\{-bt\}\left[\mathrm{erfc}\left(\frac{1}{2}\sqrt{\frac{a}{t}}\right) - \frac{2}{\sqrt{\pi}}\int_{\frac{1}{2}\sqrt{\frac{a}{t}}}^{\infty}\exp\left\{-u^2\right\}du\right] \\
& +\frac{2}{\sqrt{\pi}}\int_{\frac{1}{2}\sqrt{\frac{a}{t}}}^{\infty} \exp\left\{-\frac{ab}{4u^2} - u^2\right\}du \\
= \;& \frac{2}{\sqrt{\pi}}\int_{\frac{1}{2}\sqrt{\frac{a}{t}}}^{\infty} \exp\left\{-\frac{ab}{4u^2} - u^2\right\}du. \qquad (6.2.27)
\end{aligned}$$

Making use of (6.2.25) and (6.2.27), one can write down the three equivalent forms

$$\begin{aligned}
& L^{-1}\left[\frac{1}{s}\exp\left\{\sqrt{a(s+b)}\right\}\right] \\
= \;& \frac{1}{2}\left[\exp\left\{-\sqrt{ab}\right\}\mathrm{erfc}\left(-\sqrt{bt} + \frac{1}{2}\sqrt{\frac{a}{t}}\right) + \exp\left\{\sqrt{ab}\right\}\mathrm{erfc}\left(\sqrt{bt} + \frac{1}{2}\sqrt{\frac{a}{t}}\right)\right] \\
= \;& \exp\{-bt\}\,\mathrm{erfc}\left(\frac{1}{2}\sqrt{\frac{a}{t}}\right) + b\int_0^t exp\{-b\tau\}\,\mathrm{erfc}\left(\frac{1}{2}\sqrt{\frac{a}{\tau}}\right)d\tau \\
= \;& \frac{2}{\sqrt{\pi}}\int_{\frac{1}{2}\sqrt{\frac{a}{t}}}^{\infty} \exp\left\{-\frac{ab}{4u^2} - u^2\right\}du. \qquad (6.2.28)
\end{aligned}$$

Thus, a third form of solution is given by

$$C(x,t) = \frac{2C^0}{\sqrt{\pi}}\exp\left\{\frac{v}{2D}x\right\}\int_{\frac{1}{2}\sqrt{\frac{a}{t}}}^{\infty} \exp\left\{-\frac{ab}{4u^2} - u^2\right\}du. \qquad (6.2.29)$$

6.3 Least squares analysis and results

Solving an inverse problem consists of adjusting the parameters of a model function so as to best fit a data set. The data set, in this case, should be experimental concentration profiles at different time levels. Let the experimental concentration values be defined as $C_{expt} = C_{expt}(x_i, t_j; D, v, \alpha)$ and the analytic concentration values as $C_A = C_A(x_i, t_j; D, v, \alpha)$. Clearly $C_{expt}(x_i, t_j)$ represents a specific concentration at a particular distance into the artery wall at a particular time. Hence, the task is to find the values of D, v and α for which the analytic solution best fits the data. In this method the 'best' is defined as when the sum, S, of the squares of the differences of the points from the analytic curve is a minimum.

$$S = \sum_{j=1}^{M} \sum_{i=1}^{N} \mid C_A(x_i, t_j; D, v, \alpha) - C_{expt}(x_i, t_j; D, v, \alpha) \mid^2 , \tag{6.3.30}$$

where N is the total number of sample points on each curve, and M is the total number of time points. The sample points were evenly spaced, although it is recognised that alternative methods that target the initial change in concentration may be developed. The application of this method results in the following set of nonlinear equations in v, D and α, which may be solved using a rootfinder such as Newton's Method:

$$\mathbf{F}(\mathbf{r}) = \begin{pmatrix} \frac{\partial S}{\partial v} \\ \frac{\partial S}{\partial D} \\ \frac{\partial S}{\partial \alpha} \end{pmatrix} = \mathbf{0}, \tag{6.3.31}$$

where

$$\mathbf{r} = \begin{pmatrix} v \\ D \\ \alpha \end{pmatrix}.$$

Following Newton's method, it is assumed that $\mathbf{r}^\star$ is the true solution so that $\mathbf{F}(\mathbf{r}^\star) = \mathbf{0}$. Letting $\mathbf{r^{n+1}} = \mathbf{r^n} + \boldsymbol{\epsilon^n}$, then one is required to solve

$$\begin{aligned} \mathbf{F}(\mathbf{r}^{n+1}) &= \mathbf{F}(\mathbf{r}^n + \boldsymbol{\epsilon}^n) = \mathbf{F}(\mathbf{r}^n) + \mathbf{J}(\mathbf{r}^n)\boldsymbol{\epsilon}^n + O(\boldsymbol{\epsilon}^{n^2}) \\ &= \mathbf{F}(\mathbf{r}^n) + \mathbf{J}(\mathbf{r}^n)(\mathbf{r}^{n+1} - \mathbf{r}^n) + O(\boldsymbol{\epsilon}^{n^2}) \\ &= \mathbf{0}, \end{aligned} \tag{6.3.32}$$

(by Taylor expansion and neglecting second order terms). Thus, rearranging (6.3.32) provides:

$$\mathbf{J}(\mathbf{r}^n)\,\mathbf{r}^{n+1} = \mathbf{J}(\mathbf{r}^n)\,\mathbf{r}^n - \mathbf{F}(\mathbf{r}^n). \tag{6.3.33}$$

The Jacobian here is defined as

$$\mathbf{J} = \begin{pmatrix} \frac{\partial F_1}{\partial v} & \frac{\partial F_1}{\partial D} & \frac{\partial F_1}{\partial \alpha} \\ \frac{\partial F_2}{\partial v} & \frac{\partial F_2}{\partial D} & \frac{\partial F_2}{\partial \alpha} \\ \frac{\partial F_3}{\partial v} & \frac{\partial F_3}{\partial D} & \frac{\partial F_3}{\partial \alpha} \end{pmatrix} = \begin{pmatrix} \frac{\partial^2 S}{\partial v^2} & \frac{\partial}{\partial D}\left(\frac{\partial S}{\partial v}\right) & \frac{\partial}{\partial \alpha}\left(\frac{\partial S}{\partial v}\right) \\ \frac{\partial}{\partial v}\left(\frac{\partial S}{\partial D}\right) & \frac{\partial^2 S}{\partial D^2} & \frac{\partial}{\partial \alpha}\left(\frac{\partial S}{\partial D}\right) \\ \frac{\partial}{\partial v}\left(\frac{\partial S}{\partial \alpha}\right) & \frac{\partial}{\partial D}\left(\frac{\partial S}{\partial \alpha}\right) & \frac{\partial^2 S}{\partial \alpha^2} \end{pmatrix} \tag{6.3.34}$$

A natural question to ask is which form of solution should be employed. The third form of the solution (6.2.29) perhaps looks the simplest since it inolves a single integral. However, in solving system (6.3.33), this integral would need to be evaluated numerically. Since several experimental data points are to be used, it may not be computationally efficient to perform so many numerical integrations. For the same reason, the second form of the solution (6.1.13) involving exponentials, a complementary error function and an integral may also not be the best

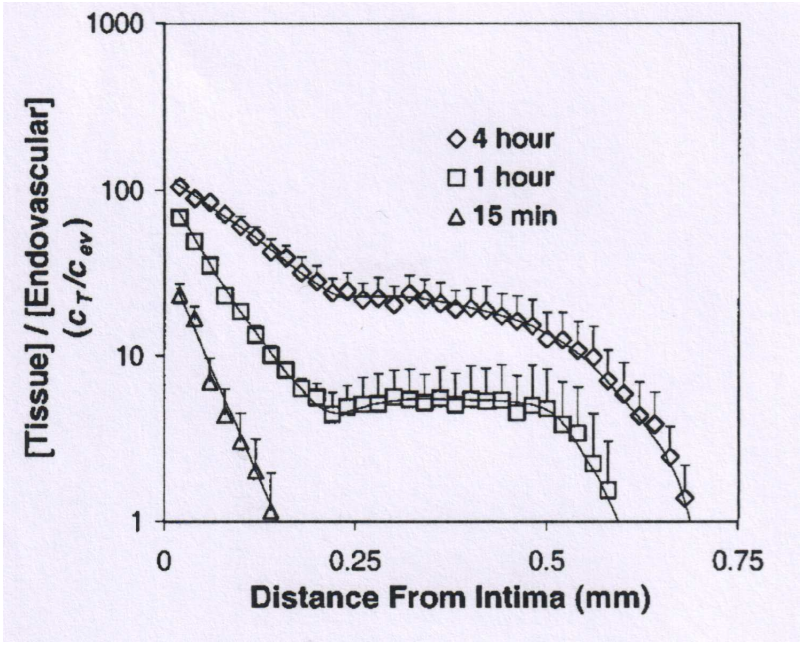

Figure 6.1: Tissue concentration normalized by the endovascularly applied concentration as a function of time, in the presence of physiological transmural hydrostatic pressure gradient. (Credit: Creel *et al.* 2000)

choice. Thus the first form of the solution (6.1.12) is used since it involves only exponentials and complementary error functions. Of course, the complementary error function itself is defined in terms of an integral and thus may also require a significant amount of computing time. The partial derivatives in (6.3.34) are lengthy expressions and thus the detail is omitted here.

The data chosen for the least squares analysis is taken from concentration profiles in Creel *et al.* (2000) and is reproduced in Figure 6.1. The graph shows experimentally measured tissue paclitaxel concentration, normalized with respect to the applied endovascular concentration. The data is obtained from experiments where arterial samples were perfused ex vivo for 15 minutes, 1 hour and 4 hours with a physiological transmural pressure gradient. Paclitaxel was applied to the endovascular aspect of the artery in buffer solution and drug distribution determined through en face cryosectioning. In applying the least squares analysis, starting

guesses for v, D and α were taken from §5.3. With these starting values, the method failed to converge. Thus an extensive search of parameter space for successful starting values was carried out. In each case, the method did not converge, suggesting that the model may be inadequate to describe this particular data. Interestingly, with $\alpha = 0$ (the advection-diffusion problem), the Newton root finder converges to $v = 2 \times 10^{-7}\text{ms}^{-1}$ and $D = 2.1 \times 10^{-13}\text{m}^2\text{s}^{-1}$ with starting guesses of $v = 1 \times 10^{-8}\text{ms}^{-1}$ and $D = 1 \times 10^{-12}\text{m}^2\text{s}^{-1}$. This result is particularly interesting, since, despite inputting starting values an order of magnitude lower, the parameters converge to values an order of magnitude higher, in line with the argument that convection is not negligible in comparison with diffusion. These results force one to ask the question: why does the method fail to converge for the full problem and yet converge to sensible values when $\alpha = 0$? The first point to note here is that the model is a very simple one; it assumes a constant applied concentration which, although not the case for a polymer coated stent, is in line with the experiments being used for comparison. Secondly, and more importantly, equation (6.1.1) accounts for a loss of drug from the system in proportion to α rather than being uptaken from the extracellular fluid into cells. Figure 6.1 clearly shows that the tissue concentration (extracellular plus cellular concentration) can greatly exceed the applied concentration. The mathematical model simply does not account for this. In order to characterize the binding to tissue properly, one would require an uptake term and partition coefficient as described in §3.3.2. Hence, in hindsight, the data is not suitable for comparison with this simple mathematical model. This does not imply, however, that the model is wrong or useless. It may still, in principle at least, be used to get a handle on v, D and α. More appropriate experimental data for comparison could be, for example, data based on a highly hydrophilic drug (partition coefficient, $K = 1$), since this would not result in tis-

sue concentrations that greatly exceed the applied concentration. Furthermore, if data were available for a purely extracellular concentration, again coupled with a highly hydrophilic drug, then the analytic solution may be fitted since there is a loss of drug from the extracellular region (to the cells) and so in this case the loss term (as opposed to an uptake and partitioning term) may be appropriate.

Chapter 7

The Polymer-Free Drug Eluting Stent

Despite the fact that the majority of drug eluting stents are coated with a drug filled polymer, the polymer is not necessary. A new technology has been developed that allows the drug to be contained within micro-pores on the surface of the stent (c.f. 'pits' and 'holes' on a compact disc). A drug-coating solution coats the pores and creates a uniform layer after evaporation of the solvent (Translumina 2006). This technology is advantageous in that when the drug has been fully released the micro-porous surface favours the adhesion of endothelial cells. This type of polymer-free stent has been named the Yukon stent. The design of this type of stent, as well as other stents, is discussed in Rogers (2005), and the results of a trial comparing a rapamycin eluting polymer-free stent with a polymer-based paclitaxel eluting stent are presented in Mehilli *et al.* (2006), where it was found that the antirestenotic effect of the rapamycin polymer-free stent was not inferior to that of the paclitaxel eluting polymer-based stent. In this chapter, a simple model is proposed to describe the elution of drug from this polymer-free stent into

the arterial wall. Solving the resulting partial differential equations analytically is non-trivial and requires the use of contour integration. The subsequent analytic expressions are obtained for the concentration and the mass in both the cellular and extracellular phases. Finally, novel release data is fitted to an exponentially decaying concentration condition at the stent/media boundary, and the resulting concentration and mass profiles are compared with clinical data.

7.1 Polymer-free model with constantly applied concentration

Since there is no polymer coating on the stent, it may be reasonable to model the micro porous stent system by considering only the media region. The drug input is then given by the boundary condition at $x = 0$, the stent/media boundary. In the first case, it is assumed that some concentration, say C_0, is constantly applied at the $x = 0$ boundary. Consider the initial value problem, defined on $x \in (0, L]$, where, here, L is the thickness of the media:

$$\phi \frac{\partial C_e}{\partial t}(x,t) + v\frac{\partial C_e}{\partial x}(x,t) = D\frac{\partial^2 C_e}{\partial x^2}(x,t) - \alpha\left(C_e(x,t) - \frac{C_i(x,t)}{K}\right), \quad (7.1.1)$$

$$(1-\phi)\frac{\partial C_i}{\partial t}(x,t) = \alpha\left(C_e(x,t) - \frac{C_i(x,t)}{K}\right), \quad (7.1.2)$$

subject to

$C_e(x,0) = C_i(x,0) = 0$, $C_e(0,t) = C^0$, $t \geq 0$, $C_e(x,t)$ and $C_i(x,t)$ bounded for all x, t, where v is the magnitude of the transmural velocity, D is the diffusion coefficient, α is the drug uptake rate constant, K is the partition coefficient and ϕ is the porosity.

7.1.1 Non-dimensionalization

The following non-dimensional variables are employed:

$$t^N = \frac{D}{L^2}t, \;\; x^N = \frac{x}{L}, \;\; C_e^N = \frac{C_e}{C_0}, \;\; C_i^N = \frac{C_i}{C_0}.$$

After dropping the subscript N for convenience, equations (7.1.1-7.1.2), are now defined on $x \in (0, 1]$ and become

$$\phi\frac{\partial C_e}{\partial t}(x,t) + Pe\frac{\partial C_e}{\partial x}(x,t) = \frac{\partial^2 C_e}{\partial x^2}(x,t) - \alpha^\star\left(C_e(x,t) - \frac{C_i(x,t)}{K}\right), \quad (7.1.3)$$

$$(1-\phi)\frac{\partial C_i}{\partial t}(x,t) = \alpha^\star\left(C_e(x,t) - \frac{C_i(x,t)}{K}\right), \quad (7.1.4)$$

subject to

$C_e(x,0) = C_i(x,0) = 0$, $C_e(0,t) = 1$, $t \geq 0$, $C_e(x,t)$ and $C_i(x,t)$ bounded for all x, t, where the Peclet number and the scaled uptake rate constant are, respectively,

$$Pe = Lv/D, \quad \alpha^\star = L^2\alpha/D.$$

7.1.2 Solution in Laplace transform space

Rearranging (7.1.4) provides

$$\frac{\partial C_i}{\partial t}(x,t) + \frac{\gamma}{K}C_i(x,t) = \gamma C_e(x,t), \quad (7.1.5)$$

where

$$\gamma = \frac{\alpha^\star}{1-\phi}.$$

Solving (7.1.5) subject to the initial condition provides

$$C_i(x,t) = \gamma \int_0^t e^{-\gamma(t-t')/K}\, C_e(x,t')\, dt'. \tag{7.1.6}$$

After substituting (7.1.6) into (7.1.3), the following integro-differential equation is obtained

$$\phi\frac{\partial C_e}{\partial t}(x,t)+Pe\frac{\partial C_e}{\partial x}(x,t) = \frac{\partial^2 C_e}{\partial x^2}(x,t)-\alpha^\star\left(C_e(x,t) - \frac{\gamma}{K}\int_0^t e^{-\gamma(t-t')/K}\, C_e(x,t')\, dt'\right). \tag{7.1.7}$$

Taking Laplace transforms of (7.1.7) yields, after making use of the initial condition and rearranging,

$$\frac{d^2\bar{C}_e}{dx^2}(x,s) - Pe\frac{d\bar{C}_e}{dx}(x,s) - \Gamma(s)\bar{C}_e(x,s) = 0, \tag{7.1.8}$$

where

$$\Gamma(s) = \frac{\phi K s\left(s + \frac{\gamma}{K} + \frac{\alpha^\star}{\phi}\right)}{Ks+\gamma}. \tag{7.1.9}$$

An expression for the extracellular concentration, in Laplace transform space, is then obtained by solving (7.1.8) subject to $C_e(0,t) = 1$ and the boundedness condition:

$$\begin{aligned}\bar{C}_e(x,s) &= \frac{1}{s}\,\exp\left\{\frac{x}{2}\left(Pe - \sqrt{Pe^2+4\Gamma(s)}\right)\right\} \\ &= \frac{1}{s}\,\exp\left\{\frac{xPe}{2}\right\}\,\exp\left\{-\frac{x}{2}\sqrt{Pe^2+4\Gamma(s)}\right\}.\end{aligned} \tag{7.1.10}$$

Using the definition of $\Gamma(s)$ from (7.1.9), it is possible to re-write (7.1.10) in a more concise form which clearly displays the dependence on s:

$$\bar{C}_e(x,s) = \frac{1}{s}\ \exp\left\{\frac{xPe}{2}\right\}\ \exp\left\{-x\sqrt{\phi}\sqrt{\frac{(s+s_1)\,(s+s_2)}{s+s_3}}\right\}, \tag{7.1.11}$$

where

$$2s_{1,2} = \frac{\gamma}{K} + \frac{\alpha^\star}{\phi} + \frac{Pe^2}{4\phi} \mp \sqrt{\left(\frac{\gamma}{K} + \frac{\alpha^\star}{\phi} + \frac{Pe^2}{4\phi}\right)^2 - \frac{Pe^2\gamma}{\phi K}},$$

and

$$s_3 = \frac{\gamma}{K}.$$

Finally, taking the Laplace transform of (7.1.6), and employing convolution, the solution for C_i in Laplace transform space is

$$\begin{aligned}\bar{C}_i(x,s) &= \frac{\gamma}{s+\gamma/K}\,\bar{C}_e(x,s) \\ &= \frac{\gamma}{s\,(s+\gamma/K)}\exp\left\{\frac{xPe}{2}\right\}\ \exp\left\{-x\sqrt{\phi}\sqrt{\frac{(s+s_1)\,(s+s_2)}{s+s_3}}\right\}\end{aligned} \tag{7.1.12}$$

7.1.3 Solution via complex inversion formula

Notice that (7.1.11) can be written in the form

$$\bar{C}_e(x,s) = \ \exp\left\{\frac{xPe}{2}\right\}\ f(s), \tag{7.1.13}$$

where

$$f(s) = \frac{\exp\left\{-x\sqrt{\phi}\sqrt{\frac{(s+s_1)(s+s_2)}{s+s_3}}\right\}}{s}. \tag{7.1.14}$$

Thus one only needs to consider

$$L^{-1}\left[f(s)\right]. \tag{7.1.15}$$

By the complex inversion formula (§4.1, Theorem 1),

$$\begin{aligned} L^{-1}\left[f(s)\right] &= L^{-1}\left[\frac{\exp\left\{-x\sqrt{\phi}\sqrt{\frac{(s+s_1)(s+s_2)}{s+s_3}}\right\}}{s}\right] \\ &= \frac{1}{2\pi\mathrm{i}}\int_{\beta-\mathrm{i}\infty}^{\beta+\mathrm{i}\infty}\frac{\exp\left\{st-x\sqrt{\phi}\sqrt{\frac{(s+s_1)(s+s_2)}{s+s_3}}\right\}}{s}\,ds. \end{aligned} \tag{7.1.16}$$

To evaluate (7.1.16) in practice, consider the modified Bromwich contour in Figure 7.1. Notice that the integrand of (7.1.16) has a simple pole at $s = 0$ (inside the contour), as well as three branch points at $-s_1$, $-s_3$ and $-s_2$. For the parameter values considered, it is always the case that $0 < s_1 < s_3 < s_2$. Thus a branch cut has has been made along the negative real axis. Now,making use of the Residue Theorem (see Chapter 4, Theorem 4),

$$\begin{aligned} & \frac{1}{2\pi\mathrm{i}}\oint_C e^{st}f(s)ds \\ = \;& \frac{1}{2\pi\mathrm{i}}\int_{AB} e^{st}f(s)ds + \frac{1}{2\pi\mathrm{i}}\int_{BC} e^{st}f(s)ds + \frac{1}{2\pi\mathrm{i}}\int_{CD} e^{st}f(s)ds \\ + \;& \frac{1}{2\pi\mathrm{i}}\int_{DE} e^{st}f(s)ds + \frac{1}{2\pi\mathrm{i}}\int_{EF} e^{st}f(s)ds + \frac{1}{2\pi\mathrm{i}}\int_{FG} e^{st}f(s)ds \\ + \;& \frac{1}{2\pi\mathrm{i}}\int_{GH} e^{st}f(s)ds + \frac{1}{2\pi\mathrm{i}}\int_{HJ} e^{st}f(s)ds + \frac{1}{2\pi\mathrm{i}}\int_{JK} e^{st}f(s)ds \\ + \;& \frac{1}{2\pi\mathrm{i}}\int_{KL} e^{st}f(s)ds + \frac{1}{2\pi\mathrm{i}}\int_{LM} e^{st}f(s)ds + \frac{1}{2\pi\mathrm{i}}\int_{MN} e^{st}f(s)ds \\ + \;& \frac{1}{2\pi\mathrm{i}}\int_{NO} e^{st}f(s)ds + \frac{1}{2\pi\mathrm{i}}\int_{OA} e^{st}f(s)ds, \\ = \;& \mathrm{Res}(s=0) \end{aligned} \tag{7.1.17}$$

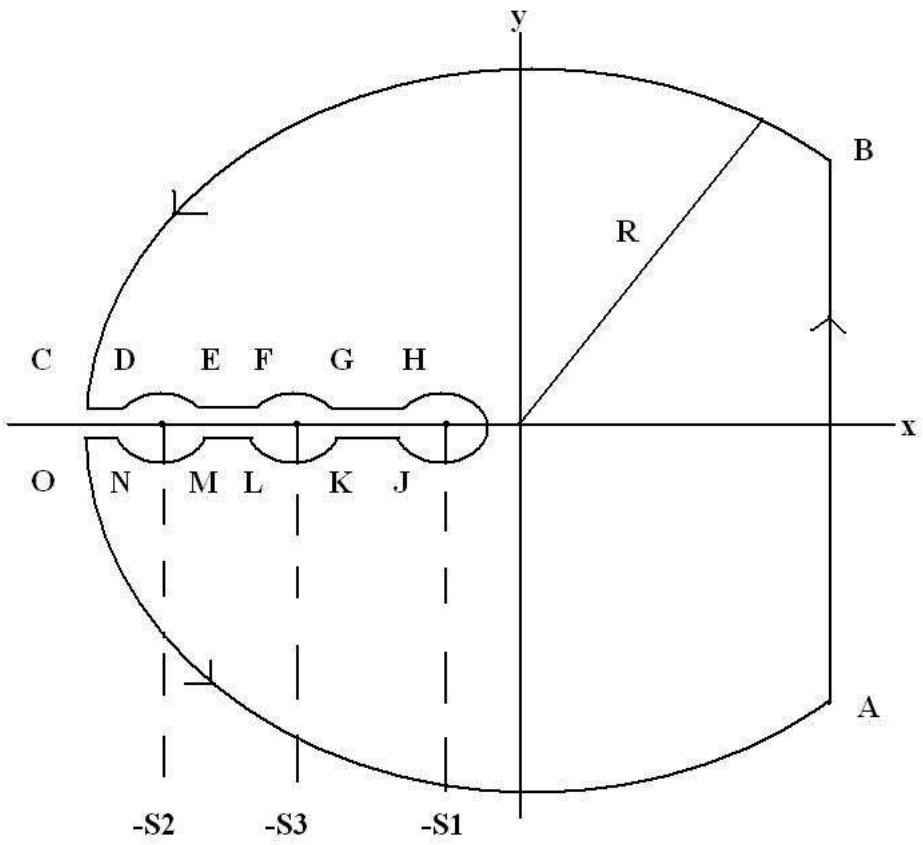

Figure 7.1: Modified Bromwich Contour. Note that the circles centred on $-s_1$, $-s_3$ and $-s_2$ have radii ϵ_1, ϵ_3 and ϵ_2, respectively.

so that there are fifteen integrals to consider. The condition in Theorem 3 (§4.1) is satisfied so that as $R \to \infty$, the integrals over BC and OA vanish.

Along CD, let $s = u\, e^{\mathrm{i}\theta}$, $\theta = \pi$, $s + s_1 = u_1\, e^{\mathrm{i}\theta_1}$, $\theta_1 = \pi$, $s + s_2 = u_2\, e^{\mathrm{i}\theta_2}$, $\theta_2 = \pi$, $s + s_3 = u_3\, e^{\mathrm{i}\theta_3}$, $\theta_3 = \pi$, from $s = -R$ to $s = -s_2 - \epsilon_2$:

$$\begin{aligned}
& \frac{1}{2\pi\mathrm{i}} \int_{CD} e^{st} f(s) ds \\
= \; & \frac{1}{2\pi\mathrm{i}} \int_{-R}^{-s_2-\epsilon_2} e^{st} f(s) ds \\
= \; & \frac{1}{2\pi\mathrm{i}} \int_{R}^{\epsilon_2+s_2} \frac{\exp\left\{-ut - x\sqrt{\phi}\sqrt{\frac{u_1 e^{\mathrm{i}\pi} u_2 e^{\mathrm{i}\pi}}{u_3 e^{\mathrm{i}\pi}}}\right\}}{-u}(-du) \\
= \; & \frac{1}{2\pi\mathrm{i}} \int_{R}^{\epsilon_2+s_2} \frac{\exp\left\{-ut - \mathrm{i}x\sqrt{\phi}\sqrt{\frac{u_1 u_2}{u_3}}\right\}}{u} du, \\
= \; & \frac{1}{2\pi\mathrm{i}} \int_{R}^{\epsilon_2+s_2} \frac{\exp\left\{-ut - \mathrm{i}x\sqrt{\phi}\sqrt{\frac{(u-s_1)(u-s_2)}{u-s_3}}\right\}}{u} du. \qquad (7.1.18)
\end{aligned}$$

Along DE, the point $-s_2$ is moved to the origin by writing $s = \epsilon_2 e^{\mathrm{i}\theta} - s_2$, $ds = \mathrm{i}\epsilon_2 \mathrm{e}^{\mathrm{i}\theta} \mathrm{d}\theta$. Thus

$$\begin{aligned}
& \frac{1}{2\pi\mathrm{i}} \int_{DE} e^{st} f(s) ds \\
= \; & \frac{\epsilon_2}{2\pi} \int_{\pi}^{0} \frac{\exp\left\{\left(\epsilon_2 e^{\mathrm{i}\theta} - s_2\right) t - x\sqrt{\phi}\sqrt{\epsilon_2} e^{\mathrm{i}\theta/2} \sqrt{\frac{\epsilon_2 e^{\mathrm{i}\theta} + s_1 - s_2}{\epsilon_2 e^{\mathrm{i}\theta} - s_2 + s_3}} + \mathrm{i}\theta\right\}}{\epsilon_2 e^{\mathrm{i}\theta} - s_2} \, d\theta \\
\to \; & 0 \quad \text{as} \quad \epsilon_2 \to 0. \qquad (7.1.19)
\end{aligned}$$

Along EF, let $s = u\ e^{\mathrm{i}\theta}$, $\theta = \pi$, $s + s_1 = u_1\ e^{\mathrm{i}\theta_1}$, $\theta_1 = \pi$, $s + s_2 = u_2\ e^{\mathrm{i}\theta_2}$, $\theta_2 = 0$, $s + s_3 = u_3\ e^{\mathrm{i}\theta_3}$, $\theta_3 = \pi$, from $s = -s_2 + \epsilon_2$ to $s = -s_3 - \epsilon_3$:

$$\begin{aligned}
& \frac{1}{2\pi\mathrm{i}} \int_{EF} e^{st} f(s) ds \\
= & \frac{1}{2\pi\mathrm{i}} \int_{-s_2+\epsilon_2}^{-s_3-\epsilon_3} e^{st} f(s) ds \\
= & \frac{1}{2\pi\mathrm{i}} \int_{s_2-\epsilon_2}^{s_3+\epsilon_3} \frac{\exp\left\{-ut - x\sqrt{\phi}\sqrt{\frac{u_1 e^{\mathrm{i}\pi} u_2 e^{\mathrm{i}0}}{u_3 e^{\mathrm{i}\pi}}}\right\}}{-u}(-du) \\
= & \frac{1}{2\pi\mathrm{i}} \int_{s_2-\epsilon_2}^{s_3+\epsilon_3} \frac{\exp\left\{-ut - x\sqrt{\phi}\sqrt{\frac{u_1 u_2}{u_3}}\right\}}{u} du, \\
= & \frac{1}{2\pi\mathrm{i}} \int_{s_2-\epsilon_2}^{s_3+\epsilon_3} \frac{\exp\left\{-ut - x\sqrt{\phi}\sqrt{\frac{(u-s_1)(s_2-u)}{u-s_3}}\right\}}{u} du. \qquad (7.1.20)
\end{aligned}$$

Along FG, the point $-s_3$ is moved to the origin by writing $s = \epsilon_3 e^{\mathrm{i}\theta} - s_3$, $ds = \mathrm{i}\epsilon_3 \mathrm{e}^{\mathrm{i}\theta} \mathrm{d}\theta$. Thus

$$\begin{aligned}
& \frac{1}{2\pi\mathrm{i}} \int_{FG} e^{st} f(s) ds \\
= & \frac{\epsilon_3}{2\pi} \int_{\pi}^{0} \frac{\exp\left\{\begin{array}{c} \left(\epsilon_3 e^{\mathrm{i}\theta} - s_3\right) t \\ -x\sqrt{\frac{\phi}{\epsilon_3}} e^{-\mathrm{i}\theta/2} \sqrt{\left(\epsilon_3 e^{\mathrm{i}\theta} + s_1 - s_3\right)\left(\epsilon_3 e^{\mathrm{i}\theta} - s_3 + s_2\right)} + \mathrm{i}\theta \end{array}\right\}}{\epsilon_3 e^{\mathrm{i}\theta} - s_3} d\theta \\
\to & \ 0 \quad \text{as} \quad \epsilon_3 \to 0. \qquad (7.1.21)
\end{aligned}$$

Along GH, let $s = u\, e^{\mathrm{i}\theta}$, $\theta = \pi$, $s + s_1 = u_1\, e^{\mathrm{i}\theta_1}$, $\theta_1 = \pi$, $s + s_2 = u_2\, e^{\mathrm{i}\theta_2}$, $\theta_2 = 0$, $s + s_3 = u_3\, e^{\mathrm{i}\theta_3}$, $\theta_3 = 0$, from $s = -s_3 + \epsilon_3$ to $s = -s_1 - \epsilon_1$:

$$\begin{aligned}
& \frac{1}{2\pi \mathrm{i}} \int_{GH} e^{st} f(s) ds \\
= & \frac{1}{2\pi \mathrm{i}} \int_{-s_3+\epsilon_3}^{-s_1-\epsilon_1} e^{st} f(s) ds \\
= & \frac{1}{2\pi \mathrm{i}} \int_{s_3-\epsilon_3}^{s_1+\epsilon_1} \frac{\exp\left\{-ut - x\sqrt{\phi}\sqrt{\frac{u_1 e^{\mathrm{i}\pi} u_2 e^{\mathrm{i}0}}{u_3 e^{\mathrm{i}0}}}\right\}}{-u}(-du) \\
= & \frac{1}{2\pi \mathrm{i}} \int_{s_3-\epsilon_3}^{s_1+\epsilon_1} \frac{\exp\left\{-ut - \mathrm{i}x\sqrt{\phi}\sqrt{\frac{u_1 u_2}{u_3}}\right\}}{u} du, \\
= & \frac{1}{2\pi \mathrm{i}} \int_{s_3-\epsilon_3}^{s_1+\epsilon_1} \frac{\exp\left\{-ut - \mathrm{i}x\sqrt{\phi}\sqrt{\frac{(u-s_1)(s_2-u)}{s_3-u}}\right\}}{u} du. \qquad (7.1.22)
\end{aligned}$$

Along HJ, the point $-s_1$ is moved to the origin by writing $s = \epsilon_1 e^{\mathrm{i}\theta} - s_1$, $ds = \mathrm{i}\epsilon_1 \mathrm{e}^{\mathrm{i}\theta} \mathrm{d}\theta$. Thus

$$\begin{aligned}
& \frac{1}{2\pi \mathrm{i}} \int_{HJ} e^{st} f(s) ds \\
= & \frac{\epsilon_1}{2\pi} \int_{\pi}^{-\pi} \frac{\exp\left\{\left(\epsilon_1 e^{\mathrm{i}\theta} - s_1\right) t - x\sqrt{\phi}\sqrt{\epsilon_1} e^{\mathrm{i}\theta/2} \sqrt{\frac{\epsilon_1 e^{\mathrm{i}\theta} - s_1 + s_2}{\epsilon_1 e^{\mathrm{i}\theta} - s_1 + s_3}} + \mathrm{i}\theta\right\}}{\epsilon_1 e^{\mathrm{i}\theta} - s_1} d\theta \\
\to & \ 0 \quad \text{as} \quad \epsilon_1 \to 0. \qquad (7.1.23)
\end{aligned}$$

Along JK, let $s = u\,e^{\mathrm{i}\theta}$, $\theta = -\pi$, $s+s_1 = u_1\,e^{\mathrm{i}\theta_1}$, $\theta_1 = -\pi$, $s+s_2 = u_2\,e^{\mathrm{i}\theta_2}$, $\theta_2 = 0$, $s+s_3 = u_3\,e^{\mathrm{i}\theta_3}$, $\theta_3 = 0$, from $s = -s_1-\epsilon_1$ to $s = -s_3+\epsilon_3$:

$$\begin{aligned}
&\frac{1}{2\pi\mathrm{i}}\int_{JK} e^{st}f(s)ds \\
= \;& \frac{1}{2\pi\mathrm{i}}\int_{-s_1-\epsilon_1}^{-s_3+\epsilon_3} e^{st}f(s)ds \\
= \;& \frac{1}{2\pi\mathrm{i}}\int_{s_1+\epsilon_1}^{s_3-\epsilon_3} \frac{\exp\left\{-ut - x\sqrt{\phi}\sqrt{\frac{u_1e^{-\mathrm{i}\pi}u_2e^{\mathrm{i}0}}{u_3e^{\mathrm{i}0}}}\right\}}{-u}(-du) \\
= \;& \frac{1}{2\pi\mathrm{i}}\int_{s_1+\epsilon_1}^{s_3-\epsilon_3} \frac{\exp\left\{-ut + \mathrm{i}x\sqrt{\phi}\sqrt{\frac{u_1u_2}{u_3}}\right\}}{u}du, \\
= \;& \frac{1}{2\pi\mathrm{i}}\int_{s_1+\epsilon_1}^{s_3-\epsilon_3} \frac{\exp\left\{-ut + \mathrm{i}x\sqrt{\phi}\sqrt{\frac{(u-s_1)(s_2-u)}{s_3-u}}\right\}}{u}du. \qquad (7.1.24)
\end{aligned}$$

Along KL, the point $-s_3$ is moved to the origin by writing $s = \epsilon_3 e^{\mathrm{i}\theta} - s_3$, $ds = \mathrm{i}\epsilon_3\mathrm{e}^{\mathrm{i}\theta}\mathrm{d}\theta$. Thus

$$\begin{aligned}
&\frac{1}{2\pi\mathrm{i}}\int_{KL} e^{st}f(s)ds \\
= \;& \frac{\epsilon_3}{2\pi}\int_0^{-\pi} \frac{\exp\left\{\begin{array}{c}\left(\epsilon_3e^{\mathrm{i}\theta}-s_3\right)t \\ -x\sqrt{\frac{\phi}{\epsilon_3}}e^{-\mathrm{i}\theta/2}\sqrt{\left(\epsilon_3e^{\mathrm{i}\theta}+s_1-s_3\right)\left(\epsilon_3e^{\mathrm{i}\theta}-s_3+s_2\right)}+\mathrm{i}\theta\end{array}\right\}}{\epsilon_3e^{\mathrm{i}\theta}-s_3}\,d\theta \\
\to \;& 0 \quad \text{as} \quad \epsilon_3 \to 0. \qquad (7.1.25)
\end{aligned}$$

Along LM, let $s = u\ e^{\mathrm{i}\theta}$, $\theta = -\pi$, $s + s_1 = u_1\ e^{\mathrm{i}\theta_1}$, $\theta_1 = -\pi$, $s + s_2 = u_2\ e^{\mathrm{i}\theta_2}$, $\theta_2 = 0$, $s + s_3 = u_3\ e^{\mathrm{i}\theta_3}$, $\theta_3 = -\pi$, from $s = -s_3 - \epsilon_3$ to $s = -s_2 + \epsilon_2$:

$$\begin{aligned}
& \frac{1}{2\pi\mathrm{i}} \int_{LM} e^{st} f(s) ds \\
= & \frac{1}{2\pi\mathrm{i}} \int_{-s_3-\epsilon_3}^{-s_2+\epsilon_2} e^{st} f(s) ds \\
= & \frac{1}{2\pi\mathrm{i}} \int_{s_3+\epsilon_3}^{s_2-\epsilon_2} \frac{\exp\left\{-ut - x\sqrt{\phi}\sqrt{\frac{u_1 e^{-\mathrm{i}\pi} u_2 e^{\mathrm{i}0}}{u_3 e^{-\mathrm{i}\pi}}}\right\}}{-u}(-du) \\
= & \frac{1}{2\pi\mathrm{i}} \int_{s_3+\epsilon_3}^{s_2-\epsilon_2} \frac{\exp\left\{-ut - x\sqrt{\phi}\sqrt{\frac{u_1 u_2}{u_3}}\right\}}{u} du, \\
= & \frac{1}{2\pi\mathrm{i}} \int_{s_3+\epsilon_3}^{s_2-\epsilon_2} \frac{\exp\left\{-ut - x\sqrt{\phi}\sqrt{\frac{(u-s_1)(s_2-u)}{u-s_3}}\right\}}{u} du. \qquad (7.1.26)
\end{aligned}$$

Along MN, the point $-s_2$ is moved to the origin by writing $s = \epsilon_2 e^{\mathrm{i}\theta} - s_2$, $ds = \mathrm{i}\epsilon_2 \mathrm{e}^{\mathrm{i}\theta} \mathrm{d}\theta$. Thus

$$\begin{aligned}
& \frac{1}{2\pi\mathrm{i}} \int_{MN} e^{st} f(s) ds \\
= & \frac{\epsilon_2}{2\pi} \int_0^{-\pi} \frac{\exp\left\{\left(\epsilon_2 e^{\mathrm{i}\theta} - s_2\right) t - x\sqrt{\phi}\sqrt{\epsilon_2} e^{\mathrm{i}\theta/2} \sqrt{\frac{\epsilon_2 e^{\mathrm{i}\theta} + s_1 - s_2}{\epsilon_2 e^{\mathrm{i}\theta} - s_2 + s_3}} + \mathrm{i}\theta\right\}}{\epsilon_2 e^{\mathrm{i}\theta} - s_2} d\theta \\
\to & \ 0 \quad \text{as} \quad \epsilon_2 \to 0. \qquad (7.1.27)
\end{aligned}$$

Along NO, let $s = u\,e^{\mathrm{i}\theta}$, $\theta = -\pi$, $s + s_1 = u_1\,e^{\mathrm{i}\theta_1}$, $\theta_1 = -\pi$,

$s + s_2 = u_2\,e^{\mathrm{i}\theta_2}$, $\theta_2 = -\pi$, $s + s_3 = u_3\,e^{\mathrm{i}\theta_3}$, $\theta_3 = -\pi$, from $s = -s_2 - \epsilon_2$ to $s = -R$

$$\begin{aligned}
& \frac{1}{2\pi\mathrm{i}} \int_{NO} e^{st} f(s) ds \\
= \; & \frac{1}{2\pi\mathrm{i}} \int_{-s_2-\epsilon_2}^{-R} e^{st} f(s) ds \\
= \; & \frac{1}{2\pi\mathrm{i}} \int_{s_2+\epsilon_2}^{R} \frac{\exp\left\{-ut - x\sqrt{\phi}\sqrt{\frac{u_1 e^{-\mathrm{i}\pi} u_2 e^{-\mathrm{i}\pi}}{u_3 e^{-\mathrm{i}\pi}}}\right\}}{-u}(-du) \\
= \; & \frac{1}{2\pi\mathrm{i}} \int_{s_2+\epsilon_2}^{R} \frac{\exp\left\{-ut + \mathrm{i}x\sqrt{\phi}\sqrt{\frac{u_1 u_2}{u_3}}\right\}}{u} du, \\
= \; & \frac{1}{2\pi\mathrm{i}} \int_{s_2+\epsilon_2}^{R} \frac{\exp\left\{-ut + \mathrm{i}x\sqrt{\phi}\sqrt{\frac{(u-s_1)(u-s_2)}{u-s_3}}\right\}}{u} du. \qquad (7.1.28)
\end{aligned}$$

Now, the residue at the simple pole $s = 0$ is

$$\lim_{s\to 0} \frac{s \exp\left\{st - x\sqrt{\phi}\sqrt{\frac{(s+s_1)(s+s_2)}{s+s_3}}\right\}}{s} = \exp\left\{-x\sqrt{\frac{\phi s_1 s_2}{s_3}}\right\}. \qquad (7.1.29)$$

By the Residue Theorem (§4.1, Theorem 4),

$$\frac{1}{2\pi\mathrm{i}} \oint_C e^{st} f(s) ds = \exp\left\{-x\sqrt{\frac{\phi s_1 s_2}{s_3}}\right\}, \qquad (7.1.30)$$

and so the left hand side of (7.1.17) reduces to $\exp\left\{-x\sqrt{\frac{\phi s_1 s_2}{s_3}}\right\}$.

Hence, with the integrals along BC, DE, FG, HJ, KL, MN and OA tending to zero in the limit, and with the integrals along EF and LM cancelling through addition, the only contributions are those from the integrals along CD, GH, JK

and NO. Thus, (7.1.17) reduces to

$$
\begin{aligned}
&\frac{1}{2\pi\mathrm{i}}\int_{AB} e^{st}f(s)ds \\
&= \exp\left\{-x\sqrt{\frac{\phi s_1 s_2}{s_3}}\right\} \\
&\quad -\frac{1}{2\pi\mathrm{i}}\lim_{R\to\infty,\epsilon_{1,2,3}\to 0}\left\{\begin{array}{l} \frac{1}{2\pi\mathrm{i}}\int_{CD} e^{st}f(s)ds + \frac{1}{2\pi\mathrm{i}}\int_{GH} e^{st}f(s)ds \\ \\ +\frac{1}{2\pi\mathrm{i}}\int_{JK} e^{st}f(s)ds + \frac{1}{2\pi\mathrm{i}}\int_{NO} e^{st}f(s)ds \end{array}\right\} \\
&= \exp\left\{-x\sqrt{\frac{\phi s_1 s_2}{s_3}}\right\} \\
&\quad -\frac{1}{2\pi\mathrm{i}}\lim_{R\to\infty,\epsilon_{1,2,3}\to 0}\left\{\begin{array}{l} \frac{1}{2\pi\mathrm{i}}\int_{R}^{\epsilon_2+s_2} \frac{\exp\left\{-ut-\mathrm{i}x\sqrt{\phi}\sqrt{\frac{(u-s_1)(u-s_2)}{u-s_3}}\right\}}{u}du \\ +\frac{1}{2\pi\mathrm{i}}\int_{s_3-\epsilon_3}^{s_1+\epsilon_1} \frac{\exp\left\{-ut-\mathrm{i}x\sqrt{\phi}\sqrt{\frac{(u-s_1)(s_2-u)}{s_3-u}}\right\}}{u}du \\ \\ +\frac{1}{2\pi\mathrm{i}}\int_{s_1+\epsilon_1}^{s_3-\epsilon_3} \frac{\exp\left\{-ut+\mathrm{i}x\sqrt{\phi}\sqrt{\frac{(u-s_1)(s_2-u)}{s_3-u}}\right\}}{u}du \\ +\frac{1}{2\pi\mathrm{i}}\int_{s_2+\epsilon_2}^{R} \frac{\exp\left\{-ut+\mathrm{i}x\sqrt{\phi}\sqrt{\frac{(u-s_1)(u-s_2)}{u-s_3}}\right\}}{u}du \end{array}\right\} \\
&= \exp\left\{-x\sqrt{\frac{\phi s_1 s_2}{s_3}}\right\} \\
&\quad -\frac{1}{2\pi\mathrm{i}}\left\{\begin{array}{l} \frac{1}{2\pi\mathrm{i}}\int_{\infty}^{s_2} \frac{\exp\left\{-ut-\mathrm{i}x\sqrt{\phi}\sqrt{\frac{(u-s_1)(u-s_2)}{u-s_3}}\right\}}{u}du \\ +\frac{1}{2\pi\mathrm{i}}\int_{s_3}^{s_1} \frac{\exp\left\{-ut-\mathrm{i}x\sqrt{\phi}\sqrt{\frac{(u-s_1)(s_2-u)}{s_3-u}}\right\}}{u}du \\ \\ +\frac{1}{2\pi\mathrm{i}}\int_{s_1}^{s_3} \frac{\exp\left\{-ut+\mathrm{i}x\sqrt{\phi}\sqrt{\frac{(u-s_1)(s_2-u)}{s_3-u}}\right\}}{u}du \\ +\frac{1}{2\pi\mathrm{i}}\int_{s_2}^{\infty} \frac{\exp\left\{-ut+\mathrm{i}x\sqrt{\phi}\sqrt{\frac{(u-s_1)(u-s_2)}{u-s_3}}\right\}}{u}du \end{array}\right\} \\
&= \exp\left\{-x\sqrt{\frac{\phi s_1 s_2}{s_3}}\right\} - \frac{1}{\pi}\left\{\begin{array}{l} \int_{s_2}^{\infty}\frac{e^{-ut}}{u}\sin\left(x\sqrt{\phi}\sqrt{\frac{(u-s_1)(u-s_2)}{u-s_3}}\right)du \\ +\int_{s_1}^{s_3}\frac{e^{-ut}}{u}\sin\left(x\sqrt{\phi}\sqrt{\frac{(u-s_1)(s_2-u)}{s_3-u}}\right)du \end{array}\right\}.
\end{aligned}
\tag{7.1.31}
$$

Thus, returning to (7.1.13), the solution for C_e can be written as

$$\begin{aligned} C_e(x,t) &= \exp\left\{\frac{xPe}{2}\right\} \\ &\quad \times \left[\begin{array}{c} \exp\left\{-x\sqrt{\frac{\phi s_1 s_2}{s_3}}\right\} \\ -\frac{1}{\pi}\left\{\begin{array}{c} \int_{s_2}^{\infty} \frac{e^{-ut}}{u}\sin\left(x\sqrt{\phi}\sqrt{\frac{(u-s_1)(u-s_2)}{u-s_3}}\right)du \\ +\int_{s_1}^{s_3} \frac{e^{-ut}}{u}\sin\left(x\sqrt{\phi}\sqrt{\frac{(u-s_1)(s_2-u)}{s_3-u}}\right)du \end{array}\right. \end{array}\right]. \end{aligned} \tag{7.1.32}$$

The solution for $C_i(x,t)$ can now be obtained directly from (7.1.12) and (7.1.32) using convolution:

$$\begin{aligned} & C_i(x,t) \\ &= \gamma\int_0^t e^{-s_3(t-t')}\exp\left\{\frac{xPe}{2}\right\} \\ &\times \left[\begin{array}{c} \exp\left\{-x\sqrt{\frac{\phi s_1 s_2}{s_3}}\right\} \\ -\frac{1}{\pi}\left\{\begin{array}{c} \int_{s_2}^{\infty} \frac{e^{-ut'}}{u}\sin\left(x\sqrt{\phi}\sqrt{\frac{(u-s_1)(u-s_2)}{u-s_3}}\right)du \\ +\int_{s_1}^{s_3} \frac{e^{-ut'}}{u}\sin\left(x\sqrt{\phi}\sqrt{\frac{(u-s_1)(s_2-u)}{s_3-u}}\right)du \end{array}\right. \end{array}\right] dt'. \\ &= \gamma\exp\left\{\frac{xPe}{2}\right\}\left[I_1 - I_2 - I_3\right], \end{aligned} \tag{7.1.33}$$

where

$$\begin{aligned} I_1 &= \exp\left\{-x\sqrt{\frac{\phi s_1 s_2}{s_3}}\right\}\int_0^t e^{-s_3(t-t')}dt' \\ &= \frac{\exp\left\{-x\sqrt{\frac{\phi s_1 s_2}{s_3}}\right\}}{s_3}\left(1-e^{-s_3 t}\right), \end{aligned} \tag{7.1.34}$$

$$
\begin{aligned}
I_2 &= \frac{1}{\pi}\int_0^t e^{-s_3(t-t')}\int_{s_2}^{\infty}\frac{e^{-ut'}}{u}\sin\left(x\sqrt{\phi}\sqrt{\frac{(u-s_1)\,(u-s_2)}{u-s_3}}\right)du\,dt' \\
&= \frac{1}{\pi}e^{-s_3t}\int_{s_2}^{\infty}\int_0^t e^{-(u-s_3)t'}dt'\,\frac{\sin\left(x\sqrt{\phi}\sqrt{\frac{(u-s_1)(u-s_2)}{u-s_3}}\right)}{u}\,du \\
&= \frac{1}{\pi}e^{-s_3t}\int_{s_2}^{\infty}\left(\frac{1-e^{-(u-s_3)t}}{u-s_3}\right)\frac{\sin\left(x\sqrt{\phi}\sqrt{\frac{(u-s_1)(u-s_2)}{u-s_3}}\right)}{u}\,du,
\end{aligned}
\tag{7.1.35}
$$

and

$$
I_3 = \frac{1}{\pi}e^{-s_3t}\int_{s_1}^{s_3}\left(\frac{e^{-(u-s_3)t}-1}{s_3-u}\right)\frac{\sin\left(x\sqrt{\phi}\sqrt{\frac{(u-s_1)(s_2-u)}{s_3-u}}\right)}{u}\,du, \tag{7.1.36}
$$

where I_3 has been simplified in a similar way to I_2 as in (7.1.35). Returning to (7.1.33) and substituting in equations (7.1.34-7.1.36), the solution for $C_i(x,t)$ is thus

$$
C_i(x,t) = \gamma\exp\left\{\frac{xPe}{2}\right\}\left[\begin{array}{c}
\frac{\exp\left\{-x\sqrt{\frac{\phi s_1 s_2}{s_3}}\right\}}{s_3}\left(1-e^{-s_3t}\right) \\
-\frac{1}{\pi}e^{-s_3t}\int_{s_2}^{\infty}\left(\frac{1-e^{-(u-s_3)t}}{u-s_3}\right)\frac{\sin\left(x\sqrt{\phi}\sqrt{\frac{(u-s_1)(u-s_2)}{u-s_3}}\right)}{u}\,du \\
-\frac{1}{\pi}e^{-s_3t}\int_{s_1}^{s_3}\left(\frac{e^{-(u-s_3)t}-1}{s_3-u}\right)\frac{\sin\left(x\sqrt{\phi}\sqrt{\frac{(u-s_1)(s_2-u)}{s_3-u}}\right)}{u}\,du
\end{array}\right]. \tag{7.1.37}
$$

7.2 Polymer-free model with exponentially decaying applied concentration

The boundary condition at $x = 0$ is somewhat unrealistic and it is outlined here how the solution may be obtained for a more general boundary condition that

ensures the drug concentration at the stent/media interface decays exponentially with time. The following form is chosen for boundary condition at $x = 0$,

$$C_e(0,t) = C_0 \exp\{-\lambda^\star t\},$$

where $\lambda^\star$ is a constant. Applying the same non-dimensionalization as in §7.1.1 provides

$$C_e(0,t) = \exp\{-\lambda t\},$$

where

$$\lambda = \lambda^\star L^2/D,$$

and the superscript N has been dropped for convenience. Then (7.1.10) now becomes

$$\begin{aligned}
\bar{C}_e(x,s) &= \frac{1}{s+\lambda}\ \exp\left\{\frac{xPe}{2}\right\}\ \exp\left\{-\frac{x}{2}\sqrt{Pe^2+4\Gamma(s)}\right\} \\
&= \frac{1}{s+\lambda}\ \exp\left\{\frac{xPe}{2}\right\}\ \exp\left\{-x\sqrt{\phi}\sqrt{\frac{(s+s_1)\,(s+s_2)}{s+s_3}}\right\} \\
&= \exp\left\{\frac{xPe}{2}\right\}\frac{s}{s+\lambda}\ f(s) \\
&= \exp\left\{\frac{xPe}{2}\right\}\left(\frac{s+\lambda-\lambda}{s+\lambda}\ f(s)\right) \\
&= \exp\left\{\frac{xPe}{2}\right\}\left(f(s)-\frac{\lambda}{s+\lambda}\ f(s)\right) \\
&= \exp\left\{\frac{xPe}{2}\right\}\ f(s) - \lambda \exp\left\{\frac{xPe}{2}\right\}\frac{f(s)}{s+\lambda}, \qquad (7.2.38)
\end{aligned}$$

where $s_1,\ s_2,\ s_3$ are as before and $f(s)$ is given by (7.1.14). Notice that the second expression in the last line of (7.2.38) can be evaluated using convolution in the same way as C_i (see the previous Section) to obtain:

$$
\begin{aligned}
C_e(x,t) &= \exp\left\{\frac{xPe}{2}\right\} \\
&\times \left[\begin{array}{c}
\exp\left\{-x\sqrt{\frac{\phi s_1 s_2}{s_3}}\right\} \\
-\frac{1}{\pi}\left\{\begin{array}{c}\int_{s_2}^{\infty}\frac{\exp\{-ut\}}{u}\sin\left(x\sqrt{\phi}\sqrt{\frac{(u-s_1)(u-s_2)}{u-s_3}}\right)du \\ +\int_{s_1}^{s_3}\frac{\exp\{-ut\}}{u}\sin\left(x\sqrt{\phi}\sqrt{\frac{(u-s_1)(s_2-u)}{s_3-u}}\right)du\end{array}\right\} \\
-\lambda\left(\begin{array}{c}\frac{\exp\left\{-x\sqrt{\frac{\phi s_1 s_2}{s_3}}\right\}}{\lambda}\left(1-e^{-\lambda t}\right) \\ -\frac{1}{\pi}\left\{\begin{array}{c}\int_{s_2}^{\infty}\frac{(e^{-\lambda t}-e^{-ut})}{u(u-\lambda)}\sin\left(x\sqrt{\phi}\sqrt{\frac{(u-s_1)(u-s_2)}{u-s_3}}\right)du \\ +\int_{s_1}^{s_3}\frac{(e^{-ut}-e^{-\lambda t})}{u(\lambda-u)}\sin\left(x\sqrt{\phi}\sqrt{\frac{(u-s_1)(s_2-u)}{s_3-u}}\right)du\end{array}\right\}\end{array}\right)
\end{array}\right] \\
&= \exp\left\{\frac{xPe}{2}\right\} \\
&\times \left[\begin{array}{c}
\exp\left\{-(x\sqrt{\frac{\phi s_1 s_2}{s_3}}+\lambda t)\right\} \\
-\frac{1}{\pi}\left\{\begin{array}{c}\int_{s_2}^{\infty}\left(e^{-ut}-\frac{\lambda(e^{-\lambda t}-e^{-ut})}{u-\lambda}\right)\frac{\sin\left(x\sqrt{\phi}\sqrt{\frac{(u-s_1)(u-s_2)}{u-s_3}}\right)}{u}du \\ +\int_{s_1}^{s_3}\left(e^{-ut}-\frac{\lambda(e^{-ut}-e^{-\lambda t})}{\lambda-u}\right)\frac{\sin\left(x\sqrt{\phi}\sqrt{\frac{(u-s_1)(s_2-u)}{s_3-u}}\right)}{u}du\end{array}\right\}
\end{array}\right].
\end{aligned}
\tag{7.2.39}
$$

Now, to evaluate $C_i(x,t)$, recall from (7.1.12) that

$$
\bar{C}_i(x,s) = \frac{\gamma}{s+s_3}\bar{C}_e(x,s). \tag{7.2.40}
$$

Thus convolution can be employed again, making use of (7.2.39) to obtain

$$\begin{aligned} C_i(x,t) &= \gamma \exp\left\{\frac{xPe}{2}\right\} \int_0^t e^{-s_3(t-t')} \\ &\times \left[\begin{array}{c} \exp\left\{-(x\sqrt{\frac{\phi s_1 s_2}{s_3}} + \lambda t')\right\} \\ -\frac{1}{\pi}\left\{ \begin{array}{l} \int_{s_2}^{\infty} \left(e^{-ut'} - \frac{\lambda\left(e^{-\lambda t'} - e^{-ut'}\right)}{u-\lambda}\right) \frac{\sin\left(x\sqrt{\phi}\sqrt{\frac{(u-s_1)(u-s_2)}{u-s_3}}\right)}{u} du \\ + \int_{s_1}^{s_3} \left(e^{-ut'} - \frac{\lambda\left(e^{-ut'} - e^{-\lambda t'}\right)}{\lambda-u}\right) \frac{\sin\left(x\sqrt{\phi}\sqrt{\frac{(u-s_1)(s_2-u)}{s_3-u}}\right)}{u} du \end{array} \right\} \end{array} \right] dt' \\ &= \gamma \exp\left\{\frac{xPe}{2}\right\} \left[I_4 - I_5 - I_6\right], \end{aligned} \tag{7.2.41}$$

where

$$\begin{aligned} I_4 &= \exp\left\{-x\sqrt{\frac{\phi s_1 s_2}{s_3}}\right\} \int_0^t e^{-s_3(t-t')-\lambda t'} dt' \\ &= \frac{\exp\left\{-x\sqrt{\frac{\phi s_1 s_2}{s_3}}\right\}}{s_3 - \lambda} \left(e^{-\lambda t} - e^{-s_3 t}\right), \end{aligned} \tag{7.2.42}$$

and I_5 and I_6 (evaluated in a similar way to I_2 and I_3) are given by :

$$I_5 = \frac{e^{-s_3 t}}{\pi} \int_{s_2}^{\infty} \left[\begin{array}{c} \left(\frac{\left(e^{(s_3-u)t} - 1\right)}{s_3 - u} - \frac{\lambda\left(\frac{(e^{(s_3-\lambda)t}-1)}{s_3-\lambda} - \frac{(e^{(s_3-u)t}-1)}{s_3-u}\right)}{u-\lambda} \right) \\ \times \frac{\sin\left(x\sqrt{\phi}\sqrt{\frac{(u-s_1)(u-s_2)}{u-s_3}}\right)}{u} \end{array} \right] du, \tag{7.2.43}$$

$$I_6 = \frac{e^{-s_3 t}}{\pi} \int_{s_1}^{s_3} \left[\begin{array}{c} \left(\frac{\left(e^{(s_3-u)t} - 1\right)}{s_3 - u} - \frac{\lambda\left(\frac{(e^{(s_3-u)t}-1)}{s_3-u} - \frac{(e^{(s_3-\lambda)t}-1)}{s_3-\lambda}\right)}{\lambda-u} \right) \\ \times \frac{\sin\left(x\sqrt{\phi}\sqrt{\frac{(u-s_1)(s_2-u)}{s_3-u}}\right)}{u} \end{array} \right] du. \tag{7.2.44}$$

Hence, substituting (7.2.42-7.2.44) into (7.2.41) provides the solution for C_i.

7.2.1 Equations of Mass

The equations for the extracellular and cellular drug concentrations subject to an exponentially decaying concentration at $x = 0$ are given by (7.2.39) and (7.2.41). Now, the total mass of drug in the media region at time t is given by:

$$M(t) = \int_0^L C_e(x,t)\, dx + \int_0^L C_i(x,t)\, dx. \tag{7.2.45}$$

To obtain the equation for total non-dimensional mass of drug in the media, the corresponding non-dimensional expressions for the extracellular and cellular concentrations are integrated over $[0,1]$:

$$\begin{aligned} M^N(t^N) &= \int_0^1 C_e^N(x^N,t^N)\, dx + \int_0^1 C_i^N(x^N,t^N)\, dx^N \\ &= M_e^N(t^N) + M_i^N(t^N), \end{aligned} \tag{7.2.46}$$

Again, for convenience, the superscript N is suppressed. Consider firstly

$$M_e(t) = \int_0^1 C_e(x,t)\, dx = I_7 - I_8 - I_9, \tag{7.2.47}$$

where

$$\begin{aligned} I_7 &= e^{-\lambda t} \int_0^1 \exp\left\{ \left(\frac{Pe}{2} - \sqrt{\frac{\phi s_1 s_2}{s_3}} \right) x \right\} dx \\ &= \frac{e^{-\lambda t}\left(\exp\left\{ \frac{Pe}{2} - \sqrt{\frac{\phi s_1 s_2}{s_3}} \right\} - 1 \right)}{\frac{Pe}{2} - \sqrt{\frac{\phi s_1 s_2}{s_3}}}, \end{aligned} \tag{7.2.48}$$

$$
\begin{aligned}
I_8 &= \frac{1}{\pi}\int_0^1 \exp\left\{\frac{xPe}{2}\right\}\int_{s_2}^{\infty} f_1(u,t)\,\sin\left(x\sqrt{\phi}\sqrt{\frac{(u-s_1)\,(u-s_2)}{u-s_3}}\right)\,du\,dx \\
&= \frac{1}{\pi}\int_{s_2}^{\infty}\int_0^1 \exp\left\{\frac{xPe}{2}\right\}\,\sin\left(x\sqrt{\phi}\sqrt{\frac{(u-s_1)\,(u-s_2)}{u-s_3}}\right)\,dx\,f_1(u,t)\,du \\
&= \frac{1}{\pi}\int_{s_2}^{\infty}\left\{\frac{\exp\{a_1\}\,[a_1\sin(b_1(u))-b_1(u)\cos(b_1(u))]+b_1(u)}{a_1^2+b_1^2(u)}\right\}f_1(u,t)\,du,
\end{aligned}
\tag{7.2.49}
$$

with

$$
f_1(u,t)=\left(e^{-ut}-\frac{\lambda(e^{-\lambda t}-e^{-ut})}{u-\lambda}\right)/u,
$$

$$
a_1=Pe/2,\quad b_1(u)=\sqrt{\frac{\phi\,(u-s_1)\,(u-s_2)}{u-s_3}}.
$$

and

$$
\begin{aligned}
I_9 &= \frac{1}{\pi}\int_0^1 \exp\left\{\frac{xPe}{2}\right\}\int_{s_1}^{s_3} f_2(u,t)\,\sin\left(x\sqrt{\phi}\sqrt{\frac{(u-s_1)\,(s_2-u)}{s_3-u}}\right)\,du\,dx \\
&= \frac{1}{\pi}\int_{s_1}^{s_3}\int_0^1 \exp\left\{\frac{xPe}{2}\right\}\,\sin\left(x\sqrt{\phi}\sqrt{\frac{(u-s_1)\,(s_2-u)}{s_3-u}}\right)\,dx\,f_2(u,t)\,du \\
&= \frac{1}{\pi}\int_{s_1}^{s_3}\left\{\frac{\exp\{a_1\}\,[a_1\sin(b_2(u))-b_2(u)\cos(b_2(u))]+b_2(u)}{a_1^2+b_2^2(u)}\right\}f_2(u,t)\,du,
\end{aligned}
\tag{7.2.50}
$$

with

$$
f_2(u,t)=\left(e^{-ut}-\frac{\lambda(e^{-ut}-e^{-\lambda t})}{\lambda-u}\right)/u,
$$

$$a_1 = Pe/2, \quad b_2(u) = \sqrt{\frac{\phi\,(u-s_1)\,(s_2-u)}{s_3-u}}.$$

In evaluating I_8 and I_9, use has been made of the following result:

$$\int_0^1 \exp\{ax\}\ \sin(bx)\,dx = \frac{\exp\{a\}\,(a\sin(b) - b\cos(b)) + b}{a^2+b^2}. \tag{7.2.51}$$

Next consider

$$M_i(t) = \int_0^1 C_i(x,t)\,dx = \gamma\,(I_{10} - I_{11} - I_{12}), \tag{7.2.52}$$

where

$$\begin{aligned} I_{10} &= \int_0^1 \frac{\exp\left\{\left(\frac{Pe}{2} - \sqrt{\frac{\phi s_1 s_2}{s_3}}\right)x\right\}\left(e^{-\lambda t} - e^{-s_3 t}\right)}{s_3-\lambda}\,dx \\ &= \frac{\left(\exp\left\{\frac{Pe}{2} - \sqrt{\frac{\phi s_1 s_2}{s_3}}\right\} - 1\right)\left(e^{-\lambda t} - e^{-s_3 t}\right)}{(s_3-\lambda)\left(\frac{Pe}{2} - \sqrt{\frac{\phi s_1 s_2}{s_3}}\right)}, \end{aligned} \tag{7.2.53}$$

$$\begin{aligned} I_{11} &= \frac{e^{-s_3 t}}{\pi}\int_0^1 \exp\left\{\frac{xPe}{2}\right\}\int_{s_2}^{\infty} f_3(u,t)\ \sin\left(x\sqrt{\phi}\sqrt{\frac{(u-s_1)\,(u-s_2)}{u-s_3}}\right)du\,dx \\ &= \frac{e^{-s_3 t}}{\pi}\int_{s_2}^{\infty}\int_0^1 \exp\left\{\frac{xPe}{2}\right\}\ \sin\left(x\sqrt{\phi}\sqrt{\frac{(u-s_1)\,(u-s_2)}{u-s_3}}\right)dx\ f_3(u,t)\,du \\ &= \frac{e^{-s_3 t}}{\pi}\int_{s_2}^{\infty}\left\{\frac{\exp\{a_1\}\,[a_1\sin(b_1(u)) - b_1(u)\cos(b_1(u))] + b_1(u)}{a_1^2 + b_1^2(u)}\right\} f_3(u,t)\,du, \end{aligned} \tag{7.2.54}$$

with

$$f_3(u,t) = \left[\frac{\left(e^{(s_3-u)t}-1\right)}{s_3-u} - \frac{\lambda\left(\frac{(e^{(s_3-\lambda)t}-1)}{s_3-\lambda} - \frac{(e^{(s_3-u)t}-1)}{s_3-u}\right)}{u-\lambda} \right] /u,$$

and

$$\begin{aligned} I_{12} &= \frac{e^{-s_3 t}}{\pi} \int_0^1 \exp\left\{\frac{xPe}{2}\right\} \int_{s_1}^{s_3} f_4(u,t)\, \sin\left(x\sqrt{\phi}\sqrt{\frac{(u-s_1)\,(s_2-u)}{s_3-u}} \right) du\, dx \\ &= \frac{e^{-s_3 t}}{\pi} \int_{s_1}^{s_3} \int_0^1 \exp\left\{\frac{xPe}{2}\right\} \sin\left(x\sqrt{\phi}\sqrt{\frac{(u-s_1)\,(s_2-u)}{s_3-u}} \right) dx\, f_4(u,t)\, du \\ &= \frac{e^{-s_3 t}}{\pi} \int_{s_1}^{s_3} \left\{ \frac{\exp\{a_1\}\left[a_1 \sin(b_2(u)) - b_2(u)\cos(b_2(u))\right] + b_2(u)}{a_1^2 + b_2^2(u)} \right\} f_4(u,t)\, du, \end{aligned} \tag{7.2.55}$$

with

$$f_4(u,t) = \left[\frac{\left(e^{(s_3-u)t}-1\right)}{s_3-u} - \frac{\lambda\left(\frac{(e^{(s_3-u)t}-1)}{s_3-u} - \frac{(e^{(s_3-\lambda)t}-1)}{s_3-\lambda}\right)}{\lambda-u} \right] /u.$$

Again, use has been made of (7.2.51) in evaluating integrals I_{11} and I_{12}.

7.2.2 Fitting exponentially decaying boundary condition to novel release data

In a study by McCormick (McCormick 2008), the release and uptake into tissue of the novel succinobucol (drug) coated Yukon stent has been investigated in vivo. In this study, experiments were carried out which allowed the total mass of drug on the stent to be measured at various time points over a period of 28 days. In the mathematical model, the stent itself is not considered. Instead, the drug available at the stent/media interface is assumed to decay exponentially with time and is accounted for in the boundary condition at $x = 0$. Here it is indicated how

the experimental measurements of drug mass in $x < 0$ are fitted to the proposed exponentially decaying boundary condition which is imposed at the stent/media interface ($x = 0$).

The objective consists of adjusting the parameters of a model function so as to best fit a data set. The experimental data set is in the form of stent drug mass measurements at different time points. These mass measurements can be normalized with respect to the initial mass on the stent so that the non-dimensional initial stent mass is taken to be unity

$$M^N = \frac{M}{M_0}, \quad M_0^N = 1.$$

In a similar manner, normalizing the stent drug concentration by the initial concentration, the initial non-dimensional stent drug concentration is also unity

$$C^N = \frac{C}{C_0}, \quad C_0^N = 1.$$

It is straightforward to see that the two non-dimensional parameters M^N and C^N are equivalent, since concentration is defined as mass divided by volume:

$$M^N = \frac{M}{M_0} = \frac{CV}{C_0 V} = \frac{C}{C_0} = C^N.$$

Recall that the non-dimensional boundary condition at $x = 0$ is

$$C_e(0, t) = \exp\{-\lambda t\}.$$

With the normalized stent mass profile taken to be the same as the normalized stent concentration profile, the assumption is then made that this data provides the concentration available at the $x = 0$ boundary and thus can be fitted to the

exponentially decaying boundary condition. In a similar manner to the previous Chapter, the experimental values are defined as $C_{expt} = C_{expt}(t_j; \lambda)$ and the analytic concentration values as $C_A = C_A(t_j; \lambda)$, where $j = 1, 2, ..., M$, are the sample time points. The task is then to find the value of λ for which the exponentially decaying boundary condition best fits the data. In this method, the 'best' is defined to be when the sum, S, of the squares of the differences of the two concentrations over M time points is a minimum.

$$S = \sum_{j=1}^{M} \mid C_A(t_j; \lambda) - C_{expt}(t_j; \lambda) \mid^2 . \tag{7.2.56}$$

Applying this least squares approach results in the following equation which can be solved for λ using a rootfinder such as Newton's Method:

$$\begin{aligned} \frac{\partial S}{\partial \lambda} &= 2 \sum_{j=1}^{M} \left[C_A(t_j; \lambda) - C_{expt}(t_j; \lambda) \right] \frac{\partial C_A}{\partial \lambda}(t_j; \lambda) \\ &= -2 \sum_{j=1}^{M} \left[\exp\{-\lambda t_j\} - C_{expt} \right] t_j \exp\{-\lambda t_j\}, \end{aligned} \tag{7.2.57}$$

since $C_A = \exp\{-\lambda t_j\}$.

In order to be able to solve for λ, it is necessary to know the parameter values for the system. In the absence of data on the drug succinobucol, the partition coefficient ($K \approx 27$) and drug uptake rate ($\alpha \approx 2 \times 10^{-5}$ s^{-1}) are taken to be that of the drug probucol (succinobucol is a derivative of probucol) (Kuzuya *et al.* 1991). The diffusion coefficient and porosity are taken to be the same values as those in Chapter 5, namely $D_m = 10^{-12}$m^2 s^{-1}, $\phi = 0.61$. Following on from the results of the sensitivity analysis in Chapter 5, the transmural velocity is taken to be of order 10^{-7}m s^{-1} and for the particular samples of tissue used, the media was

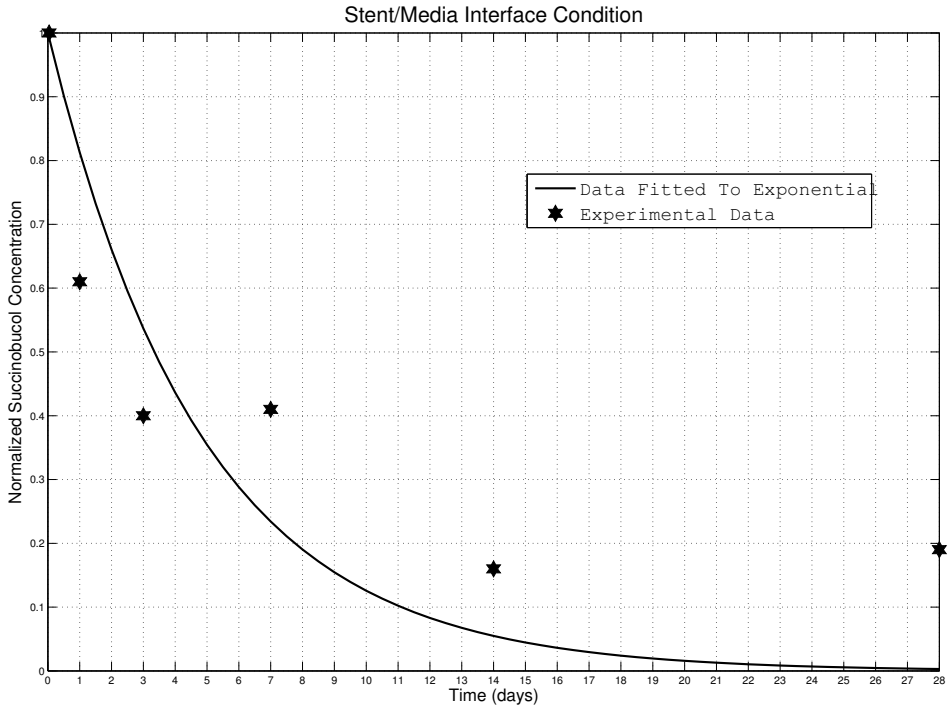

Figure 7.2: Comparison between experimental data and fitted boundary condition

found to have a thickness of around 2×10^{-4}m (personal communication, Roger Wadsworth). Using Newton's method, the value of λ converges to 0.096007. Figure 7.2 displays the fitted normalized concentration at the $x = 0$ boundary against dimensional time, together with the experimental data points.

It should be stressed that exponential decay of drug at the stent/media interface is a mathematical idealization, based on how one would expect such a concentration to decay. Figure 7.2 shows that the exponential decay is a reasonable approximation to the behaviour at early times. However, the long-term behaviour does not appear to be captured. This discrepancy may well be due to the limited number of experiments carried out. Alternatively, it may be that some portion of the drug is, in fact, retained in the stent, even at long times.

7.3 Graphical results and comparison with novel data

In this section the solution obtained for total mass is compared to experimental data (McCormick 2008). Despite obtaining an analytic solution for the total mass of drug in tissue, it is necessary to evaluate the integrals numerically. This can be achieved, for example, by using the trapezoidal rule as described in Chapter 5. Figure 7.3 displays the analytic solution (as computed from the trapezoidal rule) of normalized tissue mass versus time. In Figure 7.4, the corresponding tissue concentration is compared with experimental data. To obtain tissue concentration from normalized mass, a comparison was made between the experimental peak tissue mass and the peak normalized tissue mass from the analytic solution. This allowed for an estimate to be made of the initial dimensional succinobucol concentration on the stent, which was subsequently normalized by the experimentally measured total tissue mass (McCormick 2008) to achieve tissue mass concentration. The results show that, in line with the experimental data, the tissue concentration rises steadily from zero at $t = 0$ to some maximum value due to the effects of diffusion "spreading" and convection "pushing" the drug through the media. At the same time, the drug is being uptaken into cells. Eventually, the fluid drug carrier concentration reduces to such a level that the tissue concentration decays for the remainder of time. Whilst the experimental peak concentration occurs much earlier (1 day compared with the analytic peak of 5 days), Figure 7.3 shows that in fact the analytic extracellular tissue mass peaks at 1 day. Figure 7.3 clearly demonstrates that most of the tissue mass is contained within the cells, most likely due to the high partition coefficient of the drug. There is an obvious anomaly in Figure 7.4: the significant drop in tissue concentration between days $1 - 3$. One

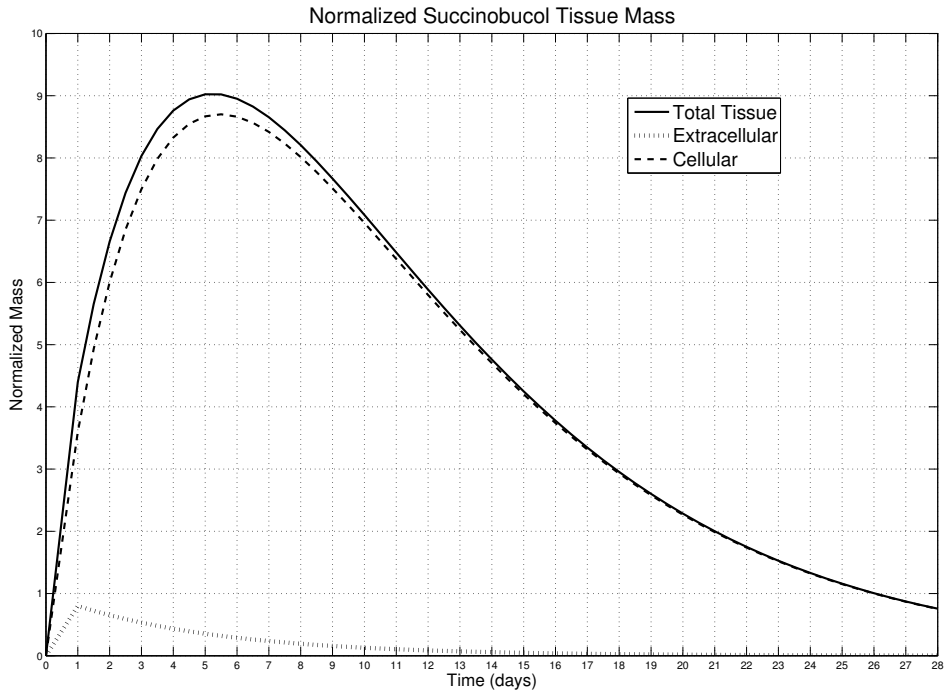

Figure 7.3: Normalized Tissue Mass

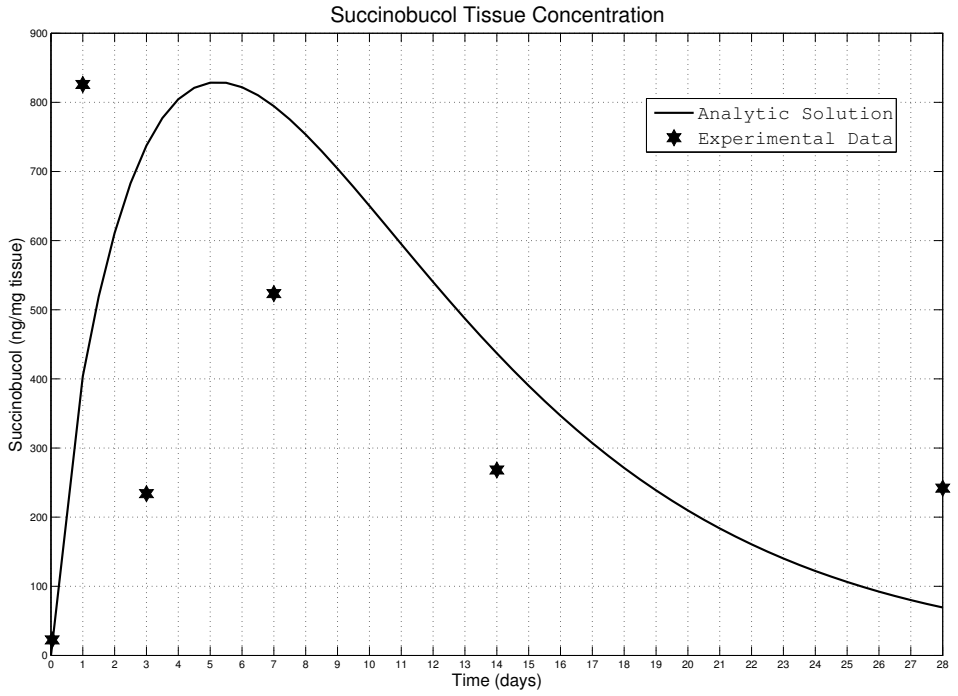

Figure 7.4: Comparison between experimental data and analytic solution

would intuitively expect the drop in concentration after the peak to be closer to the shape of the analytic solution. This is most likely due to experimental error since only a very small number of experiments were actually carried out (due to the high costs involved). There is another possible explanation; the properties of the arterial wall change with healing, resulting in a variation in parameter values. This idea that is explored in the following section. It is also worth noting that the long time behaviour again is not captured, reinforcing the idea that there may be significant experimental error or that the model needs to be improved.

7.3.1 Hypothesis: time-dependent parameters

Recall that the implantation of a stent damages the arterial wall and often the endothelial layer of cells are badly damaged or even completely removed. Since the endothelium acts as a barrier to fluid transport into the wall, the damage to these cells may result in increased transport through the wall, associated with a higher transmural velocity. However, the regrowth of the endothelium, coupled with the migration of smooth muscle cells may coincide with a return to the increased resistance to flow and an increase in cellular density. This could lead to both a decrease in transmural velocity, v, and a decrease in porosity, ϕ. Thus it is of interest to consider these parameters to be time-dependent to reflect the changing nature of the arterial wall. However, doing this adds a degree of complexity to the model equations, making an analytic solution difficult to obtain. Nonetheless, it is straightforward to evaluate the solution, $M(t)$ using different parameter values at different times. In Figure 7.5, the transmural velocity is reduced linearly by one order of magnitude over the period $3 - 7$ days. During the same period, the porosity is steadily reduced from 0.61 to 0.51, which is equivalent to increasing the cellular density. The result is a reduction in total tissue mass over the period

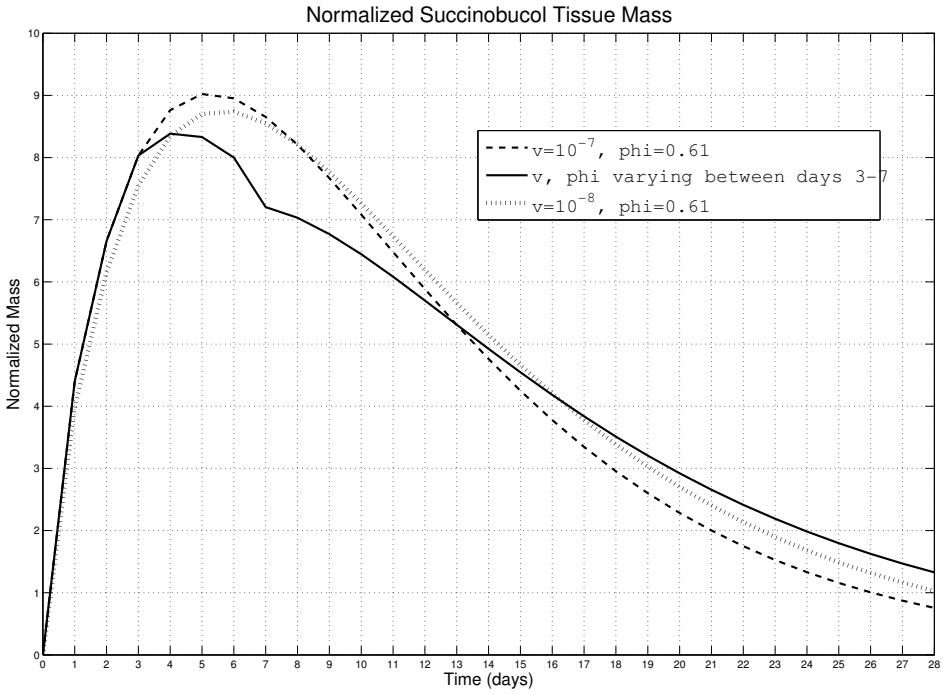

Figure 7.5: Time-dependent parameters

$3-7$ days, compared with the fixed higher parameter values over the same period. Thus it has been demonstrated that, should some of the model parameters be time-dependent, then this does indeed have an effect on the total mass of drug that accumulates in the arterial wall.

7.3.2 Varying the Peclet number

Recall that in the sensitivity analysis on the polymer coated stent in Chapter 5, it was found that the cellular drug concentration was extremely sensitive to changes in the transmural velocity. In Figure 7.6 it is evident that for the polymer-free pitted stent, the transmural velocity does not play as significant a role. Reducing the transmural velocity from $v = 10^{-7}(Pe = 20)$ to $v = 10^{-8}(Pe = 2)$ results

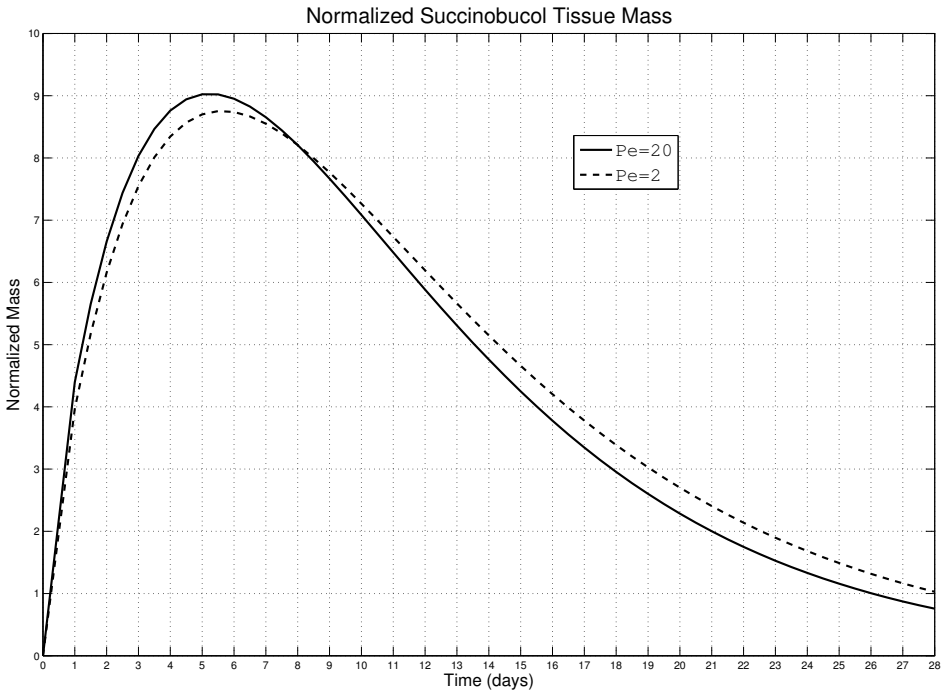

in a small change in total tissue mass. For the higher Peclet number, a higher peak tissue mass is achieved. However, as time progresses, the faster transmural velocity results in a faster clearance of drug through the system, so that the lower Peclet number case results in a higher tissue mass at later times.

An obvious question that arises is: why in the case of a polymer coated stent is the effect of the transmural velocity so much greater? This remains an open question.

Chapter 8

Analytic Solutions of Newtonian and Non-Newtonian Pipe Flow

Whilst it is well established that the initial stages of atherosclerosis are characterized by abnormal accumulation of white blood cells in the arterial wall, the cause of this abnormal accumulation is not fully understood. Blood flow in the main arteries is known to be pulsatile, leading to variable flow rates and shear stresses being exerted on the arterial wall. Atherosclerosis tends to occur at sites of low wall shear stress as well as areas of recirculation and stasis (Zarins *et al.* 1983). Clearly, an understanding of blood flow in the arteries is essential in helping to understand atherosclerosis.

8.1 Introduction and motivation

Blood is known to exhibit viscoelastic properties (Thurston 1976). Unlike a Newtonian fluid, the stress-strain curve of blood is nonlinear since the properties of blood are significantly affected by arrangement, orientation and deformability of red blood cells. The viscous properties of blood are related to the energy dissipated

during flow, due to sliding and deformation of red blood cells. The elastic properties, on the other hand, are related to energy stored during flow due to orientation and deformation. Whilst Newtonian models can provide a reasonable approximation of blood flow in large arteries, in general, non-Newtonian models are required.

The flow in a long straight pipe due to a periodic pressure gradient was first examined theoretically by Sexl (1928) and experimentally by Richardson and Tyler (1929). Sexl, using Stokes' equation, developed the solution

$$u(r,t) = C\left\{J_0\left(\sqrt{\frac{-i\omega}{\nu}}R\right) - J_0\left(\sqrt{\frac{-i\omega}{\nu}}r\right)\right\}e^{i\omega t},$$

where the pressure gradient is proportional to $\exp\{i\omega t\}$, r is the radial distance from the pipe centre, R is the pipe radius, ν and ω are the kinematic viscosity and the frequency of the pulsatile flow respectively and $J_0(x)$ denotes the zero order Bessel function of the first kind (Watson 1966). Note that this solution is finite at $r = 0$ and satisfies the usual no-slip condition at $r = R$.

Although Szymanski (1932) produced some exact solutions for flows in a cylindrical tube it was not until the nineteen-fifties that there was a resurgence of interest in pulsatile flow (Lambossy 1952, Ito 1953, Peterson 1954, Uchida 1956, Sanyal 1956, Lance 1956). However, it was probably McDonald's work on the physiology of blood flow (McDonald 1952, McDonald 1953, Helps & McDonald 1953, McDonald 1955) that was the catalyst for two important papers by Womersley (Womersley 1955a, Womersley 1955b) in which he studied (Newtonian) flows in arteries subject to a known oscillating pressure. In these papers he introduced the non-dimensional number, $R\sqrt{\omega/\nu}$. This non-dimensional number is now well known as the Womersley number.

Since this seminal work there have been a number of publications. Although not of direct relevance to this work, Robertson *et al.* (1996) and Shen *et al.* (2008) examined Oldroyd B flows in curved pipes using perturbation methods. Ku (1997) has written an interesting review of blood flow in arteries. (See also the more recent review by Gündoğdu & Carpinlioğlu 1999). Pontrelli and Bhatnagar (1997) numerically examined the flow of a viscoelastic fluid between rotating cylinders and the following year, the first author (Pontrelli 1998) obtained some numerical solutions for the non-Newtonian flow of blood in a pipe subject to a known pressure gradient. Das and Arakeri (2000) have considered the case of volume flow rate variation. Rohlf and Teuti (2000) discusses an interpretation of the Womersley number in small blood vessels while El Khatib and Damiano (2003), recognising the inadequacy of a Newtonian model for blood, proposed a non-Newtonian shear thinning constitutive relationship for which they obtained an analytic solution. Fetecau (2004) examined Oldroyd B flows in both cylindrical and annular pipes subject to zero initial flow and an impulsively started constant pressure gradient. Chen (2004) also studied the Oldroyd B model, but with given (arbitrary) inlet volume flow rate which varied with time. Hayat *et al.* (2004) looked at the exact solutions of Oldroyd B problems in Cartesian coordinates, including Couette flow and unsteady flow between parallel plates.

More recently, Agarwal *et al.* (2008) studied pulsatile flow in carotid artery bifurcation, and Peterson and Plesniak (2008) experimentally studied the influence of inlet velocity profile and secondary flow on pulsatile flow in a model artery with stenosis. Ünsal (2005) carried out a combined analytical and experimental investigation of sinusoidal mass-flow controlled, pulsating pipe flow, discussing deviations of the analytic solution from the experimental as the Reynolds number increased. Other earlier authors performing similar experimental work include

Clamen & Minto (1977) and Shemer *et al.* (1985).

In this chapter, a different tack is taken: non-Newtonian flow in rigid cylindrical and annular pipes subject to a general time-dependent pressure gradient and general initial flow conditions is considered. The particular model of non-Newtonian flow chosen is the Oldroyd B model and its corresponding analytic solution is easily shown to provide, as special cases, analytic solutions for both Maxwellian and Newtonian flows.

This chapter is organized as follows. Since the Newtonian case is of interest in its own right, this shall be presented first. Indeed it is surprising that no one appears to have written down the (correct) expression for pulsatile Newtonian flow. Next, a partial integro-differential equation is derived for the Oldroyd B model of non-Newtonian pipe flow. This is then solved by separation of variables of the homogeneous problem followed by Laplace transforms of the resulting integro-differential equation. The Maxwellian and Newtonian cases are then derived as special cases. Furthermore, when the pressure gradient is constant, "Poiseuille flows" for all three cases emerge as t tends to infinity. A similar analysis is then performed for annular pipe flow. Finally, using pressure gradient data from a dog's femoral artery, solutions are displayed graphically.

8.2 The differential equations governing the flow

The flow of an isothermal, incompressible fluid is described by the equations of conservation of mass and momentum

$$\nabla \cdot \mathbf{u} = 0 \tag{8.2.1}$$

$$\rho \frac{D\mathbf{u}}{Dt} = -\nabla p + \nabla \cdot \mathbf{T} \tag{8.2.2}$$

where $\mathbf{T}$ is the symmetric extra-stress tensor, and ρ, $\mathbf{u}$ and p denote density, velocity and pressure respectively.

8.2.1 Newtonian fluid

The constitutive equation for a Newtonian fluid is

$$\mathbf{T} = 2\mu\mathbf{d}, \tag{8.2.3}$$

where $\mathbf{d}$ is the rate of deformation tensor

$$\mathbf{d} = \frac{1}{2}\left(\nabla\mathbf{u} + (\nabla\mathbf{u})^T\right) \tag{8.2.4}$$

and μ is the viscosity.

8.2.2 Maxwellian fluid

For the case of Maxwellian flow there is an additional material constant, λ_1, known as the relaxation time. The relaxation time is defined as the time taken for the shear stress in a viscoelastic material obeying the Maxwellian model to reduce to e^{-1} of its initial value. In this case the constitutive equation is

$$\mathbf{T} + \lambda_1 \overset{\nabla}{\mathbf{T}} = 2\mu_p\mathbf{d}, \tag{8.2.5}$$

where $\overset{\nabla}{\mathbf{A}}$, the upper convected derivative of $\mathbf{A}$, is defined as

$$\begin{aligned} \overset{\nabla}{\mathbf{A}} &= \frac{D\mathbf{A}}{Dt} - (\nabla\mathbf{u})^T \cdot \mathbf{A} - \mathbf{A} \cdot (\nabla\mathbf{u}) \\ &= \frac{\partial\mathbf{A}}{\partial t} + (\mathbf{u} \cdot \nabla)\mathbf{A} - (\nabla\mathbf{u})^T \cdot \mathbf{A} - \mathbf{A} \cdot (\nabla\mathbf{u}), \end{aligned} \tag{8.2.6}$$

and μ_p is the polymeric viscosity. The upper convected derivative takes into account the deformation induced by the rate of strain, a feature typical of elastic fluids, and adds to the usual material derivative describing the flow.

8.2.3 Oldroyd B fluid

In the Oldroyd B model of viscoelastic fluid flow (Oldroyd 1950), the characteristic retardation time for the fluid, λ_2, is included. The retardation time is defined as the time taken for the strain to reach $(1 - e^{-1})$ of its final value, starting from zero strain, after the imposition of a constant shear stress. Here the constitutive equation is

$$\mathbf{T} + \lambda_1 \overset{\nabla}{\mathbf{T}} = 2\mu(\mathbf{d} + \lambda_2 \overset{\nabla}{\mathbf{d}}) \tag{8.2.7}$$

and the total viscosity is defined as $\mu = \mu_s + \mu_p$. For an Oldroyd B fluid,

$$\lambda_2 = \frac{\lambda_1 \mu_s}{\mu_s + \mu_p} = \frac{\mu_s}{\mu}\lambda_1. \tag{8.2.8}$$

Thus Maxwellian flow may be obtained from Oldroyd B by letting $\mu_s \to 0$ with the consequence that $\lambda_2 \to 0$. Newtonian flow may be obtained from Oldroyd B by letting $\mu_p \to 0$ and then $\lambda_1 = \lambda_2 \to 0$.

8.3 Newtonian pipe flow

Consider unsteady flow within a circular pipe driven by a time-dependent pressure gradient. The flow is unidirectional with $u(r, t)$ in the axial direction satisfying

$$\frac{\partial u}{\partial t} = g(t) + \nu \left(\frac{\partial^2 u}{\partial r^2} + \frac{1}{r}\frac{\partial u}{\partial r} \right), \tag{8.3.9}$$

with

$$u(a,t) = 0 \quad ; \quad u(0,t) \quad \text{bounded}, \quad \text{all} \quad t. \tag{8.3.10}$$

Here ν, ρ and a are respectively the kinematic viscosity, the density and the pipe radius and $\rho g(t) = -\partial p/\partial z$, with $-\partial p/\partial z$ the pressure gradient (z is the axial direction). As well as those authors mentioned in §8.1, Verma (1960) and Smith (1997) have also worked on closely related problems. Drazin and Riley (2006) provide the solution

$$u(r,t) = \frac{P}{4\mu}\left(a^2 - r^2\right) - \mathrm{Re}\left\{\frac{\mathrm{i}c}{\omega\rho}\left(1 - \frac{\mathrm{J}_0\left(\mathrm{i}^{3/2}kr\right)}{\mathrm{J}_0\left(\mathrm{i}^{3/2}ka\right)}\right)\mathrm{e}^{\mathrm{i}\omega t}\right\}, \quad k^2 = \frac{\omega}{\nu}, \tag{8.3.11}$$

where, here,

$$\frac{\partial p}{\partial z} = -P - \mathrm{Re}\left\{c\mathrm{e}^{\mathrm{i}\omega t}\right\}, \quad c = c_1 - \mathrm{i}c_2 \tag{8.3.12}$$

which is essentially the form given by Sexl (1928), Uchida (1956) and Womersley (1955a). This form is ubiquitous in the literature and yet it is unsatisfactory. The problem one wishes to solve is (8.3.9) with (8.3.10) together with an arbitrary initial condition, let us say

$$u(r,0) = f(r). \tag{8.3.13}$$

In fact it is relatively straightforward to write down a solution to (8.3.9) subject to (8.3.10) and (8.3.13). The eigenfunctions of the related homogeneous problem satisfy

$$\frac{d}{dr}\left(r\frac{d\Phi(r)}{dr}\right) + \alpha r\Phi(r) = 0, \tag{8.3.14}$$

$$\Phi(a) = 0, \tag{8.3.15}$$

and admit the general solution

$$\Phi(r) = A\mathrm{J}_0(\sqrt{\alpha}r) + B\mathrm{Y}_0(\sqrt{\alpha}r), \tag{8.3.16}$$

where J_0 and Y_0 are, respectively, the zero order Bessel functions of the first and second kind (Watson 1966). Boundedness and the no slip condition then imply, respectively, that $B = 0$ and

$$\mathrm{J}_0(\sqrt{\alpha}a) = 0, \tag{8.3.17}$$

yielding, through superposition, the general solution

$$u(r,t) = \sum_{n=1}^{\infty} a_n(t)\mathrm{J}_0(\sqrt{\alpha_n}r). \tag{8.3.18}$$

With $f(r) = \sum_{n=1}^{\infty} a_n(0)\mathrm{J}_0(\sqrt{\alpha_n}r)$ it is deduced, using orthogonality, that

$$a_n(0) = \frac{2}{a^2(\mathrm{J}_1(\sqrt{\alpha_n}a))^2}\int_0^a rf(r)\mathrm{J}_0(\sqrt{\alpha_n}r)dr. \tag{8.3.19}$$

Substitution of (8.3.18) into the inhomogeneous problem results in

$$\sum_{n=1}^{\infty}\left\{\frac{da_n(t)}{dt} + \nu\alpha_n a_n(t)\right\}\mathrm{J}_0(\sqrt{\alpha_n}r) = g(t). \tag{8.3.20}$$

From orthogonality,

$$a_n(t) = a_n(0)\mathrm{e}^{-\nu\alpha_n t} + \frac{2}{a\sqrt{\alpha_n}\mathrm{J}_1(\sqrt{\alpha_n}a)}\int_0^t g(t')\mathrm{e}^{-\nu\alpha_n(t-t')}dt', \tag{8.3.21}$$

giving rise to solution (8.3.22):

$$u(r,t) = 2\sum_{n=1}^{\infty} \frac{\mathrm{J}_0(\sqrt{\alpha_n}r)\mathrm{e}^{-\nu\alpha_n t}}{a\mathrm{J}_1(\sqrt{\alpha_n}a)} \left\{ \frac{\int_0^a rf(r)\mathrm{J}_0(\sqrt{\alpha_n}r)dr}{a\mathrm{J}_1(\sqrt{\alpha_n}a)} + \frac{\int_0^t \mathrm{e}^{\nu\alpha_n t'}g(t')dt'}{\alpha_n} \right\}, \tag{8.3.22}$$

where $\sqrt{\alpha_n}, n = 1, 2, ...,$ are the countably infinite roots of $\mathrm{J}_0(\sqrt{\alpha_n}a) = 0$.
The volume flow rate is given by

$$Q = 4\pi\sum_{n=1}^{\infty} \frac{\mathrm{e}^{-\nu\alpha_n t}}{\sqrt{\alpha_n}} \left\{ \frac{\int_0^a rf(r)\mathrm{J}_0(\sqrt{\alpha_n}r)dr}{a\mathrm{J}_1(\sqrt{\alpha_n}a)} + \frac{\int_0^t \mathrm{e}^{\nu\alpha_n t'}g(t')dt'}{\sqrt{\alpha_n}} \right\}. \tag{8.3.23}$$

Immediately, one observes that this is a solution for any initial flow and time-dependent pressure gradient, with no possible singularities: $\mathrm{J}_1(\sqrt{\alpha_n}a)$ is never zero since the zeros of $\mathrm{J}_0(z)$ and $\mathrm{J}_1(z)$ interlace. When the flow is initially quiescent, the same expression as Szymanski (1932) is obtained and, additionally, if $\partial p/\partial z =$ constant, then as $t \to \infty$ Poiseuille flow is retrieved, since the solution of Poiseuille flow can be expanded in terms of Bessel functions as

$$a^2 - r^2 = \sum_{n=1}^{\infty} b_n \mathrm{J}_0(\sqrt{\alpha_n}r), \tag{8.3.24}$$

where b_n is determined by making use of orthogonality and the recurrence relations of Bessel functions. This leads to

$$a^2 - r^2 = \frac{8}{a}\sum_{n=1}^{\infty} \frac{\mathrm{J}_0(\sqrt{\alpha_n}r)}{\alpha_n^{3/2}\mathrm{J}_1(\sqrt{\alpha_n}a)}. \tag{8.3.25}$$

Of course, because of the generality of the above expressions, flows subject to impulsive pressure gradients and gradients subject to exponential decay, for example, may in principle be derived from (8.3.22). Furthermore, whilst Sexl's solution provides only the first fundamental mode, solution (8.3.22) captures all the modes.

Flow in an annular region subject to an arbitrary time-dependent pressure gradient may also be considered, where the outer radius is a while the inner radius is b ($b < a$). This results in

$$u(r,t) = \pi \sum_{n=1}^{\infty} \frac{\mathrm{V}_0(\sqrt{\alpha_n}r)\mathrm{e}^{-\nu\alpha_n t}}{1+\mathrm{X}_0(\sqrt{\alpha_n})} \left\{ \frac{\pi\alpha_n \int_b^a r f(r)\mathrm{V}_0(\sqrt{\alpha_n}r)dr}{2(1-\mathrm{X}_0(\sqrt{\alpha_n}))} + \int_0^t \mathrm{e}^{\nu\alpha_n t'} g(t')dt' \right\} \tag{8.3.26}$$

where

$$\mathrm{V}_0(\sqrt{\alpha_n}r) = \mathrm{J}_0(\sqrt{\alpha_n}r)\mathrm{Y}_0(\sqrt{\alpha_n}b) - \mathrm{J}_0(\sqrt{\alpha_n}b)\mathrm{Y}_0(\sqrt{\alpha_n}r),$$

$$\mathrm{X}_0(\sqrt{\alpha_n}) = \mathrm{J}_0(\sqrt{\alpha_n}b)/\mathrm{J}_0(\sqrt{\alpha_n}a), \quad n = 1, 2, ...,$$

where here $\sqrt{\alpha_n}$ are the countably infinite zeros of $\mathrm{V}_0(\sqrt{\alpha_n}a) = 0$. The corresponding volumetric flow rate is

$$Q = 4\pi \sum_{n=1}^{\infty} \frac{\mathrm{e}^{-\nu\alpha_n t}(1-\mathrm{X}_0(\sqrt{\alpha_n}))}{\alpha_n(1+\mathrm{X}_0(\sqrt{\alpha_n}))} \left\{ \frac{\pi\alpha_n \int_b^a r f(r)\mathrm{V}_0(\sqrt{\alpha_n}r)dr}{2(1-\mathrm{X}_0(\sqrt{\alpha_n}))} + \int_0^t \mathrm{e}^{\nu\alpha_n t'} g(t')dt' \right\}. \tag{8.3.27}$$

It is straightforward to show that as $b \to 0$ expressions (8.3.26) and (8.3.27) reduce to (8.3.22) and (8.3.23) respectively.

8.4 The Oldroyd B equation for viscoelastic flow in a rigid cylinder

Consider the flow of an Oldroyd B fluid in a rigid cylinder of radius R. Cylindrical symmetry (no θ dependence) and the absence of radial flow (ie $u_r = 0$) are assumed. The continuity equation then implies that $u_z = u_z(r,t)$. It is further assumed that the stress tensor has no dependence on the axial direction and that

the initial flow is steady.

Define

$$\mathbf{T} = \begin{pmatrix} T_{rr} & T_{rz} \\ T_{zr} & T_{zz} \end{pmatrix}, \tag{8.4.1}$$

so that

$$\begin{aligned} \overset{\nabla}{\mathbf{T}} &= \frac{\partial \mathbf{T}}{\partial t} + (\mathbf{u}\cdot\nabla)\mathbf{T} - (\nabla\mathbf{u})^T\cdot\mathbf{T} - \mathbf{T}\cdot(\nabla\mathbf{u}) \\ &= \begin{pmatrix} T_{rr,t} & T_{rz,t} \\ T_{zr,t} & T_{zz,t} \end{pmatrix} - \begin{pmatrix} 0 & 0 \\ u_{z,r} & 0 \end{pmatrix}\begin{pmatrix} T_{rr} & T_{rz} \\ T_{zr} & T_{zz} \end{pmatrix} - \begin{pmatrix} T_{rr} & T_{rz} \\ T_{zr} & T_{zz} \end{pmatrix}\begin{pmatrix} 0 & u_{z,r} \\ 0 & 0 \end{pmatrix} \\ &= \begin{pmatrix} T_{rr,t} & T_{rz,t} - T_{rr}u_{z,r} \\ T_{zr,t} - T_{rr}u_{z,r} & T_{zz,t} - 2T_{rz}u_{z,r} \end{pmatrix}, \end{aligned} \tag{8.4.2}$$

making use of (8.2.1) and the fact that $\mathbf{u}$ only has a z component. The rate of deformation tensor then becomes

$$\begin{aligned} &\frac{1}{2}\left[\begin{pmatrix} 0 & u_{z,r} \\ 0 & 0 \end{pmatrix} + \begin{pmatrix} 0 & 0 \\ u_{z,r} & 0 \end{pmatrix}\right] \\ &= \begin{pmatrix} 0 & \frac{1}{2}u_{z,r} \\ \frac{1}{2}u_{z,r} & 0 \end{pmatrix}. \end{aligned} \tag{8.4.3}$$

Upon taking the upper convective derivative the following is obtained

$$\begin{aligned}
\overset{\nabla}{\mathbf{d}} &= \frac{D\mathbf{d}}{Dt} - (\nabla\mathbf{u})^T \cdot \mathbf{d} - \mathbf{d} \cdot (\nabla\mathbf{u}) \\
&= \frac{D\mathbf{d}}{Dt} - \left[\begin{pmatrix} 0 & 0 \\ 0 & \frac{1}{2}u_{z,r}^2 \end{pmatrix} + \begin{pmatrix} 0 & 0 \\ 0 & \frac{1}{2}u_{z,r}^2 \end{pmatrix} \right] \\
&= \begin{pmatrix} 0 & \frac{1}{2}u_{z,r,t} \\ \frac{1}{2}u_{z,r,t} & -u_{z,r}^2 \end{pmatrix},
\end{aligned} \tag{8.4.4}$$

since $D/Dt \equiv \partial/\partial t$ under the stated assumptions. Hence, the Oldroyd B constitutive equation (8.2.7) can be written as

$$\begin{aligned}
\begin{pmatrix} T_{rr} & T_{rz} \\ T_{zr} & T_{zz} \end{pmatrix} &+ \lambda_1 \left\{ \begin{pmatrix} T_{rr,t} & T_{rz,t} \\ T_{zr,t} & T_{zz,t} \end{pmatrix} - \begin{pmatrix} 0 & T_{rr}u_{,r} \\ u_{,r}T_{rr} & 2u_{,r}T_{rz} \end{pmatrix} \right\} \\
&= \mu \begin{pmatrix} 0 & u_{,r} + \lambda_2 u_{,r,t} \\ u_{,r} + \lambda_2 u_{,r,t} & -2\lambda_2 u_{,r}^2 \end{pmatrix},
\end{aligned} \tag{8.4.5}$$

where subscript z on u has been dropped for convenience. The first component of (8.4.5) provides $T_{rr} + \lambda_1 T_{rr,t} = 0$, which can be solved to give

$$T_{rr} = T_{rr}(r,0)e^{-t/\lambda_1} = 0 \tag{8.4.6}$$

since $T_{rr}(r,0) = 0$ has been assumed. The argument is that there exists some initial steady flow in which case $\overset{\nabla}{T}_{rr}$ and $\overset{\nabla}{d}_{rr}$ are both identically zero. Thus at $t = 0$, $T_{rr} = 2\mu d_{rr} = 0$. From the second component of (8.4.5):

$$T_{rz} + \lambda_1(T_{rz,t} - T_{rr}u_{,r}) = \mu(u_{,r} + \lambda_2 u_{,r,t}). \tag{8.4.7}$$

Substituting (8.4.6) into (8.4.7) and rearranging, gives

$$T_{rz,t} + \frac{1}{\lambda_1} T_{rz} = \frac{\mu}{\lambda_1} u_{,r} + \frac{\mu\lambda_2}{\lambda_1} u_{,r,t}. \tag{8.4.8}$$

Equation (8.4.8) can be easily solved with the initial condition $T_{rz}(r,0) = \mu u_{,r}$ to obtain

$$T_{rz} = \frac{\mu}{\lambda_1} \int_0^t e^{-(t-t')/\lambda_1} (u_{,r}(r,t') + \lambda_2 u_{,r,t'}(r,t'))dt' + \mu e^{-t/\lambda_1} u_{,r}(r,0). \tag{8.4.9}$$

The initial condition, $T_{rz}(r,0) = \mu u_{,r}$, follows directly from (8.4.5) by noting that $T_{rr}(r,t) \equiv 0$. Using integration by parts, it is possible to write

$$\begin{aligned} & \frac{\mu\lambda_2}{\lambda_1} \int_0^t e^{-(t-t')/\lambda_1} u_{,r,t'} dt' \\ = \; & \frac{\mu\lambda_2}{\lambda_1} e^{-t/\lambda_1} \left[e^{t/\lambda_1} \frac{\partial u}{\partial r}(r,t) - \frac{\partial u}{\partial r}(r,0) - \frac{1}{\lambda_1} \int_0^t e^{t'/\lambda_1} \frac{\partial u}{\partial r}(r,t') dt' \right] \end{aligned} \tag{8.4.10}$$

Substitution of (8.4.10) into (8.4.9) results in

$$\begin{aligned} T_{rz} \;=\; & \frac{\mu}{\lambda_1}(1 - \frac{\lambda_2}{\lambda_1}) \int_0^t e^{-(t-t')/\lambda_1} \frac{\partial u}{\partial r}(r,t') dt' \\ & + \mu \left[\frac{\lambda_2}{\lambda_1} \frac{\partial u}{\partial r}(r,t) - e^{-t/\lambda_1} \frac{\partial u}{\partial r}(r,0) \left(\frac{\lambda_2}{\lambda_1} - 1 \right) \right]. \end{aligned} \tag{8.4.11}$$

In cylindrical polars

$$\begin{aligned} \nabla \cdot \mathbf{T} \;&=\; \begin{pmatrix} \frac{1}{r}\frac{\partial}{\partial r}(rT_{rr}) + \frac{\partial}{\partial z}(T_{zr}) \\ \frac{1}{r}\frac{\partial}{\partial r}(rT_{rz}) + \frac{\partial}{\partial z}(T_{zz}) \end{pmatrix} \\ &=\; \begin{pmatrix} 0 \\ \frac{1}{r}\frac{\partial}{\partial r}(rT_{rz}) \end{pmatrix}, \end{aligned} \tag{8.4.12}$$

since $T_{rr} = T_{zr,z} = T_{zz,z} = 0$. Also, in cylindrical polars

$$\nabla p = \begin{pmatrix} p_{,r} \\ \\ p_{,z} \end{pmatrix}. \tag{8.4.13}$$

Hence, the conservation of momentum equation (8.2.2) can be written as

$$\rho \begin{pmatrix} 0 \\ \\ u_{,t} \end{pmatrix} = - \begin{pmatrix} p_{,r} \\ \\ p_{,z} \end{pmatrix} + \begin{pmatrix} 0 \\ \\ \frac{1}{r}\frac{\partial}{\partial r}(rT_{rz}) \end{pmatrix}. \tag{8.4.14}$$

since u_r has been assumed to be zero. From the first component it is observed that

$$p_{,r} = 0 \Rightarrow p = p(z,t).$$

From the second component of (8.4.14) one obtains

$$u_{,t} = -\frac{p_{,z}}{\rho} + \frac{1}{\rho r}\frac{\partial}{\partial r}(rT_{rz}), \tag{8.4.15}$$

from which the pressure gradient is easily shown to be a linear function of z and so

$$p(z,t) = p_0(t) + z(p_1(t) - p_0(t))/L,$$

so that

$$p_{,z} = (p_1(t) - p_0(t))/L = \triangle p(t)/L. \tag{8.4.16}$$

Combining (8.4.15) and (8.4.11) then delivers

$$\frac{\partial u}{\partial t} = -\frac{1}{\rho}\frac{\partial p}{\partial z} \quad + \quad \frac{\nu}{r}\frac{\partial}{\partial r}\left\{ r \left[\begin{array}{c} \frac{1}{\lambda_1}\left(1-\frac{\lambda_2}{\lambda_1}\right)\int_0^t e^{-(t-t')/\lambda_1}\frac{\partial u}{\partial r}(r,t')dt' \\ +\frac{\lambda_2}{\lambda_1}\frac{\partial u}{\partial r}(r,t) - e^{-t/\lambda_1}\frac{\partial u}{\partial r}(r,0)\left(\frac{\lambda_2}{\lambda_1}-1\right) \end{array} \right] \right\} \tag{8.4.17}$$

subject to

$$u(R,t) = 0, \qquad \text{no slip condition,} \tag{8.4.18}$$

$$u(0,t) \qquad \text{remains finite} \tag{8.4.19}$$

$$\text{and an initial (given) flow velocity} \quad u(r,0) = F(r) \tag{8.4.20}$$

where $\nu = \mu/\rho$, and R is the radius of the cylinder.

8.4.1 Non-dimensionalization

The following non-dimensional variables are employed:

$$u_N = u/U, \quad r_N = r/R, \quad p_N = p/P, \quad t_N = t/\tau, \quad t_N^{'} = t'/\tau \text{ and } z_N = z/R.$$

This leads to

$$\frac{\partial u}{\partial t} = -\gamma g(t) \quad + \quad \frac{Q}{r}\frac{\partial}{\partial r}\left\{ r \left[\begin{array}{c} \epsilon\int_0^t e^{-\tau(t-t')/\lambda_1}\frac{\partial u}{\partial r}(r,t')dt' \\ +\kappa\frac{\partial u}{\partial r}(r,t) - (\kappa-1)\,e^{-\tau t/\lambda_1}\frac{\partial u}{\partial r}(r,0) \end{array} \right] \right\} \tag{8.4.21}$$

subject to

$$u(1,t) = 0, \quad \text{no slip condition,} \tag{8.4.22}$$

$$u(0,t) \quad \text{remains finite,} \tag{8.4.23}$$

$$\text{an initial flow velocity,} \, u(r,0) = f(r), \tag{8.4.24}$$

and $g(t)$ is the time dependent pressure gradient. (8.4.25)

The subscript N in this non-dimensional form has been omitted. The associated constants and functions are defined as follows:

$$Q = \nu\tau/R^2, \quad \epsilon = \tau(1-\lambda_2/\lambda_1)/\lambda_1, \quad \kappa = \lambda_2/\lambda_1, \quad g(t) = \partial p/\partial z,$$
$$\gamma = P\tau/\rho RU\ , \quad f(r) = F/U.$$

8.4.2 General analytic solution in Laplace transform space

The eigenfunctions of the related homogeneous problem satisfy

$$\frac{d}{dr}\left(r\frac{d\Phi(r)}{dr}\right) + \alpha r\Phi(r) = 0, \tag{8.4.26}$$
$$\Phi(1) = 0, \tag{8.4.27}$$

which admits the general solution

$$\Phi(\sqrt{\alpha}r) = aJ_0(\sqrt{\alpha}r) + bY_0(\sqrt{\alpha}r), \tag{8.4.28}$$

where J_0 and Y_0 are the zeroth order Bessel functions of the first and second kind, and a and b are arbitrary constants. Since Φ must be finite, it is necessary that $b = 0$. Applying the boundary condition (8.4.27) then implies that

$$J_0(\sqrt{\alpha}) = 0. \tag{8.4.29}$$

There are a countably infinite number of roots, $\sqrt{\alpha_n}$, that satisfy (8.4.29). Thus the general solution for the homogeneous problem may be written down as

$$u(r,t) = \sum_{n=1}^{\infty} a_n(t) J_0(\sqrt{\alpha}_n r). \tag{8.4.30}$$

The initial condition (8.4.24) becomes

$$u(r,0) = \sum_{n=1}^{\infty} a_n(0) J_0(\sqrt{\alpha}_n r) = f(r).$$

Orthogonality of Bessel functions then implies that

$$\begin{aligned} a_n(0) &= \frac{\int_0^1 r f(r) J_0(\sqrt{\alpha}_n r) dr}{\int_0^1 r J_0^2(\sqrt{\alpha}_n r) dr} \\ &= \frac{2}{(J_1(\sqrt{\alpha_n}))^2} \int_0^1 r f(r) J_0(\sqrt{\alpha_n} r) dr. \end{aligned} \tag{8.4.31}$$

The next step is to substitute (8.4.30) into the inhomogeneous problem (8.4.21). First it is noted that

$$\frac{\partial u}{\partial t} = \sum_{n=1}^{\infty} \frac{\partial a_n(t)}{\partial t} J_0(\sqrt{\alpha_n} r), \tag{8.4.32}$$

$$\frac{\partial u}{\partial r} = \sum_{n=1}^{\infty} a_n(t) \sqrt{\alpha_n} J_{-1}(\sqrt{\alpha_n} r) \tag{8.4.33}$$

$$\text{and} \quad \frac{\partial^2 u}{\partial r^2} = -\sum_{n=1}^{\infty} a_n(t) \left(\alpha_n J_0(\sqrt{\alpha_n} r) + \frac{\sqrt{\alpha_n}}{r} J_{-1}(\sqrt{\alpha_n} r) \right), \tag{8.4.34}$$

using the standard Bessel function recurrence relationships.

Thus

$$\frac{1}{r}\frac{\partial u}{\partial r} + \frac{\partial^2 u}{\partial r^2} = -\sum_{n=1}^{\infty} a_n(t) \alpha_n J_0(\sqrt{\alpha}_n r) \tag{8.4.35}$$

and so with (8.4.30), equation (8.4.21) may be rewritten in the form

$$\sum_{n=1}^{\infty} \left\{ \begin{array}{l} \frac{da_n}{dt}(t) + Q\alpha_n \epsilon \int_0^t e^{-\tau(t-t')/\lambda_1} a_n(t')dt' \\ +Q\alpha_n \kappa a_n(t) - Q\alpha_n(\kappa-1)e^{-\tau t/\lambda_1} a_n(0) \end{array} \right\} J_0(\sqrt{\alpha}_n r) = -\gamma g(t).$$

Again employing orthogonality gives rise to

$$\begin{aligned} &\frac{da_n}{dt}(t) + Q\alpha_n \epsilon \int_0^t e^{-\tau(t-t')/\lambda_1} a_n(t')dt' + Q\alpha_n \left[\kappa a_n(t) - (\kappa-1)e^{-\tau t/\lambda_1} a_n(0)\right] \\ &= \frac{-\gamma g(t) \int_0^1 r J_0(\sqrt{\alpha}_n r)dr}{\int_0^1 r J_0^2(\sqrt{\alpha}_n r)dr} \quad = \quad \frac{-2\gamma g(t)}{\sqrt{\alpha}_n J_1(\sqrt{\alpha}_n)}, \end{aligned} \tag{8.4.36}$$

using standard properties of Bessel functions.

Taking Laplace transforms gives

$$\begin{aligned} &sA_n(s) - a_n(0) + \frac{Q\alpha_n \epsilon}{s+\tau/\lambda_1} A_n(s) + Q\alpha_n \left[\kappa A_n(s) - (\kappa-1)\frac{a_n(0)}{s+\tau/\lambda_1}\right] \\ &= -\frac{2\gamma G(s)}{\sqrt{\alpha_n} J_1(\sqrt{\alpha}_n)}, \end{aligned} \tag{8.4.37}$$

where

$$A_n(s) = \int_0^\infty e^{-st} a_n(t)dt \qquad \text{and} \qquad G(s) = \int_0^\infty e^{-st} g(t)dt.$$

Solving for $A_n(s)$ delivers

$$\begin{aligned} A_n(s) &= \left\{ \frac{s+\tau/\lambda_1}{(s+Q\alpha_n\kappa)(s+\tau/\lambda_1) + Q\alpha_n\epsilon} \right\} \\ &\times \left\{ a_n(0)\left(1 + \frac{Q\alpha_n(\kappa-1)}{s+\tau/\lambda_1}\right) - \frac{2\gamma G(S)}{\sqrt{\alpha_n} J_1(\sqrt{\alpha}_n)} \right\}. \end{aligned} \tag{8.4.38}$$

Two forms of the solution will now be considered, depending upon the positivity (or otherwise) of the discriminant of $(s+Q\alpha_n\kappa)(s+\tau/\lambda_1) + Q\alpha_n\epsilon$.

8.4.3 The solution forms

The denominator of the first factor in (8.4.38) can be written as

$$(s + Q\alpha_n\kappa)(s + \tau/\lambda_1) + Q\alpha_n\epsilon = s^2 + \left(\frac{\tau}{\lambda_1} + Q\alpha_n\kappa\right)s + \frac{Q\tau}{\lambda_1}\alpha_n. \tag{8.4.39}$$

The inverse transform will be qualitatively different depending on whether (8.4.39) has real or complex roots. In the first case, (8.4.38) may be inverted by using partial fractions, leading to exponential functions. For complex roots, however, it is necessary to complete the square resulting in a negative exponential multiplying sine and cosine functions. These will be denoted Type 1 and Type 2 solutions. In certain cases, as will be show, a solution can be made up of both types: such a solution will be denoted a hybrid solution.

To examine when these types of solutions occur, consider the discriminant

$$\Delta_n = \left(\frac{\tau + Q\alpha_n\lambda_2}{\lambda_1}\right)^2 - \frac{4Q\alpha_n\tau}{\lambda_1},$$

or, equivalently,

$$\Delta_n = (Q\kappa)^2\left(\alpha_n^2 + \frac{2\tau}{Q\lambda_2^2}(\lambda_2 - 2\lambda_1)\alpha_n + \left(\frac{\tau}{Q\lambda_2}\right)^2\right), \tag{8.4.40}$$

where use has been made of the definitions of κ and ϵ.

A further possible form of the solution exists when the roots of (8.4.39) are equal. This of course will only occur when the discriminant is zero, that is, for at most two values of α which must coincide with one (or two) of the roots of the first order Bessel function. Consequently this case is omitted.

8.4.3.1 Oldroyd B forms of solution

A sufficient condition for Δ_n to be positive is $\lambda_2 - 2\lambda_1 \geq 0$, or, $\lambda_2/\lambda_1 \geq 2$, which would give rise to real roots and a Type 1 form of solution. Note from (8.2.8), however, that this condition is not physical. If $\lambda_2 - 2\lambda_1 < 0$ then, depending on the other parameters involved, there is a possibility of the roots being complex, at least for some values of the zeros of the first kind Bessel function. Nonetheless, since the zeros of the Bessel function are strictly monotonic increasing and can be arbitrarily large, there must be a value of n, say n_2, such that for $n > n_2$, Δ_n becomes positive again, indicating a return to real roots. Such a solution would be a hybrid solution.

Completing the square in α_n gives

$$\Delta_n = (Q\kappa)^2 \left[\left(\alpha_n + \frac{\tau(\lambda_2 - 2\lambda_1)}{Q\lambda_2^2} \right)^2 - \lambda_1 (\lambda_1 - \lambda_2) \left(\frac{2\tau}{Q\lambda_2^2} \right)^2 \right]. \tag{8.4.41}$$

Thus a Type 1 solution will occur if

$$\left(\alpha_n + \frac{\tau(\lambda_2 - 2\lambda_1)}{Q\lambda_2^2} \right)^2 \geq \lambda_1 (\lambda_1 - \lambda_2) \left(\frac{2\tau}{Q\lambda_2^2} \right)^2, \tag{8.4.42}$$

which would always be satisfied if $\lambda_2 \geq \lambda_1$, leading again to a non-physical solution. Consequently one needs only to look at the case $\lambda_1 > \lambda_2$. Treating the discrete variable α_n as a continuous variable, say α,

$$\Delta(\alpha) = (Q\kappa)^2 \left[\left(\alpha + \frac{\tau(\lambda_2 - 2\lambda_1)}{Q\lambda_2^2} \right)^2 - \lambda_1 (\lambda_1 - \lambda_2) \left(\frac{2\tau}{Q\lambda_2^2} \right)^2 \right], \tag{8.4.43}$$

then clearly, α has a minimum occurring at

$$\alpha^\star = \frac{\tau(2\lambda_1 - \lambda_2)}{Q\lambda_2^2}. \tag{8.4.44}$$

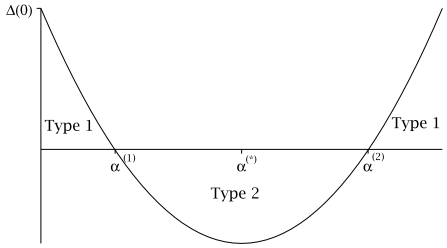

Figure 8.1: Sketch of Oldroyd B Forms of Solution: $\Delta(\alpha)$ versus α

Substituting (8.4.44) into (8.4.43), one finds that

$$\Delta(\alpha^\star) = -\lambda_1 (\lambda_1 - \lambda_2) \left(\frac{2\tau}{Q\lambda_2^2} \right)^2 < 0, \tag{8.4.45}$$

since it has been assumed that $\lambda_1 > \lambda_2$. The quadratic (8.4.43) therefore has a negative minimum which implies that there exists $\alpha^{(1)}$ and $\alpha^{(2)}$ such that $\Delta(\alpha^{(1)}) = \Delta(\alpha^{(2)}) = 0$. Indeed, these values are given by

$$\alpha^{(1),(2)} = \frac{\tau}{Q\lambda_2^2} \left(2\lambda_1 - \lambda_2 \pm 2\sqrt{\lambda_1(\lambda_1 - \lambda_2)} \right). \tag{8.4.46}$$

Under our assumption that $\lambda_1 > \lambda_2$, the two values $\alpha^{(1)}$ and $\alpha^{(2)}$ are positive. Define n_1 as the largest possible n (if it exists) that satisfies $\alpha_n \leq \alpha^{(1)}$ and n_2 as the smallest possible n that satisfies $\alpha_n \geq \alpha^{(2)}$. This now establishes the partition of the Oldroyd B summation into Type 1 and Type 2 solutions. Figure 8.1 shows a schematic of the forms of solution for the Oldroyd B case.

8.4.3.2 Maxwellian forms of solution

For Maxwellian flow when $\lambda_2 = 0$, it is observed from (8.4.40) that the discriminant is linear in α_n and is given by

$$\Delta_n = \frac{\tau^2}{\lambda_1^2} - 4\frac{Q\alpha_n\tau}{\lambda_1}. \tag{8.4.47}$$

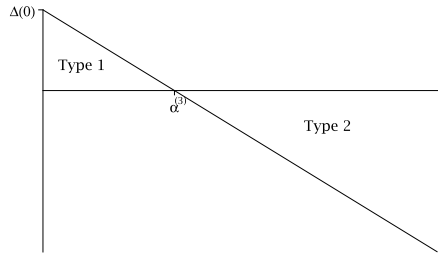

Figure 8.2: Sketch of Maxwellian Forms of Solution: $\Delta(\alpha)$ versus α

Treating the discrete variable α_n once again as a continuous variable, say α, there exists an $\alpha^{(3)}$ such that $\Delta(\alpha^{(3)}) = 0$. This value is given by

$$\alpha^{(3)} = \frac{\tau}{4Q\lambda_1}. \tag{8.4.48}$$

Define n_3 as the smallest possible n that satisfies $\alpha_n > \alpha^{(3)}$. Hence, if $\alpha_n \leq \alpha^{(3)}$ then there will be a Type 1 solution, at least for some values of the zeros of the first kind Bessel function, but since the zeros of the Bessel function are strictly monotonic increasing and can be arbitrarily large, there must exist an α_n such that Δ_n becomes negative, indicating a switch to complex roots and a Type 2 solution. Figure 8.2 displays a schematic of the forms of solution for the Maxwellian case. Note that

$$\Delta(0) = \left(\frac{\tau}{\lambda_1}\right)^2. \tag{8.4.49}$$

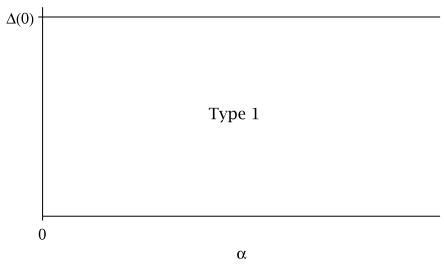

Figure 8.3: Sketch of Newtonian Form of Solution: $\Delta(\alpha)$ versus α

8.4.3.3 Newtonian form of solution

To obtain Newtonian flow, one must consider $\lambda_1 = \lambda_2 \to 0$ (and $\mu_p \to 0$). In this case, it is clear that $\Delta_n > 0$, and in fact $\Delta_n \to +\infty$. Hence, the roots are always real and so the solution is always of Type 1. Figure 8.3 displays a schematic of the form of the solution for the Newtonian case. Note that

$$\Delta(0) = \lim_{\lambda_1 \to 0} \left(\frac{\tau}{\lambda_1} \right)^2 = \infty. \tag{8.4.50}$$

8.4.3.4 Summary

To summarise, the possible forms of solution are

Oldroyd B

(a) No physical solution of Type 1 exists, that is a Type 1 solution on its own would only exist if $\lambda_2 \geq \lambda_1$.

(b) Type 2 solutions can never exist for all n.

(c) Type 1/Type2/Type 1 hybrid solutions exist when $\exists\, n_1, n_2$ such that
for $n \leq n_1$, Type 1 solution exists,
for $n\, \epsilon [n_1 + 1, n_2 - 1]$, Type 2 solution exists,

and for $n \geq n_2$, Type 1 solution exists.

(d) If $\alpha_1 > \alpha_{n_1}$, then there exists a Type 2/Type 1 hybrid solution.

Maxwellian

(a) Type 1 solution can never exist for all n.

(b) Type 2 solution exists if $\alpha_1 > R^2/4\nu_p\lambda_1$, $\nu_p = \mu_p/\rho$.

(c) Hybrid solutions exist when $\exists\, n_3$ such that

for $n < n_3$, Type 1 solution exists,

and for $n \geq n_3$, Type 2 solution exists.

Newtonian

(a) Type 1 solution exists only (this has already been derived in dimensional form, viz. equation 8.3.22)

(b) Type 2 and Hybrid solutions can never exist.

8.4.4 Oldroyd B solution

If (8.4.39) can be factorised as $(s - s_1)(s - s_2)$ with s_1 and s_2 real and given by

$$2s_{1,2} = -\left(\frac{\tau}{\lambda_1} + Q\alpha_n\kappa\right) \pm \sqrt{\left(\frac{\tau}{\lambda_1} + Q\alpha_n\kappa\right)^2 - 4\frac{Q\tau}{\lambda_1}\alpha_n}, \tag{8.4.51}$$

then the first factor in (8.4.38) can be rewritten in terms of partial fractions as

$$\frac{s + \tau/\lambda_1}{(s + Q\alpha_n\kappa)(s + \tau/\lambda_1) + Q\alpha_n\epsilon} = \frac{1}{s_1 - s_2}\left[\frac{s_1 + \tau/\lambda_1}{s - s_1} - \frac{s_2 + \tau/\lambda_1}{s - s_2}\right] \tag{8.4.52}$$

which has the inverse Laplace transform

$$L^{-1}\left[\frac{s+\tau/\lambda_1}{(s-s_1)(s-s_2)}\right] = \frac{1}{s_1-s_2}\left[(s_1+\tau/\lambda_1)e^{s_1 t} - (s_2+\tau/\lambda_1)e^{s_2 t}\right]. \quad (8.4.53)$$

Note that there exists a $s_{1,2}$ for each n but for reasons of clarity the subscript n has been suppressed. Similarly

$$\frac{Q\alpha_n(\kappa-1)}{(s-s_1)(s-s_2)} = \frac{Q\alpha_n(\kappa-1)}{s_1-s_2}\left[\frac{1}{s-s_1} - \frac{1}{s-s_2}\right] \quad (8.4.54)$$

admits the inverse Laplace transform

$$L^{-1}\left[\frac{Q\alpha_n(\kappa-1)}{(s-s_1)(s-s_2)}\right] = \frac{Q\alpha_n(\kappa-1)}{s_1-s_2}\left[e^{s_1 t} - e^{s_2 t}\right]. \quad (8.4.55)$$

Using (8.4.53) and (8.4.55) together with convolution allows the inverse Laplace transform of (8.4.38) to be written as

$$\begin{aligned} a_n(t) &= \frac{a_n(0)}{s_1-s_2}\left((s_1+\tau/\lambda_1)e^{s_1 t} - (s_2+\tau/\lambda_1)e^{s_2 t} + Q\alpha_n(\kappa-1)(e^{s_1 t} - e^{s_2 t})\right) \\ &- \frac{2\gamma}{(s_1-s_2)\sqrt{\alpha_n}J_1(\sqrt{\alpha_n})}\int_0^t \begin{pmatrix} (s_1+\tau/\lambda_1)e^{s_1(t-t')} \\ -(s_2+\tau/\lambda_1)e^{s_2(t-t')} \end{pmatrix} g(t')dt', \end{aligned} \quad (8.4.56)$$

where $a_n(0)$ is given by (8.4.31). This is the Type 1 form of $a_n(t)$.
Completing the square of (8.4.39), on the other hand, yields

$$\left[s + \frac{1}{2}\left(\tau/\lambda_1 + Q\alpha_n\kappa\right)\right]^2 + \eta^2, \quad (8.4.57)$$

where $\eta^2 = Q\tau\alpha_n/\lambda_1 - \left(\tau/\lambda_1 + Q\alpha_n\kappa\right)^2/4$.

Again, note that there exists an η for each n but it is convenient not to include the subscript n.

The first expression in (8.4.38) may then be rewritten as

$$\frac{s+\frac{1}{2}(\tau/\lambda_1+Q\alpha_n\kappa)}{[s+\frac{1}{2}(\tau/\lambda_1+Q\alpha_n\kappa)]^2+\eta^2}+\frac{(\tau/\lambda_1-Q\alpha_n\kappa)}{2\eta}\frac{\eta}{[s+\frac{1}{2}(\tau/\lambda_1+Q\alpha_n\kappa)]^2+\eta^2}, \tag{8.4.58}$$

yielding the inverse Laplace transform

$$e^{-\frac{1}{2}(\tau/\lambda_1+Q\alpha_n\kappa)t}\left(\cos\eta t+\frac{(\tau/\lambda_1-Q\alpha_n\kappa)}{2\eta}\sin\eta t\right). \tag{8.4.59}$$

Furthermore,

$$L^{-1}\left[\frac{s+\tau/\lambda_1}{(s+Q\alpha_n\kappa)(s+\tau/\lambda_1)+Q\alpha_n\kappa}\left(\frac{Q\alpha_n(\kappa-1)}{s+\tau/\lambda_1}\right)\right]$$

$$= \quad \frac{Q\alpha_n(\kappa-1)}{\eta}\ e^{-\frac{1}{2}(\tau/\lambda_1+Q\alpha_n\kappa)t}\sin\eta t. \tag{8.4.60}$$

Thus, upon employing convolution, the inverse Laplace transform of (8.4.38) becomes

$$\begin{aligned} a_n(t) \ &= a_n(0)\ e^{-\frac{1}{2}(\tau/\lambda_1+Q\alpha_n\kappa)t}\left(\cos\eta t+\frac{(\tau/\lambda_1+Q\alpha_n(\kappa-2))}{2\eta}\sin\eta t\right) \\ - \quad &\frac{2\gamma}{\sqrt{\alpha_n}J_1(\sqrt{\alpha}_n)}\int_0^t e^{-\frac{1}{2}(\tau/\lambda_1+Q\alpha_n\kappa)(t-t')}\left(\begin{array}{c}\cos\eta(t-t')\\ +\frac{(\tau/\lambda_1-Q\alpha_n\kappa)}{2\eta}\sin\eta(t-t')\end{array}\right)g(t')dt'. \end{aligned} \tag{8.4.61}$$

This is the Type 2 form of $a_n(t)$.

8.4.4.1 Hybrid solution

The hybrid solution switches from a Type 1 to a Type 2 solution when the (n_1+1)th root, α_{n_1+1}, is reached and then switches back to Type 1 when the n_2th root, α_{n_2}, is attained. Hence, making use of (8.4.56) and (8.4.61) along with (8.4.30) and (8.4.31), allows us to write down the hybrid solution as

$$u(r,t) = 2\left[\sum_{n=1}^{n_1} \text{Type 1} + \sum_{n=n_1+1}^{n_2-1} \text{Type 2} + \sum_{n=n_2}^{\infty} \text{Type 1}\right],$$

or

$$
\begin{aligned}
& u(r,t) \\
&= \quad 2\sum_{n=1}^{n_1} \left\{ \begin{array}{c} \frac{(s_1+\tau/\lambda_1)e^{s_1 t}-(s_2+\tau/\lambda_1)e^{s_2 t}+Q\alpha_n(\kappa-1)(e^{s_1 t}-e^{s_2 t})}{(J_1(\sqrt{\alpha_n}))^2} \int_0^1 r f(r) J_0(\sqrt{\alpha_n} r) dr \\ -\frac{\gamma \int_0^t \left((s_1+\tau/\lambda_1)e^{s_1(t-t')} - (s_2+\tau/\lambda_1)e^{s_2(t-t')} \right) g(t') dt'}{\sqrt{\alpha_n} J_1(\sqrt{\alpha_n})} \end{array} \right\} \\
&\qquad \times \frac{J_0(\sqrt{\alpha_n} r)}{s_1 - s_2} \\
&+ \quad 2\sum_{n=n_1+1}^{n_2-1} \left\{ \begin{array}{c} \frac{e^{-\frac{1}{2}(\tau/\lambda_1+Q\alpha_n\kappa)t}}{J_1(\sqrt{\alpha}_n)^2} \left(\cos\eta t + \frac{(\tau/\lambda_1+Q\alpha_n(\kappa-2))}{2\eta} \sin\eta t \right) \\ \times \int_0^1 r f(r) J_0(\sqrt{\alpha}_n r) dr \\ -\gamma \int_0^t \frac{e^{-\frac{1}{2}(\tau/\lambda_1+Q\alpha_n\kappa)(t-t')}}{\sqrt{\alpha_n} J_1(\sqrt{\alpha_n})} \left(\begin{array}{c} \cos\eta(t-t') \\ +\frac{(\tau/\lambda_1-Q\alpha_n\kappa)}{2\eta} \sin\eta(t-t') \end{array} \right) g(t') dt' \end{array} \right\} \\
&\qquad \times J_0(\sqrt{\alpha}_n r) \\
&+ \quad 2\sum_{n=n_2}^{\infty} \left\{ \begin{array}{c} \frac{(s_1+\tau/\lambda_1)e^{s_1 t}-(s_2+\tau/\lambda_1)e^{s_2 t}+Q\alpha_n(\kappa-1)(e^{s_1 t}-e^{s_2 t})}{(J_1(\sqrt{\alpha_n}))^2} \int_0^1 r f(r) J_0(\sqrt{\alpha_n} r) dr \\ -\frac{\gamma \int_0^t \left((s_1+\tau/\lambda_1)e^{s_1(t-t')} - (s_2+\tau/\lambda_1)e^{s_2(t-t')} \right) g(t') dt'}{\sqrt{\alpha_n} J_1(\sqrt{\alpha_n})} \end{array} \right\} \\
&\qquad \times \frac{J_0(\sqrt{\alpha_n} r)}{s_1 - s_2}.
\end{aligned}
\tag{8.4.62}
$$

Of course, if the first root, α_1, is greater than α_{n_1}, then there exists the following Type 2/Type 1 form of hybrid solution:

$$
\begin{aligned}
& u(r,t) \\
&= 2\sum_{n=1}^{n_2-1} \left\{ \begin{array}{c} \frac{e^{-\frac{1}{2}(\tau/\lambda_1+Q\alpha_n\kappa)t}}{J_1(\sqrt{\alpha}_n)^2}\left(\cos\eta t + \frac{(\tau/\lambda_1+Q\alpha_n(\kappa-2))}{2\eta}\sin\eta t\right) \\ \times \int_0^1 r f(r) J_0(\sqrt{\alpha}_n r) dr \\ -\gamma\int_0^t \frac{e^{-\frac{1}{2}(\tau/\lambda_1+Q\alpha_n\kappa)(t-t')}}{\sqrt{\alpha_n}J_1(\sqrt{\alpha_n})}\left(\begin{array}{c}\cos\eta(t-t') \\ +\frac{(\tau/\lambda_1-Q\alpha_n\kappa)}{2\eta}\sin\eta(t-t')\end{array}\right) g(t')dt' \end{array} \right\} \\
&\quad \times J_0(\sqrt{\alpha}_n r) \\
&+ 2\sum_{n=n_2}^{\infty} \left\{ \begin{array}{c} \frac{(s_1+\tau/\lambda_1)e^{s_1 t}-(s_2+\tau/\lambda_1)e^{s_2 t}+Q\alpha_n(\kappa-1)(e^{s_1 t}-e^{s_2 t})}{(J_1(\sqrt{\alpha_n}))^2}\int_0^1 r f(r) J_0(\sqrt{\alpha_n} r) dr \\ -\frac{\gamma\int_0^t \left((s_1+\tau/\lambda_1)e^{s_1(t-t')}-(s_2+\tau/\lambda_1)e^{s_2(t-t')}\right) g(t')dt'}{\sqrt{\alpha_n}J_1(\sqrt{\alpha_n})} \end{array} \right\} \\
&\quad \times \frac{J_0(\sqrt{\alpha_n} r)}{s_1-s_2}
\end{aligned}
\tag{8.4.63}
$$

8.4.5 Oldroyd B pulsatile flow

Up until now the non-dimensional scaling has been rather general. For pulsatile flow it is appropriate to replace P with $\rho\omega RU$ and τ with $1/\omega$, where ω is a measure of the frequency.

This results in

$\gamma = 1$, $Q = 1/Wo^2$,

$2s_{1,2} = (1/\omega\lambda_1 + \alpha_n\kappa/Wo^2)\left(-1 \pm \sqrt{1 - 4\alpha_n\omega\lambda_1 Wo^2/(Wo^2+\alpha_n\omega\lambda_2)^2}\right)$ and

$\eta = \sqrt{\alpha_n/(\omega Wo^2\lambda_1) - (1/(\omega\lambda_1)+\alpha_n\kappa/Wo^2)^2/4}$, where $Wo = R\sqrt{\omega/\nu}$ is the well-known Womersley number.

8.5 The Maxwellian equation for viscoelastic flow in a rigid cylinder

Recall from §8.3.3 that to obtain the corresponding Maxwellian solutions, one should let $\mu_s \to 0$ in the Oldroyd B solutions, with the consequence that $\lambda_2 \to 0$. Recall that the condition for a Type 1 only solution for Oldroyd B was the non-physical condition, $\lambda_2 \geq \lambda_1$. For Maxwellian flow, $\lambda_2 = 0$ and hence this condition is never satisfied. This confirms that there cannot exist a Type 1 only solution for Maxwellian flow.

The hybrid solution switches from a Type 1 to a Type 2 solution when the n_3th root, α_{n_3}, of the Bessel function $J(\sqrt{\alpha})$ is reached. The n_3th root is the first root that satisfies $\alpha_{n_3} > R^2/4\nu_p\lambda_1$. Of course, it is possible that no such root exists: this would occur when $\alpha_1 > R^2/4\nu_p\lambda_1$, resulting in a Type 2 solution for all values of n. The limiting process $\mu_s \to 0$ and $\lambda_2 \to 0$ is straightforward and yields the following two cases

8.5.1 Maxwellian hybrid solution

$$
\begin{aligned}
& u(r,t) \\
&= 2\sum_{n=1}^{n_3-1}\Bigg\{ \frac{(s_{M_1}+\tau/\lambda_1)e^{s_{M_1}t}-(s_{M_2}+\tau/\lambda_1)e^{s_{M_2}t})-Q_p\alpha_n\left(e^{s_{M_1}t}-e^{s_{M_2}t}\right)}{(J_1(\sqrt{\alpha_n}))^2} \\
&\qquad \times\int_0^1 rf(r)J_0(\sqrt{\alpha_n}r)dr \\
&- \frac{\gamma\int_0^t\left[(s_{M_1}+\tau/\lambda_1)e^{s_{M_1}(t-t')}-(s_{M_2}+\tau/\lambda_1)e^{s_{M_2}(t-t')}\right]g(t')dt'}{\sqrt{\alpha_n}J_1(\sqrt{\alpha_n})}\Bigg\}\frac{J_0(\sqrt{\alpha_n}r)}{s_{M_1}-s_{M_2}} \\
&+ 2\sum_{n=n_3}^{\infty}\Bigg\{\frac{e^{-\frac{1}{2}\tau t/\lambda_1}}{J_1(\sqrt{\alpha}_n)^2}\left(\cos\eta_M t+\frac{\tau/\lambda_1-2Q_p\alpha_n}{2\eta_M}\sin\eta_M t\right)\int_0^1 rf(r)J_0(\sqrt{\alpha}_n r)dr \\
&- \frac{\gamma\int_0^t e^{-\frac{1}{2}\tau(t-t')/\lambda_1}\left(\cos\eta_M(t-t')+\frac{\tau/\lambda_1}{2\eta_M}\sin\eta_M(t-t')\right)g(t')dt'}{\sqrt{\alpha_n}J_1(\sqrt{\alpha}_n)}\Bigg\}J_0(\sqrt{\alpha}_n r).
\end{aligned}
\tag{8.5.1}
$$

The variables s_{M_1}, s_{M_2}, Q_p and η_M manifest themselves as a result of the limiting process. They are: $2s_{M_1,M_2} = -\tau/\lambda_1 \pm \sqrt{(\tau/\lambda_1)^2 - 4Q_p\tau\alpha_n/\lambda_1}$,
$Q_p = \nu_p\tau/R^2, \quad \eta_M = \sqrt{Q_p\tau\alpha_n/\lambda_1 - \tau^2/4\lambda_1^2}$, where M denotes Maxwellian.

8.5.2 Maxwellian Type 2 solution

If $\alpha_1 > R^2/4\nu_p\lambda_1$ then there exists a Type 2 solution only, given by

$$\begin{aligned} & u(r,t) \\ &= 2\sum_{n=1}^{\infty}\Bigg\{\frac{e^{-\frac{1}{2}\tau t/\lambda_1}}{J_1(\sqrt{\alpha}_n)^2}\left(\cos\eta_M t+\frac{\tau/\lambda_1-2Q_p\alpha_n}{2\eta_M}\sin\eta_M t\right)\int_0^1 rf(r)J_0(\sqrt{\alpha}_n r)dr \\ &- \frac{\gamma\int_0^t e^{-\frac{1}{2}\tau(t-t')/\lambda_1}\left(\cos\eta_M(t-t')+\frac{\tau/\lambda_1}{2\eta_M}\sin\eta_M(t-t')\right)g(t')dt'}{\sqrt{\alpha_n}J_1(\sqrt{\alpha}_n)}\Bigg\}J_0(\sqrt{\alpha}_n r). \end{aligned} \tag{8.5.2}$$

8.5.3 Maxwellian Pulsatile flow

For pulsatile flow, P is replaced with $\rho\omega RU$ and τ with $1/\omega$, where ω is a measure of the frequency. This results in
$\gamma = 1$, $Q_p = 1/Wo_p^2$, $2s_{M1,M2} = (1/(\omega\lambda_1))\left(-1 \pm \sqrt{1-4\alpha_n\omega\lambda_1/Wo_p^2}\right)$ and
$\eta_M = \sqrt{\alpha_n/(\omega Wo_p^2\lambda_1) - (1/2\omega\lambda_1)^2}$, where $Wo_p = R\sqrt{\omega/\nu_p}$ is the Womersley number containing only the polymeric part of the viscosity.

8.6 The Newtonian equation for flow in a rigid cylinder

Recall from §8.3.3 that to obtain the corresponding Newtonian solutions, one should let $\mu_p \to 0$ and then $\lambda_1 = \lambda_2 \to 0$ in the Oldroyd B solutions. Immediately, it is observed from (8.4.46) that as $\lambda_1 = \lambda_2 \to 0$, $\alpha^{(1),(2)} \to \infty$. Hence there exist no switchover points, confirming that there can never exist a Type 2 solution for the Newtonian case. The limiting process, although requiring an expansion of the square root term in the expression for s, is nevertheless straightforward and the

solution is provided directly.

8.6.1 General analytic solution of Newtonian flow

The solution of Newtonian flow in a rigid cylinder can be written as

$$u(r,t) = 2\sum_{n=1}^{\infty}\left\{\frac{e^{-Q_s\alpha_n t}\int_0^1 rf(r)J_0(\sqrt{\alpha_n}r)dr}{(J_1(\sqrt{\alpha_n}))^2} - \frac{\gamma\int_0^t e^{-Q_s\alpha_n(t-t')}g(t')dt'}{\sqrt{\alpha_n}J_1(\sqrt{\alpha_n})}\right\}J_0(\sqrt{\alpha_n}r) \tag{8.6.1}$$

where $Q_s = \nu_s\tau/R^2$. Note that equation (8.6.1) is the dimensional form of (8.2.14), with $R = a$.

8.6.2 Pulsatile Newtonian flow

For pulsatile flow, P is again replaced with $\rho\omega RU$ and τ with $1/\omega$, where ω is a measure of the frequency. This results in $\gamma = 1$ and $Q_s = 1/Wo_s^2$, where $Wo_s = R\sqrt{\omega/\nu_s}$ is the Womersley number containing only the solvent part of the viscosity.

8.7 Poiseuille flow in a rigid cylinder

Consider the steady solution for the flow of an incompressible viscous fluid through a hollow cylinder of length L and fixed radius R. In cylindrical polars, the non-dimensionalized Navier-Stokes equations reduce to (assuming no θ dependence)

$$\frac{1}{r}\frac{d}{dr}\left(r\frac{du}{dr}\right) = \frac{PR}{\mu_s U}\frac{dp}{dz}, \tag{8.7.1}$$

Solving (8.7.1) subject to the usual no-slip and boundedness conditions yields the well known solution of Poiseuille flow

$$u(r) = -\frac{PR}{4\mu_s U}\frac{dp}{dz}\left(1-r^2\right) = -\frac{Re}{4}\frac{dp}{dz}\left(1-r^2\right), \tag{8.7.2}$$

where $Re = RU/\nu_s$ is the Reynolds number and the non-dimensional scaling $P = \rho U^2$ has been selected.

8.7.1 Poiseuille flow as a special case of Oldroyd B

To show that Poiseuille flow is a special case of Oldroyd B (Equation 8.4.62 or 8.4.63), it is necessary to show that as $\mu_p \to 0$, $\lambda_1 = \lambda_2 \to 0$ and $t \to \infty$, the Oldroyd B solutions tend to the expression (8.7.2). Since it has already been shown that the Oldroyd B solution tends to the Newtonian solution as $\mu_p \to 0$ and $\lambda_1 = \lambda_2 \to 0$, one needs only to show that the Newtonian solution, expression (8.6.1), tends to (8.7.2) as $t \to \infty$. Recall that for Newtonian flow

$$u(r,t) = 2\sum_{n=1}^{\infty}\left\{\frac{e^{-Q_s\alpha_n t}\int_0^1 rf(r)J_0(\sqrt{\alpha_n}r)dr}{(J_1(\sqrt{\alpha_n}))^2} - \frac{\gamma\int_0^t e^{-Q_s\alpha_n(t-t')}g(t')dt'}{\sqrt{\alpha_n}J_1(\sqrt{\alpha_n})}\right\}J_0(\sqrt{\alpha_n}r) \tag{8.7.3}$$

where $g(t) = \partial p/\partial z$ is constant for Poiseuille flow. Note that

$$\frac{P\tau}{\rho RU}\frac{\partial p}{\partial z}\int_0^t e^{-Q_s\alpha_n(t-t')}dt' = \frac{PR}{\alpha_n\mu_s U}\frac{\partial p}{\partial z}\left(1-e^{-Q_s\alpha_n t}\right) \tag{8.7.4}$$

since $Q_s = \nu_s\tau/R^2$, allowing (8.7.3) to be written as

$$u(r,t) = 2\sum_{n=1}^{\infty}\left\{\frac{e^{-Q_s\alpha_n t}\int_0^1 rf(r)J_0(\sqrt{\alpha_n}r)dr}{(J_1(\sqrt{\alpha_n}))^2} - \frac{PR\left(1-e^{-Q_s\alpha_n t}\right)}{\alpha_n^{3/2}\mu_s U J_1(\sqrt{\alpha_n})}\frac{\partial p}{\partial z}\right\}J_0(\sqrt{\alpha_n}r). \tag{8.7.5}$$

To return to Poiseuille flow, with the particular scaling $P = \rho U^2$, the limit of (8.7.5) as $t \to \infty$ is taken, giving rise to

$$\begin{aligned} u(r) &= -\frac{2PR}{\mu_s U}\frac{dp}{dz}\sum_{n=1}^{\infty}\alpha_n^{-3/2}\frac{J_0(\sqrt{\alpha_n}r)}{J_1(\sqrt{\alpha_n})} \\ &= -2Re\frac{dp}{dz}\sum_{n=1}^{\infty}\alpha_n^{-3/2}\frac{J_0(\sqrt{\alpha_n}r)}{J_1(\sqrt{\alpha_n})} \\ &= -\frac{Re}{4}\frac{dp}{dz}\left(1-r^2\right), \end{aligned} \tag{8.7.6}$$

since the Bessel function expansion of $1 - r^2$ is $\sum_{n=1}^{\infty} b_n J_0(\sqrt{\alpha_n}r)$, with $b_n = 8\alpha_n^{-3/2}/J_1(\sqrt{\alpha_n})$.

8.7.2 Oldroyd B steady flow

To obtain the equations of Oldroyd B steady flow, the time-derivative contributions to $\overset{\nabla}{\mathbf{T}}$ and $\overset{\nabla}{\mathbf{d}}$ are neglected. The Oldroyd B constitutive equation (8.3.7) then reduces to (after omitting the subscript z in the velocity component)

$$\begin{pmatrix} T_{rr} & T_{rz} \\ T_{zr} & T_{zz} \end{pmatrix} + \lambda_1 \begin{pmatrix} 0 & -u_{,r}T_{rr} \\ -u_{,r}T_{rr} & -2u_{,r}T_{rz} \end{pmatrix} = 2\mu \begin{pmatrix} 0 & \frac{1}{2}u_{,r} \\ \frac{1}{2}u_{,r} & -\lambda_2 u_{,r}^2 \end{pmatrix}. \tag{8.7.7}$$

Solving the first and second components gives rise to

$$T_{rz} = \mu u_{,r}. \tag{8.7.8}$$

Then, from the conservation of momentum equation (8.2.2),

$$-\begin{pmatrix} p_{,r} \\ p_{,z} \end{pmatrix} + \begin{pmatrix} 0 \\ \frac{1}{r}\frac{d}{dr}(r\mu u_{,r}) \end{pmatrix} = 0, \tag{8.7.9}$$

since the radial component of velocity has been assumed to be zero and the stress tensor has been assumed to have no z dependence. From the first component of (8.7.9) it is observed that

$$p_{,r} = 0 \Rightarrow p = p(z).$$

It is assumed that the pressure is the same linear function of z as in (8.4.15) . Thus, the following is obtained from the second component of (8.7.9):

$$-p_{,z} + \frac{\mu}{r}\frac{d}{dr}(ru_{,r}) = 0. \tag{8.7.10}$$

Rearranging (8.7.10) and applying the non-dimensionalization as before gives rise to

$$\frac{1}{r}\frac{d}{dr}\left(r\frac{du}{dr}\right) = \frac{PR}{\mu U}\frac{dp}{dz}. \tag{8.7.11}$$

Notice that (8.7.10) is the same as the Poiseuille equation (8.7.1), except that μ_s has been replaced by $\mu = \mu_s + \mu_p$.

8.7.3 Maxwellian steady flow

Starting from the Maxwellian constitutive equation, and neglecting the time-derivative contributions it is found that the expressions obtained for T_{rr} and T_{rz} are the same as for Oldroyd B steady flow, except that μ is replaced by μ_p (no solute viscosity for Maxwellian flows). Hence, the equation of Maxwellian steady flow is the following:

$$\frac{1}{r}\frac{d}{dr}\left(r\frac{du}{dr}\right) = \frac{PR}{\mu_p U}\frac{dp}{dz}, \tag{8.7.12}$$

that is, the Poiseuille equation (8.7.1) with μ_s replaced by μ_p.

8.8 Oldroyd B flow in an annular region

This work has in part been motivated by Womersley's early papers (Womersley 1955a, 1955b) in his attempt to model blood flow in a main artery. Recent industrial work has emphasized the need to study blood flow when a circular catheter is inserted in an artery to continuously monitor cardiac output (Fotheringham *et al.* 2005). Assuming that the catheter sits along the centre-line of the artery then it could be useful to extend the present work to flow in an annular region. In this section, it is indicated how this may be achieved.

In this case, the normalized boundary conditions consist of the following two non-slip conditions

$$\Phi(R_I/R) = \Phi(1) = 0, \tag{8.8.1}$$

where R is the artery radius and R_I is the inner (catheter) radius.
Then, solving the homogeneous problem associated with (8.4.26), as before, results in

$$\Phi(\sqrt{\xi}r) = aJ_0(\sqrt{\xi}r) + bY_0(\sqrt{\xi}r). \tag{8.8.2}$$

Applying the two boundary conditions leads to

$$J_0(\sqrt{\xi}R_I/R)Y_0(\sqrt{\xi}) = J_0(\sqrt{\xi})Y_0(\sqrt{\xi}R_I/R) \tag{8.8.3}$$

which has a countably infinite number of solutions or eigenvalues, ξ_n. The general solution of (8.4.26) is then a linear combination of the infinite modes

$$V_0(\sqrt{\xi_n}r) = \left(J_0(\sqrt{\xi_n}r)Y_0(\sqrt{\xi_n}) - J_0(\sqrt{\xi_n})Y_0(\sqrt{\xi_n}r)\right),\ n = 1, 2, ... \tag{8.8.4}$$

Now let

$$u(r,t) = \sum_{n=1}^{\infty} a_n(t) V_0(\sqrt{\xi_n} r), \tag{8.8.5}$$

where, using the initial condition (8.4.24),

$$u(r,0) = \sum_{n=1}^{\infty} a_n(t) V_0(\sqrt{\xi}_n r) = f(r). \tag{8.8.6}$$

Or, after making use of the orthogonality property of the functions $V_0(\sqrt{\xi}_n r)$,

$$a_n(0) = \frac{\displaystyle\int_{R_I/R}^{1} r f(r) V_0(\sqrt{\xi}_n r) dr}{\displaystyle\int_{R_I/R}^{1} r V_0^2(\sqrt{\xi}_n r) dr}. \tag{8.8.7}$$

Differentiation of (8.8.5) yields

$$\begin{aligned}
\frac{\partial u}{\partial t} &= \sum_{n=1}^{\infty} \frac{da_n}{dt}(t) V_0(\sqrt{\xi}_n r), \\
\frac{\partial u}{\partial r} &= \sum_{n=1}^{\infty} a_n(t) \sqrt{\xi}_n \left[J_{-1}(\sqrt{\xi}_n r) Y_0(\sqrt{\xi}_n) - J_0(\sqrt{\xi}_n) Y_{-1}(\sqrt{\xi}_n r) \right] \\
\frac{\partial^2 u}{\partial r^2} &= -\sum_{n=1}^{\infty} a_n(t) \sqrt{\xi}_n \left[\left(\frac{1}{r} J_{-1}(\sqrt{\xi}_n r) + \sqrt{\xi}_n J_0(\sqrt{\xi}_n r) \right) Y_0(\sqrt{\xi}_n) \right. \\
&- \left. \left(\frac{1}{r} Y_{-1}(\sqrt{\xi}_n r) + \sqrt{\xi}_n Y_0(\sqrt{\xi}_n r) \right) J_0(\sqrt{\xi}_n) \right]
\end{aligned}$$

so that

$$\frac{\partial^2 u}{\partial r^2} + \frac{1}{r} \frac{\partial u}{\partial r} = -\sum_{n=1}^{\infty} a_n(t) \xi_n V_0(\sqrt{\xi}_n r). \tag{8.8.8}$$

Substitution of (8.8.5) and (8.8.8) into (8.4.21) gives

$$\sum_{n=1}^{\infty}\left\{\frac{da_n}{dt}(t) \;+\; Q\xi_n\epsilon\int_0^t e^{-\tau(t-t')/\lambda_1}a_n(t')dt' \right. \tag{8.8.9}$$

$$\left. +\; Q\xi_n\kappa a_n(t) - Q\xi_n(\kappa-1)e^{-\tau t/\lambda_1}a_n(0)\right\}V_0(\sqrt{\xi}_n r) = -\gamma g(t).$$

Making use of orthogonality again provides

$$\frac{da_n}{dt}(t) \;+\; Q\xi_n\epsilon\int_0^t e^{-\tau(t-t')/\lambda_1}a_n(t')dt' + Q\xi_n\kappa a_n(t) - Q\xi_n(\kappa-1)e^{-\tau t)/\lambda_1}a_n(0)$$

$$= \frac{-\gamma g(t)\int_{R_I/R}^1 rV_0(\sqrt{\xi}_n r)dr}{\int_{R_I/R}^1 rV_0^2(\sqrt{\xi}_n r)dr}. \tag{8.8.10}$$

The right-hand side of (8.8.10) can be simplified by noting that (Carslaw & Jaeger 1986)

$$\int_{R_I/R}^1 rV_0(\sqrt{\xi}_n r)dr = \frac{2(J_0(\sqrt{\xi}_n R_I/R) - J_0(\sqrt{\xi}_n))}{\pi\xi_n J_0(\sqrt{\xi}_n R_I/R)}$$

$$\int_{R_I/R}^1 rV_0^2(\sqrt{\xi}_n r)dr = \frac{2(J_0^2(\sqrt{\xi}_n R_I/R) - J_0^2(\sqrt{\xi}_n))}{\pi^2\xi_n J_0^2(\sqrt{\xi}_n R_I/R)}. \tag{8.8.11}$$

Substituting these expressions into (8.8.10) gives

$$\frac{da_n}{dt}(t) \;+\; Q\xi_n\epsilon\int_0^t e^{-\tau(t-t')/\lambda_1}a_n(t')dt' + Q\xi_n\kappa a_n(t) - Q\xi_n(\kappa-1)e^{-\tau t/\lambda_1}a_n(0)$$

$$= \frac{-\gamma g(t)\pi}{1+X_0} \tag{8.8.12}$$

where $X_0 = J_0(\sqrt{\xi}_n)/J_0(\sqrt{\xi}_n R_I/R)$. Taking Laplace Transforms of (8.8.12) results in

$$sA_n(s) - a_n(0) + \frac{Q\epsilon\xi_n}{s+\tau/\lambda_1}A_n(s) + Q\xi_n\kappa A_n(s) - \frac{Q\xi_n(\kappa-1)a_n(0)}{s+\tau/\lambda_1} = \frac{-\gamma G(s)\pi}{1+X_0}, \tag{8.8.13}$$

where

$$A_n(s) = \int_0^\infty e^{-st}a_n(t)dt \quad \text{and} \quad G(s) = \int_0^\infty e^{-st}g(t)dt.$$

Solving for $A_n(s)$ delivers

$$A_n(s) = \left\{\frac{s+\tau/\lambda_1}{(s+Q\xi_n\kappa)(s+\tau/\lambda_1)+Q\xi_n\epsilon}\right\}\left\{a_n(0)\left(1+\frac{Q\xi_n(\kappa-1)}{s+\tau/\lambda_1}\right) - \frac{\gamma G(S)\pi}{1+X_0}\right\}. \tag{8.8.14}$$

8.8.1 Oldroyd B annular solution

Note that (8.8.14) takes the same form as the cylindrical case (8.4.38), except that α_n has been replaced by ξ_n and the term that multiplies $G(s)$ is different. Hence, the analysis of the different solution forms follows through, resulting in the annular Type 1 form of $a_n(t)$ as

$$\begin{aligned} a_n(t) &= \frac{a_n(0)\left((\tilde{s}_1+\tau/\lambda_1)e^{\tilde{s}_1 t} - (\tilde{s}_2+\tau/\lambda_1)e^{\tilde{s}_2 t} + Q\xi_n(\kappa-1)(e^{\tilde{s}_1 t} - e^{\tilde{s}_2 t})\right)}{\tilde{s}_1-\tilde{s}_2} \\ &- \frac{\gamma\pi\int_0^t\left((\tilde{s}_1+\tau/\lambda_1)e^{\tilde{s}_1(t-t')} - (\tilde{s}_2+\tau/\lambda_1)e^{\tilde{s}_2(t-t')}\right)g(t')dt'}{(\tilde{s}_1-\tilde{s}_2)(1+X_0)}, \end{aligned} \tag{8.8.15}$$

where $2\tilde{s}_{1,2} = -(\tau/\lambda_1 + Q\xi_n\kappa) \pm \sqrt{(\tau/\lambda_1 + Q\xi_n\kappa)^2 - 4Q\tau\xi_n/\lambda_1}$. Similarly, the annular Type 2 form of $a_n(t)$ can be written as

$$\begin{aligned} a_n(t) &= a_n(0)\ e^{-\frac{1}{2}(\tau/\lambda_1+Q\xi_n\kappa)t}\left(\cos\tilde{\eta}t + \frac{(\tau/\lambda_1 - Q\xi_n\kappa)}{2\tilde{\eta}}\sin\tilde{\eta}t + \frac{Q\xi_n(\kappa-1)}{\tilde{\eta}}\sin\tilde{\eta}t\right) \\ &- \frac{\gamma\pi\int_0^t e^{-\frac{1}{2}(\tau/\lambda_1+Q\xi_n\kappa)(t-t')}\left(\cos\tilde{\eta}(t-t') + \frac{(\tau/\lambda_1-Q\xi_n\kappa)}{2\tilde{\eta}}\sin\tilde{\eta}(t-t')\right)g(t')dt'}{1+X_0}, \end{aligned} \tag{8.8.16}$$

where $\tilde{\eta}^2 = Q\tau\xi_n/\lambda_1 - (\tau/\lambda_1 + Q\xi_n\kappa)^2/4$. Note also that the denominator in (8.8.7) can be simplified by using the second expression in (8.8.11):

$$\begin{aligned} a_n(0) &= \frac{\int_{R_I/R}^1 rf(r)V_0(\sqrt{\xi}_n r)dr}{\int_{R_I/R}^1 rV_0^2(\sqrt{\xi}_n r)dr} \\ &= \frac{\pi^2\xi_n\int_{R_I/R}^1 rf(r)V_0(\sqrt{\xi}_n r)dr}{2(1-X_0^2)}. \end{aligned} \tag{8.8.17}$$

8.8.1.1 Oldroyd B hybrid solution

As with cylindrical pipe flow an Oldroyd B Type 1 solution would only exist if $\lambda_2 \geq \lambda_1$, which is non-physical. The hybrid solution switches between the Type 1 and Type 2 solutions when the (n_1+1)th root, ξ_{n_1+1} is reached, and then switches back to Type 1 when the n_2th root, ξ_{n_2} is reached. Following §8.4.3, ξ_{n_1} is defined as the largest possible ξ_n that satisfies $\xi_n \leq \alpha^{(1)}$ and ξ_{n_2} as the smallest possible ξ_n that satisfies $\xi_n \geq \alpha^{(2)}$. This now defines the partition of the Oldroyd B summation into Type 1 and Type 2 solutions. Hence, making use of (8.8.15-8.8.17) and (8.8.5),

the hybrid solution can be written as

$$
\begin{aligned}
&u(r,t)\\
&= \sum_{n=1}^{n_1} \left\{ \begin{array}{c} \frac{\pi^2\xi_n\left((\tilde{s}_1+\tau/\lambda_1)e^{\tilde{s}_1 t}-(\tilde{s}_2+\tau/\lambda_1)e^{\tilde{s}_2 t}+Q\xi_n(\kappa-1)(e^{\tilde{s}_1 t}-e^{\tilde{s}_2 t})\right)}{2(1-X_0^2)} \\ \times \int_{R_I/R}^{1} r f(r) V_0(\sqrt{\xi_n} r) dr \\ -\frac{\gamma\pi \int_0^t \left((\tilde{s}_1+\tau/\lambda_1)e^{\tilde{s}_1(t-t')}-(\tilde{s}_2+\tau/\lambda_1)e^{\tilde{s}_2(t-t')}\right) g(t') dt'}{1+X_0} \end{array} \right\} \\
&\quad \times \frac{V_0(\sqrt{\xi_n} r)}{\tilde{s}_1-\tilde{s}_2} \\
&+ \sum_{n=n_1+1}^{n_2-1} \left\{ \begin{array}{c} \frac{\pi^2\xi_n e^{-\frac{1}{2}(\tau/\lambda_1+Q\xi_n\kappa)t}}{2(1-X_0^2)} \left(\cos\tilde{\eta}t + \frac{(\tau/\lambda_1+Q\xi_n(\kappa-2))}{2\tilde{\eta}} \sin\tilde{\eta}t\right) \\ \times \int_{R_I/R}^{1} r f(r) V_0(\sqrt{\xi}_n r) dr \\ -\gamma\pi \int_0^t \frac{e^{-\frac{1}{2}(\tau/\lambda_1+Q\xi_n\kappa)(t-t')}}{1+X_0} \left(\begin{array}{c} \cos\tilde{\eta}(t-t') \\ +\frac{(\tau/\lambda_1-Q\xi_n\kappa)}{2\tilde{\eta}} \sin\tilde{\eta}(t-t') \end{array} \right) \\ \times g(t') dt' \end{array} \right\} \\
&\quad \times V_0(\sqrt{\xi}_n r) \\
&+ \sum_{n=n_2}^{\infty} \left\{ \begin{array}{c} \frac{\pi^2\xi_n\left((\tilde{s}_1+\tau/\lambda_1)e^{\tilde{s}_1 t}-(\tilde{s}_2+\tau/\lambda_1)e^{\tilde{s}_2 t}+Q\xi_n(\kappa-1)(e^{\tilde{s}_1 t}-e^{\tilde{s}_2 t})\right)}{2(1-X_0^2)} \\ \times \int_{R_I/R}^{1} r f(r) V_0(\sqrt{\xi_n} r) dr \\ -\frac{\gamma\pi \int_0^t \left((\tilde{s}_1+\tau/\lambda_1)e^{\tilde{s}_1(t-t')}-(\tilde{s}_2+\tau/\lambda_1)e^{\tilde{s}_2(t-t')}\right) g(t') dt'}{1+X_0} \end{array} \right\} \\
&\quad \times \frac{V_0(\sqrt{\xi_n} r)}{\tilde{s}_1-\tilde{s}_2}.
\end{aligned}
\tag{8.8.18}
$$

Of course, if the first root, ξ_1, is greater than ξ_{n_1}, then the following Type 2/Type 1 form of hybrid solution exists:

$$
\begin{aligned}
& u(r,t) \\
& = \sum_{n=1}^{n_2-1} \left\{ \begin{array}{c} \frac{\pi^2 \xi_n e^{-\frac{1}{2}(\tau/\lambda_1 + Q\xi_n\kappa)t}}{2(1-X_0^2)} \left(\cos\tilde{\eta}t + \frac{(\tau/\lambda_1 + Q\xi_n(\kappa-2))}{2\tilde{\eta}} \sin\tilde{\eta}t \right) \\ \times \int_{R_I/R}^{1} r f(r) V_0(\sqrt{\xi}_n r) dr \\ -\gamma\pi \int_0^t \frac{e^{-\frac{1}{2}(\tau/\lambda_1 + Q\xi_n\kappa)(t-t')}}{1+X_0} \left(\begin{array}{c} \cos\tilde{\eta}(t-t') \\ + \frac{(\tau/\lambda_1 - Q\xi_n\kappa)}{2\tilde{\eta}} \sin\tilde{\eta}(t-t') \end{array} \right) \\ \times g(t') dt' \end{array} \right\} \\
& \quad \times V_0(\sqrt{\xi}_n r) \\
& + \sum_{n=n_2}^{\infty} \left\{ \begin{array}{c} \frac{\pi^2 \xi_n \left((\tilde{s}_1 + \tau/\lambda_1) e^{\tilde{s}_1 t} - (\tilde{s}_2 + \tau/\lambda_1) e^{\tilde{s}_2 t} + Q\xi_n(\kappa-1)(e^{\tilde{s}_1 t} - e^{\tilde{s}_2 t}) \right)}{2(1-X_0^2)} \\ \times \int_{R_I/R}^{1} r f(r) V_0(\sqrt{\xi_n} r) dr \\ -\frac{\gamma\pi \int_0^t \left((\tilde{s}_1 + \tau/\lambda_1) e^{\tilde{s}_1(t-t')} - (\tilde{s}_2 + \tau/\lambda_1) e^{\tilde{s}_2(t-t')} \right) g(t') dt'}{1+X_0} \end{array} \right\} \\
& \quad \times \frac{V_0(\sqrt{\xi_n} r)}{\tilde{s}_1 - \tilde{s}_2}.
\end{aligned}
\tag{8.8.19}
$$

8.8.2 Oldroyd B pulsatile flow in an annular region

Choosing the form of P and τ for pulsatile flow as in §8.4.5, one obtains

$\gamma = 1$, $Q = 1/Wo^2$,

$2\tilde{s}_{1,2} = (1/(\omega\lambda_1) + \xi_n\kappa/Wo^2)\left(-1 \pm \sqrt{1 - 4\xi_n\omega\lambda_1 Wo^2/(Wo^2 + \xi_n\omega\lambda_2)^2}\right)$ and $\tilde{\eta} = \sqrt{\xi_n/(\omega Wo^2\lambda_1) - (1/(\omega\lambda_1) + \xi_n\kappa/Wo^2)^2/4}$.

8.8.3 Reducing Oldroyd B annular solution to Oldroyd B cylindrical solution

To show that the Oldroyd B annular solution reduces to the Oldroyd B cylindrical solution, it is necessary to show that, as $R_I \to 0$,

$$\frac{V_0(\sqrt{\xi_n}r)\pi^2\xi_n \int_{R_I/R}^1 rf(r)V_0(\sqrt{\xi_n}r)dr}{2(1-\frac{J_0^2(\sqrt{\xi_n})}{J_0^2(\sqrt{\xi_n}R_I/R)})} \to 2\frac{\int_0^1 rf(r)J_0(\sqrt{\alpha_n}r)dr}{(J_1(\sqrt{\alpha_n}))^2}, \tag{8.8.20}$$

$$\frac{\pi V_0(\sqrt{\xi_n}r)}{1+\frac{J_0(\sqrt{\xi_n})}{J_0(\sqrt{\xi_n}R_I/R)}} \to \frac{2J_0(\sqrt{\alpha_n}r)}{\sqrt{\alpha_n}J_1(\sqrt{\alpha_n})}, \tag{8.8.21}$$

$$\tilde{s}_{1,2}(\xi_n) \to s_{1,2}(\alpha_n), \tag{8.8.22}$$

$$\tilde{\eta}(\xi_n) \to \eta_(\alpha_n). \tag{8.8.23}$$

Recall from (8.8.3) that the ξ_n are the eigenvalues satisfying

$$J_0(\sqrt{\xi_n}R_I/R)Y_0(\sqrt{\xi_n}) = J_0(\sqrt{\xi_n})Y_0(\sqrt{\xi_n}R_I/R). \tag{8.8.24}$$

Rearranging provides

$$\frac{J_0(\sqrt{\xi_n})}{J_0(\sqrt{\xi_n}R_I/R)} = \frac{Y_0(\sqrt{\xi_n})}{Y_0(\sqrt{\xi_n}R_I/R)}. \tag{8.8.25}$$

Now, let $R_I \to 0$, $J_0(\sqrt{\xi_n}R_I/R) \to 1$ and $\frac{Y_0(\sqrt{\xi_n})}{Y_0(\sqrt{\xi_n}R_I/R)} \to 0$ so that equation(8.8.25) reduces to

$$J_0(\sqrt{\xi_n}) = 0. \tag{8.8.26}$$

Hence, from (8.4.29) it is inferred that as $R_I \to 0$, $\xi_n \to \alpha_n$. Recall that from (8.8.4)

$$V_0(\sqrt{\xi_n}r) = J_0(\sqrt{\xi_n}r)Y_0(\sqrt{\xi_n}) - J_0(\sqrt{\xi_n})Y_0(\sqrt{\xi_n}r). \tag{8.8.27}$$

It has been shown that as $R_I \to 0$, $\xi_n \to \alpha_n$ so that (8.8.27) reduces to

$$V_0(\sqrt{\alpha_n}r) = J_0(\sqrt{\alpha_n}r)Y_0(\sqrt{\alpha_n}) - J_0(\sqrt{\alpha_n})Y_0(\sqrt{\alpha_n}r). \tag{8.8.28}$$

But from (8.4.29), $J_0(\sqrt{\alpha_n}) = 0$ and so (8.8.28) becomes

$$V_0(\sqrt{\alpha_n}r) = J_0(\sqrt{\alpha_n}r)Y_0(\sqrt{\alpha_n}). \tag{8.8.29}$$

Since it has been shown that as $R_I \to 0$, $\xi_n \to \alpha_n$, then (8.8.22) and (8.8.23) follow. Since $Y_0(\sqrt{\alpha_n})$ is a constant value for each α_n, it is clear that as $R_I \to 0$,

$$V_0(\sqrt{\xi_n}r)\frac{\pi^2\xi_n \int_{R_I/R}^1 rf(r)V_0(\sqrt{\xi_n}r)dr}{2(1 - \frac{J_0^2(\sqrt{\xi_n})}{J_0^2(\sqrt{\xi_n}R_I/R)})}$$

$$\to \frac{J_0(\sqrt{\alpha_n}r)(Y_0(\sqrt{\alpha_n}))^2\alpha_n\pi^2 \int_0^1 rf(r)J_0(\sqrt{\alpha_n}r)dr}{2}. \tag{8.8.30}$$

Hence, in order to demonstrate the validity of (8.8.20) the following must be demonstrated:

$$\frac{(Y_0(\sqrt{\alpha_n}))^2\alpha_n\pi^2}{2} \equiv \frac{2}{(J_1(\sqrt{\alpha_n}))^2}, \tag{8.8.31}$$

or equivalently,

$$Y_0(\sqrt{\alpha_n})J_1(\sqrt{\alpha_n}) \equiv \frac{2}{\pi\sqrt{\alpha_n}}. \tag{8.8.32}$$

In a similar manner, in order to show that (8.8.21) is true, it is also necessary to

demonstrate the validity of (8.8.32). However, this is simply a special case of the following relationship [3, 34]:

$$J_{m+1}(z)Y_m(z) - J_m(z)Y_{m+1}(z) = \frac{2}{\pi z}. \tag{8.8.33}$$

Clearly, selecting $m = 0$ confirms that (8.8.32) is true.

8.9 Maxwellian flow in an annular region

To obtain the corresponding Maxwellian annular solutions, let $\mu_s \to 0$ in the Oldroyd B solutions, with the consequence that $\lambda_2 \to 0$. The hybrid solution switches from a Type 1 to a Type 2 solution when the n_3th root, ξ_{n_3} is reached. The n_3 root is the first root that satisfies $\xi_{n_3} > R^2/4\nu_p\lambda_1$. Of course, it is possible that there does not exist such a root: this would occur when $\xi_1 > R^2/4\nu_p\lambda_1$, resulting in a Type 2 solution for all values of n. The limiting process $\mu_s \to 0$ and $\lambda_2 \to 0$ again is straightforward and yields the following two cases.

8.9.1 Maxwellian annular hybrid solution

$$
\begin{aligned}
&u(r,t)\\
&= \sum_{n=1}^{n_3-1} \left\{ \begin{array}{c} \frac{\pi^2\xi_n((\tilde{s}_{M_1}+\tau/\lambda_1)e^{\tilde{s}_{M_1}t}-(\tilde{s}_{M_2}+\tau/\lambda_1)e^{\tilde{s}_{M_2}t}-Q_p\xi_n(e^{\tilde{s}_{M_1}t}-e^{\tilde{s}_{M_2}t}))}{2(1-X_0^2)} \\ \times \int_{R_I/R}^{1} r f(r) V_0(\sqrt{\xi_n} r) dr \\ -\frac{\gamma\pi \int_0^t \left((\tilde{s}_{M_1}+\tau/\lambda_1)e^{\tilde{s}_{M_1}(t-t')} - (\tilde{s}_{M_2}+\tau/\lambda_1)e^{\tilde{s}_{M_2}(t-t')} \right) g(t') dt'}{1+X_0} \end{array} \right\} \\
&\quad \times \frac{V_0(\sqrt{\xi_n} r)}{\tilde{s}_{M_1} - \tilde{s}_{M_2}} \\
&+ \sum_{n=n_3}^{\infty} \left\{ \begin{array}{c} \frac{\pi^2 \xi_n e^{-\frac{1}{2}\tau t/\lambda_1}}{2(1-X_0^2)} \left(\cos\tilde{\eta}_M t + \frac{(\tau/\lambda_1 - 2Q_p\xi_n)}{2\tilde{\eta}_M} \sin\tilde{\eta}_M t \right) \\ \times \int_{R_I/R}^{1} r f(r) V_0(\sqrt{\xi}_n r) dr \\ -\gamma\pi \int_0^t \frac{e^{-\frac{1}{2}\tau(t-t')/\lambda_1}}{1+X_0} \left(\begin{array}{c} \cos\tilde{\eta}_M(t-t') \\ + \frac{\tau}{2\lambda_1\tilde{\eta}_M} \sin\tilde{\eta}_M(t-t') \end{array} \right) g(t') dt' \end{array} \right\} \\
&\quad \times V_0(\sqrt{\xi}_n r).
\end{aligned}
\tag{8.9.1}
$$

The variables $\tilde{s}_{M_1}$, $\tilde{s}_{M_2}$, Q_p and $\tilde{\eta}_M$ manifest themselves as a result of the limiting process. They are:

$2\tilde{s}_{M_1,M_2} = -\tau/\lambda_1 \pm \sqrt{(\tau/\lambda_1)^2 - Q_p\tau\xi_n/\lambda_1}, \quad Q_p = \nu_p\tau/R^2, \quad \tilde{\eta}_M = \sqrt{Q_p\tau\xi_n/\lambda_1 - \tau^2/4\lambda_1^2}.$

8.9.2 Maxwellian annular Type 2 solution

If $\xi_1 > R^2/4\nu_p\lambda_1$ then there exists a Type 2 solution only, given by

$$u(r,t) = \sum_{n=1}^{\infty} \left\{ \begin{array}{c} \frac{\pi^2 \xi_n e^{-\frac{1}{2}\tau t/\lambda_1}}{2(1-X_0^2)} \left(\cos\tilde{\eta}_M t + \frac{(\tau/\lambda_1 - 2Q_p\xi_n)}{2\tilde{\eta}_M} \sin\tilde{\eta}_M t \right) \\ \times \int_{R_I/R}^1 r f(r) V_0(\sqrt{\xi}_n r) dr \\ -\gamma\pi \int_0^t \frac{e^{-\frac{1}{2}\tau(t-t')/\lambda_1}}{1+X_0} \left(\begin{array}{c} \cos\tilde{\eta}_M(t-t') \\ + \frac{\tau}{2\lambda_1\tilde{\eta}_M} \sin\tilde{\eta}_M(t-t') \end{array} \right) g(t')dt' \end{array} \right\} \times V_0(\sqrt{\xi}_n r). \tag{8.9.2}$$

8.9.3 Maxwellian pulsatile flow in an annular region

Choosing the form of P and τ for pulsatile flow as before results in $\gamma = 1$, $Q_p = 1/Wo_p^2$, $2\tilde{s}_{M1,M2} = (1/(\omega\lambda_1))\left(-1 \pm \sqrt{1 - \xi_n\omega\lambda_1/Wo_p^2}\right)$ and $\tilde{\eta}_M = \sqrt{\xi_n/(\omega Wo_p^2\lambda_1) - (1/(2\omega\lambda_1))^2}$.

8.9.4 Reducing Maxwellian annular solution to Maxwellian cylindrical solution

Clearly the Maxwellian annular solutions reduce to the corresponding cylindrical solutions when the limits

$$\tilde{s}_{M1,2}(\xi_n) \to s_{M1,2}(\alpha_n) \tag{8.9.3}$$

$$\tilde{\eta}_M(\xi_n) \to \eta_M(\alpha_n) \tag{8.9.4}$$

hold and, additionally, (8.8.20) and (8.8.21) are valid.

Since it has already been demonstrated that as $R_I \to 0$, $\xi_n \to \alpha_n$ then it is clear

that these conditions are satisfied.

8.10 Newtonian flow in an annular region

To obtain the corresponding Newtonian annular solutions, one should let $\mu_p \to 0$ and $\lambda_1 = \lambda_2 \to 0$ in the Oldroyd B annular solutions. The limiting process is again relatively straightforward and the solution is provided directly.

8.10.1 General analytic solution of Newtonian flow in an annular region

$$u(r,t) = \sum_{n=1}^{\infty} \left\{ \begin{array}{c} \frac{e^{-Q_s \xi_n t} \pi^2 \xi_n \int_{R_I/R}^{1} r f(r) V_0(\sqrt{\xi_n} r) dr}{2(1-X_0^2)} \\ -\frac{\gamma\pi \int_0^t e^{-Q_s \xi_n (t-t')} g(t') dt'}{1+X_0} \end{array} \right\} V_0(\sqrt{\xi_n} r). \tag{8.10.1}$$

Note that equation (8.10.1) is the dimensional form of (8.3.26), with $R = a$, $R_I = b$.

8.10.2 Newtonian pulsatile flow in an annular region

Choosing the form of P and τ for pulsatile flow as in §8.6.2 results in $\gamma = 1$ and $Q_s = 1/Wo_s^2$.

8.10.3 Reducing Newtonian annular solution to Newtonian cylindrical solution

The Newtonian annular solution reduces to the corresponding cylindrical solution since the limits (8.8.20) and (8.8.21) have been shown to hold.

8.11 Poiseuille flow in an annular region

Recall that from (8.7.1)

$$\frac{1}{r}\frac{d}{dr}\left(r\frac{du}{dr}\right) = \frac{PR}{\mu_s U}\frac{dp}{dz}, \tag{8.11.1}$$

subject to the boundary conditions

$$u(R_I/R) = u(1) = 0. \tag{8.11.2}$$

The solution of (8.11.1) subject to (8.11.2) is the well-known solution of Poiseuille flow in an annular region

$$u(r) = -\frac{Re}{4}\frac{dp}{dz}\left(1 - r^2 + \frac{[(R_I/R)^2 - 1]\, ln(r)}{ln(R_I) - ln(R)}\right), \tag{8.11.3}$$

where the non-dimensional scaling $P = \rho U^2$ has been employed. Clearly as $R_I \to 0$, $u(r) \to -Re(dp/dz)(1 - r^2)/4$; i.e. (8.7.2), the equation for Poiseuille flow in a rigid cylinder.

8.12 Simulations

In this section numerical simulations of some of the aforementioned analytic solutions for the velocity profile of blood in a dog's femoral artery are considered. It is assumed that the artery is a rigid cylinder of radius R. The required data is obtained from (McDonald 1974): $R = 0.0012\ m$, $\mu_s = 0.004939\ kg\ m^{-1}\ s^{-1}$, $\rho = 1060\ kg\ m^{-3}$, $\omega = 2\pi \times 2.85\ s^{-1}$, and the peak (measured) velocity $U = 1.05\ m\ s^{-1}$. In the absence of data on the relaxation and retardation times for blood, the choice $\lambda_1 = 0.05s$, $\lambda_2 = 0.009s$ is made, satisfying $\lambda_1 > \lambda_2$ (personal communication, Ken Walters). Primarily, the reason for this selection was to ex-

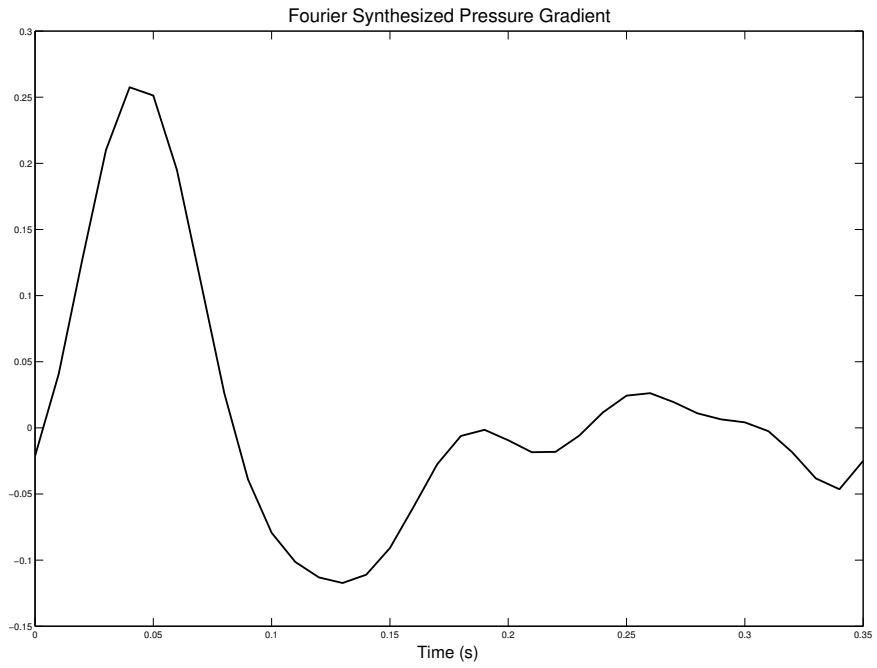

Figure 8.4: Fourier synthesized pressure gradient using data from McDonald (1974)

hibit the more complicated hybrid solution. Although there was no physiological reason for this choice, several evaluations of the different type analytic solutions were made and no substantially qualitative differences were discovered. These values of λ_1 and λ_2 result in $\mu = 0.02744\ kg\ m^{-1}\ s^{-1}$ (since $\mu = \mu_s\lambda_1/\lambda_2$) and $\mu_p = 0.022501\ kg\ m^{-1}\ s^{-1}$ (since $\mu = \mu_s + \mu_p$). The graphs all show two periods of flow in dimensional variables. Zero initial flow is chosen for simplicity. This is reasonable, since the term involving $f(r)$ tends to zero extremely rapidly as a consequence of the negative exponentials that multiply it. The zeros of the first kind Bessel function up to $n = 10$ were employed for the computations; choosing more terms did not appear to significantly alter the profiles. McDonald (1974) provides pressure gradient data. This is expanded as a Fourier series with five terms to provide an analytic expression for the function $g(t)$. The Fourier synthesized pressure gradient is displayed in Figure 8.4.

8.12.1 Rigid cylinder simulations

In Figures $8.5 - 8.7$, the solutions of the velocity profile for Oldroyd B (hybrid), Maxwellian (hybrid) and Newtonian flow in a rigid cylinder are compared. It is observed that the three profiles have different peak velocities, occurring at $r = 0$, the centre of the artery. In Figure 8.8 a slice is taken through the solution resulting in the $r = 0$ profiles. Backflow occurs during a substantial part of the cycle for each case. One noticeable difference is that the peak backflow velocity is four times greater for the Maxwellian case than the Newtonian case, with Oldroyd B half that of the Maxwellian value. Moreover, for Newtonian flow backflow is observed for a longer period of time than either of the Oldroyd B and Maxwellian cases; Oldroyd B and Maxwellian switch from positive to negative velocity twice in one cycle, whereas Newtonian only switches once. In Figures $8.9 - 8.11$, the profiles at four different times during the first cycle are considered. These graphs display, perhaps more clearly, the greatest peak velocity and backflow for Maxwellian flow, and the least peak velocity for Oldroyd B.

The three fluids react differently to the asymmetries in the applied pressure gradient, due to the systolic (when heart is contracting) and diastolic (when heart is relaxing and expanding) pressures. In particular, whilst the Newtonian velocity profile mimics the applied pressure gradient, the Maxwellian and Oldroyd B fluids show significant deviations as a result of the stress relaxation and retardation effects. Furthermore, memory effects are observed, since in both Maxwellian and Oldroyd B fluids, the stress at any time depends on the whole strain history. The grestest peak velocity for Maxwellian may be explained by the fact that the value of λ_1 chosen results in a $1/\lambda_1$ of 20, whilst the lowest peak velocity for Oldroyd B may be explained by the small ratio of retardation to relaxation time, $\lambda_2/\lambda_1 = 0.18$. Further simulations are undoubtedly required to properly investigate the effect of

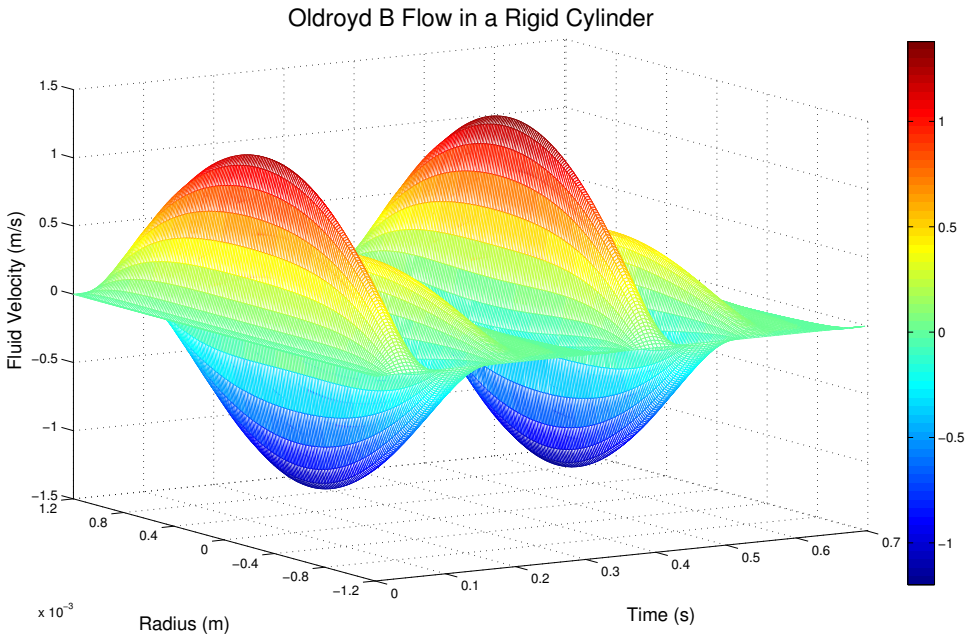

Figure 8.5: Two periods of Oldroyd B flow in a rigid cylinder with zero initial flow.

retardation and relaxation on the velocity profiles.

8.12.2 Annular region simulations

In this section a cylindrical catheter inside the artery is considered, and hence the blood velocity profiles in this annular region are analysed. The further simplifying assumption that the catheter lies along the centre line of the artery is made. If the catheter is small, it is not unreasonable to select $R_I/R = 0.1$. In Figures 8.12−8.14 the solutions of the velocity profile for Oldroyd B (hybrid), Maxwellian (hybrid) and Newtonian flow in an annular region are compared. Again, Maxwellian provides the largest peak velocity, followed by Newtonian and then Oldroyd B. The catheter is in the centre of the artery and so the peak velocity can no longer occur at $r = 0$. For each of the three cases, the peak velocity does not occur half way between R and R_I as one might have anticipated. The profile is in fact skewed,

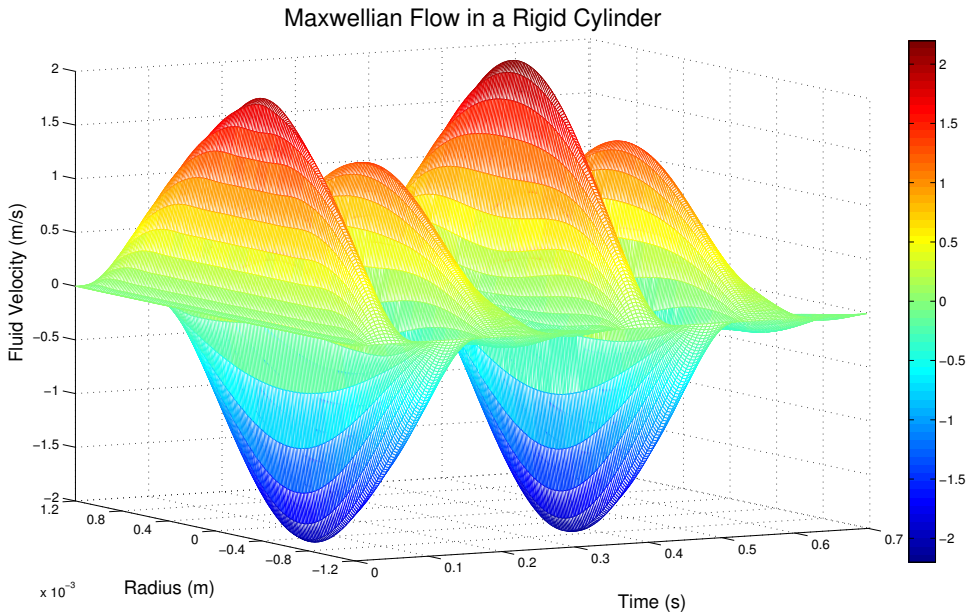

Figure 8.6: Two periods of Maxwellian flow in a rigid cylinder with zero initial flow.

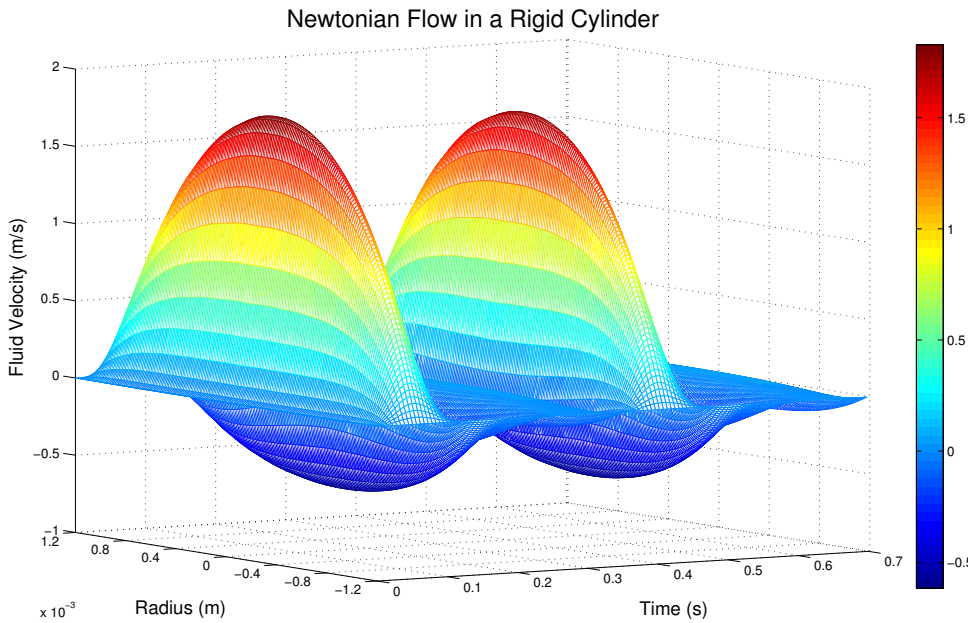

Figure 8.7: Two periods of Newtonian flow in a rigid cylinder with zero initial flow.

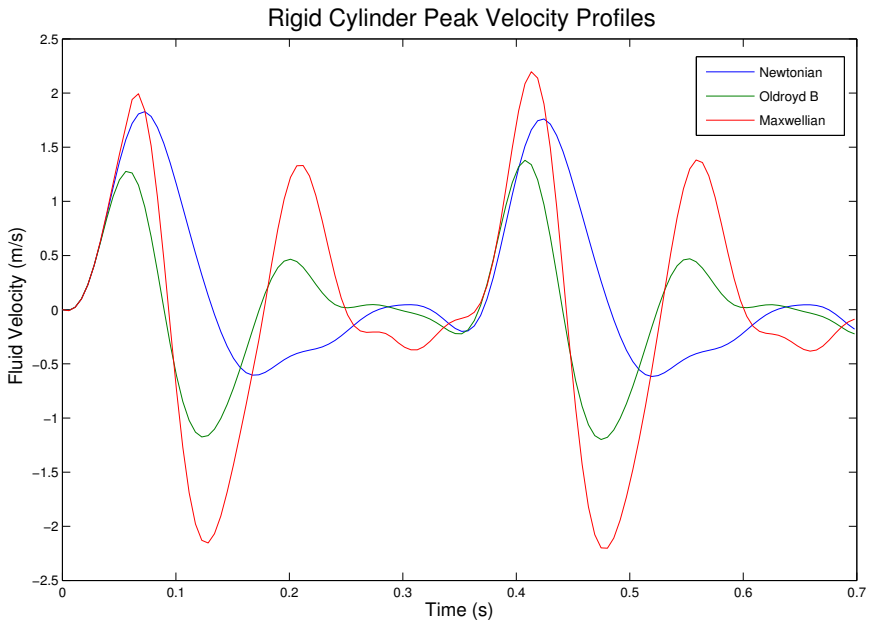

Figure 8.8: Rigid cylinder peak velocity profiles over two cycles

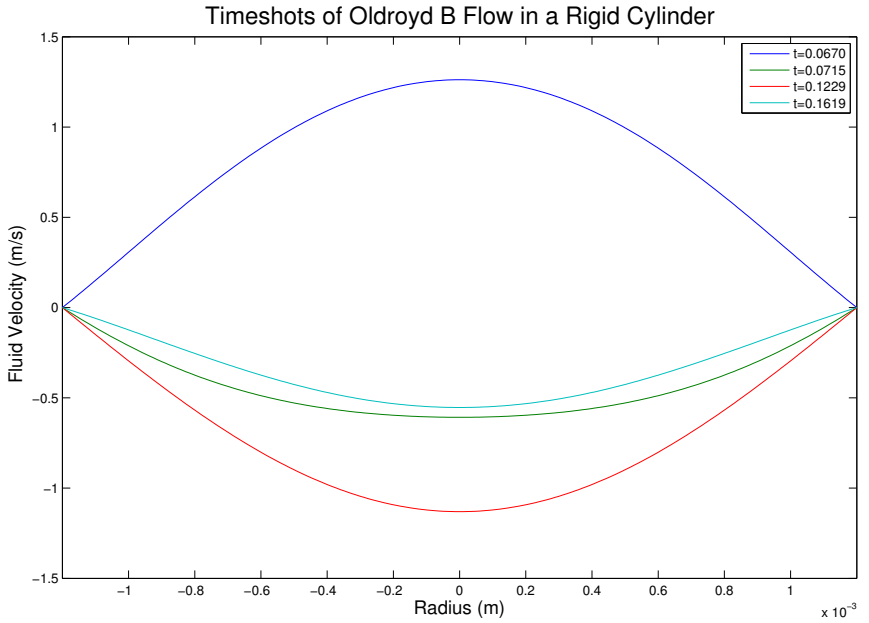

Figure 8.9: Timeshots of Oldroyd B flow in a rigid cylinder with zero initial flow.

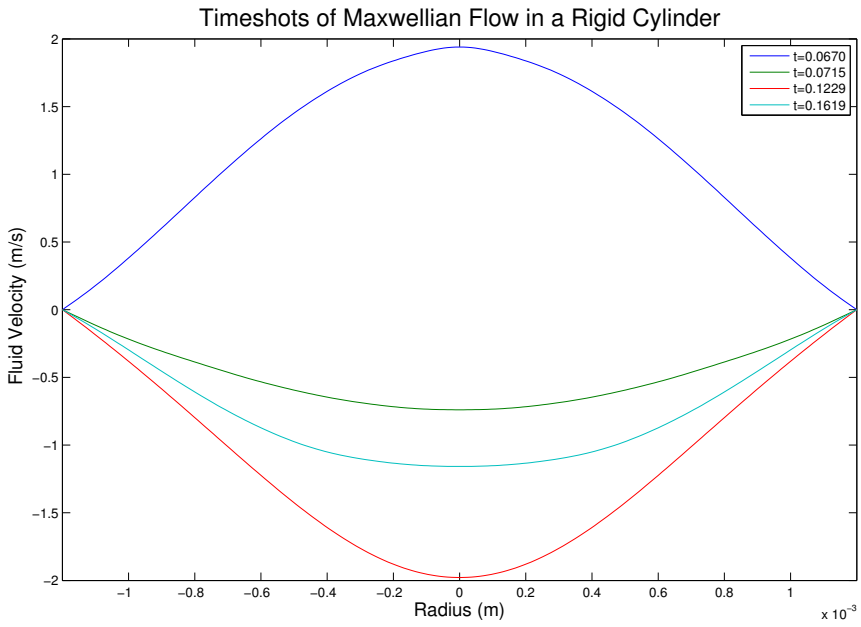

Figure 8.10: Timeshots of Maxwellian flow in a rigid cylinder with zero initial flow.

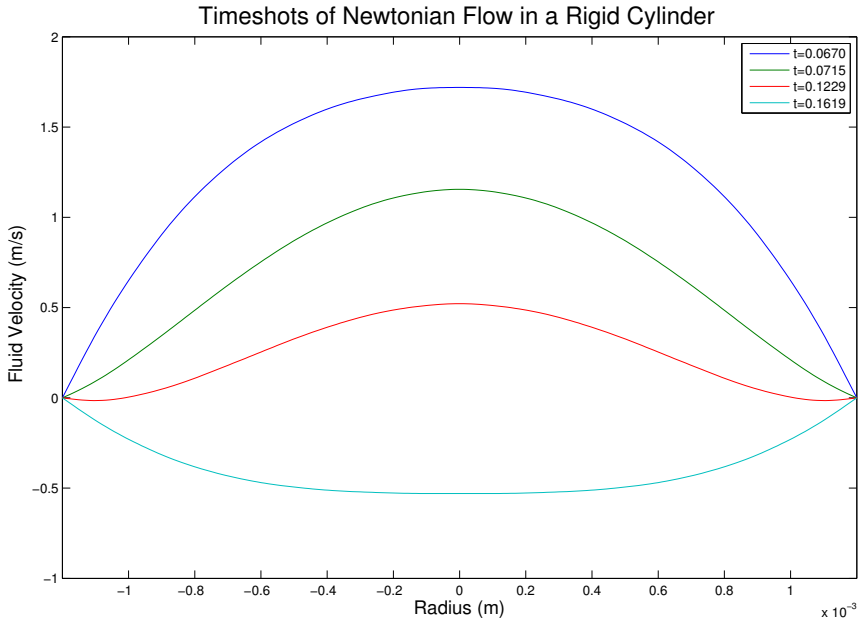

Figure 8.11: Timeshots of Newtonian flow in a rigid cylinder with zero initial flow.

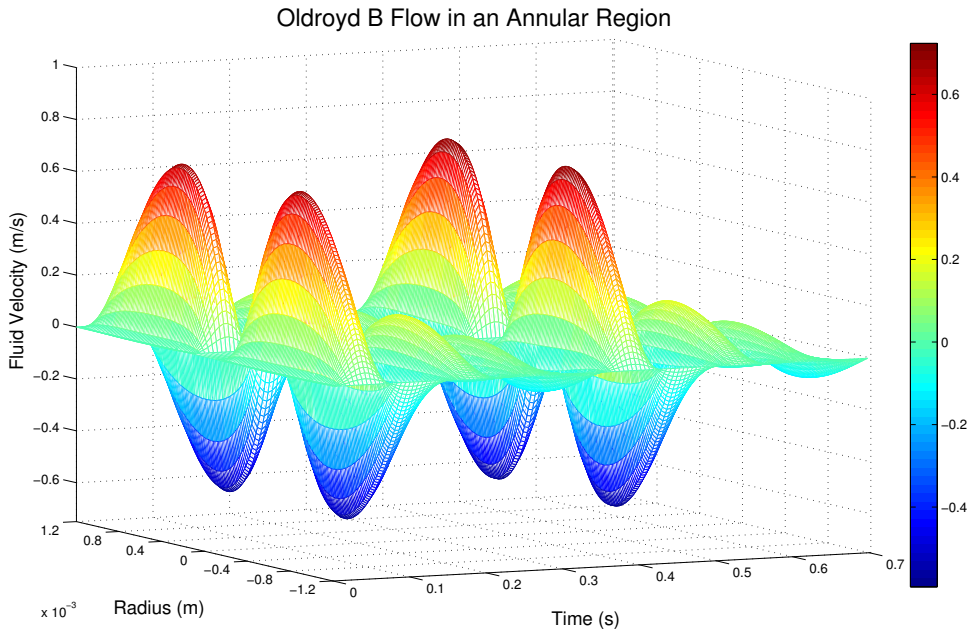

Figure 8.12: Two periods of Oldroyd B flow in annular region with zero initial flow.

with the peak closer to the catheter. This is best seen in Figures 8.16 – 8.18. In Figure 8.15 backflow occurs during a substantial part of the cycle for all three cases.

It should be pointed out, while Newtonian flow (with an appropriate effective viscosity) may adequately be used to describe blood flow in a large artery, it is not at all clear that Oldroyd B or Maxwell are suitable models. Thus, the diagrams displayed in this chapter must be regarded as illustrative of their corresponding analytic solutions rather than assigning any physiological meaning. Finally, the limitations of this work should be stressed. So that the mathematics would be tractable, a rigid cylinder, cylindrical symmetry and zero radial flow have all been assumed. In addition, it has been assumed that the stress tensor has no axial dependence, that the initial flow is steady and that the resulting flow is laminar.

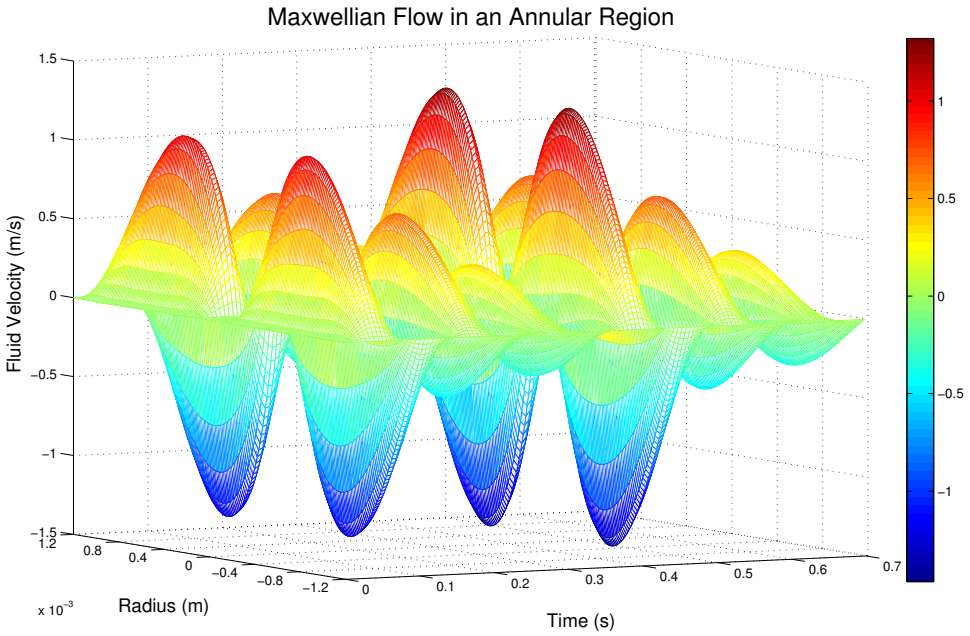

Figure 8.13: Two periods of Maxwellian flow in annular region with zero initial flow.

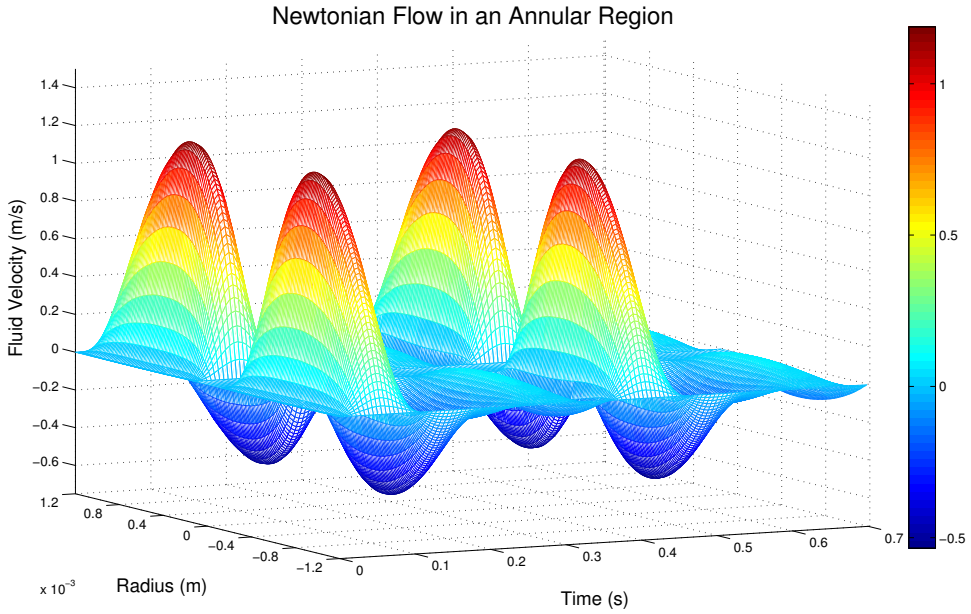

Figure 8.14: Two periods of Newtonian flow in an annular region with zero initial flow.

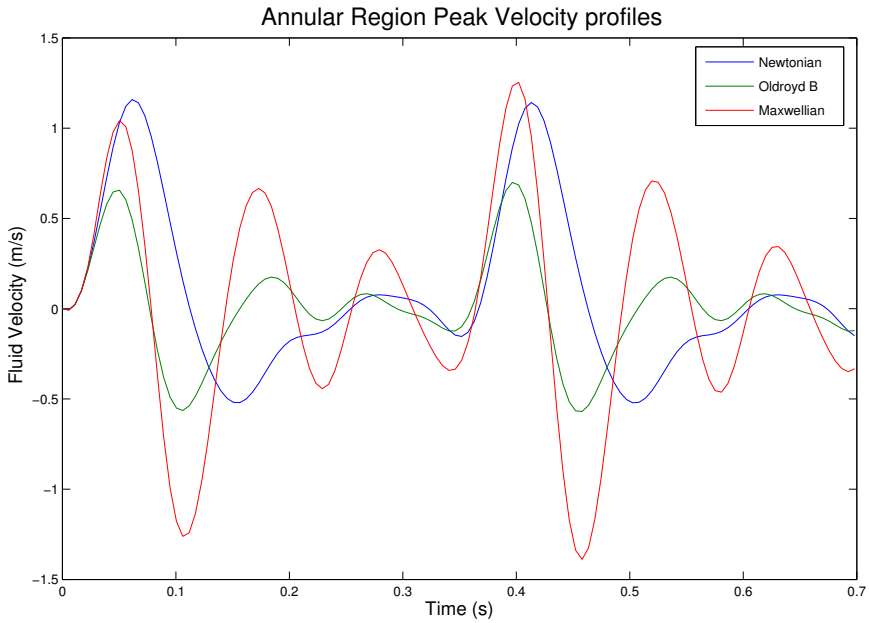

Figure 8.15: Annular region peak velocity profiles over two cycles

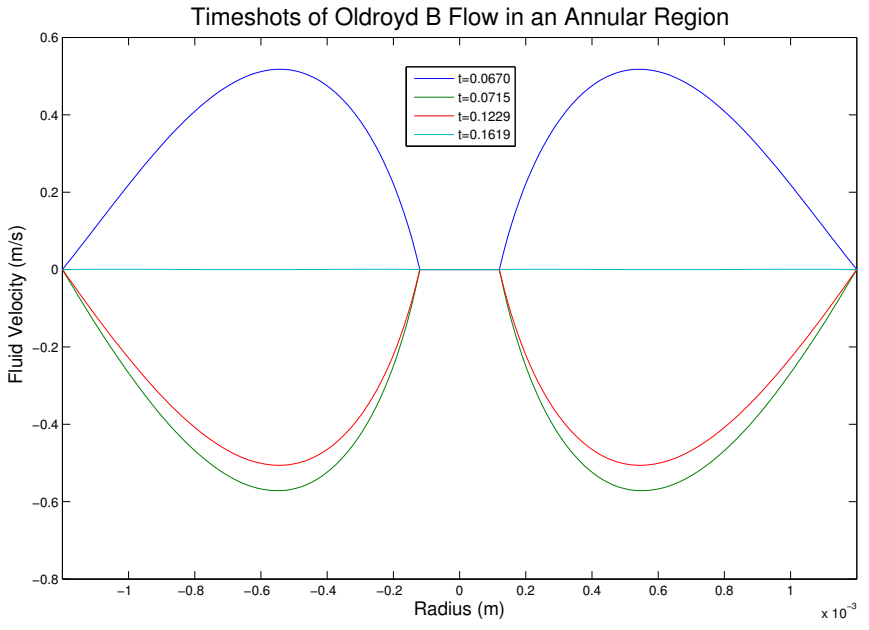

Figure 8.16: Timeshots of Oldroyd B flow in an annular region with zero initial flow.

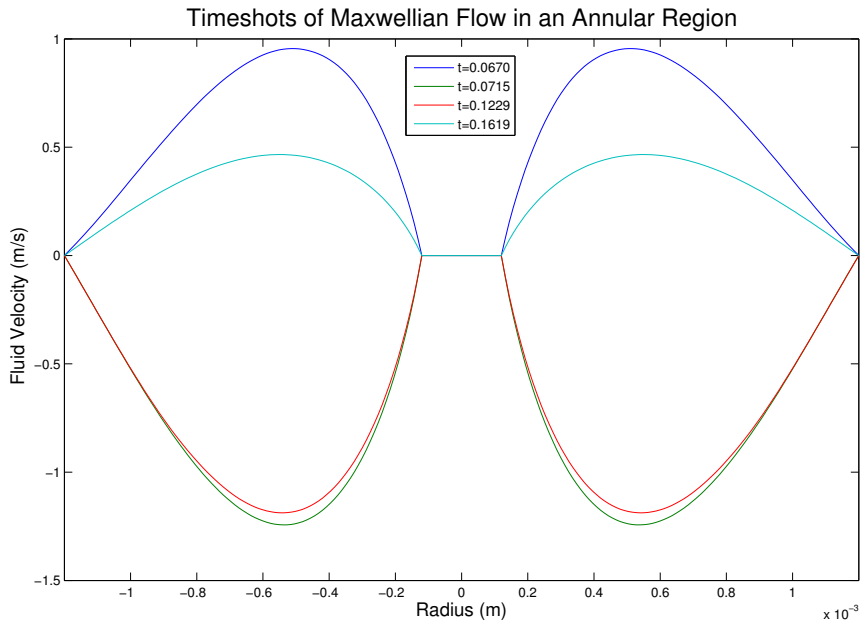

Figure 8.17: Timeshots of Maxwellian flow in an annular region with zero initial flow.

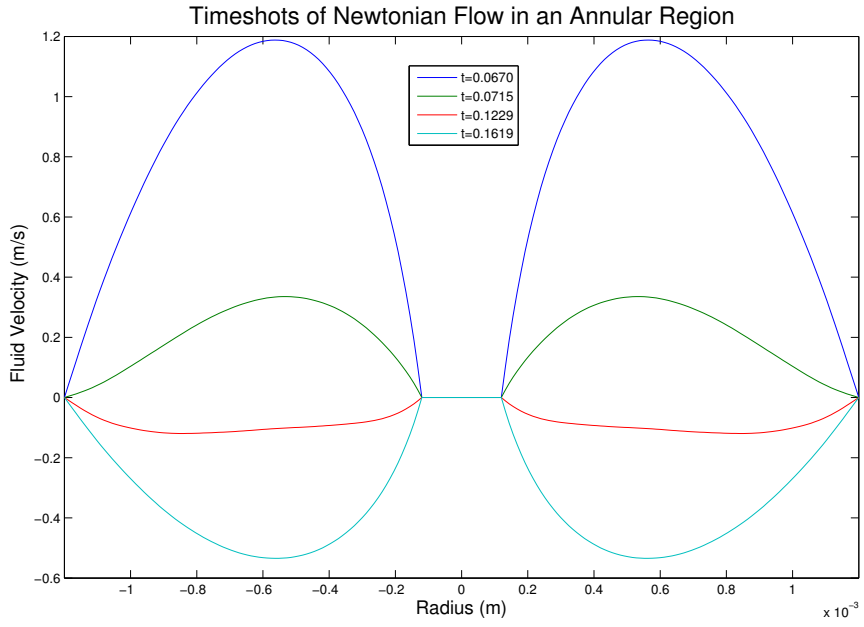

Figure 8.18: Timeshots of Newtonian flow in an annular region with zero initial flow.

In reality, an artery is elastic rather than rigid and blood almost certainly requires a more sophisticated rheological model. Furthermore, the stability of the flow, the transition to turbulence and turbulence itself have not been considered.

Chapter 9

Conclusions and Future Research

9.1 Conclusions

In this work four models have been developed to describe the elution of a drug from polymer coated stents. The solution for model I has been written down in Laplace transform space, and the inverted solution has been derived for a specific limiting case. This case has been compared with the results of a numerical scheme for the full problem and showed good agreement, thus in part validating the code. Through a thorough sensitivity analysis, four parameters have been identified which play a significant role in determining the resulting cellular drug concentrations. The transmural velocity, v, has been measured in studies to be at least 10^{-8}ms^{-1} and even, in some cases, an order of magnitude higher. It is understood that the transmural velocity may increase with disease (Baldwin et al. 1997), as well as with disruption to the endothelium (Lovich & Edelman 1999), resulting in a convection dominated system. Furthermore, there is evidence to suggest that the transmural fluid flux increases with blood pressure. It may be reasonable to assume that patients with atherosclerois have high blood pressure and thus they may

experience increased transmural flux as a result of this. Since the solutions have been found to be very sensitive to changes in v, it is suggested that the extent of atherosclerosis may have a significant effect on drug delivery and deposition. Two of the drug dependent parameters, drug uptake rate into smooth muscle cells, α_i, and partitioning into cells, K_i, also have a large effect on the therapeutic time and the drug concentration in the arterial wall. Whilst the partition coefficient is easily measured, the uptake rate is not. To date, our estimates of α_i have come from fitting a first order reaction kinetic model to tissue concentration profiles. It is important that both α_i and K_i are accurately determined since the therapeutic time and cellular concentration levels can vary significantly with changes in these parameters. Given the importance of the parameter v, the significance of the effect of changes in α_i on the results is no surprise since, according to the timescale estimates, the Damköhler number is typically of order unity, indicating that advection and reaction are of comparable importance and dominate over diffusion in the media region.

The results confirm that adding a drug-free topcoat polymer layer can slow the release of drug from the stent. The thicker the coating and the smaller the diffusion coefficient, the longer the release time. Even without a topcoat, this effect is observed: the thicker the polymer and the smaller the polymer diffusion coefficient, the longer the release time.

The results from the sensitivity analysis suggest that therapeutic time increases with the proportion of plaque, suggesting that the plaque acts as a reservoir for the drug. Thus patients with a higher degree of atherosclerosis may continue to receive therapeutic levels of drug for longer than patients with a lesser degree of plaque. A more sophisticated model of plaque, taking into account its complicated structure, may provide more insight into the effect of plaque on the cellular drug

concentrations. A series of release profiles have been generated and confirm that the main factors which influence release of the drug from the polymer coated stent are polymer thickness and the polymer diffusion coefficient. A period of release of up to three weeks can be obtained for polymer thickness 10^{-5} m coupled with polymer diffusion coefficient of order 10^{-16} m^2 s^{-1}. In this case, diffusion across the polymer is clearly the rate-limiting step since its associated timescale is at least an order of magnitude greater than the faster processes (convection, reaction and diffusion) in the media region. The other parameters in the model, including the drug-dependent ones, have little effect on drug release from the polymer.

Two of the difficult-to-determine parameters, v and D_m, have been estimated by fitting an analytic solution to experimental data. The values obtained reinforce the idea that convection is not negligible in comparison with diffusion. A Yukon polymer-free micro-porous stent system has also been modelled. A comparison has been made with experimental data on the drug succinobucol. The analytic tissue mass profile follows a similar shape to that of the experimental data, with discrepancies being attributed to the very small number of experiments performed. It is also found that if parameters such as transmural velocity and cellular density are time-dependent to reflect changes in artery structure during healing, then this may result in lower values of drug tissue mass.

To fully understand the complex progressive disease of atherosclerosis, an understanding of blood flow in the arteries is essential. To this end, analytic solutions have been obtained for Newtonian and non-Newtonian pipe flows subject to an arbitrary time-dependent pressure gradient and arbitrary initial flow. Solutions for both cylindrical and annular pipes have been simulated using data for blood flow in a dog's femoral artery and presented graphically.

9.2 Future Research

A natural extension to the work on modelling drug-eluting stents is to consider models in two and three dimensions. Such models would take into account the anisotropic nature of the arterial tissue and thus allow for differing diffusion coefficients in different directions, a property which cannot be handled in the current one-dimensional configuration. Models in higher dimensions would necessarily require numerical solutions due to the extra levels of complexity involved. A more sophisticated model of plaque could be devised to take into account its complicated structure. Ultimately, the various parameters of the models (diffusion coefficients, tissue thickness, transmural velocity, partition coefficient, drug uptake rate, etc.) should be measured experimentally for one test case, rather than drawing the data from various different studies. The measurement of these parameters would help characterize the optimal design of a stent. Finally, the pulmonary artery is believed to be more elliptical than cylindrical in shape, and thus it would be useful to extend the work on pipe flow to consider an elliptical tube.

Medical Glossary

- **Anisotropic**: having physical properties that differ according to the direction of measurement
- **Adventitia**: the outer layer of the arterial wall
- **Atheroma**: a fatty deposit in the inner lining of the arterial wall
- **Atherosclerosis**: the build up of lipid, cholesterol, cellular waste products, calcium and other substances in the inner lining of the arterial wall
- **Carotid artery**: an artery that supplies the head and neck with oxygenated blood
- **Catheter**: a thin flexible tube inserted into the body to permit introduction or withdrawal of fluids or to keep the passageway open
- **Collagen**: the fibrous protein constituent of bone, cartilage, tendon and other connective tissues
- **Dextran**: an antithrombotic drug
- **Dipyridamole**: a drug that inhibits thrombus formation when given chronically and causes vasodilation when given at high doses over short time

- **Elastin**: a protein, similar to collagen, that is the principal structural component of elastic fibres
- **Elastomeric**: a polymer with elastic properties
- **Endothelium**: a single layer of thin flattened cells that line the interior surface of blood vessels
- **Extracellular fluid**: fluid outwith cells
- **Femoral artery**: an artery in the leg used as an access point to insert a device such as a catheter or stent, which are pushed through the artery to the site of the lesion or blockage.
- **Fibrin**: an elastic, insoluble protein
- **Fibroblast cells**: cells found in the adventitia that produce collagen
- **Heart attack**: occurs when the blood supply to part of the heart is interrupted causing some heart cells to die
- **Heparin**: an anticoagulent drug
- **Hydrophilic**: having a strong affinity for water; tending to dissolve in, mix with, or be wetted by water
- **Hydrophobic**: lacking affinity for water; tending to repel and not absorb water; tending not to dissolve in or mix with or be wetted by water
- **Iliac artery**: one of the large arteries supplying blood to the pelvis and legs
- **Internal elastic lamina**: a fenestrated layer of elastic tissue that is the outermost part of the intima of an artery

- **Intima**: The innermost region of the arterial wall
- **Ischemia**: a restriction in blood supply
- **LDL**: Low Density Lipoprotein. The primary cholesterol-carrying blood substance
- **Lipid**: fatty substances
- **Lipophilic**: having an affinity for lipids
- **Lipophobic**: having no affinity for lipids
- **Lumen**: interior of a blood vessel
- **Macrophage**: a type of white blood cell that ingests (takes in) foreign material
- **Media**: the middle region of the arterial wall, containing smooth muscle cells, collagen and elastin
- **Myocardium**: heart muscle
- **Non-resorbable**: a substance that shows relatively limited in vivo degredation
- **Paclitaxel**: a highly lipophilic drug used for the prevention of restenosis
- **Plasma**: the fluid part of blood that remains when the blood cells are removed
- **Pulmonary artery**: a blood vessel that carries blood from the heart to the lungs

- **Rapamycin**: an anti-rejection drug which has an anti-proliferative effect on smooth muscle cells
- **Restenosis**: the re-narrowing of an artery
- **Shear stress**: a stress which is applied parallel or tangential to a face of a material
- **Sirolimus**: also known as rapamycin
- **Smooth muscle**: muscle that contracts without conscious control and found in the media layer of the arterial wall
- **Smooth muscle cells**: cells made of smooth muscle
- **Stroke**: a sudden loss of consciousness resulting when the rupture or occlusion of a blood vessel leads to lack of oxygen in the brain
- **Strut**: the wires making up the stent
- **Succinobucol**: an antioxidant drug
- **Thrombosis**: the formation or presence of a thrombus (a clot of coagulated blood attached at the site of its formation) in a blood vessel
- **Vasa vasorum**: a network of small blood vessels that supply blood to the adventitia
- **Vasoconstriction**: decrease in diameter of a blood vessel
- **Vasodilation**: widening of blood vessels
- **White blood cells**: (or leucocytes) cells that act as an immune system in the blood

Bibliography

Agarwal, R., Katiyar, V. K. & Pradhan, P. (2008), 'A mathematical model of pulsatile flow in carotid artery bifurcation', *J. Fluid Mech.* **81**, 421–431.

Ai, L. & Vafai, K. (2006), 'A coupling model for macromolecule transport in a stenosed arterial wall', *Int. J. Heat Mass Trans.* **49**, 1568–1591.

Alberding, J. P., Baldwin, A. L., Barton, J. K. & Wiley, E. (1992), 'Effects of pulsation frequency and endothelial integrity on enhanced arterial transmural filtration produced by pulsatile pressure', *Am. J. Physiol. Heart Circ. Physiol.* **289**, H931–H937.

Alexis, F., Venkatraman, S., Rath, S. K. & Boey, F. (2004), 'In vitro study of release mechanisms of paclitaxel and rapamycin from drug-incorporated biodegradable stents', *J. Control. Release* **98(1)**, 67–74.

Angioplasty.org (2009).
*http://www.ptca.org/stentcenter/index.html 15/03/10

Baldwin, A. L., Wilson, L. M., Gradus-Pizlo, I., Wilensky, R. & March, K. (1997), 'Effect of atherosclerosis on transmural convection and arterial ultrastructure', *Arterio. Thromb. Vasc. Biol.* **17**, 3365–3375.

Beavers, G. S. & Joseph, D. (1967), 'Boundary conditions at a naturally permeable wall', *J. Fluid Mech.* **30(1)**, 197–207.

Beers, M. H. (2004), *The Merck Manual of Health & Aging*, Elsevier Health Sciences.

Buzzle (2009).
*http://www.buzzle.com/articles/facts-about-open-heart-surgery.html 15/03/10

Carslaw, H. S. & Jaeger, J. C. (1986), *Conduction of Heat in Solids*, second edn, Oxford University Press.

Chen, C. I., Chen, C. K. & Yang, Y. Y. (2004), 'Unsteady unidirectional flow of an Oldroyd-B fluid in a circular duct with different given volume flow rate conditions', *J. Heat Mass Transfer* **40**, 203–209.

Clamen, M. & Minton, P. (1977), 'An experimental investigation of flow in an oscillating pipe', *Int. J. Eng. Sci.* **46**, 1147–1156.

Cordis (2009).
*www.cordis.com 15/03/10

Crank, J. (1956), *The Mathematics of Diffusion*, Oxford University Press.

Creel, C. J., Lovich, M. A. & Edelman, E. R. (2000), 'Arterial paclitaxel distribution and deposition', *Circ. Res.* **86**, 879–884.

Das, D. & Arakeri, J. H. (2000), 'Unsteady laminar duct flow with a given volume flow rate variation', *Trans. Am. Soc. Mech. Eng.* **67**, 274–281.

Davia, L., Grassi, G., Pontrelli, G., Lapasin, R., Perin, D. & Grassi, M. (2009), 'Mathematical modelling of NABD release from endothelium gel paved stent', *Comput. Biol. Chem.* **33**, 33–40.

Drazin, P. & Riley, N. (2006), *The Navier-Stokes Equations: A Classification of Flows and Exact Solutions*, Cambridge University Press.

Duraiswamy, N., Schoephoerster, R. T., Moreno, M. R. & Moore, J. E. (2007), 'Stented artery flow patterns and their effects on the artery wall', *Annu. Rev. Fluid Mech.* **39**, 357–382.

El Khatib, F. H. & Damiano, E. R. (2003), 'Linear and nonlinear analyses of pulsatile blood flow in a cylindrical tube', *Biorheology* **40**, 503–522.

Fetecau, C. (2004), 'Analytical solutions for non-Newtonian flows in pipe-like domains', *Int. J. Non-Linear Mech.* **39**.

Fotheringham, P., Gourlay, A. R., McKee, S. & Andrews, S. (2005), 'A numerical investigation of heat transfer cardiac output measurements', *J. Theoret. Med.* **6**.

Garasic, J. M., Edelman, E. R., Squire, J. C., Seifert, P., Williams, M. S. & Rogers, C. (2000), 'Stent and artery geometry determine intimal thickening independent of arterial injury', *Circulation* **101(7)**, 812–818.

Gradshteyn, I. S. & Ryzhik, I. M. (2007), *Tables of Integrals, Series and Products*, 7th edn, Elsevier.

Green, J. E. F., Jones, G. W., Band, L. R. & Grief, A. (2005), 'Arterial stents: modelling drug release and restenosis', *Proc. of the 4th Math. Med. Study Group* .

Gündoğdu, M. Y. & Carpinlioğlu, M. O. (1999), 'Present state of art on pulsatile flow theory (Part I: laminar flow regime)', *JSME Int. J. Series B* **42**, 384–397.

Hayat, T., Khan, M. & Ayub, M. (2004), 'Exact solutions of flow problems of an Oldroyd-B fluid', *Appl. Math. Comput.* **151**, 105–119.

Helps, E. P. & McDonald, D. A. (1953), 'Systolic backflow in the dog femoral artery', *J. Physiol.* **122**, 73P.

Hwang, C.-W., Wu, D. & Edelman, E. R. (2001), 'Physiological transport forces govern drug distribution for stent based delivery', *Circulation* **104(7)**, 600–605.

Ito, H. (1953), 'Theory of laminar flow through a pipe with non-steady pressure gradients', *Rep. Inst. High-speed Mech., Tohoku University No.3* pp. 163–180.

Karner, G. & Perktold, K. (2000), 'Effect of endothelial injury and increased blood pressure on albumin accumulation in the arterial wall: a numerical study', *J. Biomech.* **33**, 709–715.

Ku, D. N. (1997), 'Blood flow in arteries', *Annual Review of Fluid Mechanics* **29**.

Kuzuya, M., Naito, M., Funaki, C., Hayashi, T., Asai, K. & Kuzuya, F. (1991), 'Probucol prevents oxidative injury to endothelial cells', *J. Lipid Res.* **32**, 197.

Labinaz, M., Zidar, J. P., Stack, R. S. & Phillips, H. R. (2007), 'Biodegradable stents: The future of interventional cardiology?', *J. Interventiaonal Cardiology* **8**, 395 – 405.

Lambossy, P. (1952), 'Oscillations forcées d'un liquide incompressible et visqueux dans un tube rigide et horizontal, calcul de la force de frottement', *Helv. Phys. Acta* **25**, 371–386.

Lance, G. N. (1956), 'Motion of a viscous fluid in a tube which is subjected to a series of pulses', *Quart. Appl. Math.* **14**, 312–315.

Lever, M. J., Tarbell, J. M. & Cargo, C. G. (1992), 'The effect of luminal flow in a rabbit carotid artery on transmural fluid transport', *Exp. Physiol.* **77**, 553–563.

Levin, A., Vukmirovic, N., Hwang, C.-W. & Edelman, E. R. (2004), 'Specific binding to intracellular proteins determines arterial transport properties for rapamycin and paclitaxel', *Proc. Natl. Acad. Sci. USA* **101(25)**, 9463–9467.

Lovich, M. A. & Edelman, E. R. (1995), 'Mechanisms of transmural heparin transport in the rat abdominal aorta after local vascular delivery', *Circ. Res.* **77**, 1143–1150.

Lovich, M. A. & Edelman, E. R. (1999), 'Tissue concentration of heparin, not administered dose, correlates with the biological response of injured arteries in vivo', *Proc. Natl. Acad. Sci. USA* **96**, 11111–11116.

McCormick, C. (2008), Characterising drug release kinetics from succinobucol-coated Yukon stents, Technical report, SIPBS, University of Strathclyde. Confidential project report submitted to Translumina.

McDonald, D. A. (1952), 'The velocity of blood flow in the rabbit aorta studied with high-speed cinematography', *J. Physiol.* **18**, 328–339.

McDonald, D. A. (1953), 'Lateral pulsatile expansion of arteries', *J. Physiol.* **119**, 28p.

McDonald, D. A. (1955), 'The relation of pulsatile pressure to flow in arteries', *J. Physiol.* **127**, 533–552.

McDonald, D. A. (1974), *Blood Flow In Arteries*, Baltimore.

McLean, D. R. & Litvack, F. (2005), *Handbook of Drug Eluting Stents: The Importance of the Drug Platform: Coated, Uncoated, Sleeves, and New Concepts*, Taylor and Francis, London.

Mehilli, J., Kastrati, A., Wessely, R., Dibra, A., Hausleiter, J., Jaschke, B., Dirschinger, J. & Schmig, A. (2006), 'Randomized trial of a nonpolymer-based rapamycin-eluting stent versus a polymer-based paclitaxel-eluting stent for the reduction of late lumen loss', *Circulation* **113**, 273–279.

NHS (2009).
*http://www.nhs.uk/Conditions/Coronary-heart-disease/Pages/Introduction.aspx 15/03/10

Oldroyd, J. G. (1950), 'On the formation of rheological equations of state', *Proc. R. Soc. Lond.* **200(1063)**, 523–541.

Pache, J., Kastrati, A. & Mehilli, J. (2003), 'Intracoronary stenting and angiographic results: strut thickness effect on restenosis outcome (isar-stereo-2) trial', *ACC Current Journal Review* **12**, 66.

Peacock, J., Hankins, S., Jones, T. & Lutz, R. (1995), 'Flow instabilities induced by coronary artery stents: Assessment with an in vitro pulse duplicator', *J. Biomechanics* **28**, 17–26.

Peterson, L. H. (1954), 'The dynamics of pulsatile blood flow', *Circ. Res.* **2**, 127–139.

Peterson, S. D. & Plesniak, M. W. (2008), 'The influence of inlet velocity profile and secondary flow on pulsatile flow in a model artery with stenosis', *J. Fluid Mech.* **616**, 263–301.

Pontrelli, G. (1998), 'Pulsatile blood flow in a pipe,', *Comput. Fluid* **27**, 367–380.

Pontrelli, G. & Bhatnagar, R. G. (1997), 'Flow of a viscoelastic fluid between two rotating circular cylinders subject to suction or injection', *Int. J. Numer. Meth. Fluids* **24**, 337–349.

Pontrelli, G. & de Monte, F. (2007), 'Mass diffusion through two-layer porous media: an application to the drug eluting stent', *Int. J. Heat Mass Tran.* **50**, 3658–3669.

Pontrelli, G. & de Monte, F. (2009), 'Modelling of mass dynamics in arterial drug eluting stents', *J. Porous Media* **12(1)**, 19–28.

Richardson, E. G. & Tyler, E. (1929), 'The transverse velocity gradients near the mouths of pipes in which an alternating continuous flow of air is established', *Proc. Phys. Soc. (London)* **42**, 1–15.

Robertson, A. M. & Muller, S. J. (1996), 'Flow of Oldroyd-B fluids in curved pipes of circular and annular cross-section', *Int. J. Non-Linear Mechanics* **31**, 1–20.

Rogers, C. (2005), 'Drug-eluting stents: clinical perspectives on drug and design-differences', *Rev. Cardiovasc. Med.* **6**, S3S12.

Rogers, C., Groothuis, A., Toegel, G., Stejskal, E., Kamath, K., Seifert, P., Hesselberg, S., Delaney, R. & Edelman, E. (2000), 'Paclitaxel release from inert polymer material-coated stents curtails coronary in-stent restenosis in pigs', *Circulation* **102**, II566–II567.

Rohlf, K. & Tenti, G. (2000), 'The role of the Womersley number in pulsatile blood flow: a theoretical study of the cassan model', *J. Biomech.* **34**, 141–148.

Sangster, J. (1997), *Octanol-Water Partition Coefficient*, John Wiley and Sons.

Sanyal, L. (1956), 'The flow of viscous liquid in a circular tube under pressure gradients varying exponentially with time', *Indian J. Phys.* **30**, 57–61.

Sexl, T. (1928), 'Uber einige Integrale der für die achsensymmetrischen Strömungen in Rohren charakteristischen Differentialgleichung', *Ann. d. Physik.* **392(20)**, 570–580.

Shemer, L., Wyganski, I. & Kit, E. (1985), 'Pulsating flow in a pipe', *J. Fluid Mech.* **153**, 313–337.

Shen, X., Zhang, M., Ma, J. & Zhang, B. (2008), 'Flow and heat transfer of Oldroyd-B fluids in a rotating curved pipe', *J. Hydrodyn.* **20**, 39–46.

Smith, S. H. (1997), 'Time-dependent Poiseuille flow', *SIAM Rev.* **39**, 511513.

Sternberg, K., Kramer, S., Nischan, C., Grabow, N., Langer, T., Hennighausen, G. & Schmitz, K.-P. (2007), 'In vitro study of drug-eluting stent coatings based on poly(l-lactide) incorporating cyclosporine a - drug release, polymer degradation and mechanical integrity', *J. Mater. Sci: Mater. Med.* **18**, 1423–1432.

Szymanski, P. (1932), 'Some exact solutions of the hydrodynamic equations of a viscous fluid in the case of a cylindrical tube', *J. Math. Pure Appl.* **11**, 67–101.

Thurston, G. B. (1976), 'The viscosity and viscoelasticity of blood in small diameter tubes', *Microvasc. Res.* **11(2)**, 133–146.

Toiyama, Y., Inoue, Y., Hiro, J., Ojima, E., Watanabe, H., Narita, Y., Hosono, A., Miki, C. & Kusunoki, M. (2007), 'The range of optimal concentration and mechanisms of paclitaxel in radio-enhancement in gastrointestinal cancer cell lines', *Cancer Chemother. Pharmacol* **59(6)**, 733–742.

Translumina (2006).

*http://www.translumina.de/products2.pml 15/03/10

Uchida, S. (1956), 'The pulsating viscous flow superimposed on the steady laminar motion of incompressible fluid in a circular pipe', *Z. Angew. Math. Phys.* **7**, 403–422.

Ünsal, B., Ray, S., Durst, F. & Ertun¸c, O. (2005), 'Pulsating laminar pipe flow with sinusoidal mass flux variations', *Fluid Dyn. Res.* **37**, 317–333.

Venkatraman, S. & Boey, F. (2007), 'Release profiles in drug-eluting stents: issues and uncertainties', *J. Control. Release* **120**, 149–160.

Verma, P. D. (1960), 'The pulsating viscous flow superimposed on the steady laminar motion of incompressible fluid between two co-axial cylinders', *Proc. Natn. Inst. Sci. India* **26**, 447–458.

Waksman, R. & Serruys, P. W. (2004), *Handbook of Vulnerable Plaque*, Informa Healthcare.

Watson, G. N. (1966), *A Treatise on the Theory of Bessel Functions*, Cambridge University Press.

Womersley, J. R. (1955a), 'Method for the calculation of velocity, rate of flow and viscous drug in arteries when the pressure gradient is known', *J. Physiol.* **127**, 553–563.

Womersley, J. R. (1955b), 'Oscillating motion of a viscous liquid in a thin-walled elastic tube–I: The linear approximation for long waves', *Philos. Mag.* **46**, 199–221.

Yang, C. & Burt, H. M. (2006), 'Drug-eluting stents: Factors governing local pharmacokinetics', *Adv. Drug Delivery Rev.* **58**, 402–411.

Zarins, C., Giddens, D. P., Bharadvaj, B. K., Sottiurai, V. S., Mabon, R. F. & Glagov, S. (1983), 'Carotid bifurcation atherosclerosis: quantatative correlation of plaque localization with flow velocity profiles and wall shear stress', *Circ. Res.* **53(4)**, 502–514.

Zhu, W., Masaki, T., Cheung, A. K. & kern, S. E. (2006), 'Cellular pharmacokinetics and pharmacodynamics of dipyridamole in vascular smooth muscle cells', *Biochem. Pharmacol.* **72**, 956–964.

Zunino, P. (2004), 'Multidimensional pharmacokinetic models applied to the design of drug-eluting stents', *Cardiov. Eng.: Int J.* **4(2)**, 181–191.

Zunino, P. (2009), 'Numerical simulation of drug eluting coronary stents: mechanics, fluid dynamics and drug release', *Comput. Meth. Appl. Mech. Eng.* **198**, 3633–3644.